Explosion Testing of Nested Can Containment System Part I: Planar Gap

Z. Liang and J. E. Shepherd
Graduate Aeronautical Laboratories, California Institute of Technology
Pasadena, CA 91125

Explosion Dynamics Laboratory Report FM2007.001

May 9, 2007

Sponsored by Los Alamos National Laboratory, Subcontract 46222-001-07.

Executive Summary

A series of tests were carried out to determine the threshold for deflagration-to-detonation transition (DDT), structural loading, and structural response of the nested can containment systems using the 3013 outer can in the case of an accidental explosion of evolved gas within the cans. Three experimental fixtures were used to examine various issues and three mixtures consisting of either stoichiometric hydrogen-oxygen, stoichiometric hydrogen-oxygen with added nitrogen, and stoichiometric hydrogen-oxygen with added nitrogen and helium were tested. Tests were carried out as a function of initial pressure from 1 to 3.5 bar and initial temperature from room temperature to 150°C. The explosions were initiated with either a small spark or hot surface.

In Part I, a planar model of the annular gap between the outer and inner cans was tested. Measurements of pressure along the gap indicated that DDT occurred in all mixtures with threshold pressures between 1 and 3 bar, depending on the mixture and gap height. The smaller the gap height, the lower the transition threshold up to the point where flames could no longer be ignited due to quenching which occurred for a gap size of less than 0.01 in for stoichiometric hydrogen-oxygen at 1 bar initial pressure. Increasing the temperature from 25°C to 150°C resulted in a slight increase in the threshold pressure for DDT.

In Part II, a thick-wall cylindrical model was tested that simulated the interior of the outer 3013 cans and with a cylindrical insert, the annular gap between outer and inner cans. The DDT thresholds occur at much higher pressures (2.6 bar for stoichiometric hydrogen-oxygen and > 3.5 for the diluted mixtures) for an empty can than with the annular gap. The size of the gap between the end of the cans did not have a significant influence on either the threshold pressure for DDT or the pressure and strain histories. The transition thresholds and pressure histories from explosions in the annular gap were very similar to those observed in the planar gap. Measurements of the hoop strain indicated that although the details of the pressure histories differed between concentric and eccentric gaps, the peak hoop strain was similar in both cases. The measured strains with the annular gap configuration were lower than for the empty can. The peak strains could be bounded by a dynamic load factor of 2 based on the Chapman-Jouguet (CJ) pressure for the annular gap case and 3.5 for the empty can.

In Part III, tests were carried out on actual 3013 cans modified with penetrations for pressure transducers, gas handling, and ignition. Only the empty can configuration was tested. The DDT thresholds and pressure histories were essentially identical to the those observed in the empty thick-wall model used in Part II although a hot surface ignition system was used for most Part III tests rather than the spark ignition used in Parts I and

II. The peak hoop strain measured in these tests was slightly less than 2000 μstrain, the generally accepted elastic limit for this material, and the strains could be bounded using the CJ pressure and a dynamic load factor of 3.5.

We conclude that DDT is possible both within the annulus between outer and inner cans and the interior of the 3013 cans at sufficiently high initial pressure with both stoichiometric hydrogen-oxygen mixtures and hydrogen-oxygen mixtures diluted with nitrogen and helium. For the three mixtures we tested, the peak hoop strains measured in the outer can are slightly less than the 0.2% strain conventionally used to determine the onset of plastic deformation. No structural failure or measurable deformation was found in the 3013 cans that were tested. Based on the results of these tests, we conclude that DDT of a stoichiometric hydrogen-oxygen mixture (and mixtures diluted with nitrogen and helium) within the 3013 nested can containment system does not pose a threat to structural integrity of the outer can at initial pressures up to 3.5 bar and temperatures up to 150°C.

We did not test the inner or convenience cans. Based on present results and past studies, we expect the DDT threshold initial pressures to be lower for small diameter cans and/or cans filled with granular material. Since peak pressures are proportional to initial pressures, all other factors being the same, this means that the peak DDT pressures measured in the 3013 outer cans will bound the peak DDT pressures that will occur in the inner and convenience cans. However, the peak strains and deformations will be higher for the inner and convenience cans than for the outer can since the outer can is constructed of much thicker wall material than inner and convenience cans. Detonations outside or inside of the inner or convenience cans may cause significant deformation of those cans. The 3013 outer can is the ultimate pressure barrier and the deformation of the inner and convenience cans will be limited by the presence of the outer can so that we do not expect the deformation of the inner or convenience cans to be a limiting factor in determining the integrity of the overall nested can containment system.

Contents

List of Figures

List of Tables

1 Introduction

This report describes the first in a series of tests being carried out to provide data that will be used in the safety assessment of triple-nested (DOE-STD-3013) containers used in the DOE complex for PuO_2 storage. The tests use deliberate ignition of explosive mixtures to determine the type of explosion, structural loading (pressure history), and structural response (strain history) in both model fixtures and actual 3013 components. Tests have initially been carried out in a planar geometry, subsequent testing will examine annular geometries.

In the planar gap tests, the threshold for Deflagration-to-Detonation Transition (DDT) was determined for a thin layer of gas simulating the annular gap between the outer and inner cans of the 3013 containment system. For simplicity, the annular geometry was developed (unrolled) into a planar geometry so that the thin layer (gap) was a space bounded by two rigid flat plates. The gap was filled with a representative explosive gas mixture, ignited with a low-energy spark, and the subsequent explosion development monitored with pressure gages. For each mixture composition, the threshold for DDT was determined by varying the initial pressure. Since the inner and outer cans may be eccentric, gap size was treated as a parameter and we examined values of 0.01, 0.02, 0.05, 0.1, 0.44 in (0.254, 0.508, 1.27, 2.54, 11.18 mm). The annular gap between the inner and outer cans of the 3013 system[1] may vary from 0 to 0.185 in (0-4.7 mm) depending on the eccentricity of the cans. The largest gap was intended to model the head space gap of approximately 0.5 in (12.7 mm).

Three mixtures were used: A (stoichiometric hydrogen-oxygen), B (stoichiometric hydrogen-oxygen added to an initial fill of 60 kPa nitrogen) and C (stoichiometric hydrogen-oxygen added to an initial fill of 16 kPa nitrogen and 60 kPa helium). See Appendix A for the precise specification of the three mixtures. The initial conditions for the preliminary tests were room temperature (20-23°C) and pressures of 0.8–3.5 bar. A set of higher temperature tests (10°C) more representative of the actual conditions expected to be present in the cans that are in service were also performed to examine the effect of the temperature on DDT transition threshold.

[1]The dimensions quoted here were determined by examining the SRS engineering drawings M-PV-F-0016 and -0017 for the PUSPS Assembly.

2 Fixture and Procedure

All the tests were conducted in a rigid vessel constructed of two rectangular plates (19 in wide, 13 in long and 1.2 in thick) of 4130 alloy steel separated by a steel spacer to form the volume simulating the annular gap (see Fig. 1). The spacer created a rectangular region 9.2 in wide (corresponding to the inside length of the outer can), 15 in long (corresponding to the length of the unrolled annular gap), and with a height equal to the thickness of the spacer. Five different spacers with a thickness of 0.01, 0.02, 0.05, 0.10, 0.44 in were tested. The surface of the two confining plates were Blanchard ground with a resulting surface roughness between 16 and 32 micro- inch.[2] The plates and spacer were held together by 26 3/4-in cap screws and the spacer was sealed to the plates using o-rings. Four reinforcing bars were added in the center of the plates for added stiffness (Fig. 1). The plate thickness and reinforcing bars were chosen to limit the deflection of the plates under the most extreme static pressures we expected based on pre-test computation. The instrumentation and gas lines were mounted on one plate, which was held vertically through an attachment to a fixed base (Fig. 1). The second plate was removable so that the spacers could be changed and the facility maintained.

The gap was filled by the method of partial pressures using bottled gas supplied by local vendors. Prior to filling, the gap and associated plumbing was evacuated below 5 Pa. Since the volume of the facility was small, it is necessary to take some care to eliminate leaks and minimize the dead volume associated with connecting lines. For the largest gap tested (0.44 in), the volume was 60.7 in^3 (995 cc) and for the smallest gap tested (0.010 in), the volume was 1.4 in^3 (22.6 cc). The filling lines were evacuated prior to switching gases in order to minimize the error in composition. Shut-off valves were located as close as possible to the Swagelok O-Seal connections to the fixed flange. The gas within the gap was circulated by a bellows pump for five minutes to ensure a homogeneous mixture.

Two ignition sources, a spark plug and glow plug (see Fig. 1b for GP, SP), were originally mounted on one of the plates. Only the spark plug was used in the present tests. Following the initial series of tests, the glow plug was removed and the access hole sealed with a flush bolt in order to eliminate the dead volume. Four piezo-electric (PCB) pressure transducers (P_1-P_4) were mounted in the fixed plate, and the sensitive surface of the transducers was flush with the interior surface of the plate. The distance of the pressure transducers to the ignition source is listed in Table 1.

The first 63 shots for the gap sizes of 0.44, 0.10 and 0.05 in were performed with the initial configuration. Substantial dead volumes were present at three locations: (1) the

[2]The surface roughness on the 3013 outer can inner surface is called out to be 1.6 μm (63 micro-inch).

volume between the inner surface of the plate and the glow plug front (3/4 in diameter, 0.55 in deep); (2) the volume between the inner surface of the plate and the Swagelok adapters for G_1, G_2, StP and T (7/16 in diameter, 0.575 in deep); (3) the volume inside the Swagelok tubing (1/8 in diameter, total 10 in long). For the smaller gaps (0.01 and 0.02 in), the amount of the dead volume is comparable to the volume inside of the gap. Therefore, after shot 63, all the mounting holes were modified to remove the dead volume at places (1) and (2), and the Swagelok tubing between the Swagelok O-Seal fittings and valves was reduced to the smallest possible length, about seven inches total. These modifications cut down the dead volume to less than five percent for all the gap sizes.

Table 1: Distance (along long axis) from the pressure transducers (P_1-P_4) to the igniter location.

	X (m)	X (in)
P_1	0.08	3.15
P_2	0.178	7.00
P_3	0.276	10.85
P_4	0.349	13.75

In order to investigate the effect of the initial temperature on the DDT thresholds, a heating system was installed on the planar fixture after shot 101. Flexible silicon heaters were glued on the outer surface of the two plates as shown in Fig 3. Thermocouples were mounted at six locations on the surface of the plates to measure the temperature. One of the thermocouple outputs was connected with a feedback controller (Omega CN76000), which regulated the heater power to maintain a set temperature. A 1/2-in thick bar of G10 glass reinforced plastic was used to insulate the bottom of the plates from the mounting surface and the fixture was surrounded by a box constructed of 1-in thick sheets of fiberglass duct board insulation. A maximum of 2 kW of electrical power could be applied through the heaters and the fixture could be heated up to 150°C in less than one hour.

The 0.05 in gap was used for all the tests with the heaters. Two Swagelok tubing connections were lengthened by 1 in to leave space for the insulation box, thus the dead volume was slightly increased from 1 to 1.5%. A few tests at room temperature were repeated to check the effect of the dead volume.

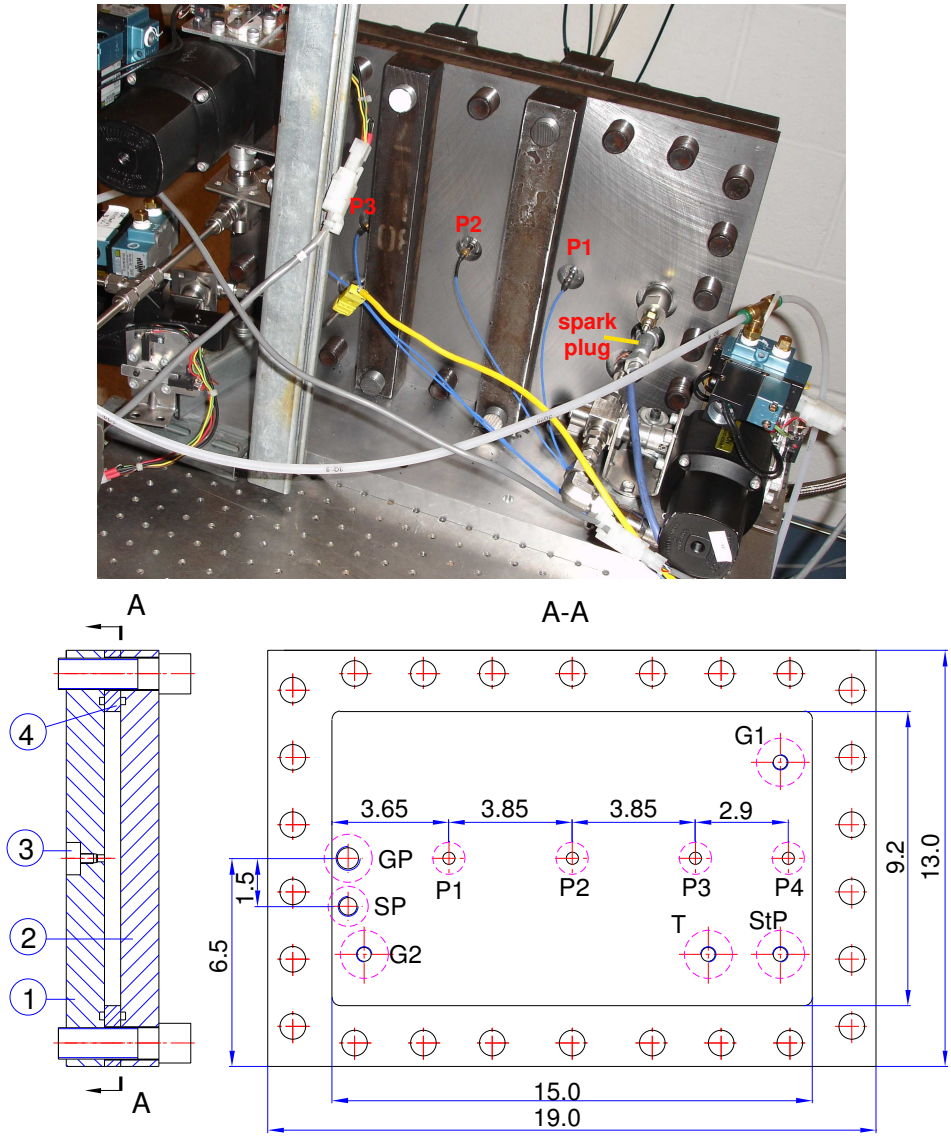

Figure 1: Setup of the planar fixture assembly without heater. 1-bottom plate, 2-top plate, 3-pressure transducer holes, 4-spacer. SP-spark plug, GP-glow plug (not used, sealed in the tests), G1, G2 - gas lines, T- thermocouple, StP- static pressure gauge. The photograph shows a view of the fixed plate (side 1) of the fixture with the instrumentation and gas feed-throughs attached.

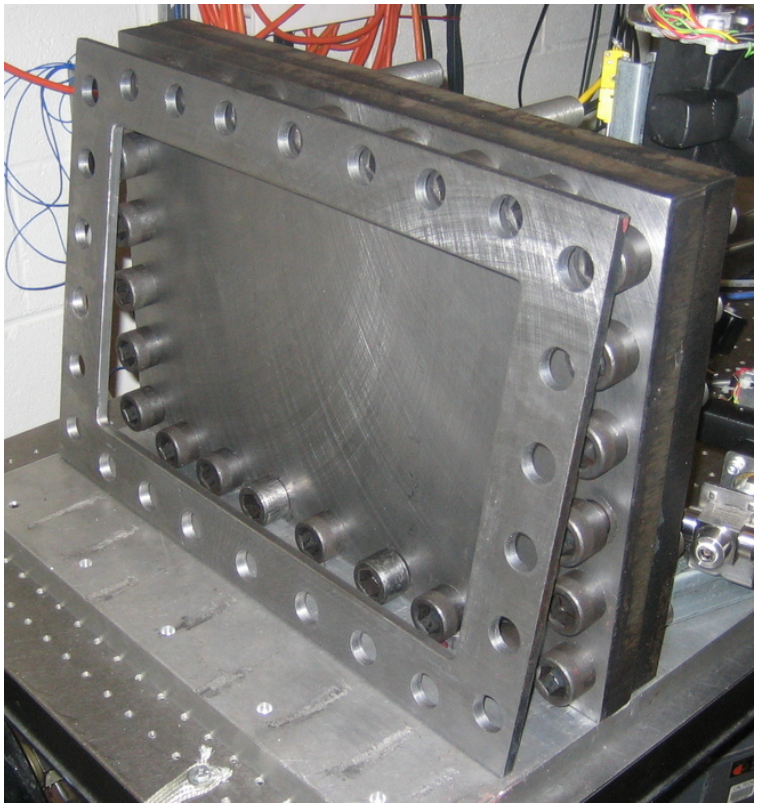

Figure 2: Photograph showing a view of the removable plate (side 2) of the fixture with a representative spacer leaning against it.

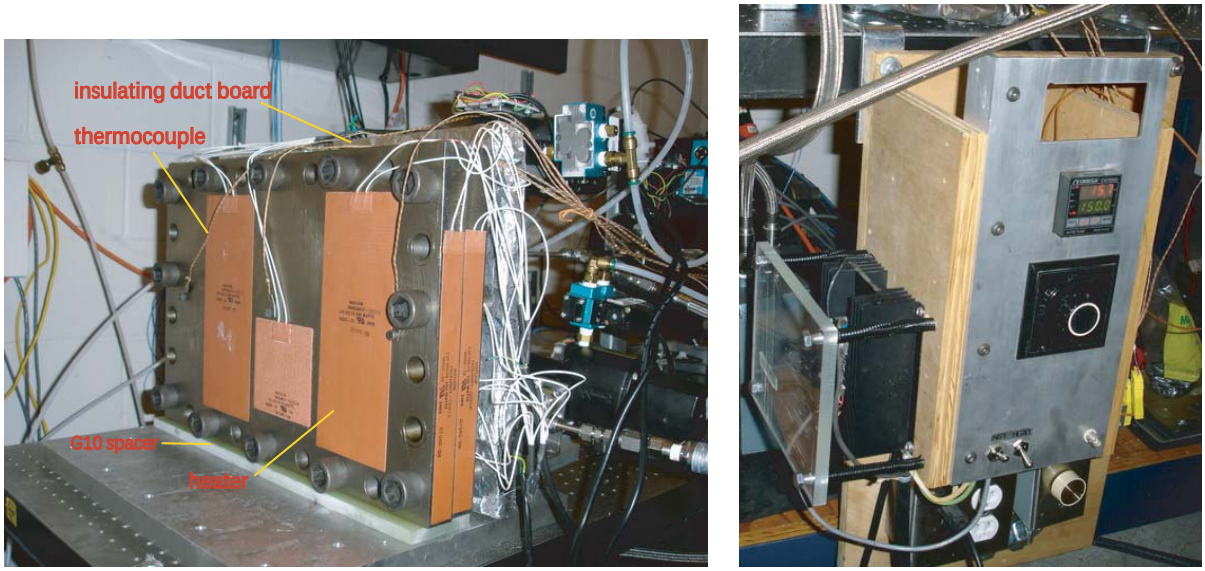

(a) (b)

Figure 3: a) Setup of the planar fixture assembly with heater and b) temperature controller. A section of insulating duct board is visible on the back of the fixture and the G10 spacer (green bar) is visible at the bottom.

3 Room Temperature Results

A total of 101 explosive tests (shots) were carried out with the unheated facility and an additional 23 shots were carried out with the heated version. A summary of the unheated test conditions is given in Table 2. The values for CJ pressure (P_{CJ}), reflected CJ pressure (P_{CJref}) and constant volume explosion pressure (P_{CV}) for each test were calculated using a chemical equilibrium program of Reynolds (1986) with realistic thermochemical properties. The results of these computations are given for each mixture and initial condition in Appendix A.

Table 2: Summary of test series at $T_0 = 21 - 25$ °C.

Gap size (in)	shots	mixture	P_0 (bar)	Threshold (bar)	dead volume
Initial setup (large dead volume)					
0.44	1-11	A	1-3.5	1.2-1.25	1.3%
	12-19	B	1-3.5	2.0-2.1	
	20-26	C	1-3.5	2.5-2.75	
0.10	27-32	A	1-3.0	∼1.0	5.5%
	33-39	B	1-3.5	1.5-1.75	
	40-45	C	1-3.0	2.0-2.25	
0.05	46-50	A	1-3.0	∼1.0	10%
	51-55	B	1-3.5	1.0-1.25	
	56-61	C	1-3.0	1.5-1.75	
Modified setup (small dead volume)					
0.05	64-66	A	1-2.0	1.0-1.25	1.0%
	67-68	B	1.5-3.0	1.5-1.75	
	69-74	C	1.75-3.0	1.75-2.0	
0.02	78-84	A	0.8-3.0	0.9-1.0	3.0%
	85-89	B	1.0-2.5	1.5-1.75	
	90-92	C	1.75-2.5	1.75-2.0	
0.01	93-96	A	0.8-2.0	0.9-1.0	5.0%
	97-99	B	1.5-2.0	1.5-1.75	
	100-101	C	1.75-2.0	1.75-2.0	

The location of DDT onset was determined by examining the pressure traces for the characteristic signatures of DDT. The pressure signals were compared to computed values of the peak pressure for idealized combustion processes. Near the DDT location, the pressure peak had a sharp front and a value which can be up to several times higher than the CJ pressure P_{CJ}. For transducers between the ignition and DDT location, a gradual rise in pressure or sometimes weak shock waves were observed prior to the DDT event. The DDT

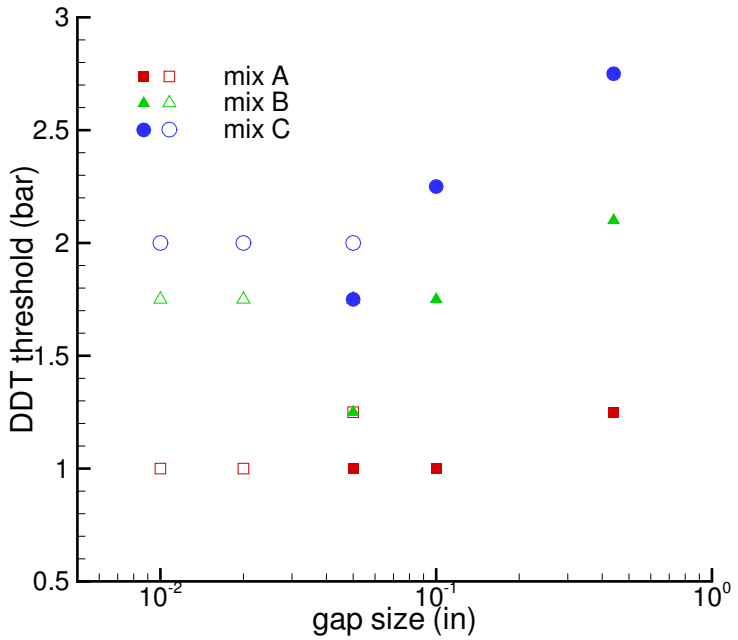

Figure 4: DDT threshold vs gap size for three mixtures. The data shown with open symbols were performed with the modified setup with the smaller dead volume.

event produced strong shock waves in the burned gas that were observed as sharp jumps in the pressure signals. These propagated away from the DDT location and can be observed in the signals from transducers adjacent to the DDT event.

Figure 4 describes the effect of the gap size on DDT transition threshold. When the gap size decreases from 0.44 to 0.05 in, the DDT thresholds for three mixtures all shift to smaller initial pressures. This behavior is associated with the flame or ZND[3] reaction zone thickness increasing with decreasing initial pressure. As the gap size is further decreased below 0.05-in, the thresholds remain constant. Below a minimum gap size, no flame propagation is possible.

In Figure 4, there are two data points for each mixture at the gap size of 0.05-in, which represent the thresholds regarding two different dead volumes. The DDT threshold shifts to a higher pressure value when the dead volume is smaller. In the original setup, there are two large dead volumes close to the spark plug (one in the glow plug mounting hole GP and one in the Swagelok O-Seal mount G2, so an explosion may have occurred in these volumes, enhancing the DDT transition process.

Figures 5-7 demonstrate the variation of the peak pressures recorded in each shot with different mixtures, gap sizes and initial pressures.[4] The experimental peaks $P_{1,max}$-$P_{4,max}$

[3]Zel'dovich, von Neumann, Döring model of an idealized steady, one-dimensional detonation

[4]In some high pressure cases, artificial spikes appeared on gauge P2 in tests 9, 24, 25, 27, 31, 36, 37, 38, 43, 44, 45, 46, 50, 54, 55, 59, 60. This peaks occur between 1-2 ms after the initial pressure jump due to

are the maximum measured pressure on the four transducers. For a given gap size, the DDT transition always occurred at lower P_0 for mixture A than mixtures B and C. For a given mixture, the DDT threshold occurred at lower initial pressures for smaller gap sizes.

Figure 8 summaries the DDT run-up distance for different gaps and mixtures. The DDT run-up distance is shorter for smaller gap size for the same mixture. The smallest run-up distance, 0.08 m (3.15-in), represents the location of P_1 and the largest, 0.349 m (13.75-in) corresponds to the location of P_4.

the detonation or shock and have a characteristic signal with negative and positive portions that strongly suggests that these are noise rather than information about pressure waves. These values are not used in reporting the peak pressures in the figures or tables.

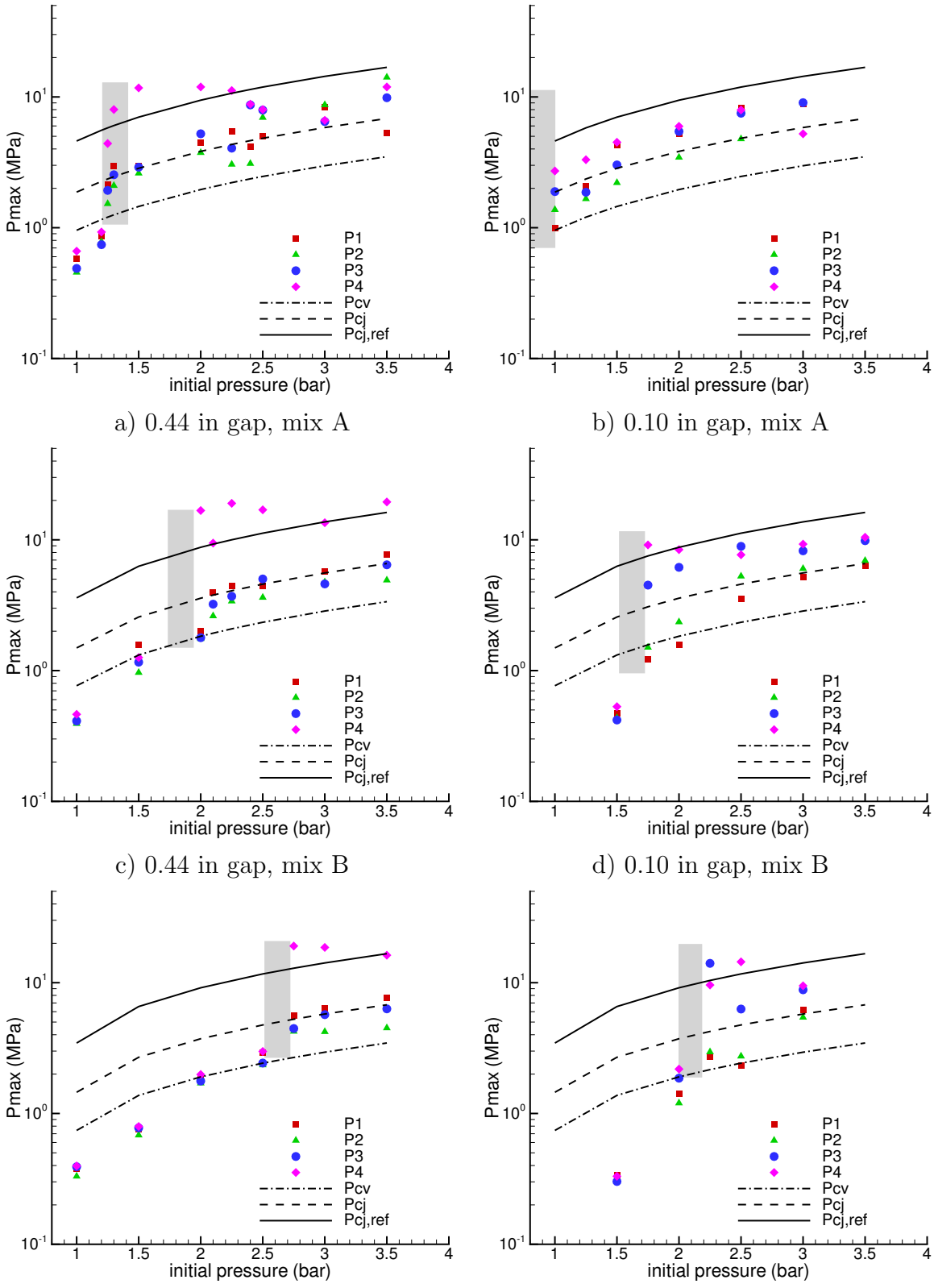

a) 0.44 in gap, mix A

b) 0.10 in gap, mix A

c) 0.44 in gap, mix B

d) 0.10 in gap, mix B

e) 0.44 in gap, mix C

f) 0.10 in gap, mix C

Figure 5: Comparison of peak pressures for gap size 0.44-in and 0.10-in. The shaded region is the estimated threshold for the onset of DDT.

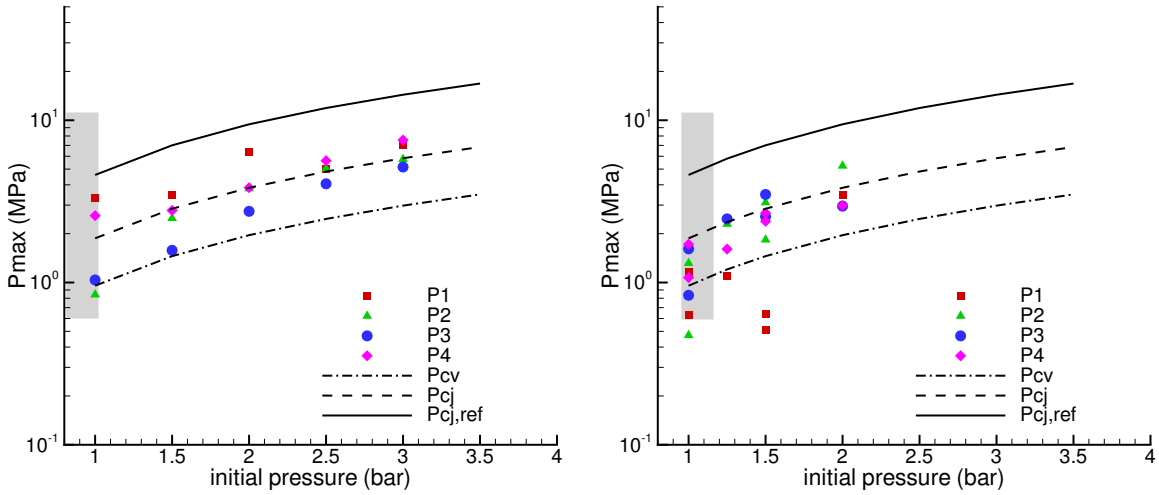

a) 0.05 in gap (10%dv), mix A

b) 0.05 in gap (1%dv), mix A

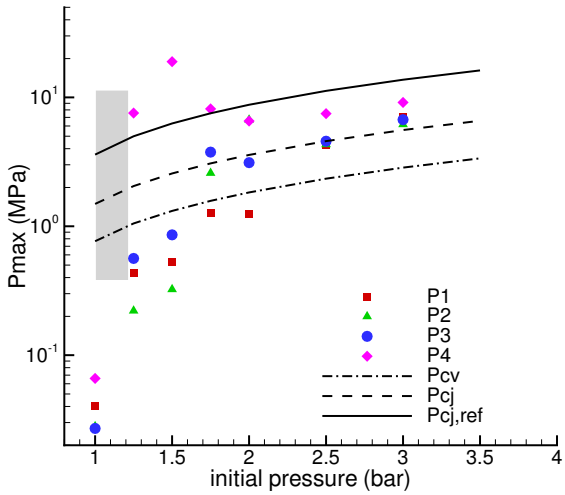

c) 0.05 in gap (10%dv), mix B

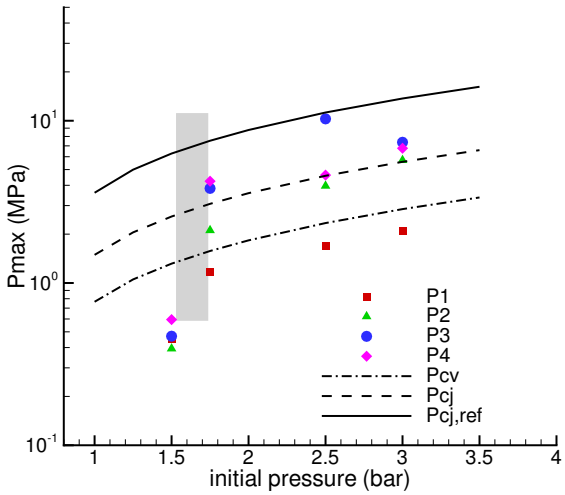

d) 0.05 in gap (1%dv), mix B

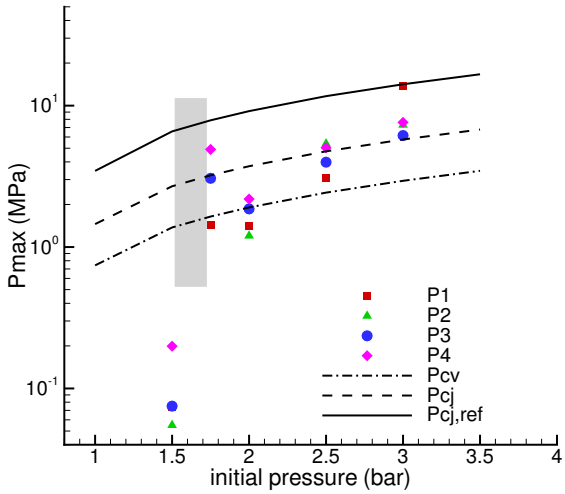

e) 0.05 in gap (10%dv), mix C

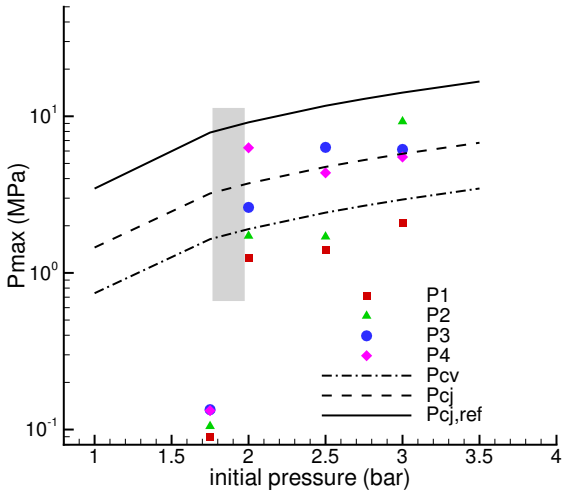

f) 0.05 in gap (1% dv), mix C

Figure 6: Comparison of peak pressures for gap size 0.05-in with 10% and 1% dead volume respectively. The shaded region is the estimated threshold for the onset of DDT.

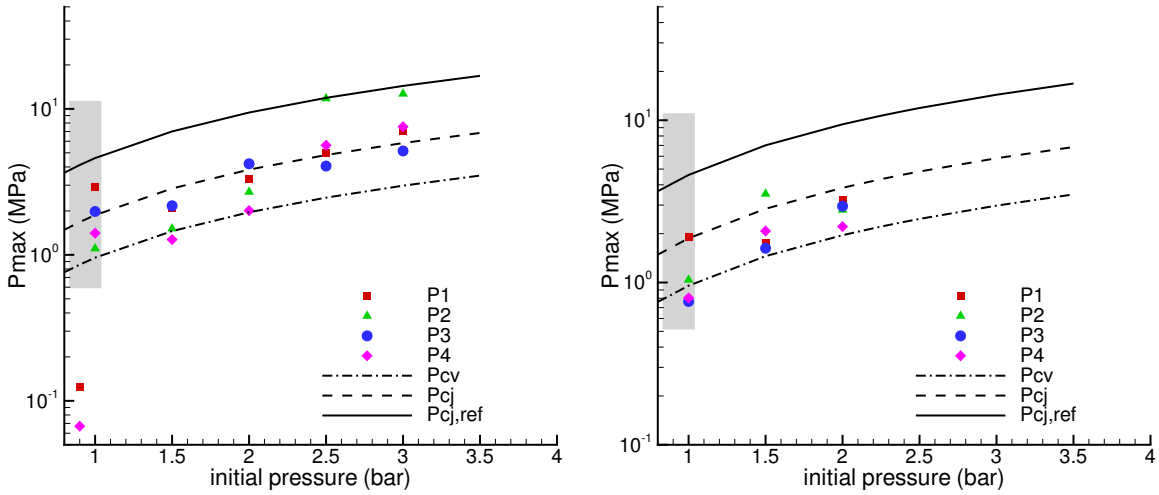

a) 0.02 in gap, mix A

b) 0.01 in gap, mix A

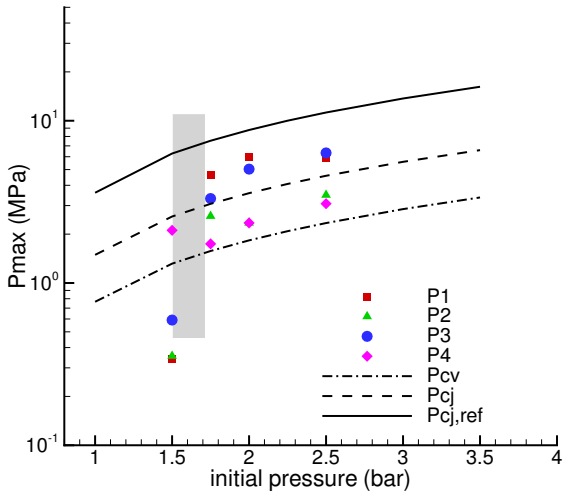

c) 0.02 in gap, mix B

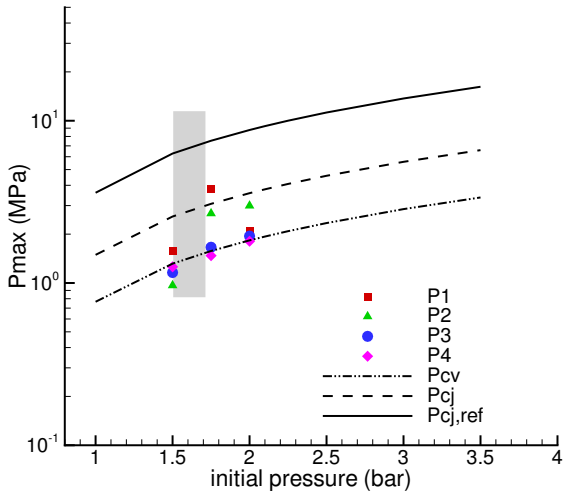

d) 0.01 in gap, mix B

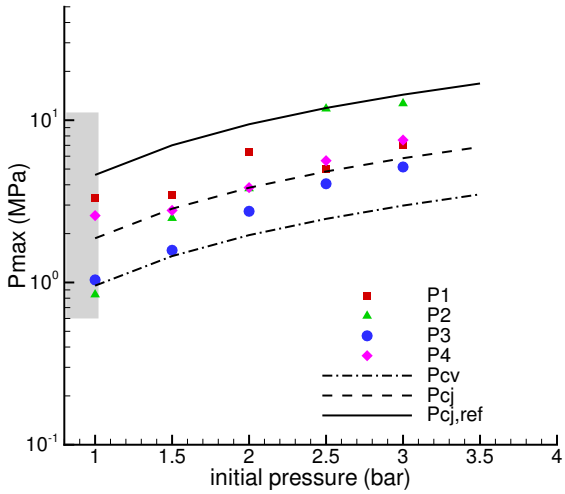

e) 0.02 in gap, mix C

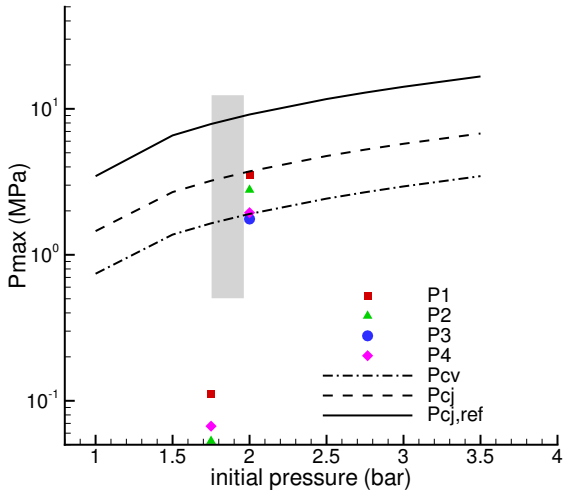

f) 0.01 in gap, mix C

Figure 7: Comparison of peak pressure for gap size 0.02 and 0.01-in. The shaded region is the estimated threshold for the onset of DDT.

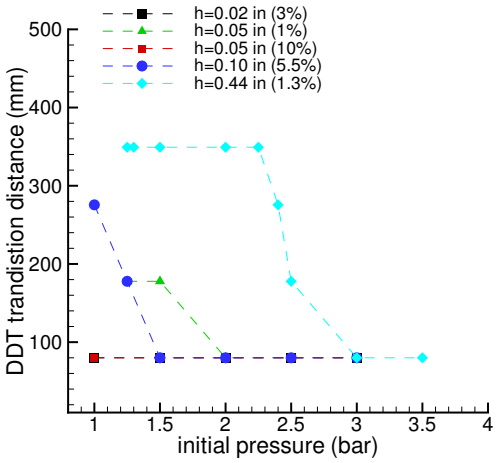

a) mixture A

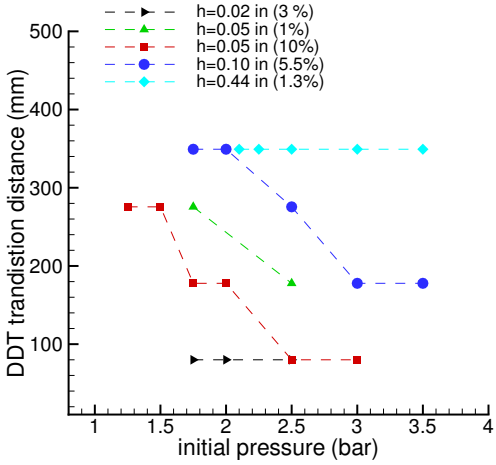

b) mixture B

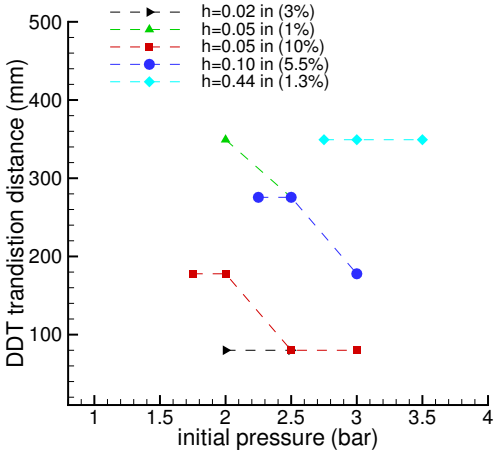

c) mixture C

Figure 8: DDT run-up distance for three mixtures.

4 Elevated Temperature Results

A total of 20 explosive tests (shots) have been carried out with the heater-equipped fixture at both room (∼21°C) and higher temperatures (44 and 150°C). A comparison of the tests is given in Fig 9; see Appendix H for more details.

Noted that the DDT thresholds are only weakly dependent on initial temperature for the gap size of 0.05 in. At the same P_0, the DDT run-up distance is slightly longer at higher T_0. As shown in Appendix H, at $P_0 = 1$ bar, DDT occurred close to P_1 at room temperature 21°C (shots 105 in Fig. 31a), but is closer to P_3 at $T_0 = 44$°C (shots 106 in Fig. 31c) and closer to P_4 at $T_0 = 150$°C (shots 114 in Fig. 31d). For $T_0 = 150$°C the location of DDT moved from near the last transducer P_4 to the first one P_1, when P_0 was increased from 1.25 to 3.0 bar. This trend is consistent with the DDT study by Card et al. (2005). It was found the transition limits are only weakly dependent on initial temperature.

Figure 10 compares the values of P_{CV}, P_{CJ} and P_{CJref} at both room temperature $T_0 = 25$ and 150°C. The values at $T_0 = 150$°C are lower since the relative energy content per unit mass at 150°C is only 70% of that at 25°C. The relative energy content is the heat of combustion divided by the internal energy of the reactants, which is proportional to the gas initial temperature.

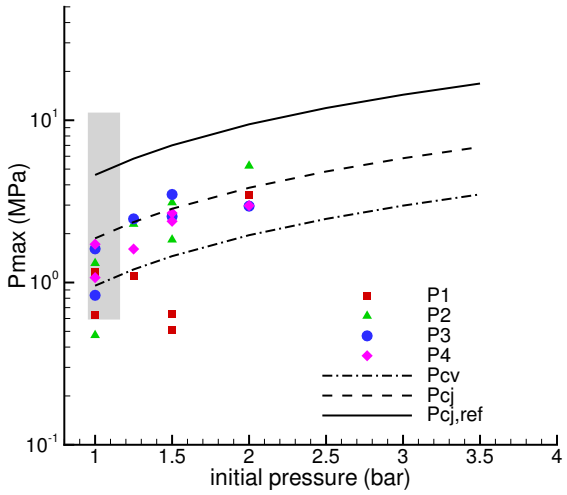

a) mix A, $T_0 = 21$ °C

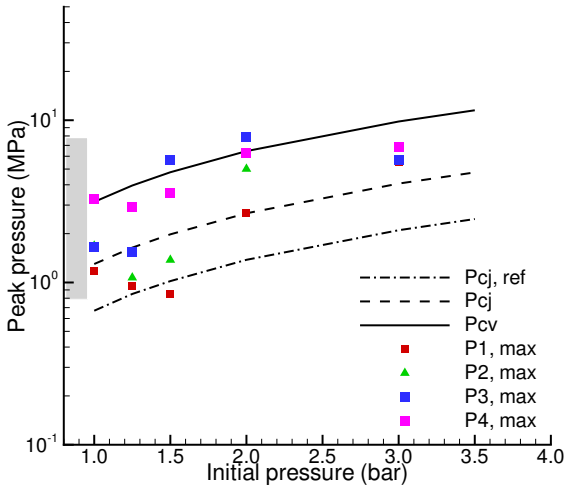

b) mix A, $T_0 = 150$ °C

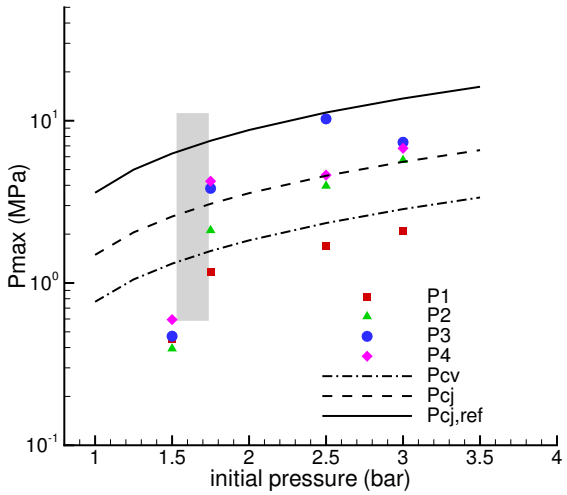

c) mix B, $T_0 = 21$ °C

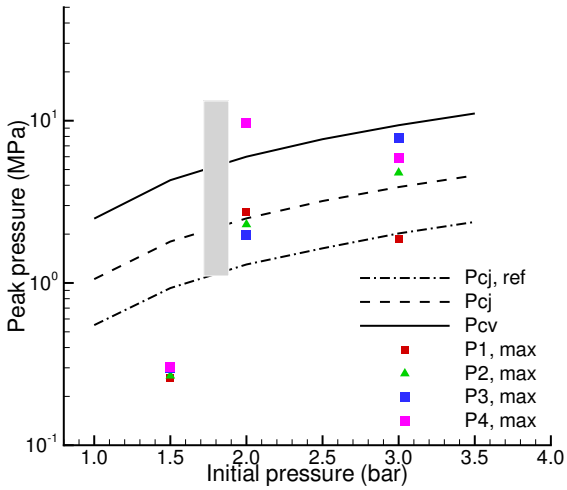

c) mix B, $T_0 = 150$ °C

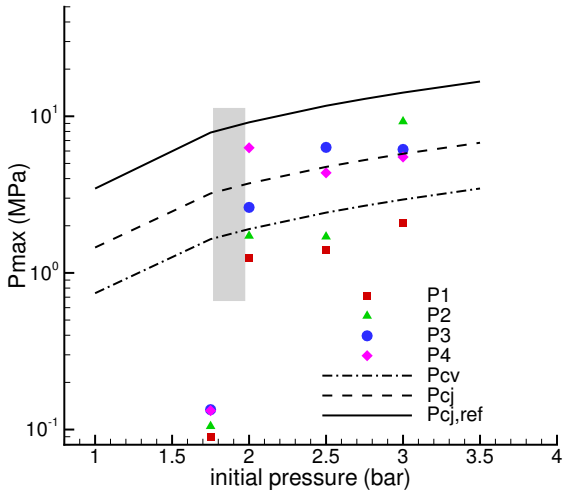

d) mix C, $T_0 = 21$ °C

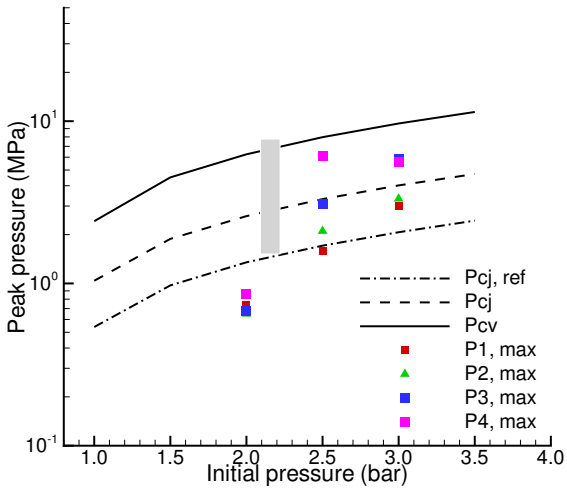

e) mix C, $T_0 = 150$ °C

Figure 9: Comparison of peak pressures for gap size 0.05 in at $T_0 = 21$ and 150 °C. The shaded region is the estimated threshold for the onset of DDT.

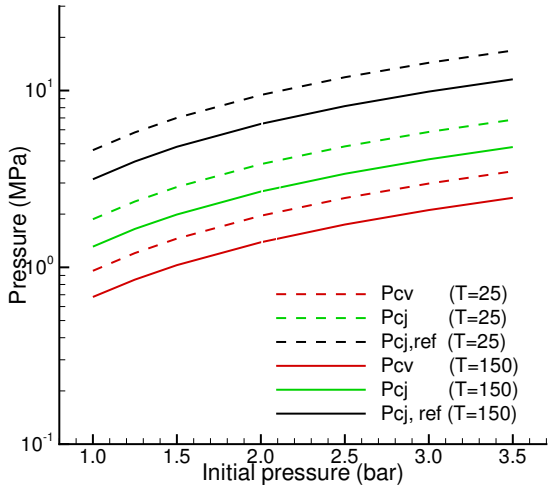

a) mix A

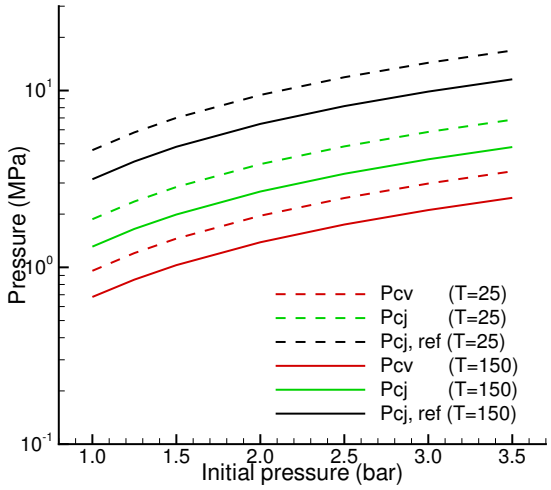

b) mix B

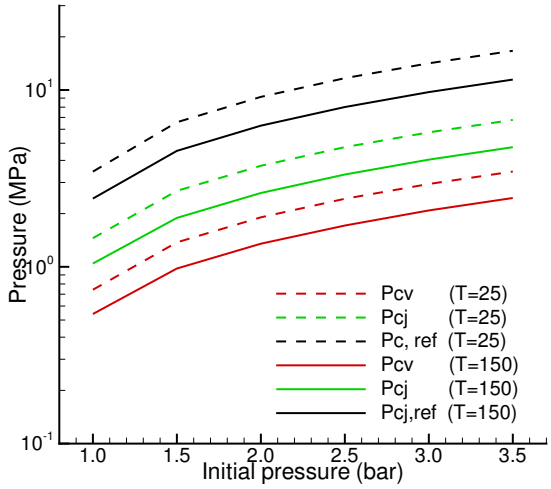

c) mix C

Figure 10: Comparison of values of P_{CV}, P_{CJ}, P_{CJref} at $T_0 = 25$ and 150 °C.

5 Summary

Our findings can be summarized as follows:

1. All three mixtures will undergo DDT with threshold initial pressures between 1 and 3 bar.

   The result, although it may appear surprising based on examining the chemical engineering literature on DDT in industrial facilities, is consistent with our past experience with hydrogen-oxygen mixtures. These mixtures have high flame speeds, high volume expansion ratios, and small induction lengths in comparison with all fuel-air mixtures. All of these factors make the mixtures much more susceptible to flame acceleration and transition to detonation than the fuel-air mixtures that have been examined in many industrial safety studies.

2. Mixture A is the most sensitive, i.e., the lowest DDT threshold pressure, mixture B is intermediate, and mixture C is the least sensitive, i.e., highest DDT threshold pressure. For example, for a gap size of 0.02 in (0.508 mm), DDT occurred at $P_0 = 1$ bar for mixture A, 1.75 bar for mixture B, and 2.0 bar for mixture C.

   This ranking of the mixtures could be anticipated on the basis of the computed CJ properties and reaction zone lengths given in the tables of Section A. Further computations of flame speed and correlations of DDT run-up distance could also be used to bolster this conclusion.

3. The smaller the gap size, the lower the threshold pressure for DDT. For example, for mixture A, DDT was observed at $P_0 = 1.25$ bar for a gap of 0.44 in (11.1 mm) and P_0 = 0.9-1.0 bar for a gap of 0.05 in (1.27 mm).

   This effect was not anticipated and was at first rather surprising. However, correlations of DDT minimum run-up distance proposed in the literature by Veser et al. (2002) and Kuznetsov et al. (2005), imply this effect with minimum run-up distance proportional to tube diameter for tubes. Extrapolating to the present planar geometry, these correlations predict that run-up distance should be proportional to gap height up to the point that quenching becomes important.

   Although the threshold pressures are lower with smaller gap sizes, the peak pressures and impulses are also lower for a smaller gap than a larger gap at the DDT threshold pressure. This is due not only to the scaling of theoretical (CJ) detonation peak pressures with the initial pressure but also due to losses associated with the narrow channel.

4. When the initial pressure is low, the reaction zone thickness is large. Therefore for small gaps, the mixture cannot be ignited when the pressure is less than some minimum value. For the smallest gap size (0.01 in), when $P_0 < 0.8$ bar, there was no ignition for mixture A, and when $P_0 \leq 1.0$ bar, there was no ignition for mixture B.

   This result is reasonable and consistent with previous work on quenching flames. The existence of a minimum gap for flame propagation is well established in the combustion literature.

5. When the initial temperature is increased from the room temperature (21-25°C) to 150°C, the DDT transition thresholds slightly increase for all three mixtures. For the same initial pressure, the higher temperature cases requires longer DDT run-up distance, and the peak pressure is lower.

   The effect of initial temperature is reasonable and consistent with previous work. Increasing the initial temperature lowers the peak pressure and volume expansion ratio, which decreases the potential for flame acceleration. In the present case, the decrease in these parameters is modest and the effect on DDT threshold is minor.

6 Implications for Safety Assessment

In Part I of this test program, we have examined only one aspect of the potential hazards associated with internal explosion in the 3013 containment system. We have shown that transition from deflagration to detonation is possible at sufficiently high pressures for the mixtures we have studied. Prior to this test program, there were no data on this combination of configuration, mixtures, and initial pressures so we were unable to draw any definite conclusions about the mode of combustion. Although we considered that DDT was unlikely in our preliminary evaluation[5], we did not rule this out absolutely and had indicated that testing would be required to settle this issue. Now we have clear evidence that DDT is possible under some conditions and this must be taken into account when examining the structural response of the 3013 containment system. Apparently these mixtures are sufficiently sensitive that flames are able to accelerate to detonations even within very thin gaps when the reaction zone is small compared to the gap height. There is a very slight influence of initial temperature on DDT threshold and lower temperature mixtures have lower DDT initial pressure thresholds and higher peak pressures.

The key implication for the safety assessment is that the impulse loading associated with DDT and detonation must be considered in addition to quasi-static loading associated with deflagration (flame). Although the peak pressures associated with DDT and detonation may be substantially higher than for deflagration, the duration of the loading is much shorter. As a consequence, the deformation of the 3013 outer can will be limited compared to static loading with the same peak pressures. If the impulse is sufficiently small, even with a DDT event it is still possible to have a structural response that maintains the integrity of the outer can.

In order to make a realistic evaluation of the structural response and the possibility of outer can rupture, the dynamic nature of the DDT and detonation loadings must be factored into the deformation computation. A preliminary estimate of the dynamic loading was made in the Safety Analysis last spring[6] for one mixture. This issue must be revisited and a new evaluation carried out. A revised estimate can be made with the present pressure data and a final evaluation will follow from measurements obtained from tests using 3013 outer cans in the later stages of the present test program.

[5]Letter from Joe Shepherd to Coyne Prenger of Los Alamos National Lab, June 11 2006

[6]AER-CW-CE-10,Rev 3, Safety Analysis for PuO_2 Triple-Nested Can Storage Systems, May 23, 2006

Bibliography

J. Card, D. Rival1, and G. Ciccarelli. DDT in fuel-air mixtures at elevated temperatures and pressures. *Shock Waves*, 14(3):167–173, 2005.

M. Kuznetsov, V. Alekseev, I. Matsukov, and S. Dorofeev. DDT in a smooth tube filled with a hydrogen-oxygen mixture. *Shock Waves*, 14(3):205–215, 2005.

W.C. Reynolds. The element potential method for chemical equilibrium analysis: implementation in the interactive program STANJAN. Technical report, Mechanical Engineering Department, Stanford University, 1986.

A. Veser, W. Breitung, and S. B. Dorofeev. Run-up distances to supersonic flames in obstacle-laden tubes. *Journal de Physique, IV France, Proceedings*, 12(7):333–340, 2002.

A Specification and characterization of gas mixture

The specifications of each mixture and the results of computations of peak pressures and reaction zone lengths are given in the tables below. The first column is the total pressure. The next three columns give the partial pressure of the components in the initial mixture. The next four columns are the constant volume explosion pressure (P_{CV}), CJ pressure (P_{CJ}), reflected CJ pressure (P_{CJref}) and CJ detonation velocity U_{CJ}. The last column Δ_{CJ} is the ZND reaction zone thickness for a CJ detonation.

Table 3: Mixture A: stoichiometric hydrogen-oxygen.

P_0 (kPa)	P_{H_2} (kPa)	P_{O_2} (kPa)	P_{CV} (MPa)	P_{CJ} (MPa)	P_{CJref} (MPa)	U_{CJ} (m/s)	Δ_{CJ} (mm)
100	66.67	33.33	0.956	1.872	4.602	2840.3	0.042
150	100.00	50.00	1.454	2.848	7.006	2862.7	0.030
200	133.33	66.67	1.958	3.836	9.441	2878.6	0.024
250	166.67	83.33	2.466	4.832	11.895	2890.9	0.021
300	200.00	100.00	2.978	5.834	14.364	2900.9	0.019
350	233.33	116.67	3.492	6.841	16.842	2909.4	0.018

Table 4: Mixture B: hydrogen-oxygen-nitrogen.

P_0 (kPa)	P_{N_2} (kPa)	P_{H_2} (kPa)	P_{O_2} (kPa)	P_{CV} (MPa)	P_{CJ} (MPa)	P_{CJref} (MPa)	U_{CJ} (m/s)	Δ_{CJ} (mm)
100	60	26.67	13.33	0.77	1.49	3.60	1904.3	0.304
150	60	60.00	30.00	1.32	2.57	6.28	2199.6	0.075
200	60	93.33	46.67	1.83	3.58	8.77	2351.2	0.046
250	60	126.67	63.33	2.34	4.58	11.24	2450.4	0.036
300	60	160.00	80.00	2.85	5.58	13.71	2521.5	0.031
350	60	193.33	96.67	3.37	6.59	16.19	2575.5	0.027

Table 5: Mixture C: hydrogen-oxygen-nitrogen-helium.

P_0 (kPa)	P_{N_2} (kPa)	P_{He} (kPa)	P_{H_2} (kPa)	P_{O_2} (kPa)	P_{CV} (MPa)	P_{CJ} (MPa)	P_{CJref} (MPa)	U_{CJ} (m/s)	Δ_{CJ} (mm)
100	16	60	16.00	8.00	0.74	1.45	3.46	2860.4	0.277
150	16	60	49.33	24.67	1.38	2.69	6.57	2997.6	0.051
200	16	60	82.67	41.33	1.91	3.73	9.14	2995.7	0.030
250	16	60	116.00	58.00	2.43	4.75	11.67	3000.1	0.022
300	16	60	149.33	74.67	2.94	5.76	14.16	2985.8	0.019
350	16	60	182.67	91.33	3.46	6.78	16.67	2983.2	0.017

B Shot list: 0.44 in gap (1.3% dead volume).

Table 6: Planar fixture with a gap of 0.44 in (1.3% dead volume). for $2H_2$-O_2 at room temperature.

shot	P_0 (bar)	P_{CV} (MPa)	P_{CJ} (MPa)	P_{CJref} (MPa)	$P_{1,max}$ (MPa)	$P_{2,max}$ (MPa)	$P_{3,max}$ (MPa)	$P_{4,max}$ (MPa)	DDT location
mixture A									
1	1.0	0.956	1.872	4.602	0.580	0.456	0.488	0.662	slow flame
3	1.2	1.154	2.260	5.560	0.868	0.780	0.742	0.927	slow flame
4	1.25	1.204	2.358	5.800	2.130	1.525	1.929	4.404	P4
2	1.3	1.254	2.456	6.041	2.966	2.098	2.540	8.011	P4
5	1.5	1.454	2.848	7.006	2.946	2.609	2.900	11.721	P4
6	2.0	1.958	3.836	9.441	4.470	3.748	5.225	11.919	P4
10	2.25	2.212	4.333	10.666	5.46	3.050	4.058	11.191	P4
11	2.4	2.364	4.632	11.402	4.186	3.092	8.685	8.807	P3
7	2.5	2.466	4.832	11.895	5.036	6.957	7.930	8.012	P2
8	3.0	2.978	5.834	14.364	8.346	8.696	6.481	6.622	P1
9	3.5	3.492	6.841	16.842	5.272	14.127	9.859	11.919	P2*
mixture B									
12	1.0	0.766	1.491	3.599	0.411	0.393	0.412	0.463	slow flame
13	1.5	1.316	2.569	6.278	1.573	0.966	1.160	1.258	slow flame
14	2.0	1.831	3.578	8.768	1.995	1.753	1.785	16.748	slow flame
19	2.1	1.933	3.778	9.263	3.964	2.616	3.220	9.438	P4
18	2.25	2.086	4.078	10.004	4.409	3.396	3.700	19.005	P4
15	2.5	2.341	4.579	11.239	4.436	3.623	5.019	16.953	P4
16	3.0	2.853	5.582	13.712	5.730	4.755	4.600	13.509	P4
17	3.5	3.366	6.589	16.194	7.708	4.914	6.440	19.472	P4
mixture C									
20	1.0	0.742	1.453	3.456	0.378	0.331	0.391	0.397	slow flame
21	1.5	1.375	2.690	6.573	0.755	0.683	0.776	0.795	slow flame
22	2.0	1.905	3.729	9.144	1.888	1.705	1.771	1.987	slow flame
23	2.5	2.426	4.752	11.669	2.933	2.347	2.430	2.980	slow flame
26	2.75	2.682	5.254	12.908	5.629	4.244	4.463	19.070	P4
24	3.0	2.941	5.762	14.160	6.404	4.217	5.698	18.607	P4
25	3.5	3.459	6.777	16.666	7.611	4.507	6.309	16.224	P4

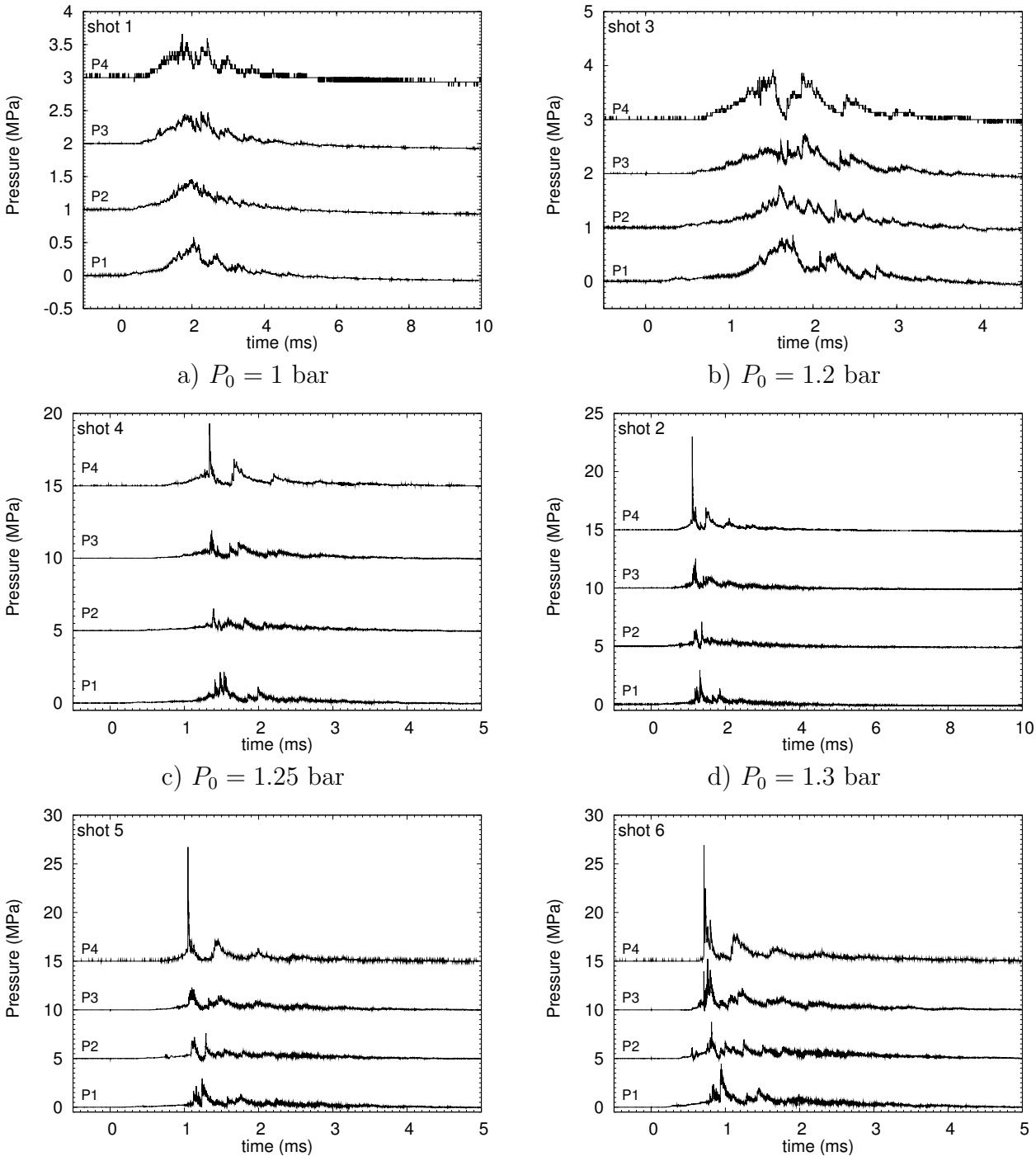

a) $P_0 = 1$ bar

b) $P_0 = 1.2$ bar

c) $P_0 = 1.25$ bar

d) $P_0 = 1.3$ bar

e) $P_0 = 1.5$ bar

f) $P_0 = 2.0$ bar

Figure 11: Pressure traces for $2H_2$-O_2 mixture with 0.44 in gap (1.3% dead volume).

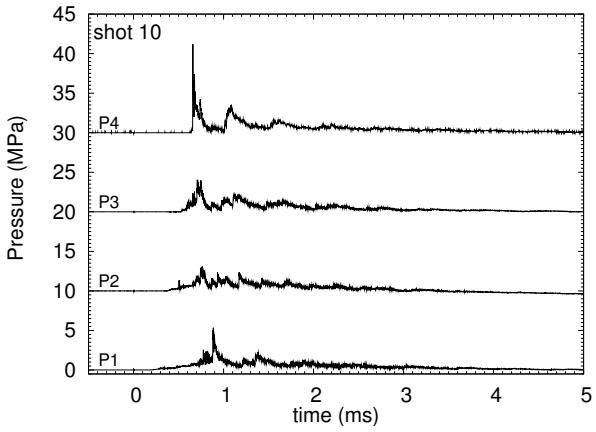

a) $P_0 = 2.25$ bar

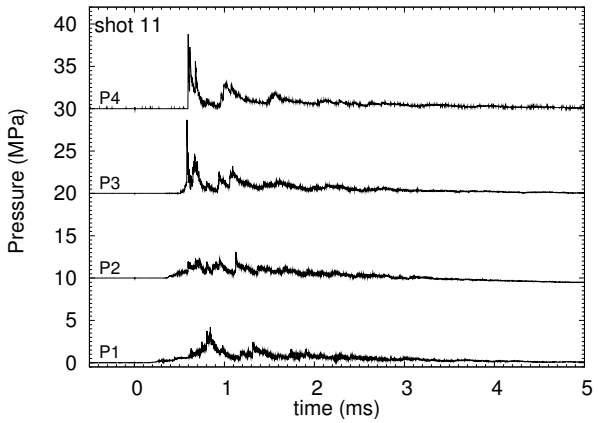

b) $P_0 = 2.4$ bar

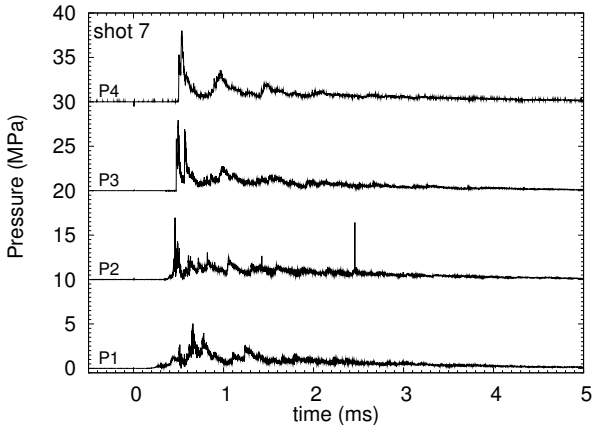

c) $P_0 = 2.5$ bar

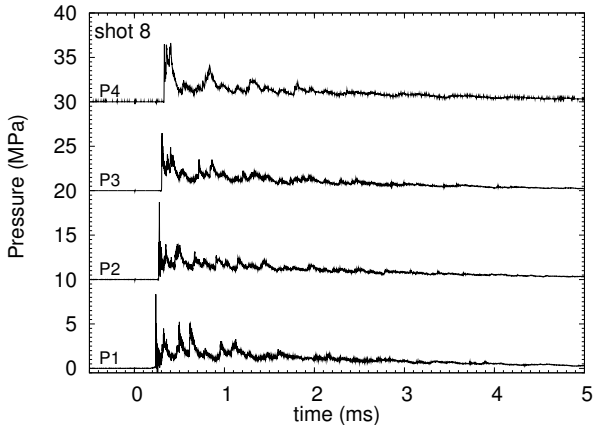

d) $P_0 = 3.0$ bar

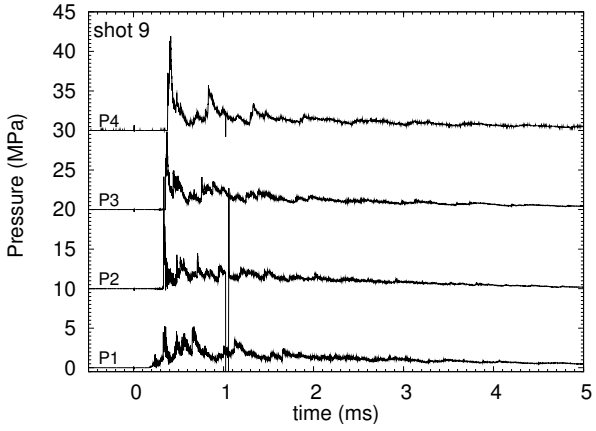

e) $P_0 = 3.5$ bar

Figure 12: Pressure traces for $2H_2$-O_2 mixture with 0.44 in gap (1.3% dead volume).

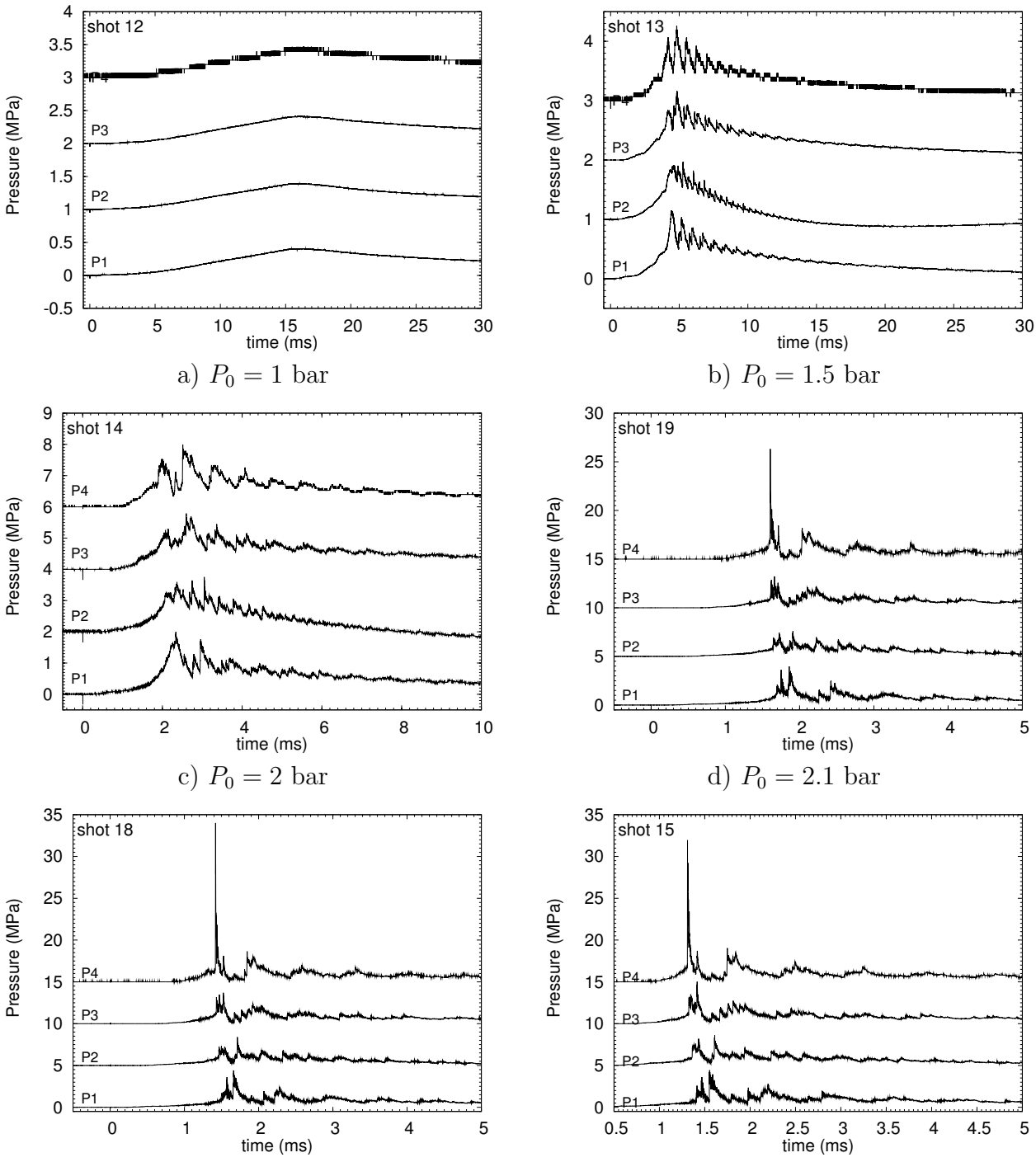

Figure 13: Pressure traces for $2H_2$-O_2-N_2 mixture with 0.44 in gap (1.3% dead volume).

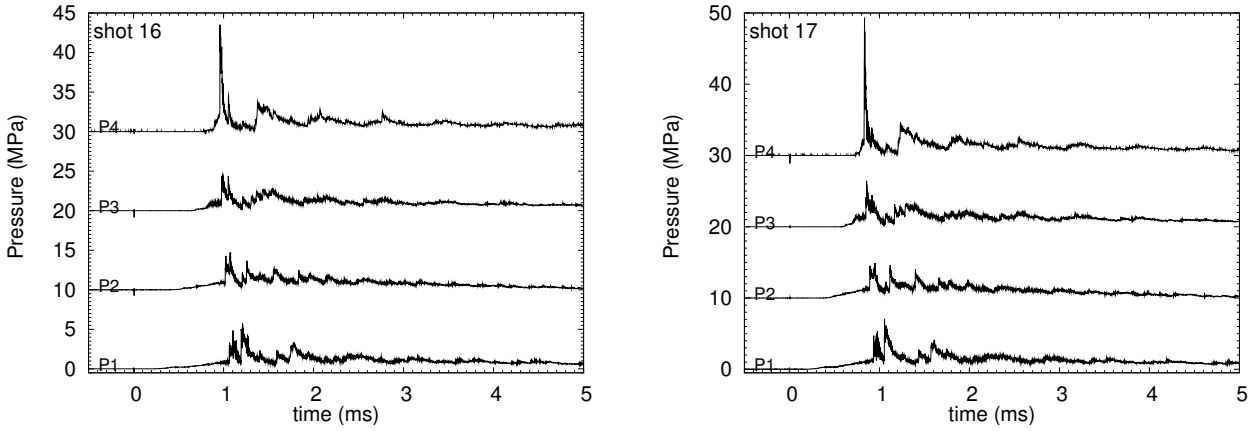

a) $P_0 = 3.0$ bar b) $P_0 = 3.5$ bar

Figure 14: Pressure traces for $2H_2$-O_2-N_2 mixture with 0.44 in gap (1.3% dead volume).

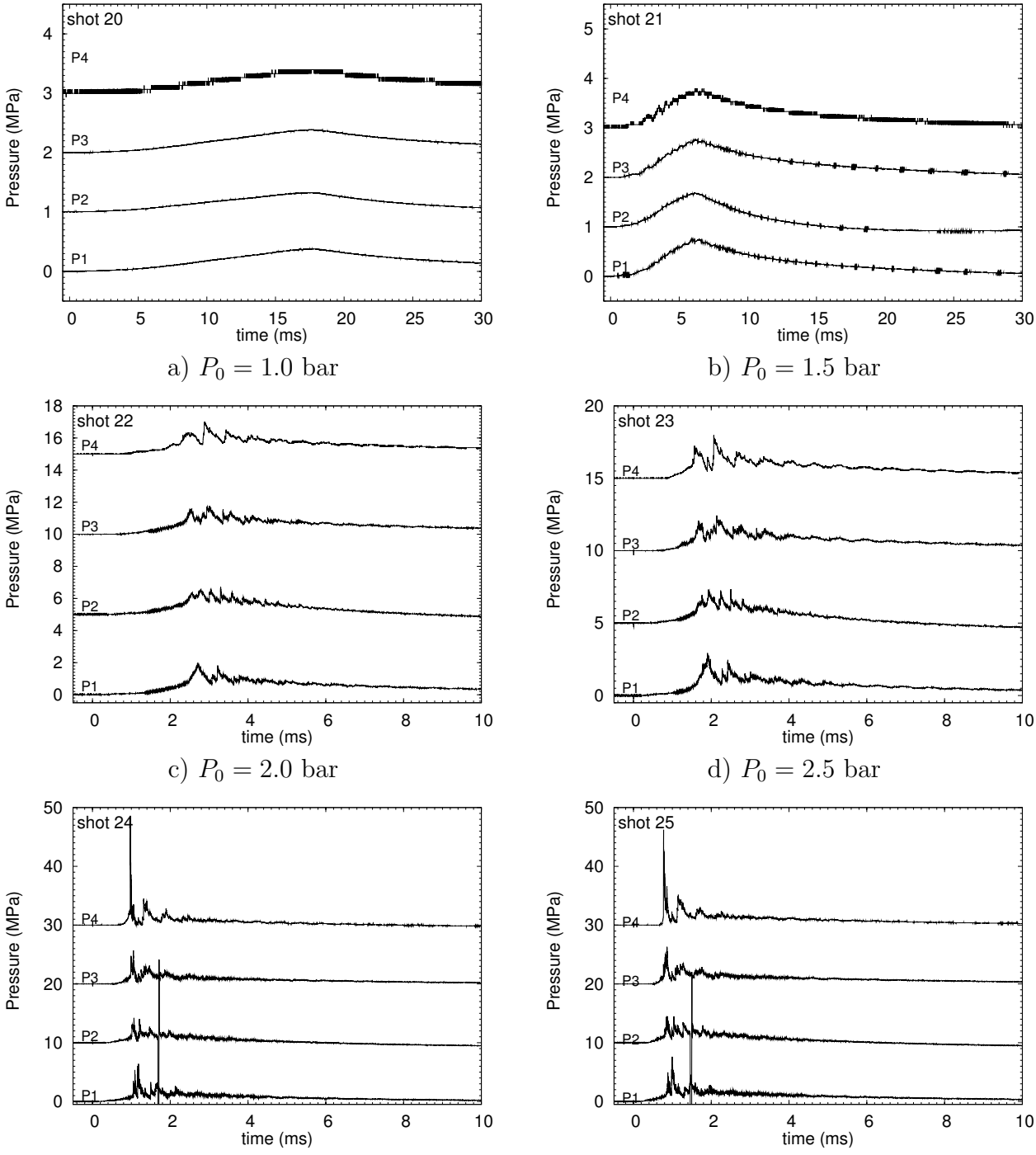

a) $P_0 = 1.0$ bar

b) $P_0 = 1.5$ bar

c) $P_0 = 2.0$ bar

d) $P_0 = 2.5$ bar

e) $P_0 = 3.0$ bar

f) $P_0 = 3.5$ bar

Figure 15: Pressure traces for $2H_2$-O_2-N_2-He mixture with 0.44 in gap (1.3% dead volume).

C Shot list: 0.10 in gap (5.5% dead volume).

Table 7: Planar fixture with a gap of 0.10 in (5.5% dead volume) for $2H_2$-O_2 at room temperature.

shot	P_0 (bar)	P_{CV} (MPa)	P_{CJ} (MPa)	P_{CJref} (MPa)	$P_{1,max}$ (MPa)	$P_{2,max}$ (MPa)	$P_{3,max}$ (MPa)	$P_{4,max}$ (MPa)	DDT location
mixture A									
28	1.0	0.956	1.872	4.602	0.998	1.373	1.888	2.715	P3
32	1.25	1.204	2.358	5.800	2.083	1.663	1.867	3.311	P2
29	1.5	1.454	2.848	7.006	4.304	2.208	3.021	4.503	P1
30	2.0	1.958	3.836	9.441	5.238	3.451	5.444	5.960	P1
31	2.5	2.466	4.832	11.895	8.225	4.776	7.504	7.946	P1
27	3.0	2.978	5.834	14.364	8.892	9.013	9.035	5.222	P1
mixture B									
33	1.0	0.766	1.491	3.599	0.034	0.034	0.034	0.0660	slow flame
34	1.5	1.316	2.569	6.278	0.472	0.435	0.419	0.530	slow flame
39	1.75	1.575	3.075	7.529	1.227	1.505	4.504	9.138	P4
35	2.0	1.831	3.578	8.768	1.564	2.353	6.158	8.410	P4
36	2.5	2.341	4.579	11.239	3.559	5.266	8.912	7.681	P3
37	3.0	2.853	5.582	13.712	5.218	6.018	8.239	9.271	P2
38	3.5	3.366	6.589	16.194	6.290	6.929	9.845	10.462	P2
mixture C									
40	1.0	0.742	1.453	3.456	0.020	0.014	0.014	0.066	slow flame
41	1.5	1.375	2.690	6.573	0.337	0.311	0.302	0.331	slow flame
42	2.0	1.905	3.729	9.144	1.409	1.201	1.861	2.185	slow flame
45	2.25	2.165	4.239	10.402	2.710	2.954	14.054	9.602	P3
43	2.5	2.426	4.752	11.669	2.330	2.740	6.288	14.436	P3
44	3.0	2.941	5.762	14.160	6.155	5.431	8.823	9.469	P2

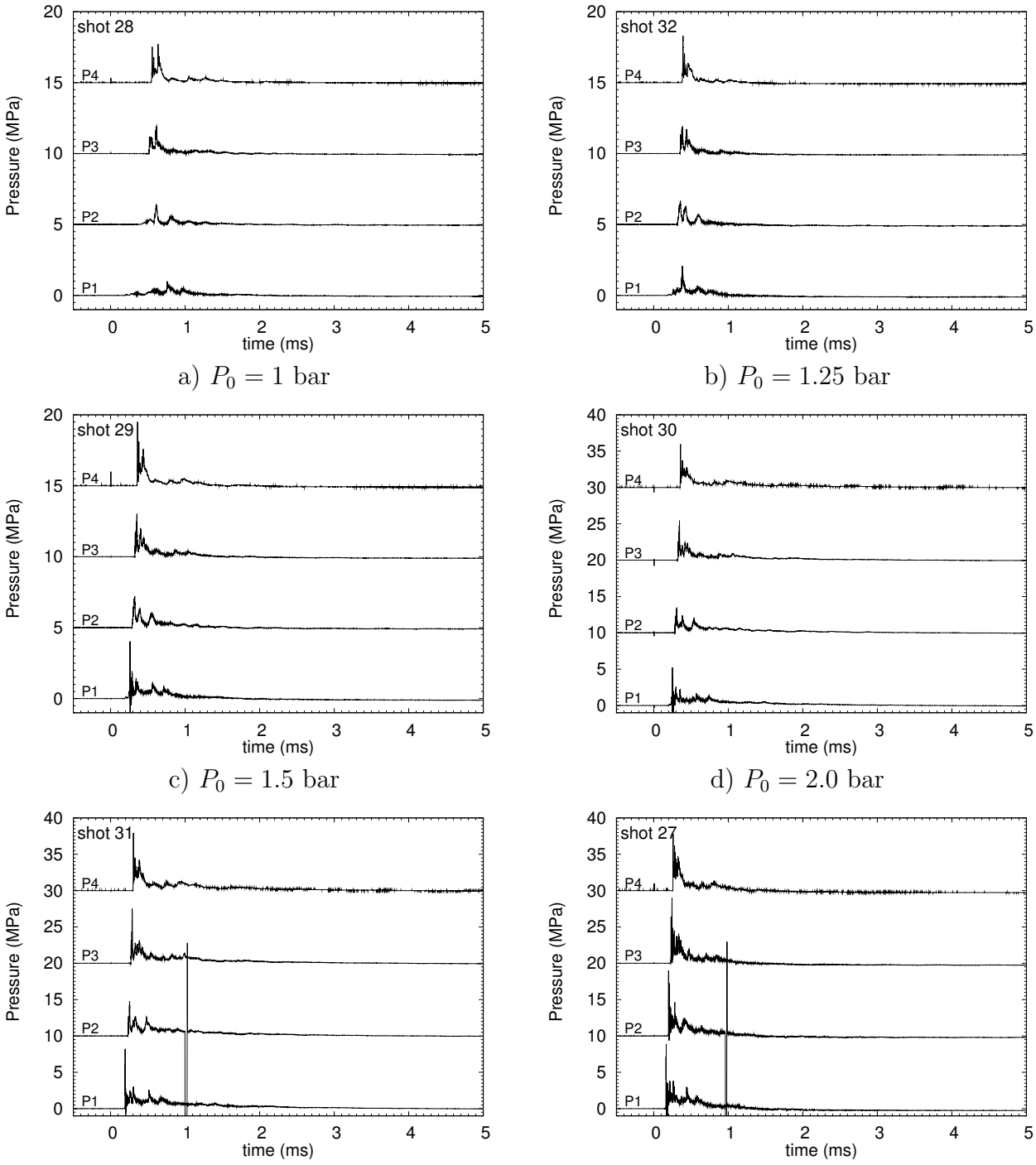

a) $P_0 = 1$ bar

b) $P_0 = 1.25$ bar

c) $P_0 = 1.5$ bar

d) $P_0 = 2.0$ bar

e) $P_0 = 2.5$ bar

f) $P_0 = 3.0$ bar

Figure 16: Pressure traces for $2H_2$-O_2 mixture with 0.1 in gap (5.5% dead volume).

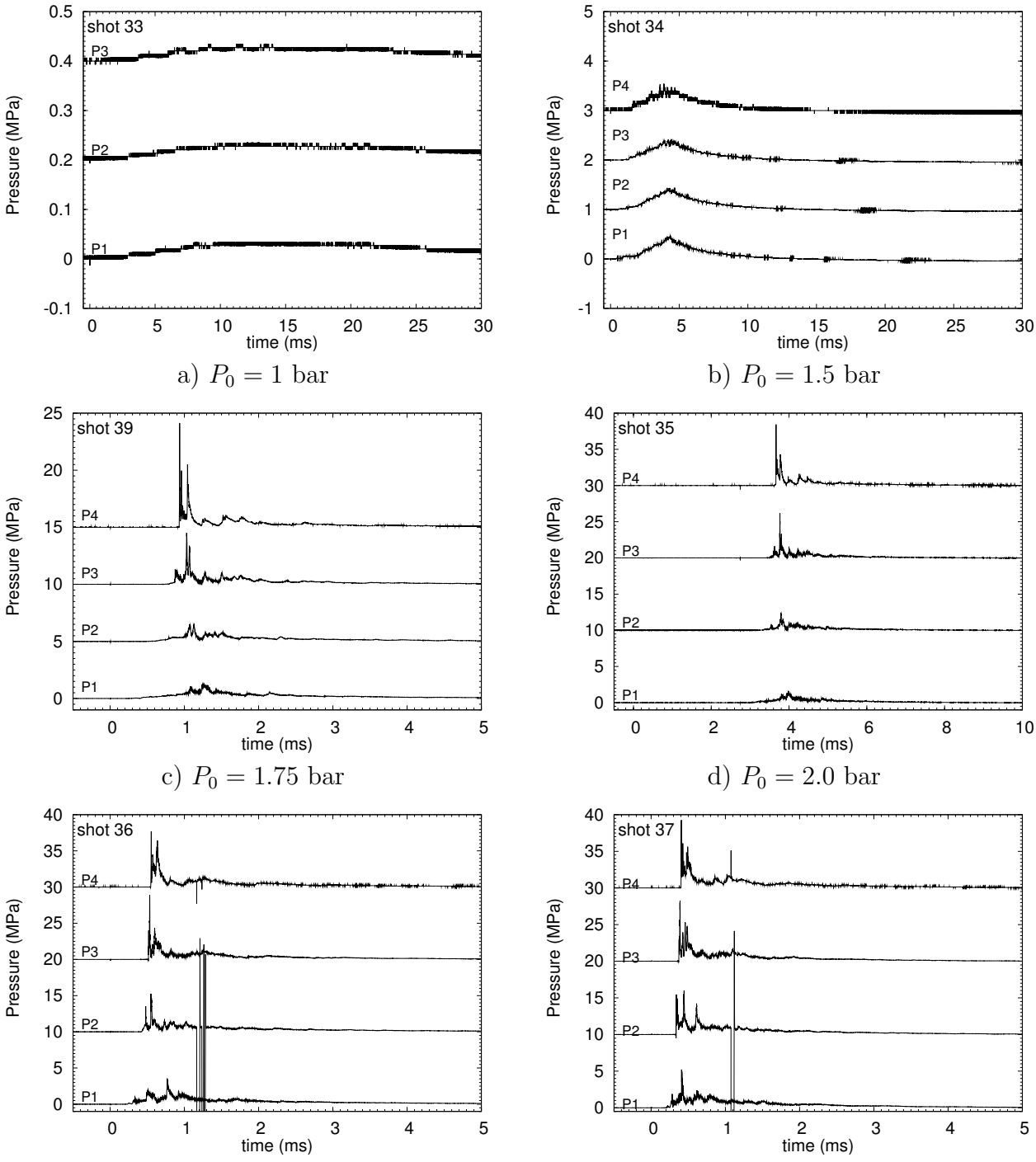

a) $P_0 = 1$ bar

b) $P_0 = 1.5$ bar

c) $P_0 = 1.75$ bar

d) $P_0 = 2.0$ bar

e) $P_0 = 2.5$ bar

f) $P_0 = 3.0$ bar

Figure 17: Pressure traces for $2H_2$-O_2-N_2 mixture with 0.1 in gap (5.5% dead volume).

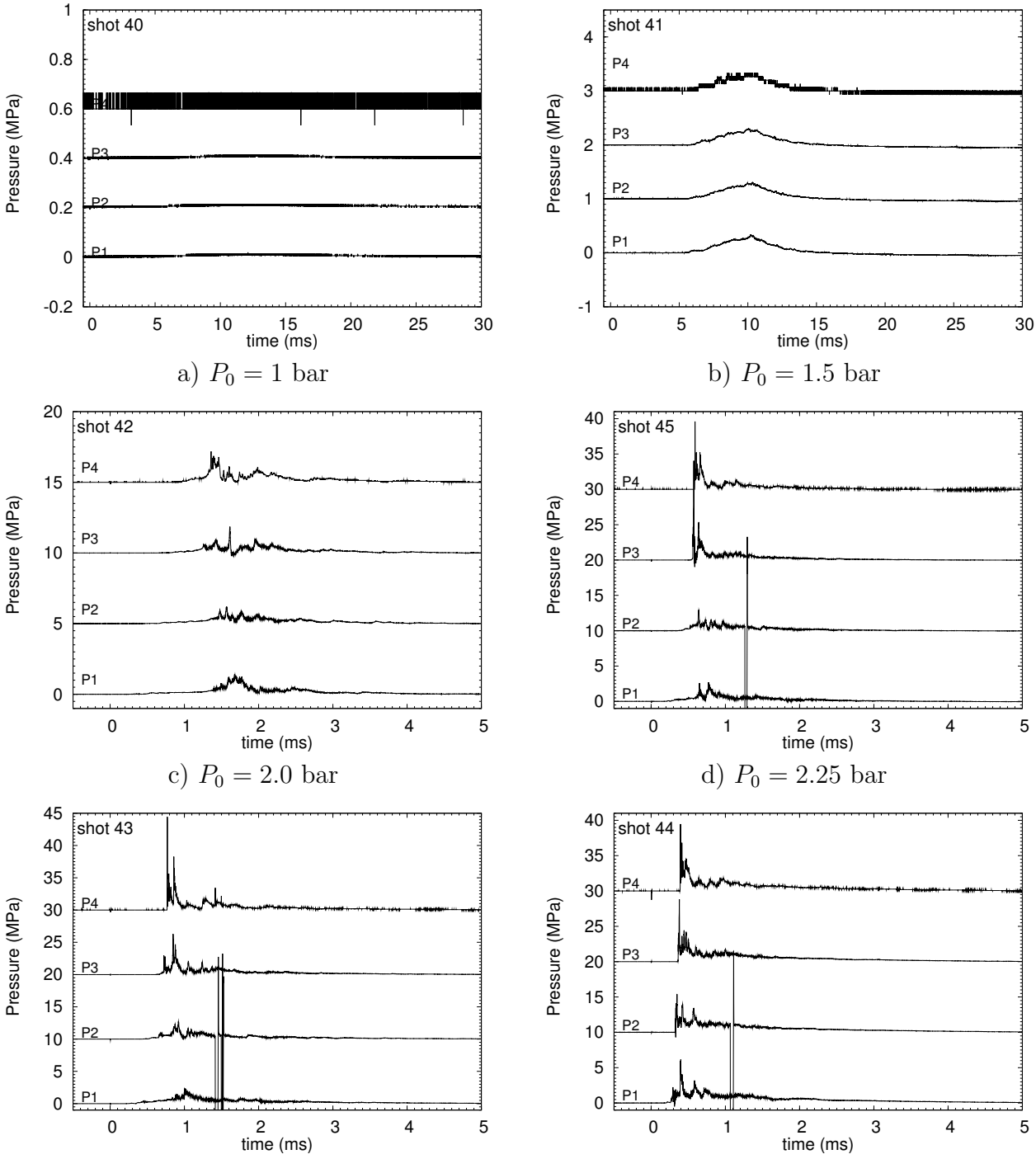

a) $P_0 = 1$ bar

b) $P_0 = 1.5$ bar

c) $P_0 = 2.0$ bar

d) $P_0 = 2.25$ bar

e) $P_0 = 2.5$ bar

f) $P_0 = 3.0$ bar

Figure 18: Pressure traces for $2H_2$-O_2-N_2-He mixture with 0.1 in gap (5.5% dead volume).

D Shot list: 0.05 in gap (10% dead volume)

Table 8: Planar fixture with a gap of 0.05 in (10% dead volume) for $2H_2$-O_2 at room temperature.

shot	P_0 (bar)	P_{CV} (MPa)	P_{CJ} (MPa)	P_{CJref} (MPa)	$P_{1,max}$ (MPa)	$P_{2,max}$ (MPa)	$P_{3,max}$ (MPa)	$P_{4,max}$ (MPa)	DDT location
mixture A									
47	1.0	0.956	1.872	4.602	3.325	0.842	1.037	2.583	P1
48	1.5	1.454	2.848	7.006	3.465	2.491	1.579	2.781	P1
49	2.0	1.958	3.836	9.441	6.337	3.796	2.746	3.841	P1
50	2.5	2.466	4.832	11.895	4.989	5.024	4.058	5.629	P1
46	3.0	2.978	5.834	14.364	7.025	5.756	5.149	7.549	P1
mixture B									
51	1.0	0.766	1.491	3.599	0.04	0.028	0.027	0.066	slow flame
62	1.25	1.052	2.051	4.994	0.432	0.221	0.563	7.562	P4
52	1.5	1.316	2.569	6.278	0.533	0.324	0.858	18.939	P4
63	1.75	1.575	3.075	7.529	1.261	2.588	3.762	8.145	P2
53	2.0	1.831	3.578	8.768	1.247	6.701	3.117	6.556	P2
54	2.5	2.341	4.579	11.239	4.261	4.320	4.572	7.483	P1
55	3.0	2.853	5.582	13.712	7.065	6.177	6.715	9.138	P1
mixture C									
56	1.0	0.742	1.453	3.456	–	–	–	–	no ignition
57	1.5	1.375	2.690	6.573	0.074	0.055	0.075	0.199	slow flame
61	1.75	1.643	3.215	7.873	1.429	3.030	3.062	4.900	P2
58	2.0	1.905	3.729	9.144	1.409	1.201	1.861	2.185	P2
59	2.5	2.426	4.752	11.669	3.054	5.383	3.982	5.033	P1
60	3.0	2.941	5.762	14.160	13.712	7.309	6.145	7.615	P1

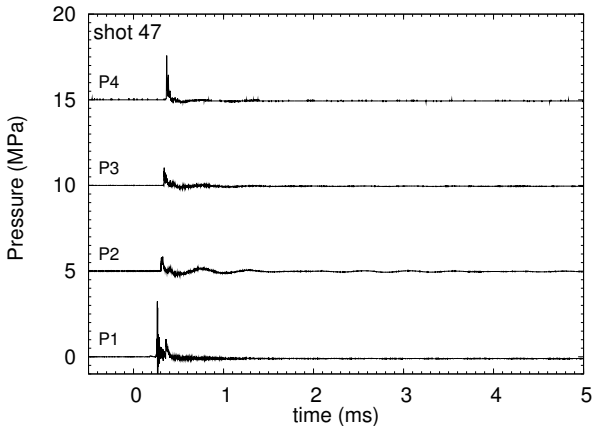

a) $P_0 = 1$ bar

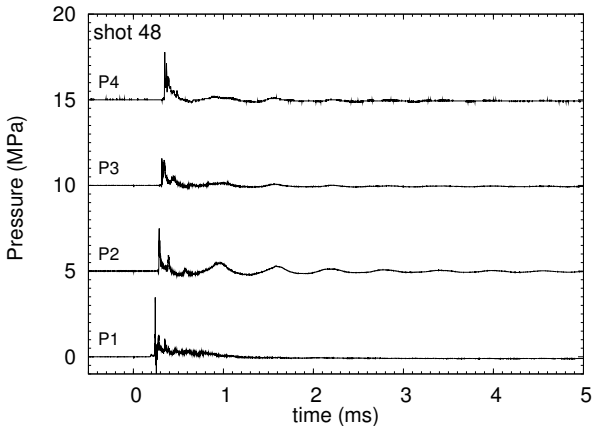

b) $P_0 = 1.5$ bar

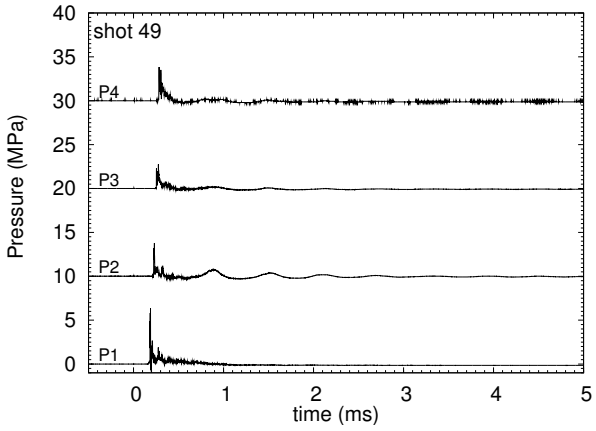

c) $P_0 = 2.0$ bar

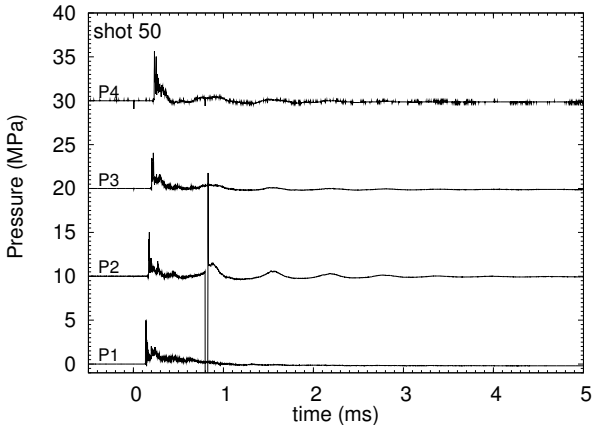

d) $P_0 = 2.5$ bar

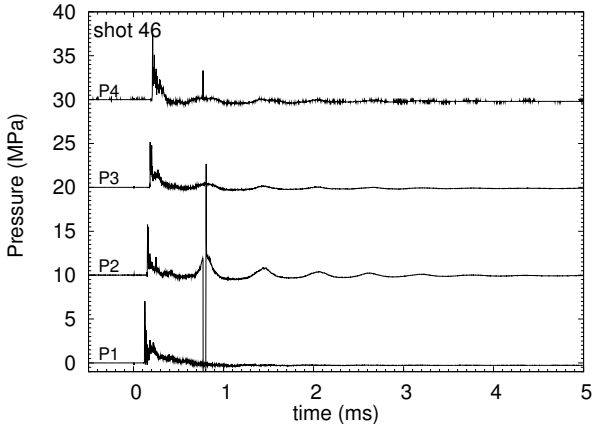

e) $P_0 = 3.0$ bar

Figure 19: Pressure traces for $2H_2$-O_2 mixture with 0.05 in gap (10% dead volume).

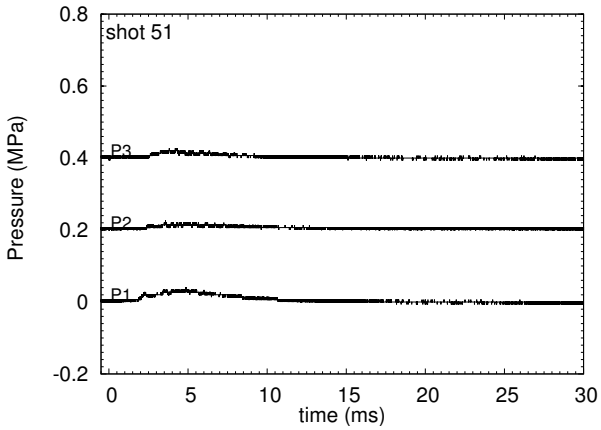

a) $P_0 = 1$ bar

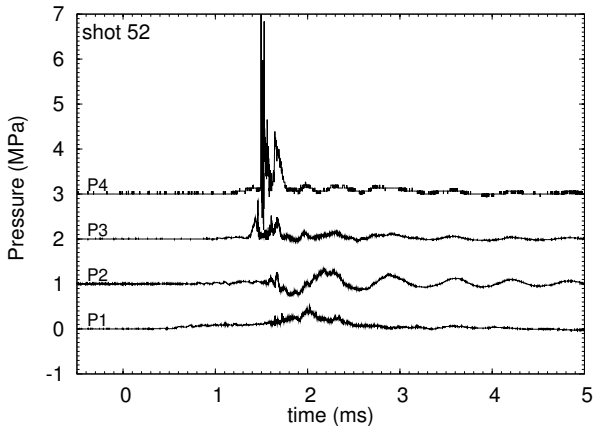

b) $P_0 = 1.5$ bar

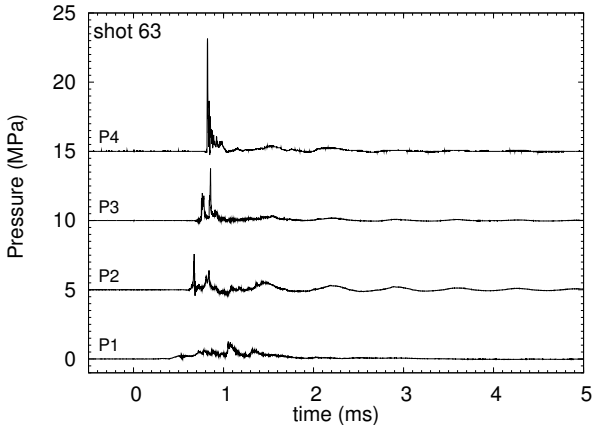

c) $P_0 = 1.75$ bar

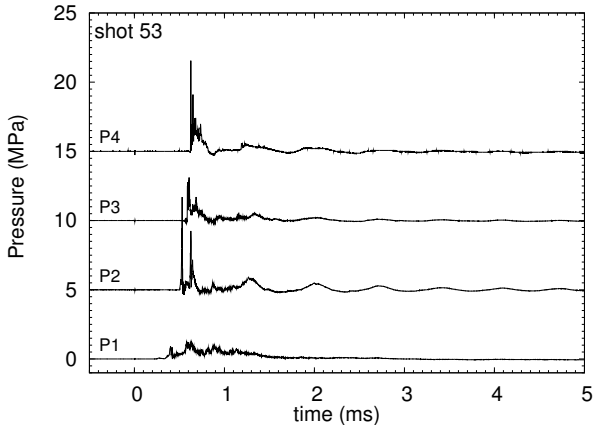

d) $P_0 = 2.0$ bar

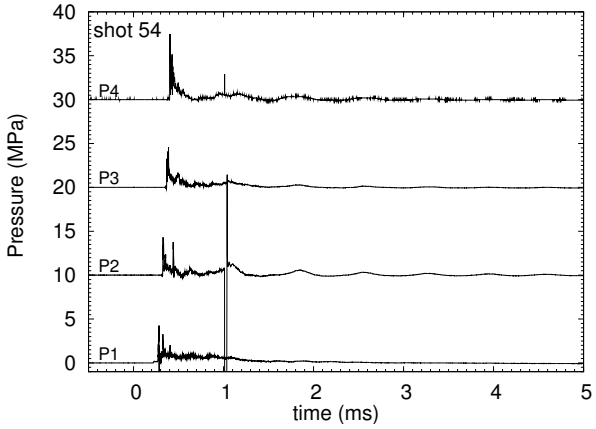

e) $P_0 = 2.5$ bar

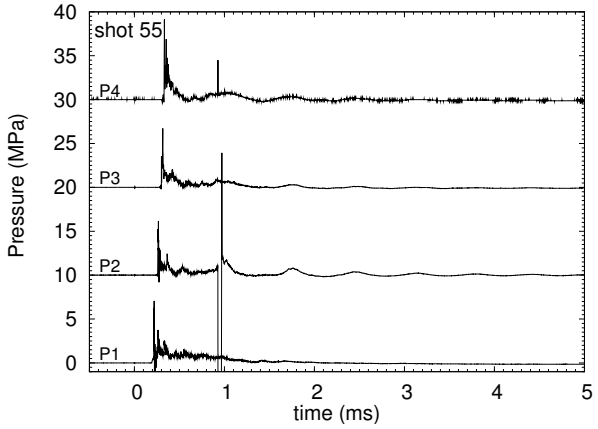

f) $P_0 = 3.0$ bar

Figure 20: Pressure traces for $2H_2$-O_2-N_2 mixture with 0.05 in gap (10% dead volume).

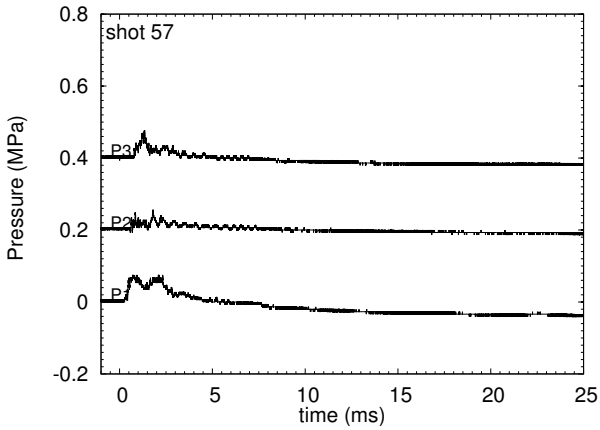

a) $P_0 = 1.5$ bar

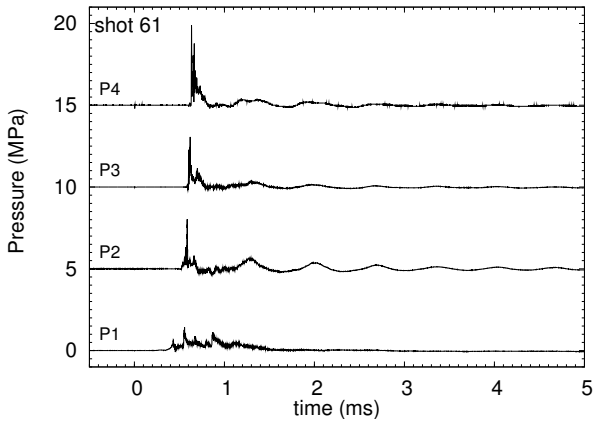

b) $P_0 = 1.75$ bar

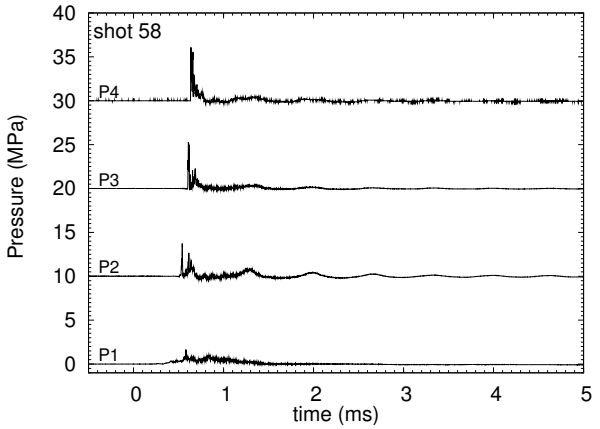

c) $P_0 = 2.0$ bar

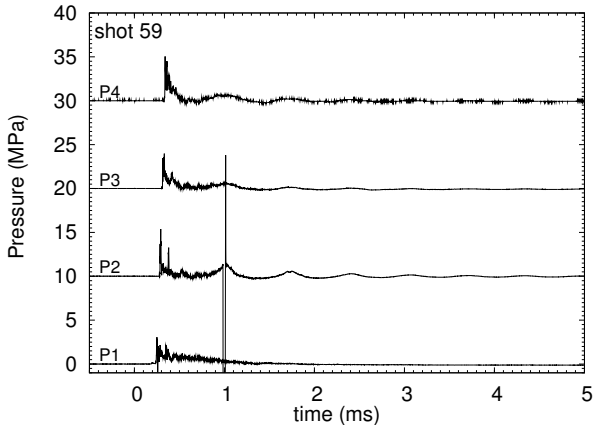

d) $P_0 = 2.5$ bar

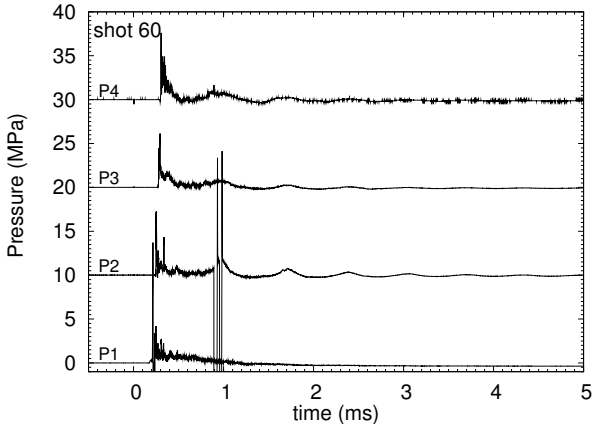

e) $P_0 = 3.0$ bar

Figure 21: Pressure traces for $2H_2$-O_2-N_2-He mixture with 0.05 in gap (10% dead volume).

E Shot list: 0.05 in gap (1% dead volume)

Table 9: Planar fixture with a gap of 0.05 in for $2H_2$-O_2 at room temperature.

shot	P_0 (bar)	P_{CV} (MPa)	P_{CJ} (MPa)	P_{CJref} (MPa)	$P_{1,max}$ (MPa)	$P_{2,max}$ (MPa)	$P_{3,max}$ (MPa)	$P_{4,max}$ (MPa)	DDT location
mixture A									
64	1.0	0.956	1.872	4.602	1.162	1.315	1.612	1.722	slow flame
71	1.0	0.956	1.872	4.602	0.629	0.473	0.834	1.072	slow flame
75	1.25	1.204	2.358	5.800	1.099	2.293	2.467	1.608	P2
65	1.5	1.454	2.848	7.006	0.636	1.835	2.553	2.384	P2
72	1.5	1.454	2.848	7.006	0.512	3.111	3.489	2.680	P2
66	2.0	1.958	3.836	9.441	3.457	5.235	2.956	2.979	P1
mixture B									
67	1.5	1.316	2.569	6.278	0.449	0.394	0.470	0.595	slow flame
68	1.75	1.575	3.075	7.529	1.162	2.111	3.829	4.238	P3
73	2.5	2.341	4.579	11.239	1.701	3.966	10.266	4.623	P2
76	3.0	2.853	5.582	13.712	2.088	5.709	7.367	6.767	P2
mixture C									
69	1.75	1.643	3.215	7.873	0.090	0.105	0.134	0.132	slow flame
70	2.0	1.905	3.729	9.144	1.251	1.723	2.620	6.291	P4
74	2.5	2.426	4.752	11.669	1.404	1.703	6.332	4.355	P3
77	3.0	2.941	5.762	14.160	2.088	9.261	6.144	5.495	P2

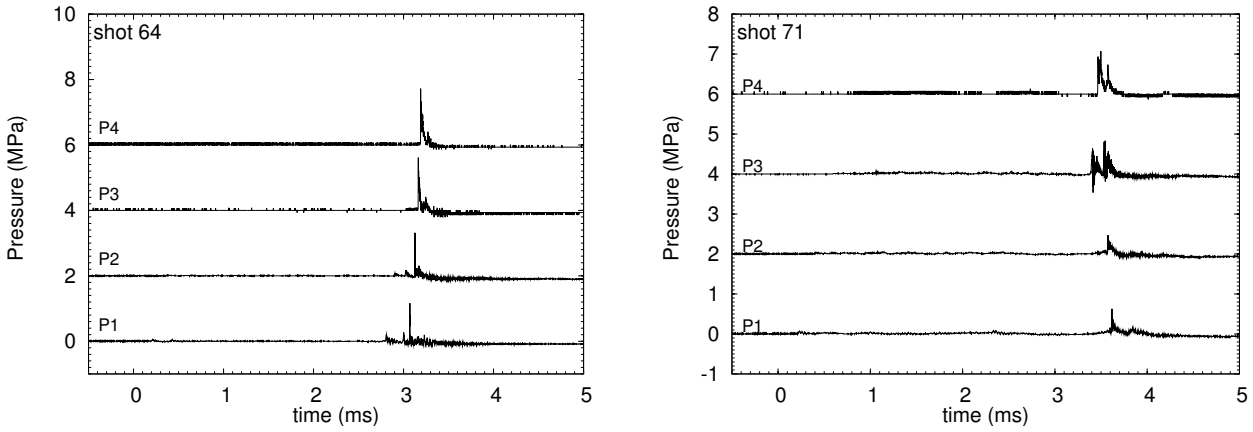

a) $P_0 = 1.0$ bar

b) $P_0 = 1.0$ bar

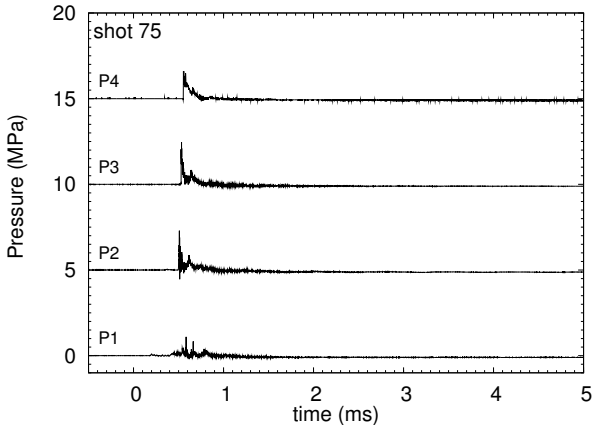

c) $P_0 = 1.25$ bar

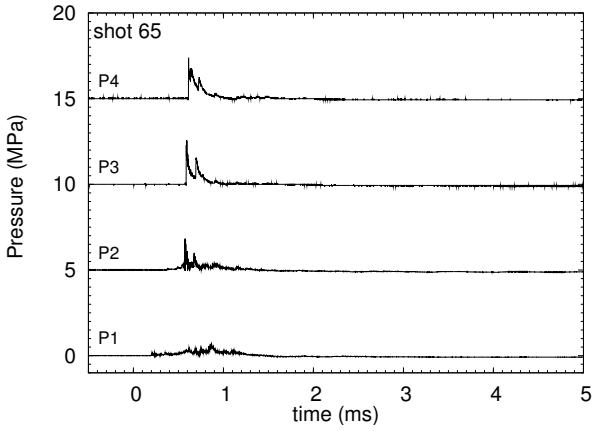

d) $P_0 = 1.5$ bar

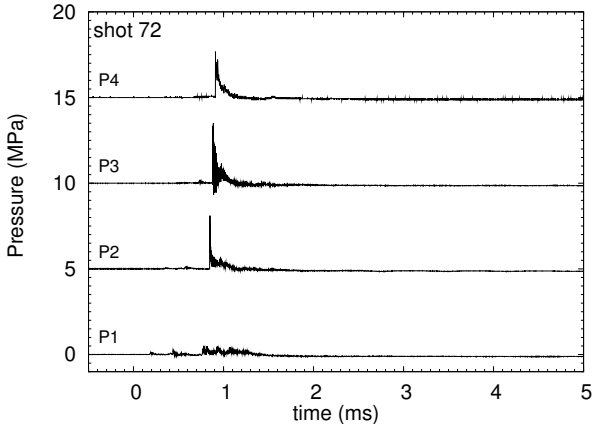

e) $P_0 = 1.5$ bar

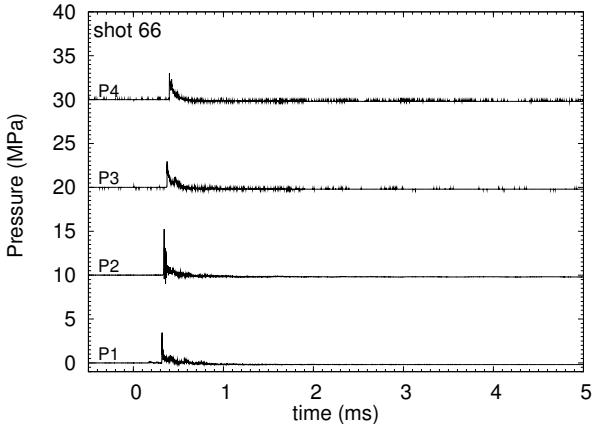

f) $P_0 = 2.0$ bar

Figure 22: Pressure traces for $2H_2$-O_2 mixture with 0.05 in gap (1% dead volume).

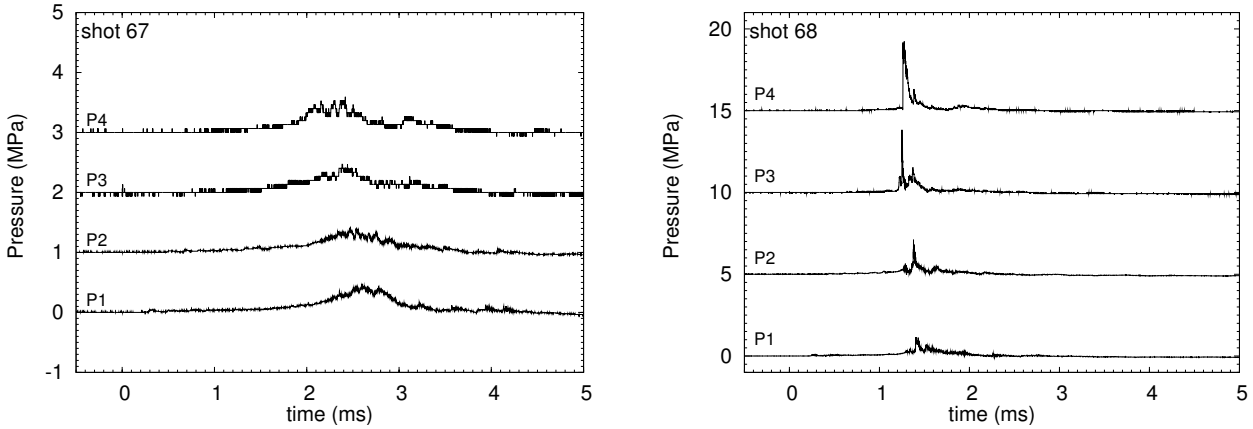

a) $P_0 = 1.5$ bar

b) $P_0 = 1.75$ bar

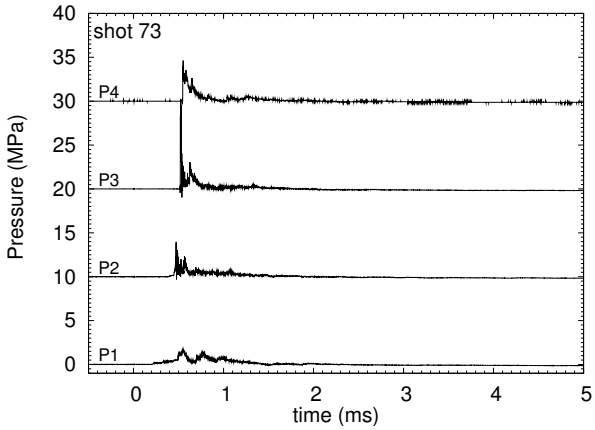

c) $P_0 = 2.5$ bar

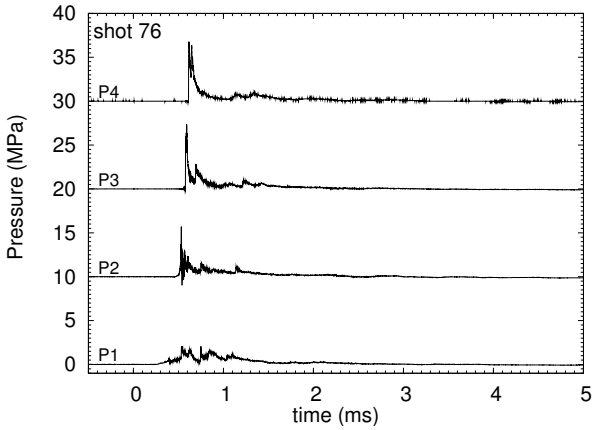

d) $P_0 = 3.0$ bar

Figure 23: Pressure traces for $2H_2$-O_2-N_2 mixture with 0.05 in gap (1% dead volume).

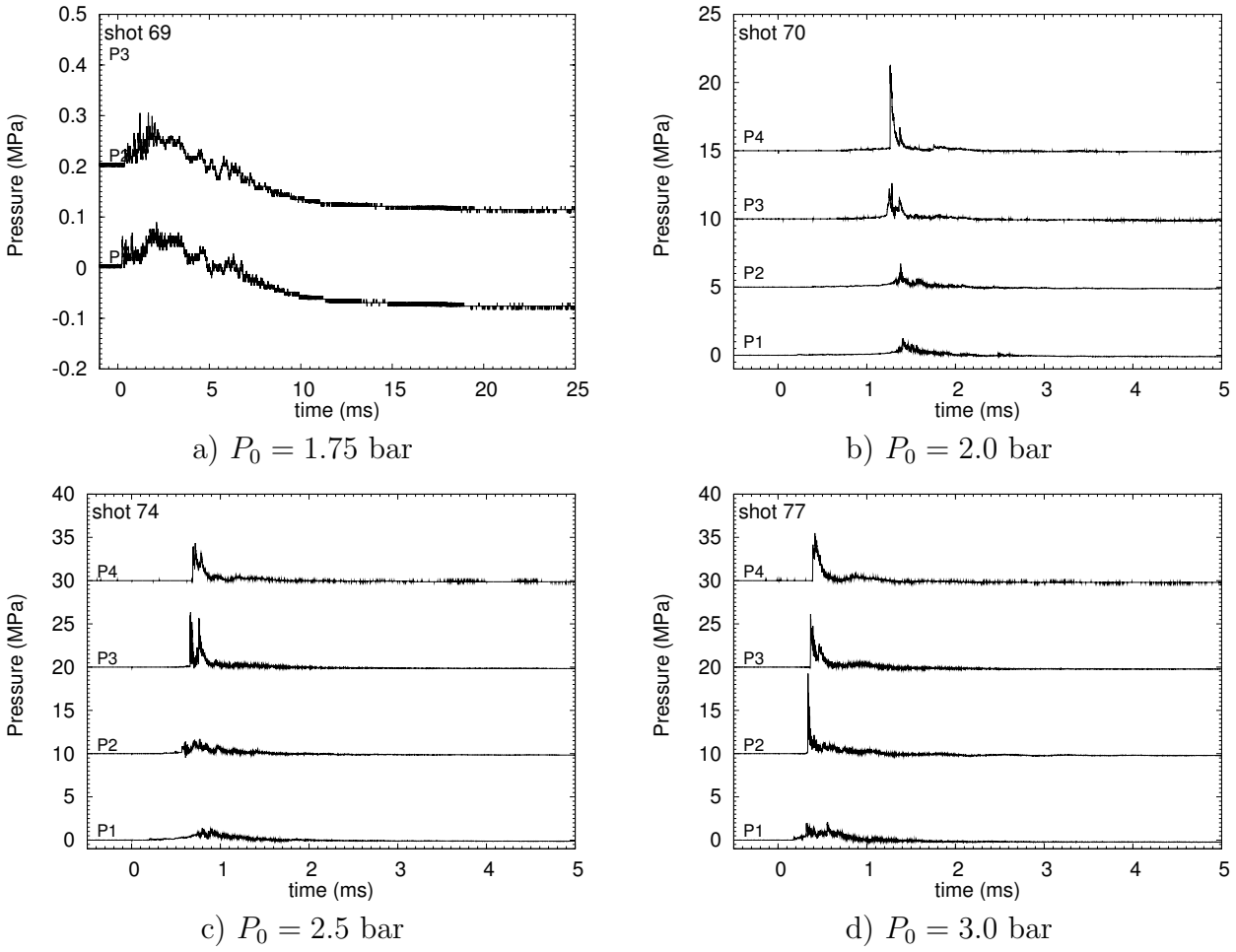

a) $P_0 = 1.75$ bar

b) $P_0 = 2.0$ bar

c) $P_0 = 2.5$ bar

d) $P_0 = 3.0$ bar

Figure 24: Pressure traces for $2H_2$-O_2-N_2-He mixture with 0.05 in gap (1% dead volume).

F Shot list: 0.02 in gap (3% dead volume)

Table 10: Planar fixture with a gap of 0.02 in (3% dead volume) for $2H_2$-O_2 at room temperature.

shot	P_0 (bar)	P_{CV} (MPa)	P_{CJ} (MPa)	P_{CJref} (MPa)	$P_{1,max}$ (MPa)	$P_{2,max}$ (MPa)	$P_{3,max}$ (MPa)	$P_{4,max}$ (MPa)	DDT location
mixture A									
83	0.8	0.759	1.485	3.651	–	–	–	–	slow flame
84	0.9	0.857	1.678	4.126	0.125	0.039	0.042	0.067	slow flame
82	1.0	0.956	1.872	4.602	2.938	1.105	1.981	1.407	P1
81	1.5	1.454	2.848	7.006	2.081	1.513	2.169	1.273	P1
80	2.0	1.958	3.836	9.441	3.284	2.697	4.205	2.010	P1
79	2.5	2.466	4.832	11.895	4.989	11.774	4.058	5.629	P1
78	3.0	2.978	5.834	14.364	7.025	12.678	5.149	7.549	P1
mixture B									
85	1.0	0.766	1.491	3.599	–	–	–	–	no ignition
86	1.5	1.316	2.569	6.278	0.339	0.355	0.591	2.112	slow flame
89	1.75	1.575	3.075	7.529	4.639	2.584	3.315	1.742	P1
87	2.0	1.831	3.578	8.768	5.995	2.348	5.032	2.345	P1
88	2.5	2.341	4.579	11.239	5.856	3.486	6.332	3.082	P1
mixture C									
90	1.75	1.643	3.215	7.873	0.131	0.046	0.034	0.067	slow flame
91	2.0	1.905	3.729	9.144	3.54	3.413	4.059	2.613	P1
92	2.5	2.426	4.752	11.669	7.993	3.025	5.477	2.412	P1

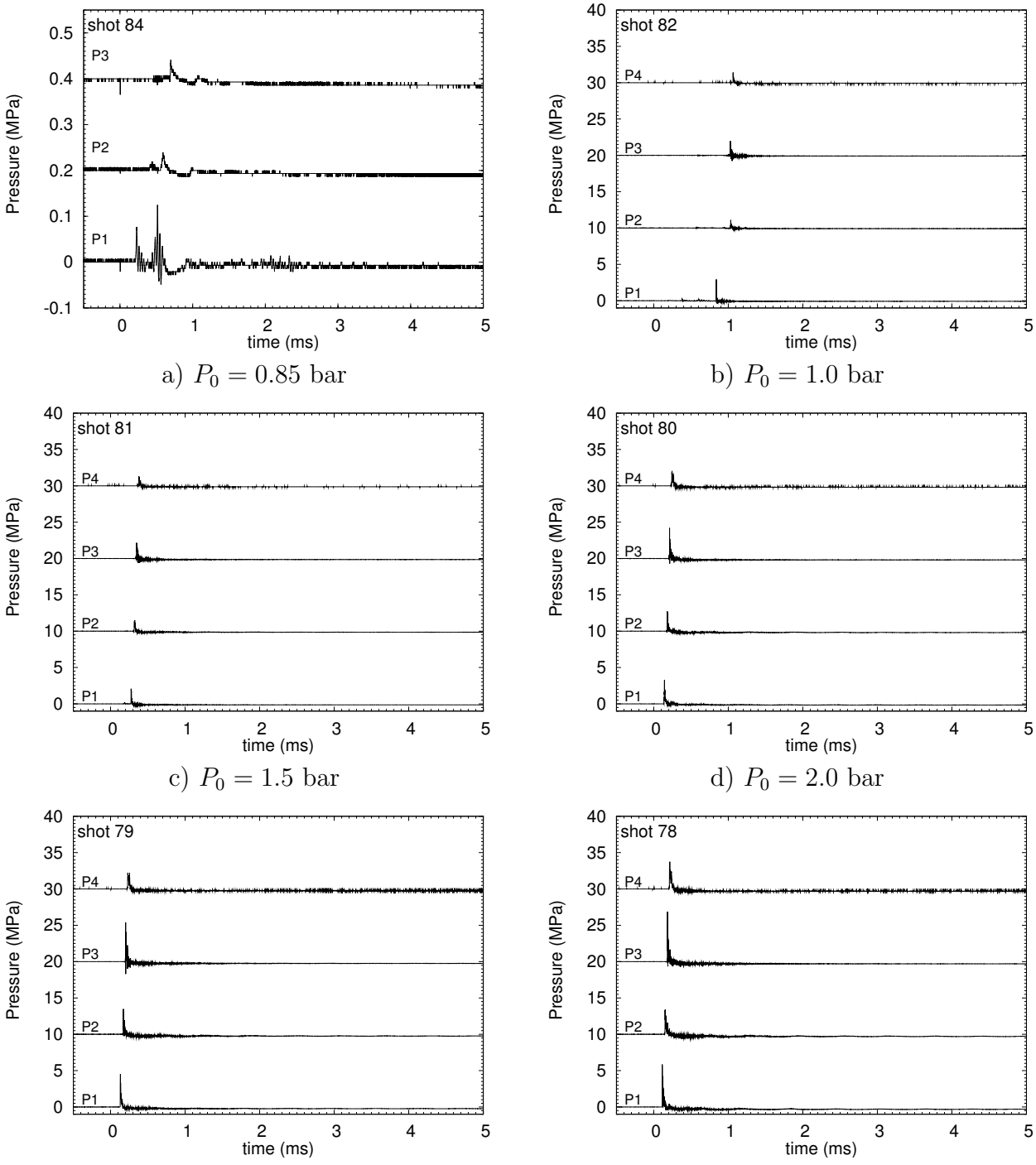

a) $P_0 = 0.85$ bar

b) $P_0 = 1.0$ bar

c) $P_0 = 1.5$ bar

d) $P_0 = 2.0$ bar

e) $P_0 = 2.5$ bar

f) $P_0 = 3.0$ bar

Figure 25: Pressure traces for $2H_2$-O_2 mixture with 0.02 in gap (3% dead volume).

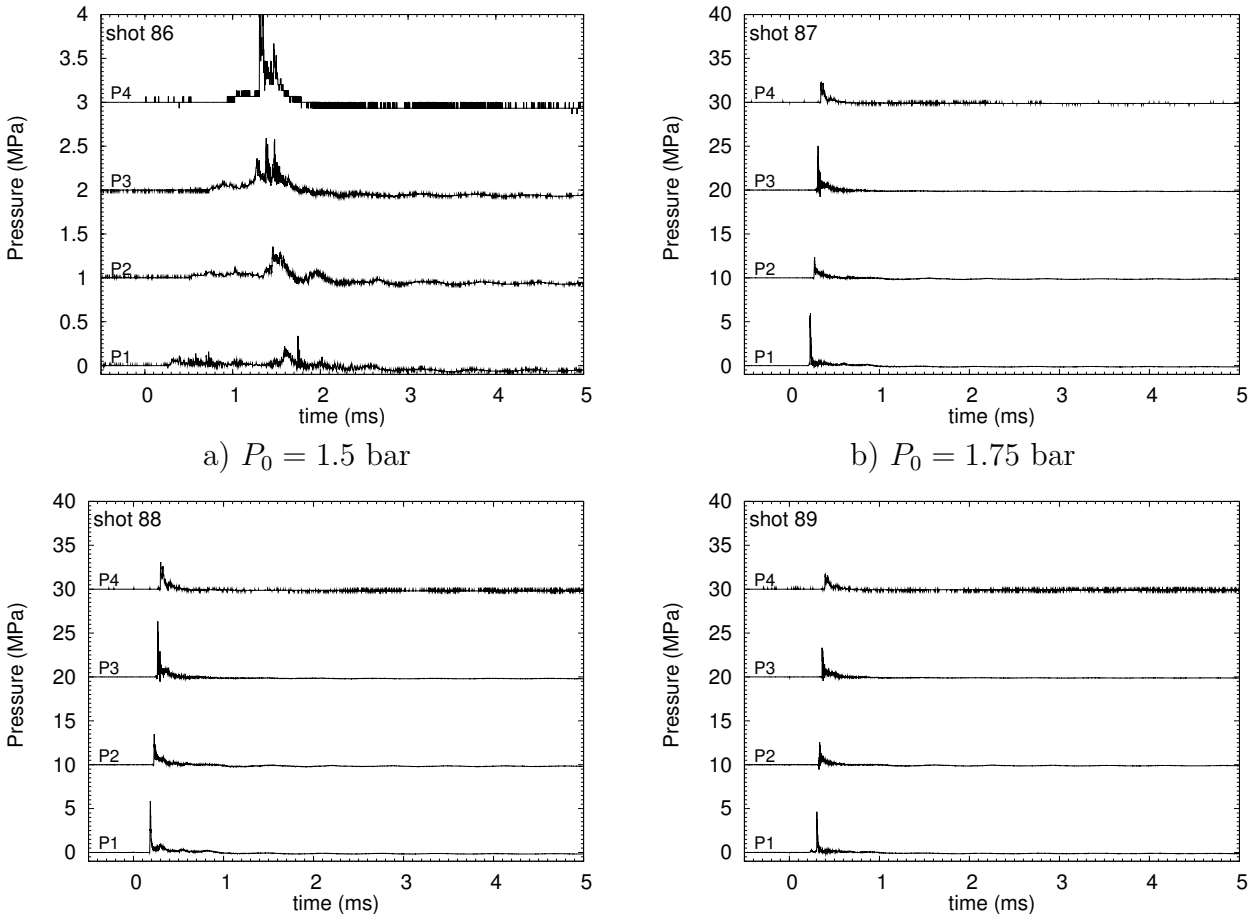

a) $P_0 = 1.5$ bar

b) $P_0 = 1.75$ bar

c) $P_0 = 2.0$ bar

d) $P_0 = 2.5$ bar

Figure 26: Pressure traces for $2H_2$-O_2-N_2 mixture with 0.02 in gap (3% dead volume).

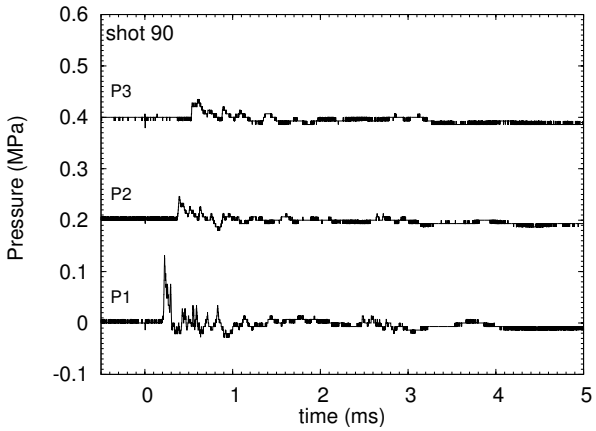

a) $P_0 = 1.75$ bar

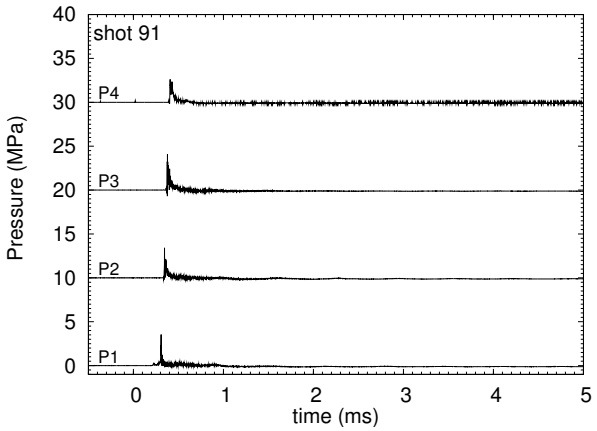

b) $P_0 = 2.0$ bar

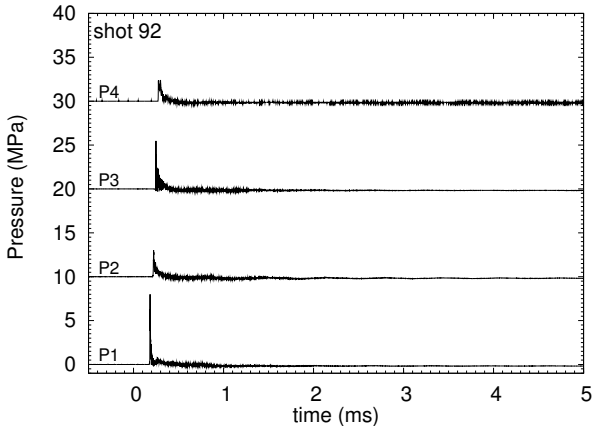

c) $P_0 = 2.5$ bar

Figure 27: Pressure traces for $2H_2$-O_2-N_2-He mixture with 0.02 in gap (3% dead volume).

G Shot list: 0.01 in gap (5% dead volume)

Table 11: Planar fixture with a gap of 0.01 in for $2H_2$-O_2 at room temperature.

shot	P_0 (bar)	P_{CV} (MPa)	P_{CJ} (MPa)	P_{CJref} (MPa)	$P_{1,max}$ (MPa)	$P_{2,max}$ (MPa)	$P_{3,max}$ (MPa)	$P_{4,max}$ (MPa)	DDT location
mixture A									
96	0.8	0.759	1.485	3.651	0.027	0.007	0.007	0.067	slow flame
95	1.0	0.956	1.872	4.602	1.901	1.039	0.764	0.804	P1
94	1.5	1.454	2.848	7.006	1.763	3.519	1.626	2.077	P1
93	2.0	1.958	3.836	9.441	3.215	2.802	2.954	2.211	P1
mixture B									
97	1.5	1.316	2.569	6.278	1.573	0.966	1.160	1.258	slow flame
99	1.75	1.575	3.075	7.529	3.803	2.683	1.661	1.474	P1
98	2.0	1.831	3.578	8.768	2.095	2.993	1.946	1.809	P1
mixture C									
100	1.75	1.643	3.215	7.873	0.111	0.053	0.028	0.067	slow flame
101	2.0	1.905	3.729	9.144	3.519	2.782	1.759	1.943	P1

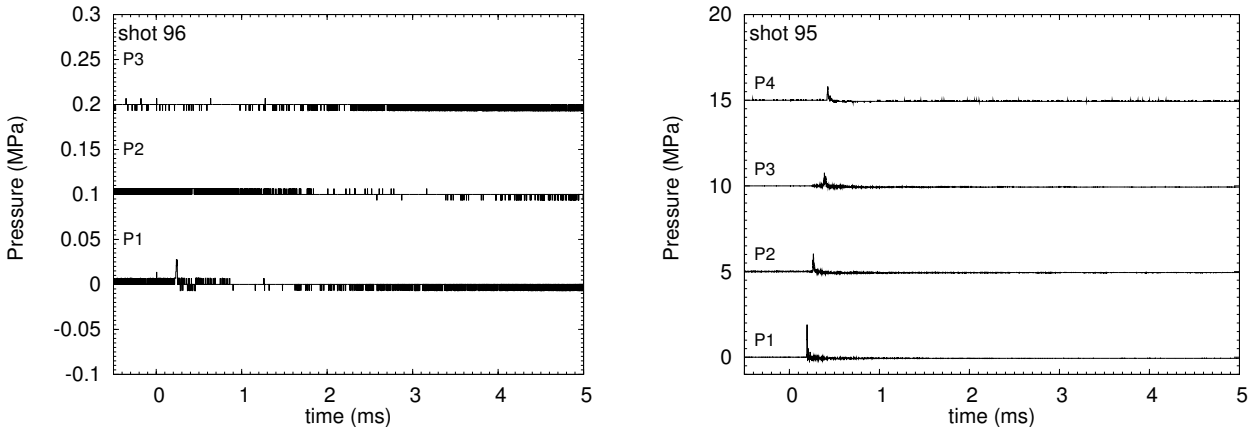

a) $P_0 = 0.8$ bar

b) $P_0 = 1.0$ bar

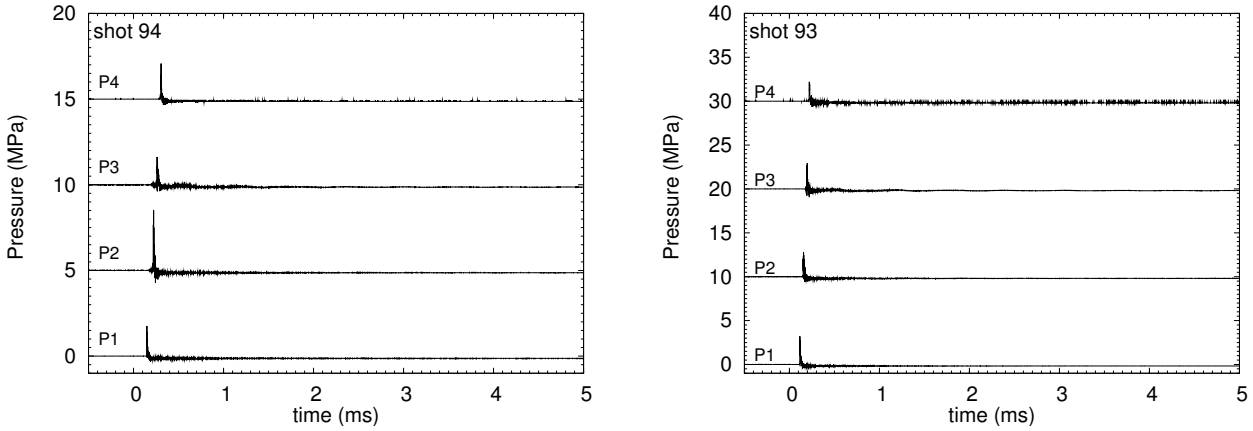

c) $P_0 = 1.5$ bar

d) $P_0 = 2.0$ bar

Figure 28: Pressure traces for $2H_2$-O_2 mixture with 0.01 in gap (5% dead volume).

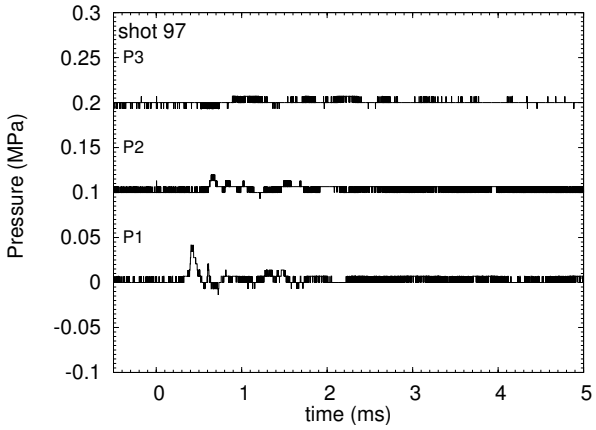

a) $P_0 = 1.5$ bar

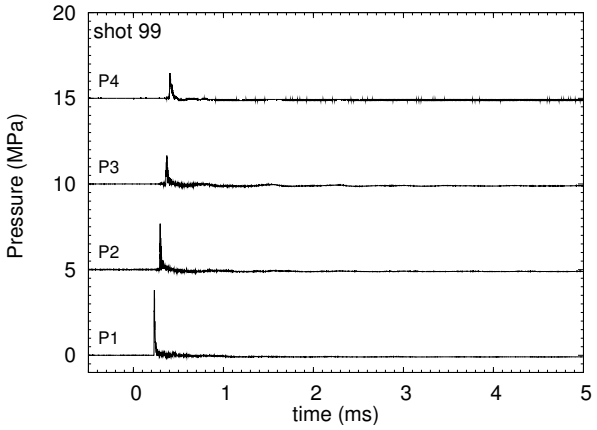

b) $P_0 = 1.75$ bar

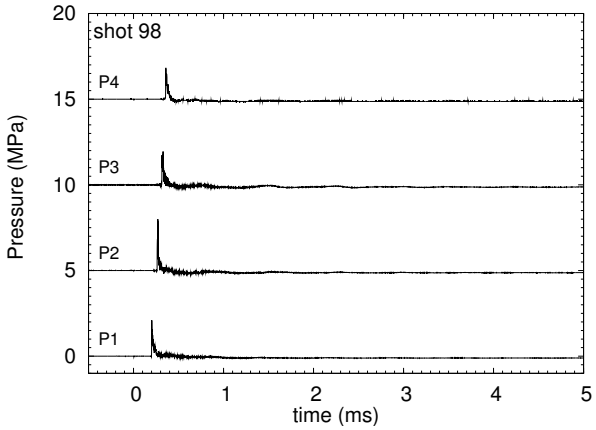

c) $P_0 = 2.0$ bar

Figure 29: Pressure traces for $2H_2$-O_2-N_2 mixture with 0.01 in gap (5% dead volume).

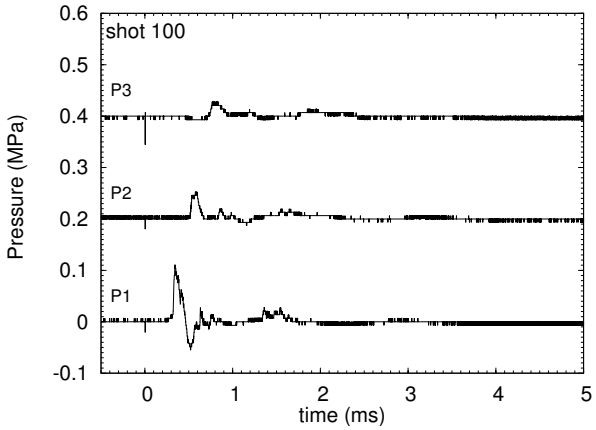

a) $P_0 = 1.75$ bar

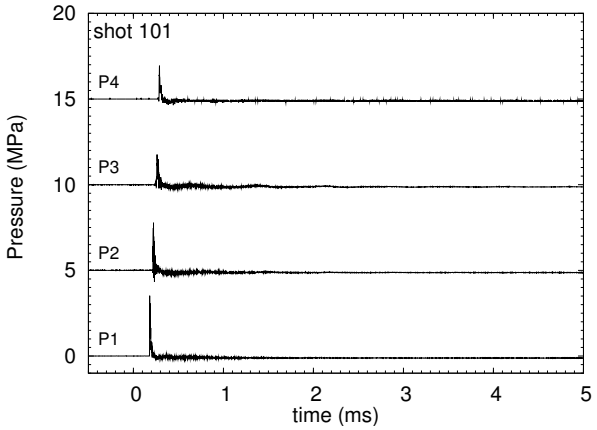

b) $P_0 = 2.0$ bar

Figure 30: Pressure traces for $2H_2$-O_2-N_2-He mixture with 0.01 in gap (5% dead volume).

H Shot list: $T_0 = 150$ °C with 0.05 in gap (1.5% dead volume).

Table 12: Planar fixture with a gap of 0.05 in (1.5% dead volume). P_0 is the expected initial pressure, $P_{0,exp}$ and $T_{0,exp}$ are the actual initial pressure and temperature before test.

shot	P_0 (bar)	$P_{0,exp}$ (bar)	$T_{0,exp}$ (°C)	P_{CV} (MPa)	P_{CJ} (MPa)	P_{CJref} (MPa)	$P_{1,max}$ (MPa)	$P_{2,max}$ (MPa)	$P_{3,max}$ (MPa)	$P_{4,max}$ (MPa)	DDT
mixture A											
105	1.0	0.95	21.2	0.96	1.87	4.60	0.295	0.994	0.674	0.490	P2
108	1.0	1.05	20.8	0.96	1.87	4.60	4.127	3.824	3.298	3.846	P1
106	1.0	1.03	42.7	0.91	1.77	4.35	0.147	0.497	2.998	4.185	P3
114	1.0	1.03	153.5	0.67	1.30	3.14	1.179	1.682	1.649	3.280	P4
109	1.25	1.19	20.9	1.20	2.39	5.80	4.385	5.047	3.223	4.298	P1
107	1.25	1.21	43.6	1.14	2.23	5.48	2.911	4.244	3.298	3.657	P1
115	1.25	1.14	151.4	0.85	1.64	3.96	0.958	1.071	1.536	2.903	P4
116	1.5	1.41	150.5	1.02	1.98	4.78	0.848	1.377	5.696	3.582	P3
120	2.0	2.12	150.1	1.38	2.67	6.45	2.690	5.009	7.832	6.259	P2
121	3.0	3.14	150.0	2.10	4.07	9.82	5.491	6.691	5.659	6.862	P1
mixture B											
110	1.5	1.45	21.0	1.32	2.57	6.28	0.184	0.191	0.187	0.226	flame
118	1.5	1.58	148.8	0.93	1.80	4.30	0.258	0.268	0.300	0.302	flame
111	2.0	2.06	21.0	1.831	3.578	8.78	1.253	2.409	5.621	13.612	P3
117	2.0	2.09	149.6	1.30	2.50	6.00	2.727	2.294	1.986	9.615	P4
122	3.0	3.12	149.0	2.02	3.90	9.38	1.879	4.780	7.832	5.882	P2
mixture C											
113	1.75	1.76	21.2	1.64	3.22	7.87	0.037	0.038	0.075	0.075	flame
112	2.0	2.03	21.1	1.91	3.73	9.14	0.516	0.726	0.712	9.275	P4
119	2.0	2.07	150.2	1.35	2.60	6.25	0.737	0.650	0.675	0.867	flame
123	2.5	2.64	149.4	1.71	3.31	7.97	1.585	2.103	3.073	6.071	P3
124	3.0	3.11	149.4	2.07	4.02	9.68	3.022	3.327	5.808	5.580	P1

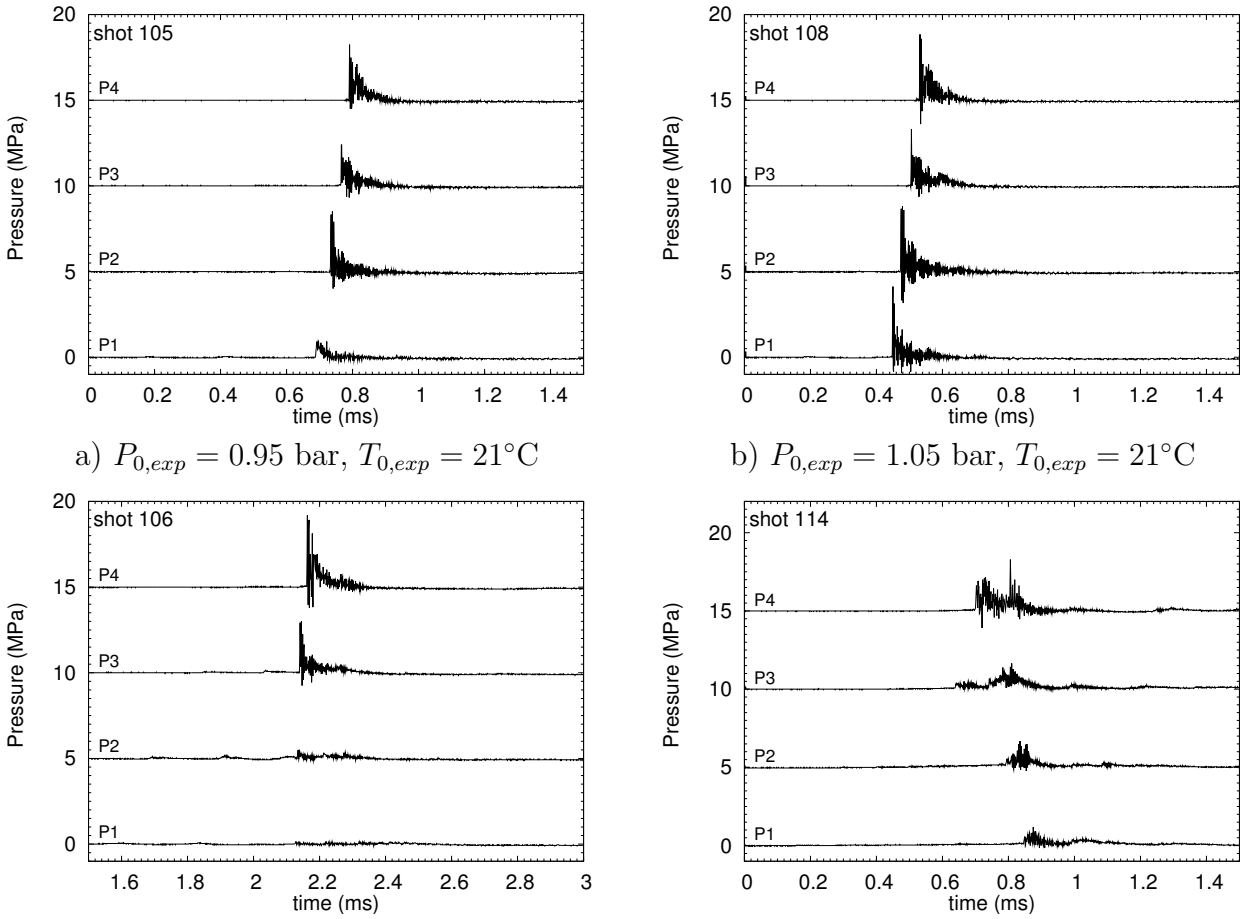

a) $P_{0,exp} = 0.95$ bar, $T_{0,exp} = 21°\text{C}$

b) $P_{0,exp} = 1.05$ bar, $T_{0,exp} = 21°\text{C}$

c) $P_{0,exp} = 1.03$ bar, $T_{0,exp} = 43°\text{C}$

d) $P_{0,exp} = 1.03$ bar, $T_{0,exp} = 154°\text{C}$

Figure 31: Pressure traces for mix A with 0.05 in gap (1.5% dead volume).

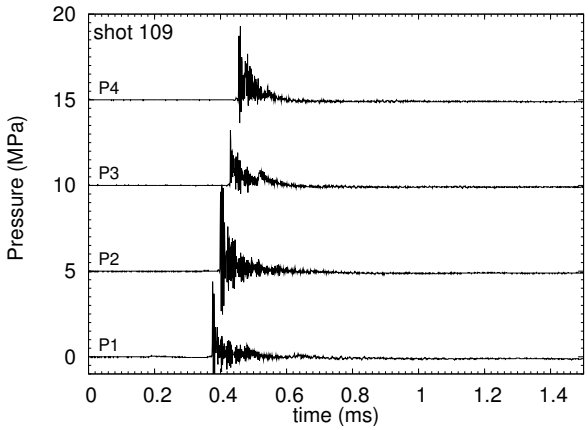

a) $P_{0,exp} = 1.19$ bar, $T_{0,exp} = 21°\text{C}$

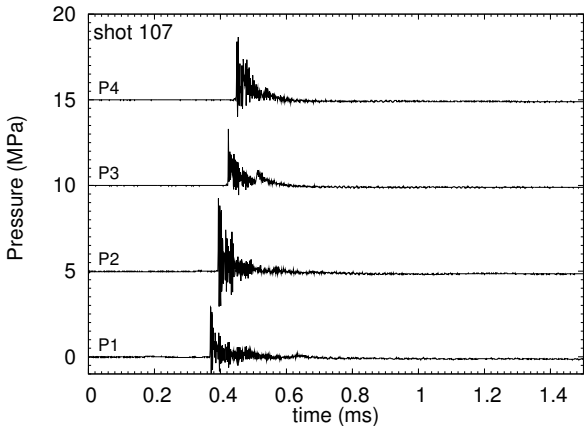

b) $P_{0,exp} = 1.21$ bar, $T_{0,exp} = 44°\text{C}$

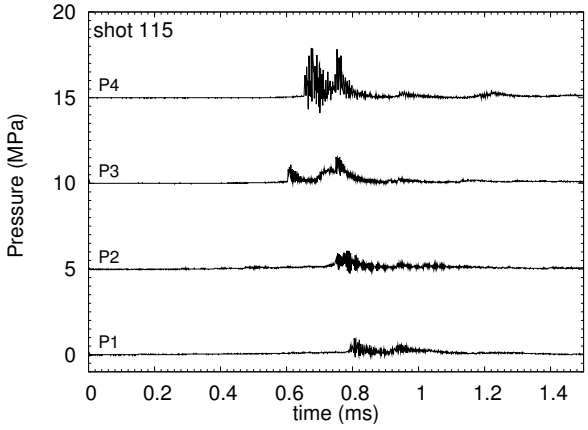

c) $P_{0,exp} = 1.14$ bar, $T_{0,exp} = 151°\text{C}$

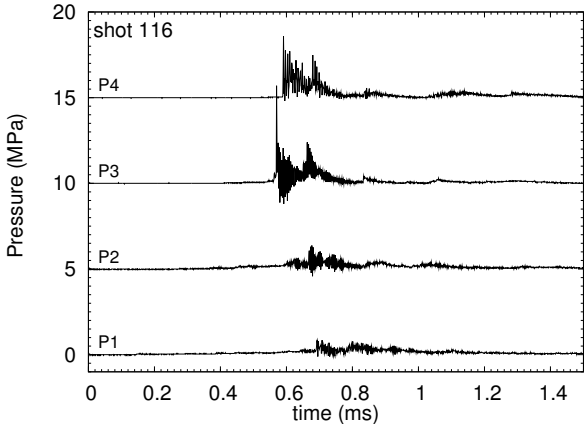

d) $P_{0,exp} = 1.41$ bar, $T_{0,exp} = 151°\text{C}$

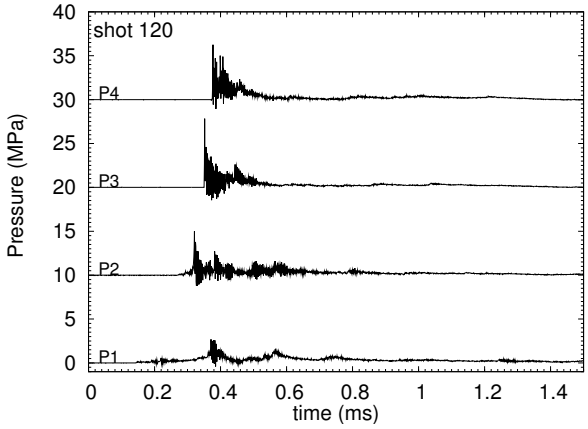

d) $P_{0,exp} = 2.12$ bar, $T_{0,exp} = 150°\text{C}$

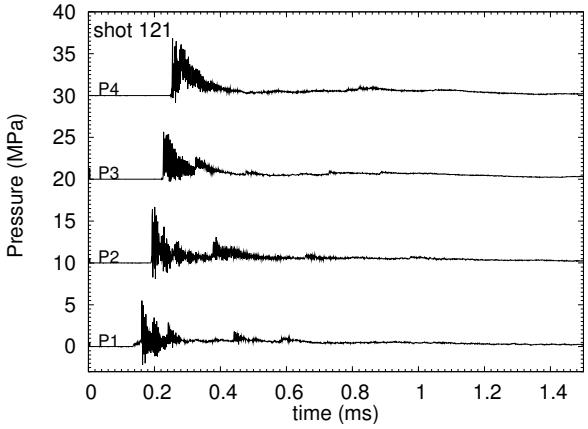

e) $P_{0,exp} = 3.14$ bar, $T_{0,exp} = 150°\text{C}$

Figure 32: Pressure traces for mix A with 0.05 in gap (1.5% dead volume).

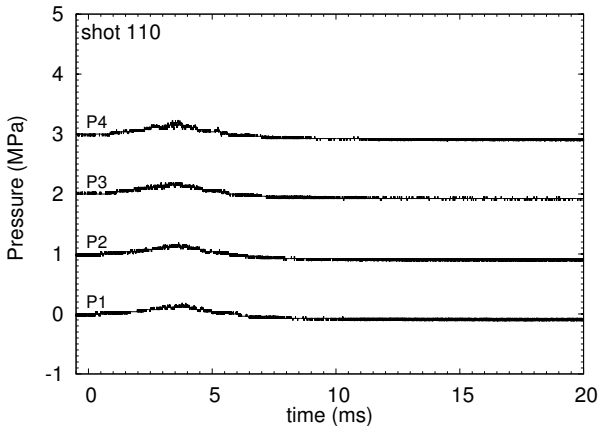

a) $P_{0,exp} = 1.45$ bar, $T_{0,exp} = 21°\text{C}$

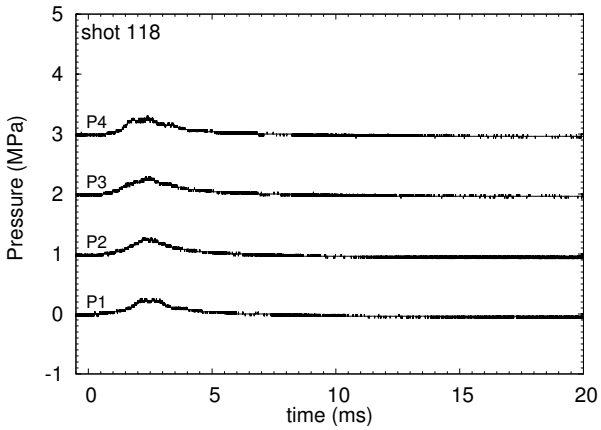

b) $P_{0,exp} = 1.58$ bar, $T_{0,exp} = 149°\text{C}$

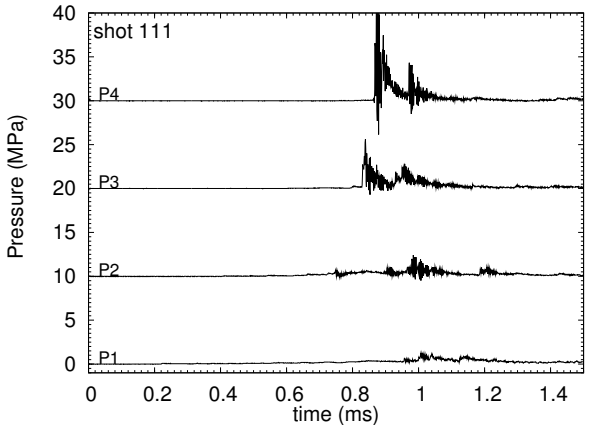

c) $P_{0,exp} = 2.06$ bar, $T_{0,exp} = 21°\text{C}$

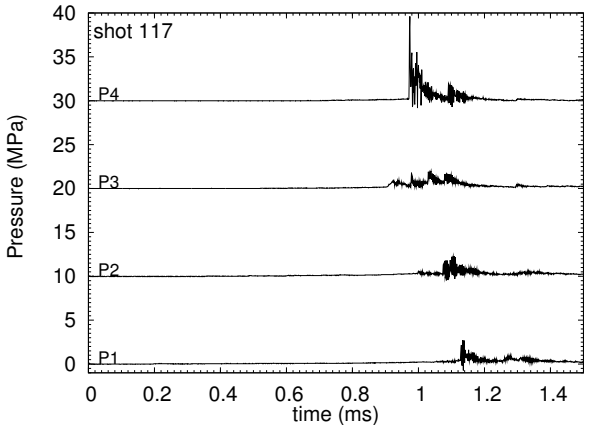

d) $P_{0,exp} = 2.09$ bar, $T_{0,exp} = 149°\text{C}$

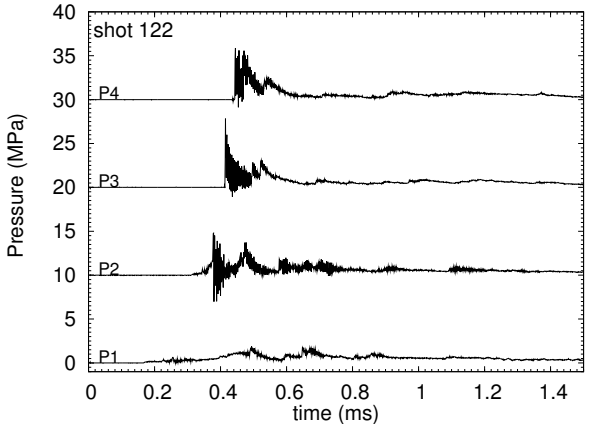

d) $P_{0,exp} = 3.12$ bar, $T_{0,exp} = 149°\text{C}$

Figure 33: Pressure traces for mix B with 0.05 in gap (1.5% dead volume).

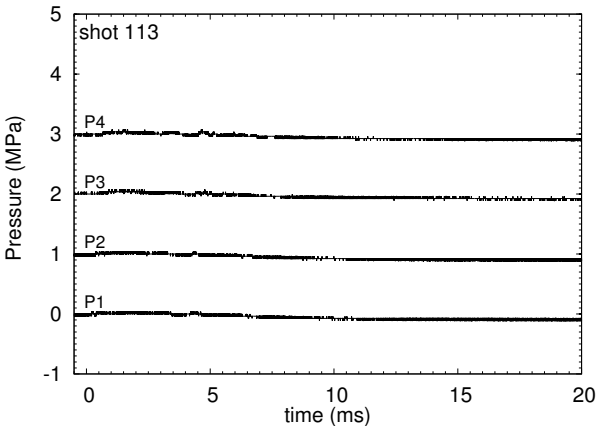

a) $P_{0,exp} = 1.76$ bar, $T_{0,exp} = 21$ °C

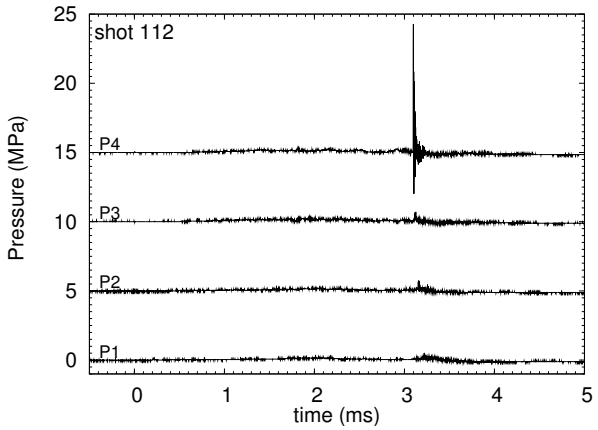

b) $P_{0,exp} = 2.03$ bar, $T_{0,exp} = 21$ °C

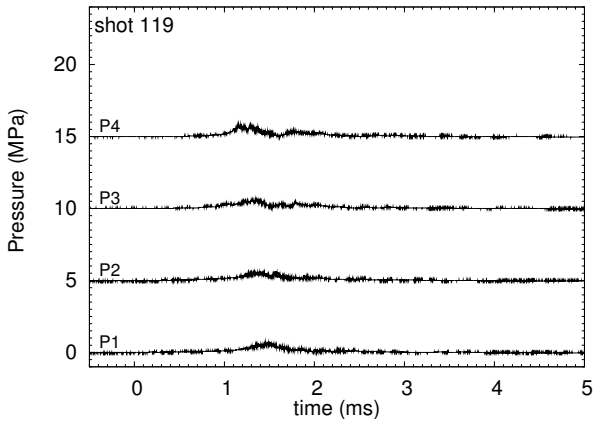

c) $P_{0,exp} = 2.07$ bar, $T_{0,exp} = 150$ °C

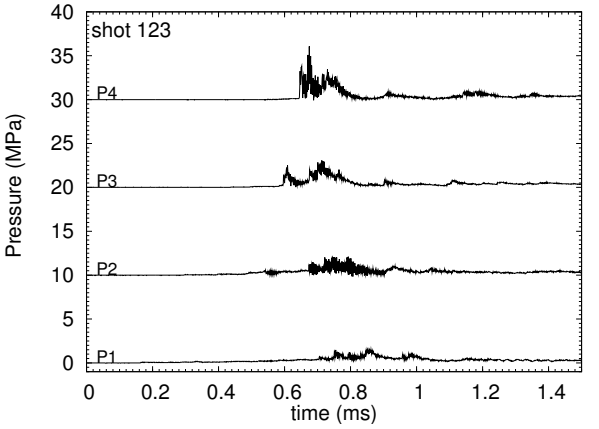

d) $P_{0,exp} = 2.64$ bar, $T_{0,exp} = 149$ °C

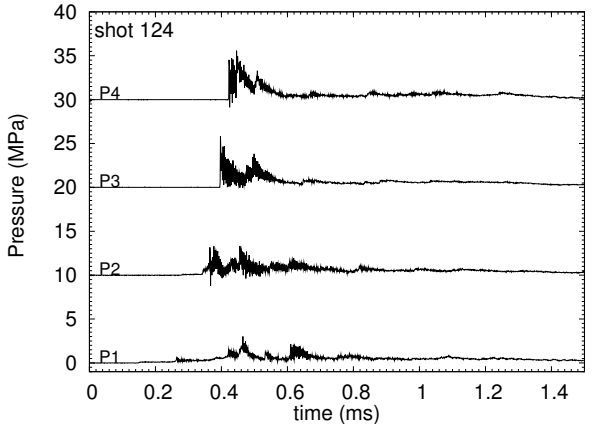

e) $P_{0,exp} = 3.11$ bar, $T_{0,exp} = 149$ °C

Figure 34: Pressure traces for mix C with 0.05 in gap (1.5% dead volume).

Explosion Testing of Nested Can Containment System Part II: Thick-walled Tube

Z. Liang and J. E. Shepherd
Graduate Aeronautical Laboratories, California Institute of Technology
Pasadena, CA 91125

Explosion Dynamics Laboratory Report FM2007.001

May 9, 2007

Sponsored by Los Alamos National Laboratory, Subcontract 46222-001-07.

Contents

List of Figures

List of Tables

1 Introduction

This report describes the second series of tests carried out to provide data that will be used in the safety assessment of triple-nested (DOE-STD-3013) containers used in the DOE complex. The tests use deliberate ignition of explosive mixtures to determine structural loading (pressure history) and structural response (stain history) in a model fixture, a thick-walled tube with a solid bar insert, simulating the annular gap between the outer and inner cans of the 3013 containment system. The threshold for Deflagration-to-Detonation Transition (DDT) was also found. Three types of tube configurations (Fig. 1) were used: (1) without tube insert (empty tube), (2) with a solid bar (concentric), and (3) with a solid bar (eccentric). Configuration (1) simulates the interior of the outermost 3013 can. Configurations (2) and (3) simulate the annular gap between the outer and inner cans of the 3013 containment system. The fixture was filled with three representative explosive gas mixtures, ignited with a low-energy spark, and the subsequent explosion development monitored with pressure gages and strain gages. For each mixture composition and tube configuration, the threshold for DDT and corresponding structural response was determined by varying the initial pressure. Based on discussions with LANL and reviewing the engineering drawings, the annular gap between the inner and outer cans of the 3013 system is between 0 and 0.16 in (0–4.06 mm) depending on the eccentricity of the cans. The gap between the lids of the two cans may vary from 0.375 to 0.6 in (9.5–15 mm) depending on the cut-off length and extent of bulging. Therefore in the current tests, an average annular gap of 0.08 in was used. Two extreme cases of the gap geometry were simulated. In configuration (2), the idealized case of a concentric inner and outer can was examined. In configuration (3), the more realistic case of can eccentricity was examined. For the end gap between the solid bar end surface and the closed flange (ignition end), two end gap sizes, 0.08 and 0.5 in, were tested.

Three mixtures were used: A (stoichiometric hydrogen-oxygen), B (stoichiometric hydrogen-oxygen added to an initial fill of 60 kPa nitrogen) and C (stoichiometric hydrogen-oxygen added to an initial fill of 16 kPa nitrogen and 60 kPa helium). See Appendix A for the precise specification of the three mixtures. The initial conditions were room temperature (20–23°C) and pressures of 1.0–3.5 bar.

2 Fixture and Procedure

All the tests were conducted in a rigid vessel constructed of a thick-walled tube (4.685 in ID, 7.9 in OD and 9.2 in long) of 4140 alloy steel closed by two flanges (see Fig. 1). The interior surface of the tube was turned with a resulting surface roughness of approximately

32 micro-inch. The flanges and the tube were held together by 16 7/8 in cap screws and sealed to the tube using o-rings. The ignition source and gas lines were mounted on one flange, and the solid bar was mounted on the second flange. Two pair of mounting holes for the solid bar were arranged on the second flange so that the gap was concentric with one pair and eccentric (annular gap size varying between 0.01 and 0.15 in) with the other pair.

The fixture was filled by the method of partial pressures using bottled gas supplied by local vendors. Prior to filling, the fixture and associated plumbing was evacuated below 5 Pa. Since the volume of the facility was small, it was necessary to take some care to eliminate leaks and minimize the dead volume associated with connecting lines. The filling lines were evacuated prior to switching gases in order to minimize errors in composition. Shut-off valves were located as close as possible to the O-Seal connections to the fixed flange. The gas within the tube was circulated by a bellows pump for five minutes to ensure a homogeneous mixture.

The ignition source, a spark plug, was used in the present tests. Four piezo-electric (PCB) pressure transducers (P_1-P_4) were mounted along the tube wall, and the sensitive surface of the transducers was flush with the interior surface of the tube. Four strain gauges (S_1-S_4) were mounted on the outer tube surface close to the reflecting end (opposite to the ignition end). $S1$ was directly opposite the pressure transducer port P_3, and the other three gauges S_2-S_4 were closely spaced. The strain gauges were of type CEA-06-125UN-350 (Vishay Measurements Group, Micro-Measurements Division), had a uni-axial strain gauge pattern, and were oriented to measure the hoop strain of the tube. The distance of the pressure transducers and strain gauges to the ignition source is listed in Table 1.

The material specification and some structural parameters of the thick tube and 3013 cans are listed in Appendix B.

Table 1: Distance (along long axis) from the pressure transducers (P_1-P_4) and strain gauges (S_1-S_4) to the igniter location.

	X (m)	X (in)		X (m)	X (in)
P_1	0.047	1.85	S_1	0.141	5.55
P_2	0.094	3.70	S_2	0.172	6.775
P_3	0.141	5.55	S_3	0.203	8.0
P_4	0.188	7.40	S_4	0.219	8.61

3 Results

A total of 38 shots were performed in this part of the project. A summary of the test conditions is given in Table 2. The values for CJ pressure (P_{CJ}), reflected CJ pressure

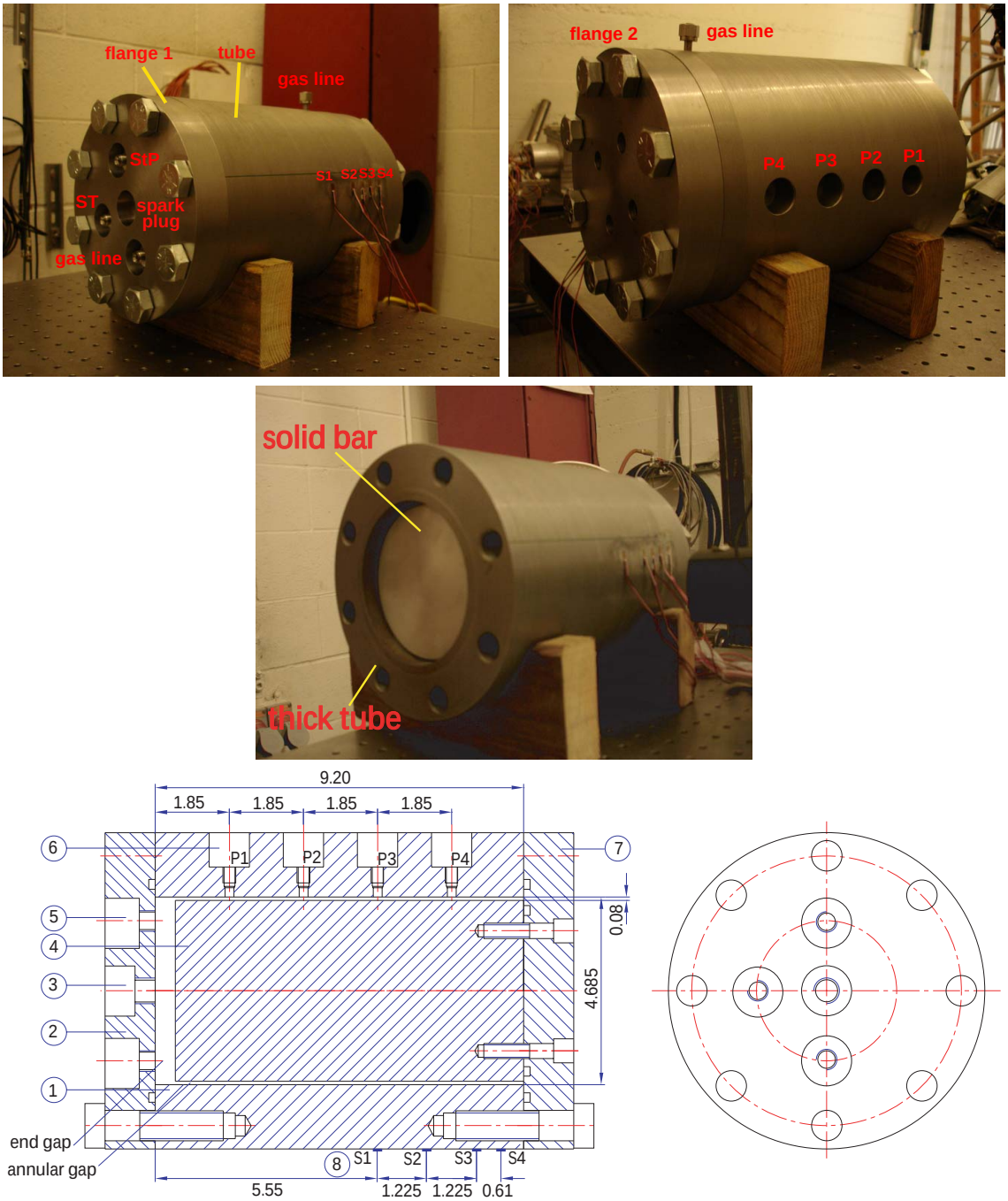

Figure 1: Setup of the thick-walled tube assembly. The top left photograph shows a view of flange 1 with spark plug and Swagelok fittings mounted and the tube side with strain gauges glued; the top right photograph shows a view of flange 2 with the solid bar attached inside and the tube side with pressure transducers mounted; the middle photograph shows a view of the solid bar from the ignition end. The CAD drawing shows configuration 2b with a concentric solid bar insert. 1-thick tube, 2-flange 1, 3-spark plug, 4-solid bar, 5-gas fill, 6-pressure transducer holes, 7-flange 2, 8-strain gauges.

(P_{CJref}) and constant volume explosion pressure (P_{CV}) for each test were calculated using a chemical equilibrium program of Reynolds (1986) with realistic thermochemical properties. The static strains, ϵ_{CJ}, ϵ_{CJref}, ϵ_{CV}, corresponding to the CJ, reflected CJ and constant volume explosion pressures, were inferred from the approximate stress-strain relation for a uniformly, statically loaded tube

$$\epsilon = \frac{(P - P_a)R}{Eh} \ , \tag{1}$$

where ϵ, E, R, h and P_a are strain, Young's modulus, average radius (R=(ID+h)/2) and thickness of the tube, and atmospheric pressure, respectively. See Appendix B for their values. The results of these computations are given in Appendix A for each mixture.

Table 2: Summary of test series. "PT" represents pressure transducers, "SG" represents strain gauges.

tube configuration	shots	mixture	P_0 (bar)	threshold (bar)
1 - without solid bar	1-5	A	2.0-3.0	2.5-2.6
	6-8	B	2.5-3.5	no DDT
	9-10	C	2.5-3.5	no DDT
2a - with concentric solid bar annular gap: 0.08 in, end gap: 0.08 in	11-15	A	1.0-3.5	<1.0
	16-19	B	1.5-3.5	1.0-1.5
	20-23	C	1.5-3.5	1.5-2.0
2b- with concentric solid bar annular gap: 0.08 in, end gap: 0.5 in	25-28	A	1.0-3.5	<1.0
	29-30	B	1.0, 3.5	–
	31-32	C	1.5, 3.5	–
3a - with eccentric solid bar 0.01 in on PT side, 0.15 in on SG side	33-35	A	1.0-3.5	<1.0
3b - with eccentric solid bar 0.15 in on PT side, 0.01 in gap on SG side	36-38	A	1.0-3.5	<1.0

3.1 Configuration 1 (empty)

The test tube has no insert in configuration 1. The summary of these tests is given in Appendix E. We have found in the planar fixture, the DDT threshold shifted to higher initial pressures for larger gap sizes. Therefore, with no gap present, we expected to observe high DDT threshold pressures for all mixtures. Figure 2 describes the peak pressures and strains for the three mixtures. For an empty tube, the DDT transition was observed at P_0 = 2.5-2.6 bar for mix A, which is twice as large as the DDT threshold, P_0 = 1.2-1.25, for the largest gap size of 0.44 in of the planar fixture. For the empty tube, when $2.6 < P_0 <$

3.5 bar, DDT transition was always observed close to the tube end. On the other hand with a planar gap of 0.44 in, the location of DDT moved from the last transducer to the first one when P_0 was increased from 2.4 to 3.5 bar. For mix B and C, no DDT transition was observed for P_0 up to 3.5 bar with the empty tube. In the planar gap, DDT was observed at $P_0 = 2.1$ bar for mix B and $P_0 = 2.75$ bar for mix C with the 0.44 in gap.

The present results are consistent with preliminary tests reported in Liang et al. (2006) in which a series of 26 tests were carried out in a test vessel (3 in inside diameter, 14 in long), closed at both ends and instrumented with pressure and strain gauges. The test mixture was 40.9% hydrogen, 22.4% oxygen, 7.7% nitrogen and 29% helium at room temperature and initial pressures up to 2.5 bar. DDT transition was observed when P_0 was increased to 2.3–2.35 bar, below which, a slow flame was observed. Although those tests are not directly comparable with present cases, the mixture and vessel size are sufficiently similar to conclude that the results are consistent.

For mix A, the peak strain was observed on the last strain gauge close to the tube end. When P_0 was increased, the peak strain also increased and the values are larger than ϵ_{CJref} (expected for a reflected CJ detonation). The maximum strain observed is on the order of 170 μstrain at $P_0 = 3.5$ bar.

For mix B and C, there is no DDT observed, but the peak strains recorded were comparable to ϵ_{CJ} (see Figure 2d, f). Considering the magnitude of the peak values, these strains must be due to the thermal effect. We have observed in previous studies of Pintgen and Shepherd (2005) that the thermal stresses could increase the peak strain on the outside of the tube up to 125% over the mechanical stress for slow combustion. In the fast combustion regime, we found the thermal stresses are negligible compared to the mechanical loading.

3.2 Configuration 2a (concentric, 0.08 in end gap)

In configuration 2a, the solid bar was inserted into the tube and mounted to be approximately concentric to the outer tube, forming an average annular gap of 0.08 in (see Fig. 18 in Appendix C). The end gap between the end surface of the solid bar and the ignition flange was initially 0.08 in. Due to the clearance of the bolt circles on the end flange, the solid bar was not completely concentric but the annular gap size was varied between 0.064 and 0.097 in. The annular gap size was measured from the ignition end by taking off the flange. The values are listed in Appendix C.

As shown in Fig. 3, the DDT transition occurred at $P_0 = 1$ bar for mix A. For mix B, it occurred at $P_0 = 1.5$ bar and for mix C, at $P_0 = 2.0$ bar. These thresholds are consistent with the results observed in the tests of the planar fixture for the gap sizes of 0.05 and 0.10

in. The peak strains were always observed on the last strain gauge. The values were between ϵ_{CJ} and ϵ_{CJref}. The maximum value was on the order of 140 micro strain at $P_0 = 3.5$ bar. See Appendix F for the summary.

3.3 Configuration 2b (concentric, 0.5 in end gap)

In configuration 2b, the solid bar was shortened to form an end gap of 0.50 in. Before the tests, the end flange was carefully adjusted so that it was visually concentric to the outer tube (not measured). See Appendix G for the summary.

As shown in Fig. 4, for mix A, the DDT threshold was found to be the same as for configuration 2a and the peak strains were also in a similar range. For mix B and C, only the cases with P_0 close to the DDT threshold and $P_0 = 3.5$ bar were carried out. For mix B, shots 29 and 30 (Fig. 32 in Appendix G) showed the same behavior as shots 17 and 19 (Fig. 26 in Appendix F) with configuration 2a. For mix C, at $P_0 = 1.5$ bar, the pressure traces of shot 31 (Fig. 33) showed that DDT transition occurred close to the tube end, while with configuration 2a, a slow flame was observed. However, the peak strain of shot 31 was negligible ($\sim$30 μstrain), so the transition thresholds are essentially the same for both configurations.

For all three mixtures, the peak strains at $P_0 = 3.5$ bar are all slightly smaller than in configuration 2a. The subsequent tests with configurations 3a and 3b also showed smaller strains. In addition to the difference of the end gap size, possible reasons that may have also led to this are: (1) DDT tests always show some variability; (2) the circulation pump used in the current tests cannot start when $P_0 > 3$ bar, so before filling the final gas component, oxygen, the pump was left running. Therefore the volume of oxygen might be different from the expected amount and the mixture may not have been stoichiometric.

3.4 Configuration 3a and 3b (eccentric)

In this test series, the solid bar inside the tube was mounted eccentrically by using the off-center pair of holes on the end flange. The nominal center-to-center offset was 0.07 in. This would give a nominal minimum gap of 0.01 in and maximum gap of 0.15 in. The two eccentric holes on the end flange were unfortunately not perpendicular to the pressure transducers, but had a 25-deg offset. When the end flange with the solid bar was mounted, some manual adjustment was performed so that the minimum gap of 0.01 in appeared close to the pressure transducer (PT) side, and the largest gap size of 0.15 in was located on the opposite side with the strain gauges (SG). The diagram of the two configurations are shown in Figure 5. See Appendix H and I for the summary.

In contrast to configuration 2b, the annular gap size for configuration 3a was reduced on the pressure transducer side, therefore one would expect faster DDT transition on this side. As shown in Figure 6, DDT indeed occurred right away at $P_0 = 1$ bar for mix A, but the maximum strain was on the same order as the values recorded in configuration 2a.

For configuration 3b, the solid bar was rotated 90-deg, therefore the largest gap, 0.15 in, appeared on the pressure transducer side and the smallest gap was on the strain gauge side. The annular gap size was measured from the ignition end by taking off the flange. The values are listed in Appendix D.

For the same mixture (P_0=1 bar, mix A), DDT appeared near the last transducer P_4 with configuration 3b (see shot 36 in Fig 35), but it was near the first transducer P_1 with configuration 3a (see shot 33 in Fig 34). This means that DDT occurred earlier on the smaller gap side and later on the larger gap side. This is consistent with our previous findings about the effect of the gap size on DDT thresholds in the planar fixture. As shown in Fig. 7, there are no significant differences in the peak pressures and strains for the two configurations.

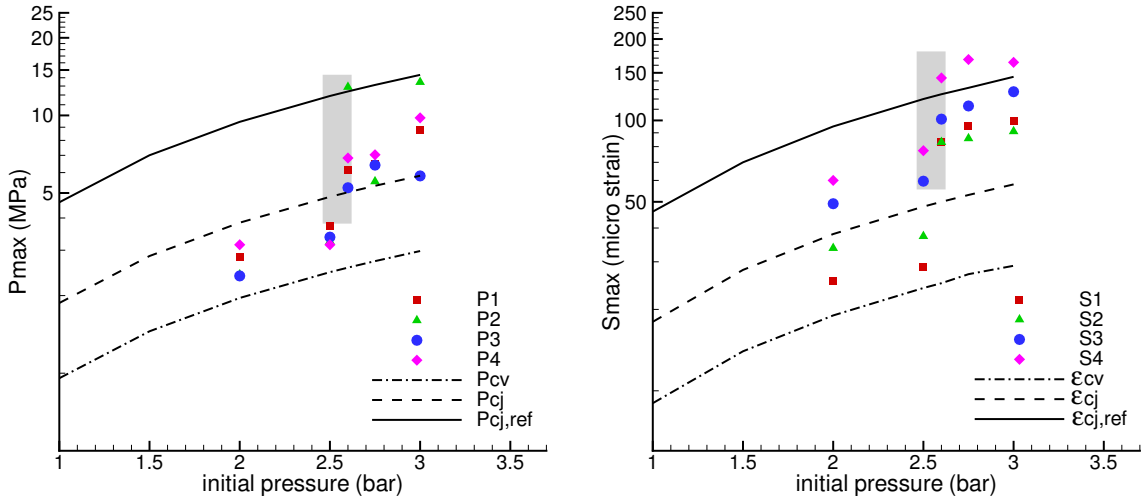

a) peak pressure, mix A

b) peak strain, mix A

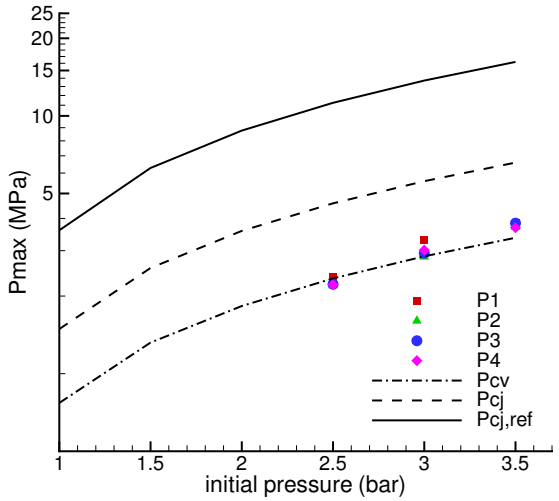

c) peak pressure, mix B

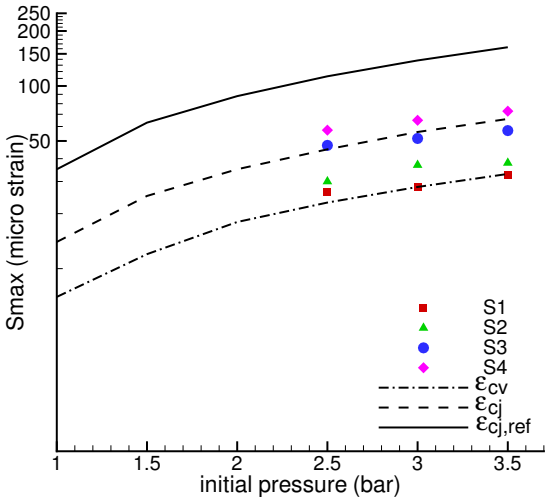

d) peak strain, mix B

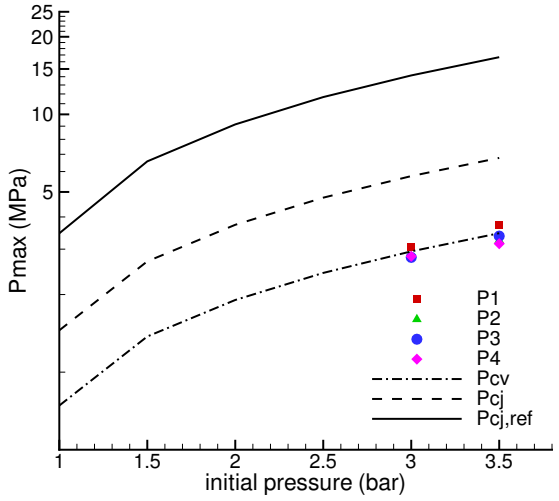

e) peak pressure, mix C

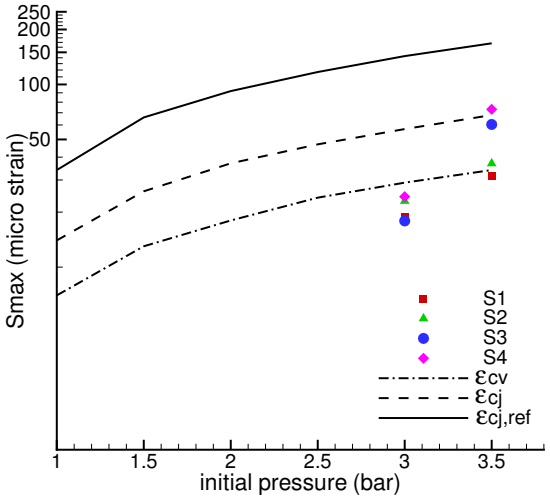

f) peak strain, mix C

Figure 2: Comparison of DDT thresholds and peak pressures for three mixtures and configuration 1 (empty tube). Gray vertical shaded region indicates the DDT threshold. No DDT observed for mix B and C.

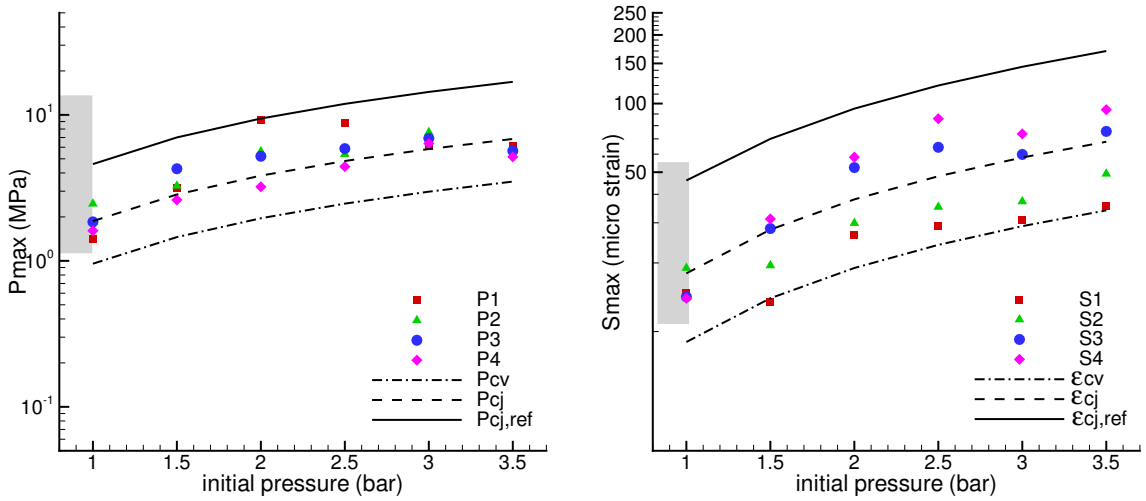

a) peak pressure, mix A

b) peak strain, mix A

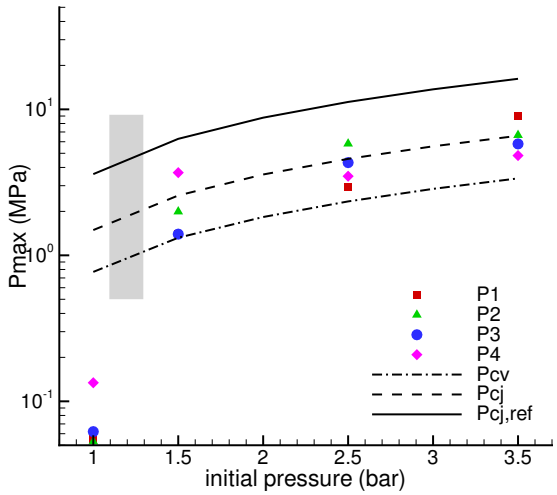

c) peak pressure, mix B

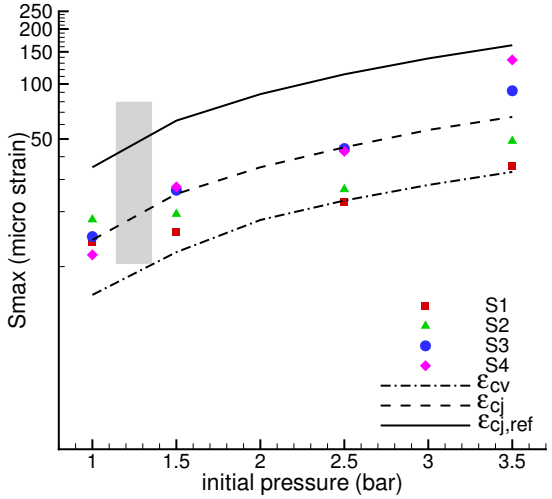

d) peak strain, mix B

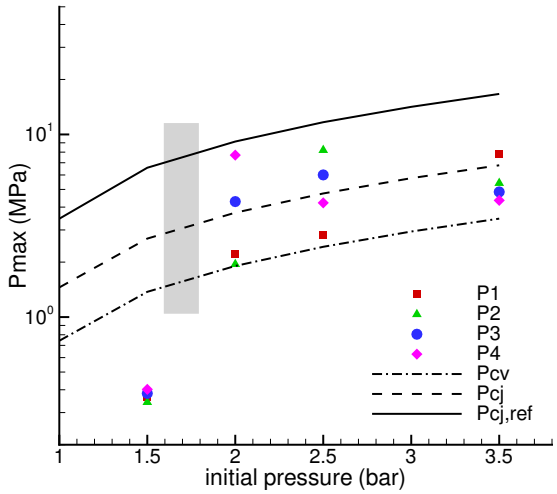

e) peak pressure, mix C

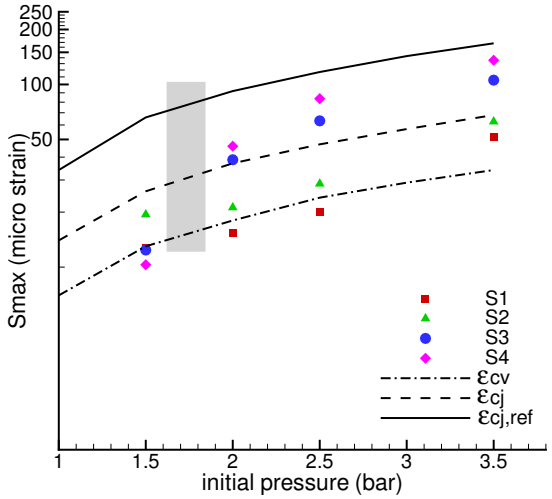

f) peak strain, mix C

Figure 3: Comparison of DDT threshold and peak pressures for three mixtures and configuration 2a. Gray vertical shaded region indicates the DDT threshold. Concentric solid bar, annular gap: 0.08 in, end gap: 0.08 in.

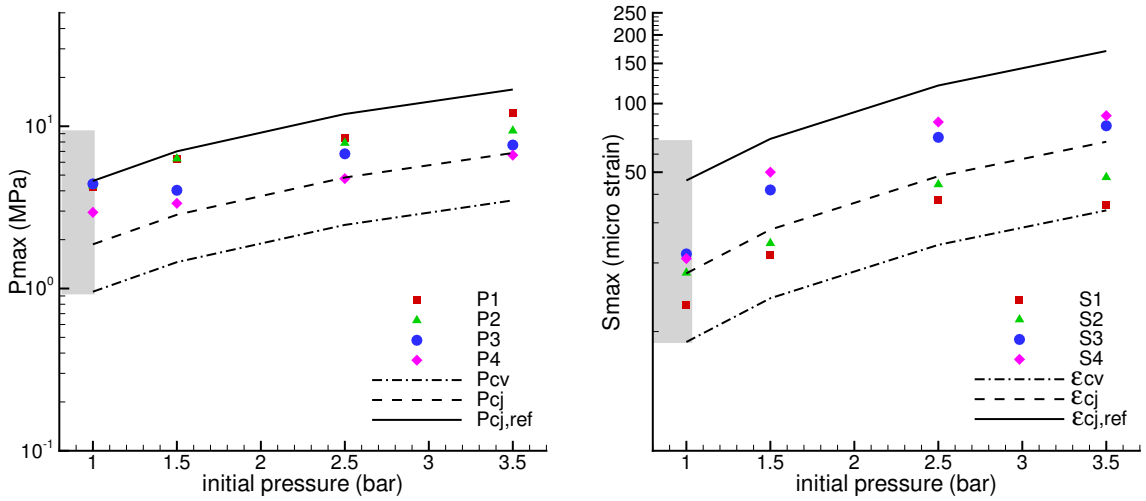

a) peak pressure, mix A

b) peak strain, mix A

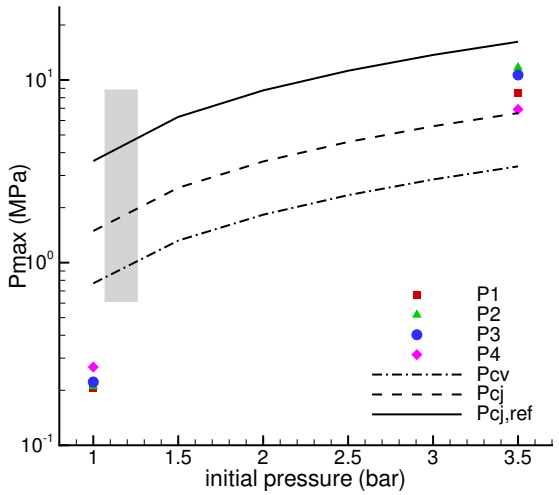

c) peak pressure, mix B

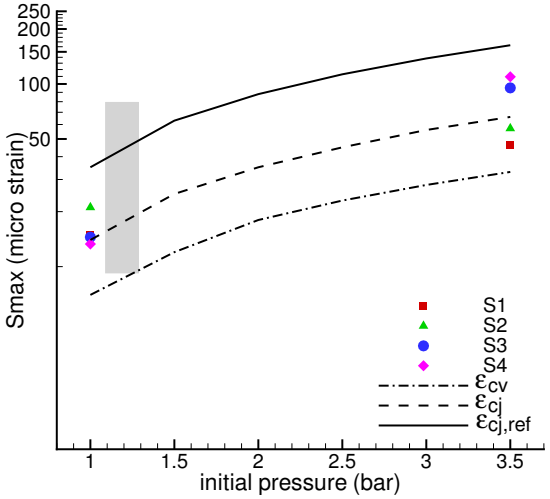

d) peak strain, mix B

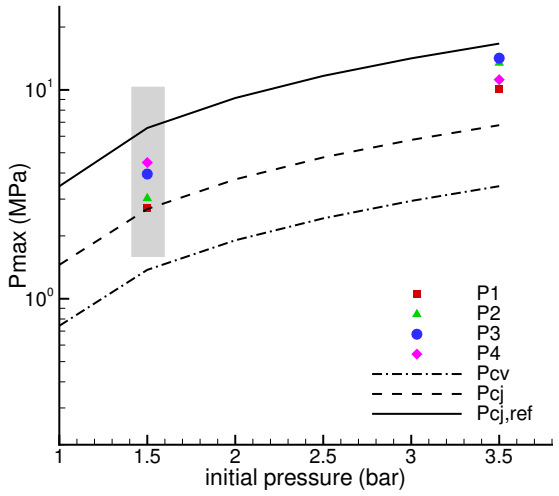

e) peak pressure, mix C

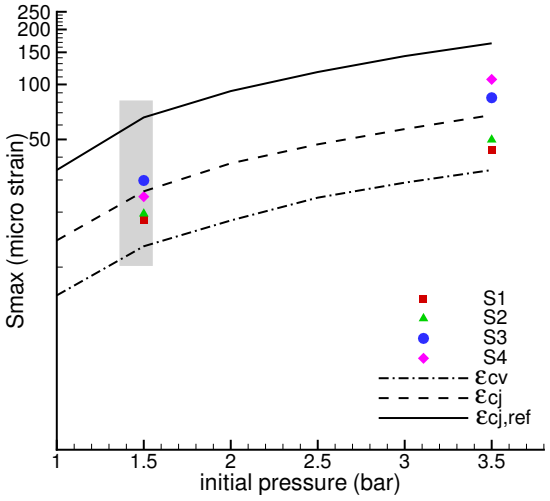

f) peak strain, mix C

Figure 4: Comparison of DDT threshold and peak pressures for three mixtures and configuration 2b. Gray vertical shaded region indicates the DDT threshold. Concentric solid bar, annular gap: 0.08 in, end gap: 0.5 in.

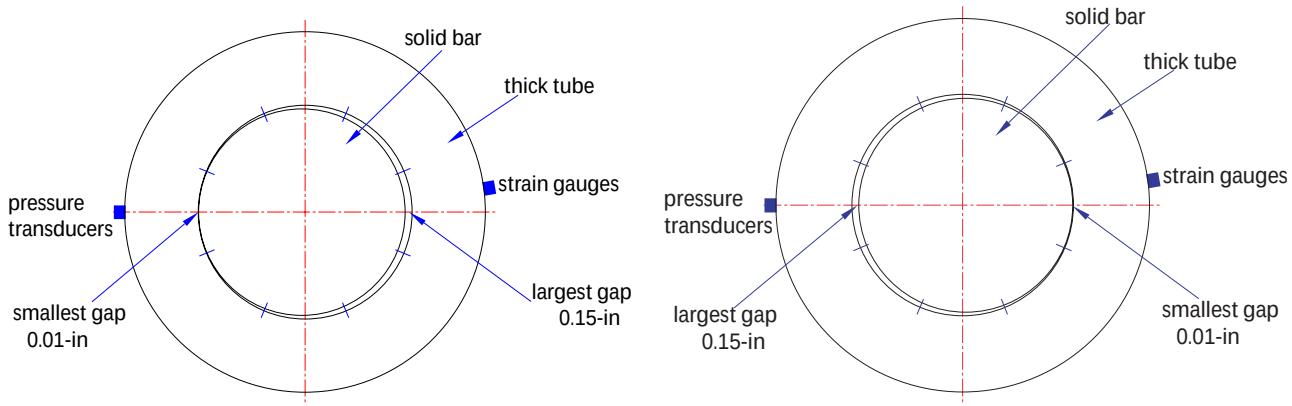

Figure 5: Diagram of the eccentric tube for a) configuration 3a (shots 33-35) and b) configuration 3b (shots 36-38).

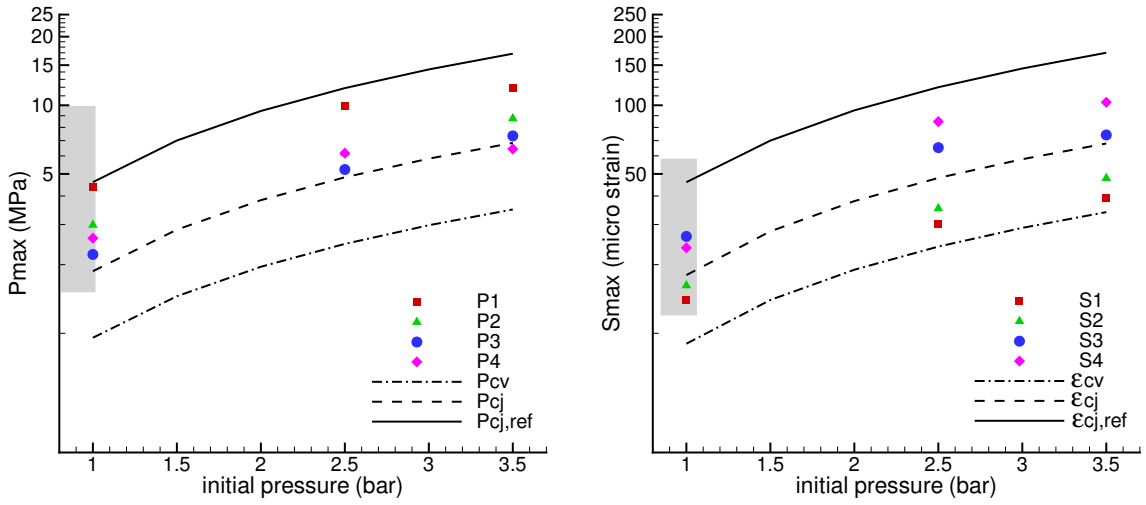

a) peak pressure, mix A

b) peak strain, mix A

Figure 6: Comparison of peak pressures for three mixtures with configuration 3a. Gray vertical shaded region indicates the DDT threshold. Eccentric solid bar, 0.01 in gap on the pressure transducer side and 0.15 in gap on the strain gauge side. End gap: 0.5 in.

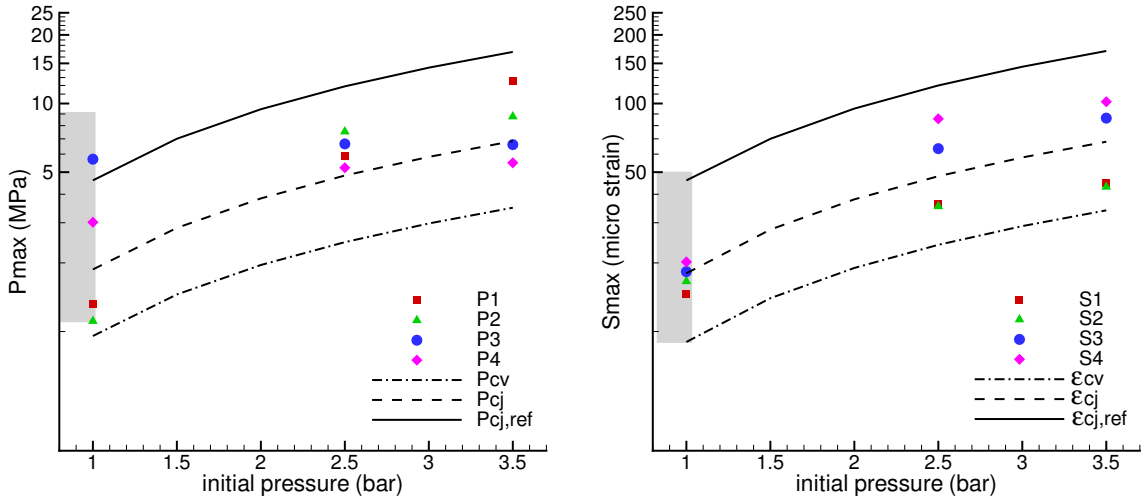

a) peak pressure, mix A

b) peak strain, mix A

Figure 7: Comparison of peak pressures for three mixtures with configuration 3b. Gray vertical shaded region indicates the DDT threshold. Eccentric solid bar, 0.15 in gap on the pressure transducer side and 0.01 in gap on the strain gauge side. End gap: 0.5 in.

4 Dynamic Load Factor

One of the most frequently used methods (Biggs, 1964, Paz and Leigh, 2004) to quickly evaluate structural response to transient loads is through the use of a Dynamic Load Factor (DLF). This method uses the measured or estimated peak pressure of the transient load corrected by the DLF to compute a static response which has an equivalent deflection to the peak transient response. This method is useful if the dynamic load factor and peak pressure can be readily computed or estimated for the cases of interest. In this section, we explore the evaluation of dynamic load factors and peak pressures from the experimental measurements and simple models of the structure.

4.1 Dynamic Load Factor

The peak value of the strain signals can be analyzed by finding the DLF Φ, which is defined as the ratio of the measured peak strain to the peak strain expected in the case of quasi-static loading[1]

$$\Phi = \frac{\epsilon_{max}}{\frac{\Delta P R}{E h}} \tag{2}$$

The peak pressure in Eq. 2 can be based on either the measured peak value in the experiment or one of the computed values. Using the experimental pressure allows a rough evaluation of what type of loading (impulsive, sudden or mixed) is taking place. For an ideal single-degree of freedom structure and a simple pressure-time history with a single jump followed by a monotonic decay (Paz and Leigh, 2004, Biggs, 1964), values of Φ close to two are associated with the limit of "sudden loading" in which the pressure jumps to a high value and does not significantly decay on the time scale of the tube radial oscillation periods. In this regime, the peak elastic deformation is proportional to the peak pressure. As the decay time of the pressure after the jump becomes shorter, the dynamic load factor becomes less than two, decreasing as the decay time decreases. In the limit of very short pressure pulses, the loading is in the impulsive regime and the peak elastic deformation is proportional to the impulse. Between these two extremes, in the mixed regime, the peak elastic deformation will depend on both the impulse and peak pressure.

Tables 3 and 4 summarize the dynamic load factors computed with Eqn. 2 for shots performed with configuration 1 (empty) and 2a (concentric). For Φ_{exp}, $\Delta P = P_{max}$, P_{max} is the maximum value of the measured pressures on transducers 1-4 in Table 17 and 18. For

[1]This expression is based on simple membrane analysis. Most sophisticated solutions using the theory of elasticity include corrections for the Poisson effect and any longitudinal strain or stress that is induced by the boundary conditions at the tube ends.

Φ_{CJ}, $\Delta P = P_{CJ}$ - P_a.

For the empty tube (see Table 3), Φ_{exp} ranged between 1.2 and 2.6 for mix A, but Φ_{CJ} varied between 1.7 and 3.5. This is consistent with the very short duration of the measured pressure spikes associated with the highest pressures. For the cases with Φ_{exp} and Φ_{CJ} greater than two, there are several reasons why this may occur. In the case of the values based on the experimental pressures, the pressure and strain measurements are not consistent since the strain gauges close to the end wall are not exactly located at the same axial distance as the pressure transducers and the two sets of gauges are on opposite sides of the tube. In the case of values based on the reflected CJ detonation pressures, the effective applied pressure may be higher than this value due to pre-compression of the gas closest to the end flange. In addition, DDT is a localized event and the point measurements of pressure and strain do not represent either average or bounding values. The DDT event is unlikely to occur on the tube axis so that the pressure measured on one side of the tube will not be consistent with the strain measured on the opposite side of the tube. Furthermore, the critical traveling load speed (Beltman and Shepherd, 2002) for the thick-walled tube is on the same order of the ideal detonation velocity, which may also result in higher dynamic load factors.

For the annular gap (see Table 4), the dynamic load factor tended to be larger for higher P_0. This may be associated with the detonation propagation modes. Previous studies in Manzhalei (1999) have shown it is possible to obtain low velocity detonations (less than U_{CJ}) in smooth narrow channels when P_0 was small, due to the competition of the chemical energy release and the effects of friction. Decreasing detonation velocity leads to decreasing post-shock pressure (peak pressure), hence decreasing the peak strain. In the current tests, when $P_0 \leq 3$ bar, all the values of Φ_{exp} were less than or equal to 1 for the three mixtures. At $P_0 = 3.5$, Φ_{exp} reached a value close to 2; $1.2 \leq \Phi_{CJ} \leq 2.2$. The dynamic load factors of the annulus configuration are less than the empty tube. One reason is that the gas volume for the annular gap is only 7.5% of the empty tube so that the total energy released in the combustion event is much smaller in the annulus than in the empty tube. Another reason is that DDT was initiated promptly for the annulus configuration, so the detonation was approximately an ideal CJ wave when it propagated to the tube end, while for the empty tube, the detonation wave was highly overdriven due to the DDT event.

4.2 Estimated strain for thick tube

In general, DDT is a localized event and point measurements of pressure and strain do not represent either average or bounding values. The DDT event is unlikely to occur on the tube axis so that the pressure measured on one side of the tube will not be consistent with the

Table 3: Dynamic load factors for configuration 1 (empty tube) and mixture A.

shot	P_0 (bar)	P_{CJ} (MPa)	P_{max} (MPa)	S_{max} (μstrain)	Φ_{exp}	Φ_{CJ}
1	2	3.836	3.149	60	2.04	1.72
3	2.5	4.832	3.737	77	2.22	1.75
5	2.6	5.032	12.884	144	1.20	3.12
4	2.75	5.332	7.036	168	2.56	3.45
2	3.0	5.834	13.463	164	1.31	3.07

Table 4: Dynamic load factors for configuration 2a (concentric solid bar).

shot	P_0 (bar)	P_{CJ} (MPa)	P_{max} (MPa)	S_{max} (μstrain)	Φ_{exp}	Φ_{CJ}
mixture A						
13	1	1.872	2.46	19	0.83	1.15
12	1.5	2.848	4.275	31.2	0.78	1.22
11	2	3.836	9.244	58.2	0.68	1.67
14	2.5	4.832	8.795	85.8	1.05	1.95
15	3	5.834	7.597	73.6	1.04	1.38
24	3.5	6.841	6.126	94	1.65	1.50
mixture B						
16	1.5	2.569	3.685	27.3	0.79	1.19
18	2.5	4.579	5.814	44.3	0.82	1.06
19	3.5	6.589	9.057	135.5	1.61	2.24
mixture C						
20	2	3.729	7.706	45.9	0.64	1.36
21	2.5	4.752	8.202	83.6	1.09	1.93
22	3.5	6.777	7.82	135.7	1.86	2.18

strain measured on the opposite side of the tube. In addition, there are often no measured peak pressure values available for engineering estimations. In this case, it is desirable to use an approximate dynamic load factor and the computed P_{CJ} for estimation of the peak strains.

In Fig. 8, the measured strains are compared with estimated strains based on P_{CJ} with dynamic load factors of 1 (impulse loading), 2 (sudden loading) and 5 (reflected detonation). For the empty tube within the DDT range ($P_0 \geq 2.6$ bar, Fig. 8a), the maximum measured strains are all larger than $\epsilon_{CJ,\ \Phi=2}$. We believe that this is because DDT occurred close to the tube end, producing much higher strains than the case where detonation was initiated promptly. However, the peak strains are bounded by using $\epsilon_{CJ,\ \Phi=5}$, which corresponds to a reflected detonation.

For the annular gap, as shown in Fig. 8b-d, the maximum measured strains are smaller than $\epsilon_{CJ,\ \Phi=2}$ for three mixtures and only slightly exceeded at $P_0 = 3.5$ bar for mix B and C. We conclude that $\Phi = 2$ and ΔP_{CJ} are appropriate for estimating peak strains in the annular configurations.

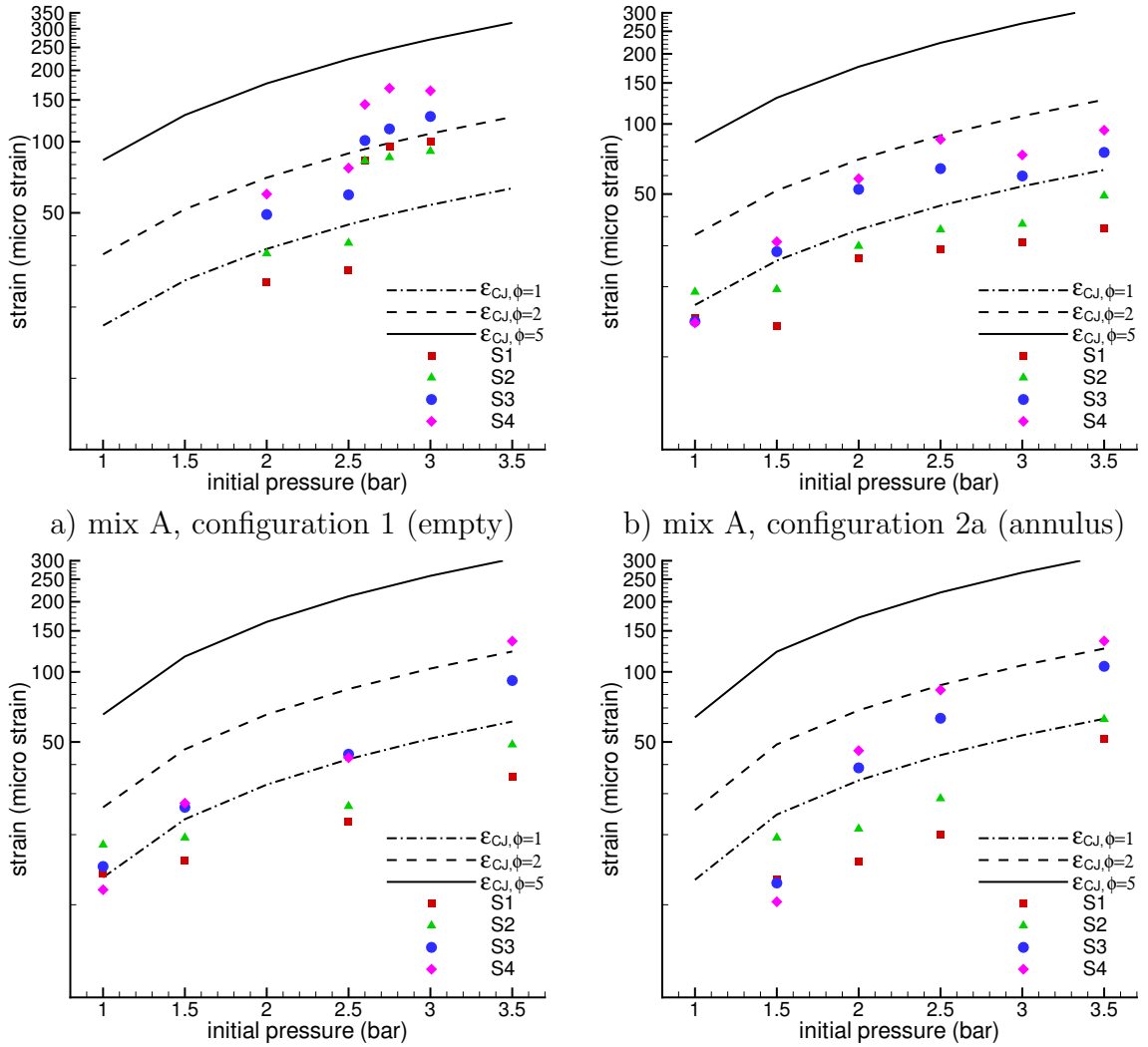

a) mix A, configuration 1 (empty)

b) mix A, configuration 2a (annulus)

c) mix B, configuration 2a (annulus)

d) mix C, configuration 2a (annulus)

Figure 8: Comparison between the measured strains (S_1-S_4) and the estimated strain (ϵ_{CJ}) based on P_{CJ} and $\Phi = 1$, 2 and 5.

4.3 Estimated strain for 3013 cans

Figure 9 and Table 5 describe the estimated strains for 3013 cans using P_{CJ} and $\Phi = 1$, 2 and 5. A strain value below 2000 μstrain (0.2%), is usually considered to be elastic deformation.[2]

[2]In a ductile material like stainless steel, the onset of yielding is gradual and there is no well defined yield point so that the choice of 0.2% as the onset of plastic deformation is arbibtrary but a long established

When P_0 is above 2 bar for any mixture, the estimated strain ϵ_{CJ} based on $\Phi = 5$ approaches the plastic deformation region. For the 3013 outer can (no inner can) tests, we expect plastic deformation may appear for $P_0 > 2.6$ bar. From the results of the annular thick-tube tests, the peak strain is bounded by ϵ_{CJ} based on $\Phi = 2$. Using this, the estimated maximum strain at $P_0 = 3.5$ bar, green lines shown in Fig. 9, is below 1500 μstrain (0.15%) for the three mixtures, so only elastic deformation is predicted to occur. Even in exceptional cases, the strains are bounded by $\Phi = 5$ so that the worst possible cases would be mix A at high pressure, and strains may slightly exceed 0.2%. Note that after plastic deformation is initiated, the elastic estimates are no longer valid, which is why we have shown these estimates as dashed lines in Fig. 5 for $\epsilon > 2000$ μstrain.

Table 5: Estimated strain for 3013 outer cans using $\Phi = 1$, 2 and 5, and computed CJ pressure P_{CJ}..

P_0	P_{CJ}	$\epsilon_{CJ,\ \Phi=1}$	$\epsilon_{CJ,\ \Phi=2}$	$\epsilon_{CJ,\ \Phi=5}$
(bar)	(MPa)	μstrain		
mixture A				
1	1.872	174.1	348.1	870.3
1.5	2.848	269.9	539.9	1349.7
2	3.836	367.0	734.0	1834.9
2.5	4.832	464.8	929.6	2324.1*
3	5.834	563.2	1126.5	2816.2*
3.5	6.841	662.2	1324.3	3310.8*
mixture B				
1	1.491	136.6	273.3	683.2
1.5	2.569	242.5	485.1	1212.6
2	3.578	341.6	683.3	1708.2
2.5	4.579	440.0	879.9	2199.8*
3	5.582	538.5	1077.0	2692.4*
3.5	6.589	637.4	1274.8	3187.0*
mixture C				
1	1.453	132.9	265.8	664.5
1.5	2.69	254.4	508.8	1272.1
2	3.729	356.5	712.9	1782.4
2.5	4.752	457.0	913.9	2284.8*
3	5.762	556.2	1112.3	2780.9*
3.5	6.777	655.9	1311.7	3279.4*
*Not reliable, indicates plastic deformation.				

practice.

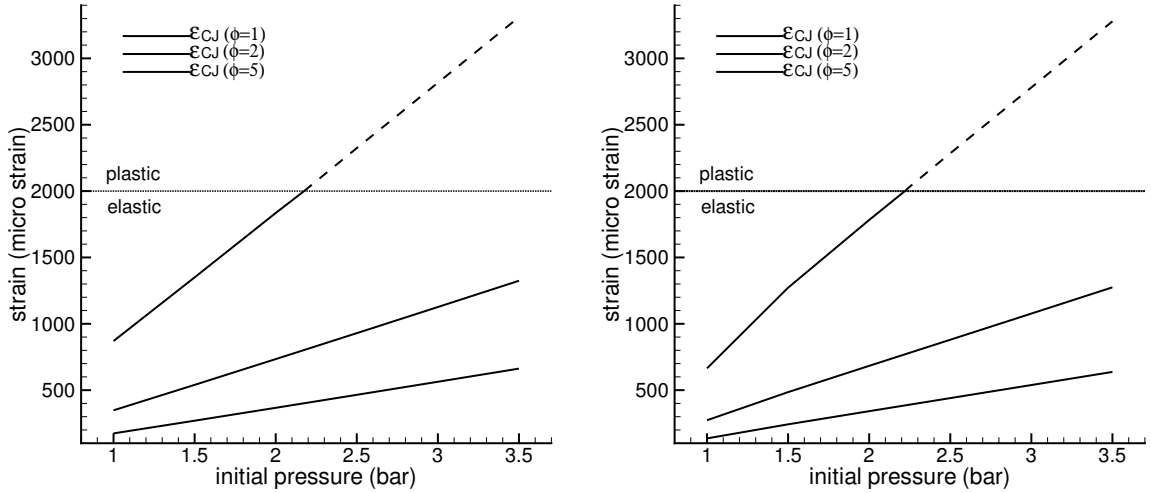

a) mix A

b) mix B

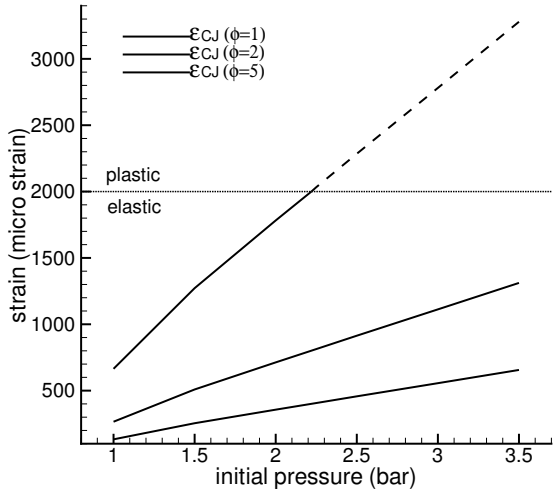

c) mix C

Figure 9: Estimated strain for 3013 outer cans based on P_{CJ} in terms of dynamic load factors of 1, 2 and 5.

5 Impulse

One of the methods used to characterize pressure-time histories for structural analysis (Biggs, 1964, Paz and Leigh, 2004) is by the impulse, which can be visualized as the area under the pressure-time curves. If the pressure transient is sufficiently short in duration so that the structure does not move appreciably during the loading duration, the subsequent structural motion is a unique function of the impulse. In this section, we explore the possibility of using impulse-based structural analysis to predict the peak strains in the test fixtures and cans. We will show that although the simplest approaches based on purely impulsive loading (Method I) are not appropriate, a more realistic approach (Method II) based on a mixed impulsive and suddenly applied constant load, is successful.

5.1 Method I

The impulse per unit area over a time interval is defined as

$$I = \int_{t_{start}}^{t_{end}} P(t)dt, \tag{3}$$

where t_{start} and t_{end} determine the integration period. The signals from the pressure transducers can be used to compute the integral with numerical methods; for example, by using the trapezoidal rule.

If the load is purely impulsive in nature (we will return to this requirement subsequently), then we can compute the peak strain by equating the initial kinetic energy $\mathcal{K}$ to the peak strain energy $\mathcal{S}_e$

$$\mathcal{K} = \mathcal{S}_e, \quad \text{or} \quad \frac{I^2}{2\rho h} = \frac{1}{2}\frac{Eh}{1-\nu^2}\epsilon_{max}^2 \ , \tag{4}$$

which shows that the peak strain depends linearly on the impulse in this limit

$$\epsilon_{max} = \sqrt{\frac{1-\nu^2}{Eh^2\rho}}I \ . \tag{5}$$

Figure 10 shows an example of the pressure trace of shot 5 (configuration 1, empty tube, mix A) and the corresponding computed impulse using Eq. 3. The first peak of the pressure signal corresponds to the incident detonation wave and the subsequent series of peaks are associated with the shock waves created by the initial detonation. The impulse has been computed as a function of $t = t_{end}$ with $t_{start} = 0$. The impulse does not equal a definite value but increases approximately linearly with time as the pressure does not return to zero but remains positive since the time scale for cooling is much greater than the observing time

of 2 ms.

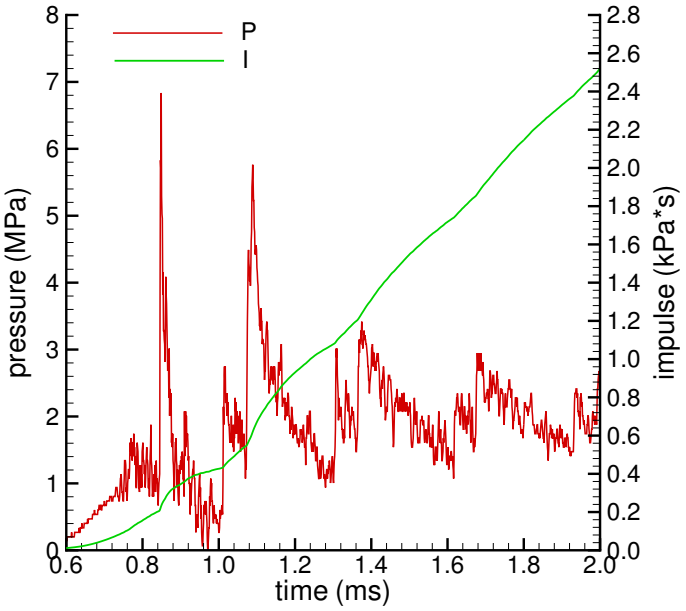

Figure 10: Pressure trace P_4 for shot 5 and the corresponding impulse I.

In order to obtain a finite impulse, we have to arbitrarily restrict the duration of the integration. To illustrate the results, we have taken t_{start} to be the detonation arrival time and the time interval, $t_{end} - t_{start}$, equal to the tube radial vibration period of 90 μs. Table 6 illustrates the computed impulse using the pressure data from configuration 2a (annulus) and the corresponding estimated strains. The estimated strains are similar to the measured values. For example, for configuration 2a (annulus) and mix A at $P_0 = 3.0$ bar, the maximum measured strain is 74 μstrain, and the estimated strains vary between 83 and 154 μstrain.

However, the predicted maximum strain values are quite sensitive to the choice of the integration interval. Since the integration interval is arbitrary and there is no obvious way to remove this limitation, there cannot be a well-defined impulse value and a more realistic model must be considered. The key to improving the model is to note that the experimental results show an initial impulse but then this is followed by an approximately constant pressure.

5.2 Method II

If we adopt a more realistic model for the loading function, then in order to compute the resulting structural response, we need to consider the equation of motion of the structure. The simplest way to do this is to consider only the radial motions and to treat these with a simplified mechanical model. The single degree of freedom model (SDOF) is the standard

Table 6: Estimated strains ϵ_1-ϵ_4 for the thick tube using Eq. 3 and computed impulse I_1-I_4 from the corresponding pressure signals P_1-P_4 for configuration 2a.

shot	P_0	I_1	ϵ_1	I_2	ϵ_2	I_3	ϵ_3	I_4	ϵ_4	τ_{CJ}
	(bar)	kPa · s	μstrain	kPa · s	μstrain	kPa · s	μstrain	kPa ·s	μstrain	μs
mixture A										
13	1	0.037	21.3	0.039	22.5	0.050	29.0	0.076	44.4	26.9
12	1.5	0.062	36.2	0.071	41.1	0.090	52.1	0.124	71.9	30.4
11	2	0.057	33.3	0.097	56.6	0.117	67.8	0.159	92.8	28.1
14	2.5	0.080	46.6	0.111	64.4	0.147	85.4	0.146	84.9	25.0
15	3	0.164	95.5	0.142	82.9	0.219	127.4	0.265	154.0	33.9
24	3.5	0.182	105.7	0.189	109.8	0.249	144.9	0.212	123.1	30.4
mixture B										
16	1.5	0.066	38.4	0.060	34.7	0.053	30.8	0.140	81.4	31.0
18	2.5	0.071	41.6	0.124	72.1	0.161	93.8	0.198	115.4	30.3
19	3.5	0.142	82.6	0.182	105.6	0.213	123.7	0.236	137.5	29.3
mixture C										
20	2	0.117	67.9	0.073	42.3	0.118	68.6	0.202	117.5	34.1
21	2.5	0.160	93.0	0.113	65.8	0.182	106.1	0.249	144.8	37.0
22	3.5	0.143	83.3	0.166	96.6	0.215	124.8	0.266	155.0	29.1

approach used by the structural analysis community. SDOF models are discussed in great detail by Biggs (1964) [Chap. 2] for a variety of forcing functions and specifically for high explosives in spherical vessels by (Duffey and Mitchell, 1973, Part 1). Some essential results for a single type of forcing function, the rectangular pulse, were sketched out in Pintgen and Shepherd (2006). The forcing function represented by a rectangular impulse followed by a step or sudden load is discussed in the following.

Assuming radially symmetric and axially uniform loading of an infinite tube structure corresponds to a SDOF model where only radial displacement x of the thin shell structure is permitted, Fig. 11. This loading condition is identical to a circular ring under uniform internal radial pressure. The radial deflection can be modeled as a forced harmonic oscillator

$$\frac{\partial^2 x}{\partial t^2} + \omega^2 x = \frac{P(t)}{\rho h} \,, \tag{6}$$

where the oscillator natural frequency (radian/s) is

$$\omega = \sqrt{\frac{\bar{k}}{\bar{m}}} \tag{7}$$

in terms of the reduced mass $\bar{m} = \rho h$ and the reduced stiffness $\bar{k} = Eh/R^2(1-\nu^2)$.

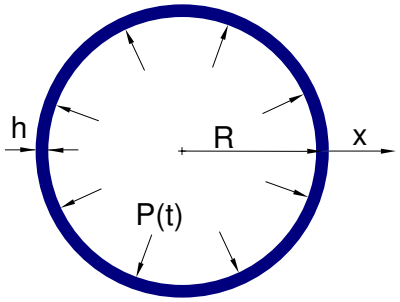

Figure 11: Single degree of freedom model of cylindrical tube structure; radius R, internal pressure $P(t)$, wall thickness h, and radial displacement x.

A program was written using MATLAB to numerically solve the equation of motion of the SDOF model, Eq. 6, for an arbitrary forcing function $P(t)$.

5.3 Estimated strain with measured pressure

As an example, Fig. 12 shows the computed strain history obtained by solving Eq. 6 with the measured pressure trace P_3 for shots 14 and 24 (see Appendix F). The strain trace S_1 is also plotted for comparison because P_3 and S_1 are located at the same distance from the igniter location. For both shots, the estimated peak strains are larger than the peak values recorded on S_1, but smaller than the ones on S_4 (Appendix F).

Figure 13, Tables 7, and 8 compare the measured peak strains for configurations 1 and 2a with the maximum estimated strains by solving Eq. 6 with the measured pressure signals. For configuration 1, the estimated values of strain are all smaller than the measured values. For the slow flame cases ($P_0 < 2.6$ bar), this is because the thermal effect produces much higher measured strains than would be predicted on the basis of pressure alone. For the DDT cases ($P_0 \geq 2.6$ bar), transition occurred close to tube end due to shock reflection, and the load was localized (asymmetric) near the strain gauges in some cases. This generated much higher peak strains (up to a factor of two) than are predicted from the pressure measurements.

For configuration 2a, when $P_0 > 2$ bar, the estimated values are all smaller than the measured ones. There are several reasons why the simple SDOF model may not always reproduce the measured strain histories. The simplest explanation is that the pressure measured on one side of the tube is not consistent with the strain measured on the opposite side of the tube. Another issue is that the annular gap was not uniform around the tube, as shown in Appendix C. Finally, the SDOF model will not be able to represent the effects of the end flanges or the possible resonant response of the tube to the traveling load aspects of the detonation.

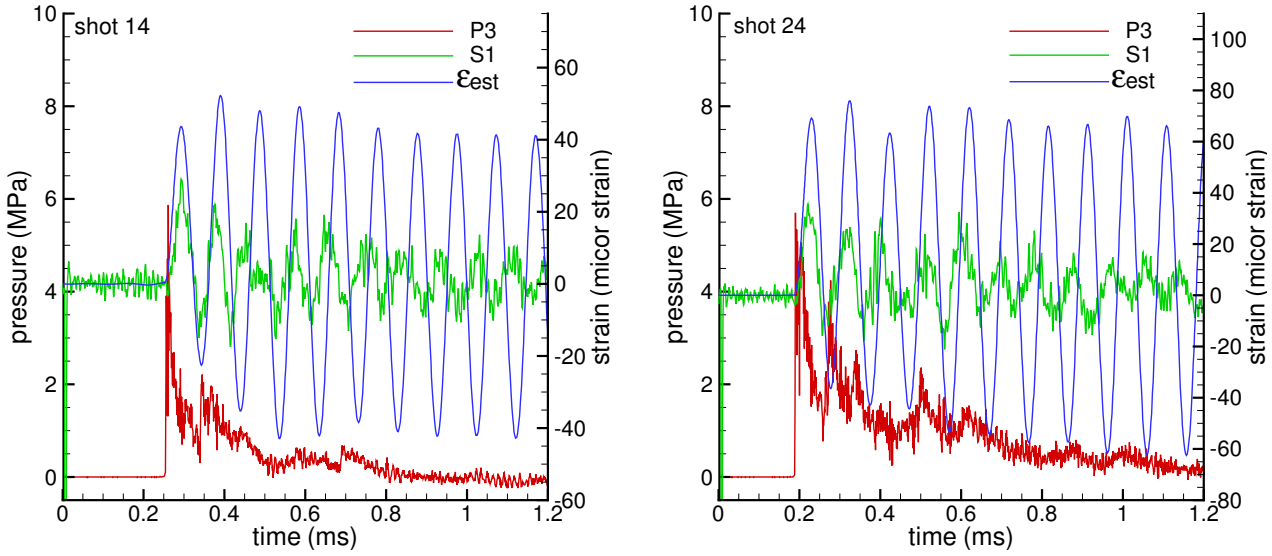

a) Shot 14 ($P_0 = 2.5$ bar) b) Shot 24 ($P_0 = 3.5$ bar)

Figure 12: Comparison between the measured strain (S_1) and the computed strain (ϵ_{est}) obtained by solving Eq. 6 with the measured pressure signal P_3 for shots 14 and 24.

Table 7: Measured maximum strains S_1-S_4 and estimated maximum strains $\epsilon_{1,max}$-$\epsilon_{4,max}$ obtained by solving Eq. 6 with the measured pressure signals P_1-P_4 for configuration 1 (empty) and mix A. For shot 2, the value of $\epsilon_{2,est}$ was large because the pressure signal was noisy due to the effect of loosened cables (see Fig. 21c). Therefore the maximum value $\epsilon_{1,est}$=106 μstrain was shown in Fig. 13a.

shot	P_0	$S_{1,max}$	$S_{2,max}$	$S_{3,max}$	$S_{4,max}$	$\epsilon_{1,est}$	$\epsilon_{2,est}$	$\epsilon_{3,est}$	$\epsilon_{4,est}$
	(bar)	(μstrain)							
1	2.0	25.5	33.7	49.2	60.0	24.1	27.7	31.0	26.7
3	2.5	28.6	37.3	59.6	77.3	31.5	47.8	34.6	36.6
5	2.6	83.0	83.1	101.1	143.6	56.2	71.7	92.7	53.0
4	2.75	95.0	85.8	113.1	168.0	66.5	79.0	94.0	49.9
2	3.0	99.6	91.1	127.7	164.0	106	156.3*	78.6	72.6

5.4 Estimated strain with P_{CJ} and P_{CV}

Instead of the experimental pressures, we can use a very simple model that is a mix of an initial impulse to model the first peak followed by a constant pressure to simulate the pressurization by the hot combustion products. We ignore all the shock waves and do not treat any of the other features that are present in the experimental pressure traces. Our goal is to develop a simplified but still realistic representation of the loading function.

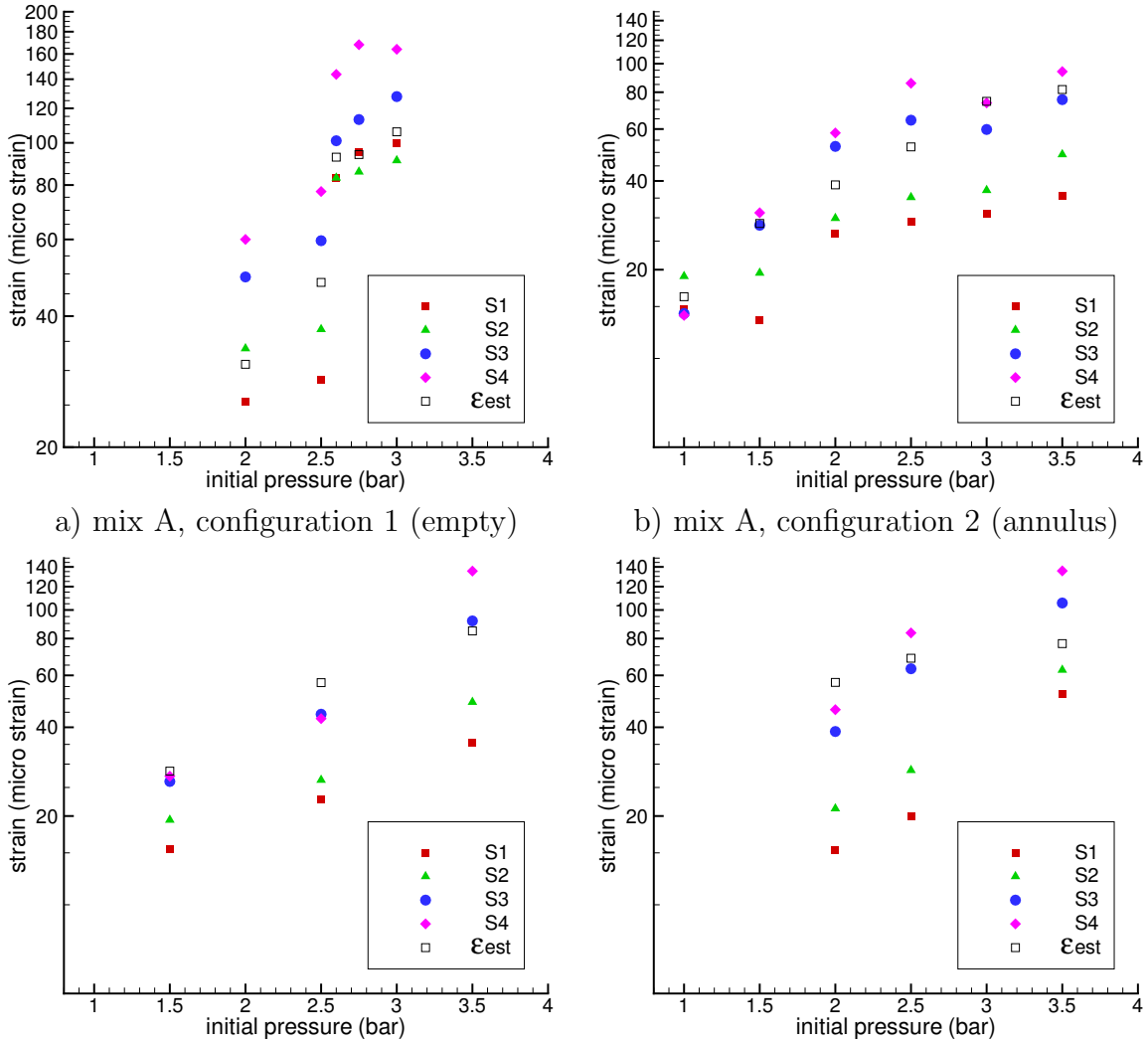

a) mix A, configuration 1 (empty)

b) mix A, configuration 2 (annulus)

c) mix B, configuration 2 (annulus)

d) mix C, configuration 2 (annulus)

Figure 13: Measured maximum strains S_1-S_4 and estimated maximum stain ϵ_{exp} obtained by solving Eq. 6 with the measured pressure signals for a) configuration 1 (empty tube), b), c), d) configuration 2a (annulus).

We have modeled the forcing function as

$$P(t) = \begin{cases} P_0 & t \leq 0 \\ P_{CJ} & 0 < t \leq \tau \\ P_{CV} & t > \tau \end{cases} \tag{8}$$

where τ is the rectangular pulse width, P_{CJ} is used to represent the peak pressure in the impulse loading, and P_{CV} is used to represent the subsequent constant pressure in the "tail" of the pressure transient. The pulse width τ_{CJ} was selected to give the same impulse as observed experimentally for the first pressure pulse, which is associated with the detonation.

Table 8: Measured maximum strains S_1-S_4 and estimated maximum strains $\epsilon_{1,max}$-$\epsilon_{4,max}$ obtained by solving Eq. 6 with the measured pressure signals P_1-P_4 for configuration 2a (annulus).

shot	P_0	$S_{1,max}$	$S_{2,max}$	$S_{3,max}$	$S_{4,max}$	$\epsilon_{1,est}$	$\epsilon_{2,est}$	$\epsilon_{3,est}$	$\epsilon_{4,est}$
	(bar)	(μstrain)							
mixture A									
13	1.0	14.7	19.0	14.2	14.0	11.0	12.8	16.2	14.1
12	1.5	13.5	19.5	28.3	31.2	21.0	21.0	28.7	23.9
11	2.0	26.5	29.9	52.4	58.2	27.8	34.5	38.8	33.7
14	2.5	29.0	35.2	64.3	85.8	33.9	38.8	52.2	41.0
15	3.0	30.9	37.2	59.8	73.6	70.6	74.5	71.8	60.0
24	3.5	35.7	49.2	75.5	94.0	66.7	81.7	75.9	65.6
mixture B									
16	1.5	15.5	19.4	26.2	27.3	11.9	18.9	12.5	28.4
18	2.5	22.7	26.5	44.3	42.8	29.9	51.8	56.7	41.1
19	3.5	35.4	48.7	91.8	135.5	80.0	56.8	84.9	58.5
mixture C									
20	2.0	15.3	21.2	38.7	45.9	24.6	21.7	34.2	56.8
21	2.5	20.0	28.6	63.2	83.6	31.7	53.8	68.6	46.0
22	3.5	51.8	62.6	105.6	135.7	58.7	64.3	76.9	54.6

The value of τ is computed by dividing the 90-μs impulse value I computed in the previous section with P_{CJ}. The results are given in the last column of Table 6 and we can see that average value of τ for all cases is approximately 30 μs.

Figure 14 illustrates the model pressure history for $P_0 = 2.0$ bar, mixture A and $\tau = 30$ μs. The corresponding strain profile is given by the solution of Eq. 6 with the pressure profile of Eq.8. The computed maximum strain is approximately 64 μstrain, which is close to the maximum measured value, 58 μstrain.

Figure 15a shows the computed peak strain as function of τ/T from the solution of Eq. 6 for mixture A at $P_0 = 1$, 2 and 3 bar. When τ/T approaches zero, the pressure function becomes a step load P_{CV}, and the estimated strain decreases to a minimum value. When $\tau > 0.5T$, ($T = 2\pi/\omega$ is the oscillation period of the structure) the pressure function is dominated by the rectangular pulse P_{CJ}, and the estimated strain reaches a maximum value. Figure 15b shows the DLF Φ_{CJ} and Φ_{CV} as a function of τ/T using Eq. 2, where ϵ_{max} is the computed strain shown in Figure 15a for $P_0 = 2$ bar, and $\Delta P = P_{CJ} - P_a$ for Φ_{CJ}, and $P_{CV} - P_a$ for Φ_{CV}.

The DLF is a monotonic function of τ/T. For long pulses, $\tau > 0.5T$, $\Phi_{CJ} \to 2$ and $\Phi_{CV} \to 4$, independent of τ. For short pulses, $\tau < 0.4T$, the DLF decreases with decreasing

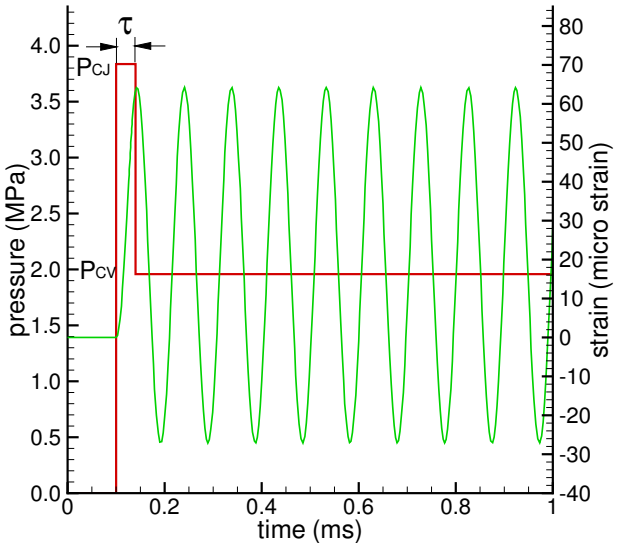

Figure 14: Defined pressure load and computed strain history for $P_0 = 2.0$ bar, mix A, $\tau = 30$ μs ($\tau/T = 0.33$).

pulse duration, this is the impulsive regime. When $\tau = 0$, $\Phi_{CV} \rightarrow 2$ and $\Phi_{CJ} \rightarrow 1$, as expected. For $P_0 = 1$ and 3 bar, Φ_{CV} and Φ_{CJ} have almost the same values as $P_0 = 2$ bar, so these results are not shown here.

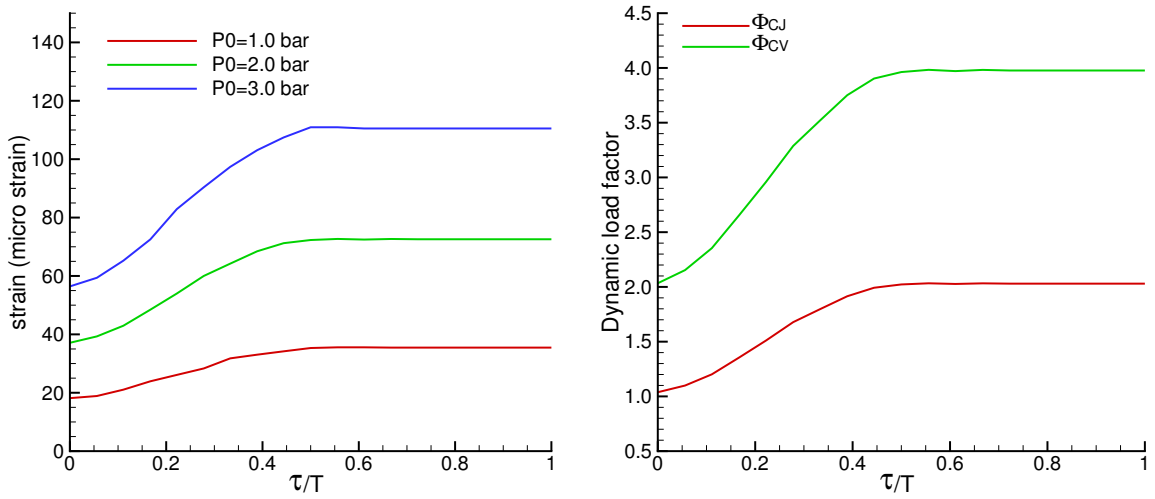

a) b)

Figure 15: a) Maximum estimated strain as a function of pulse duration τ for mix A and $P_0 = 1$, 2 and 3 bar, computed by solving Eq.6 with the defined pressure function of Eq. 8; b) dynamic load factors using the strain values in a) for $P_0 = 2$ bar.

Figure 16 compares the measured and the computed peak strains from the solution of Eq. 6 with the pressure model of Eq. 8 and $\tau = 30$ μs. For all the mixtures, the computed

strains show the same trend as the measured values with increasing P_0. The maximum measured strains are smaller than or equal to ϵ_{est} for almost all cases and are only slightly exceeded at $P_0 = 3.5$ bar for mix B and C. We conclude that impulse method II is appropriate for estimating the upper bound on the peak strains in the annular configurations.

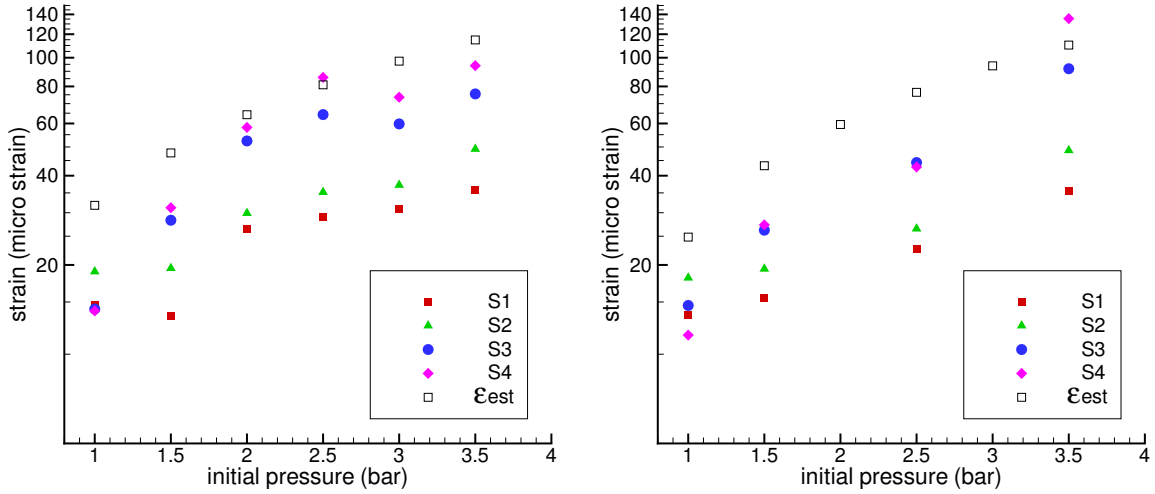

a) mix A

b) mix B

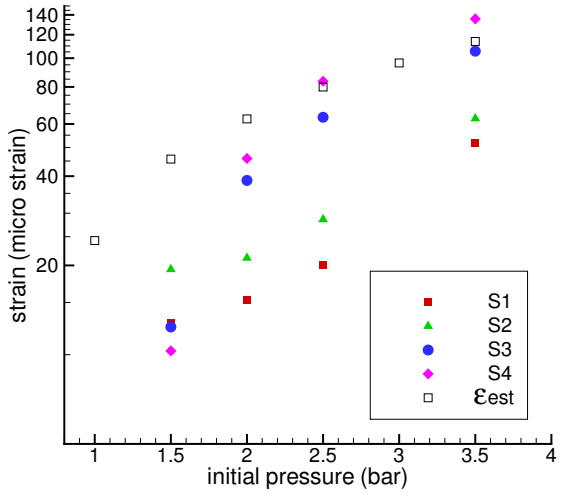

c) mix C

Figure 16: Comparison between the measured strain ($S_1 - S_4$) and the maximum computed strain (ϵ_{est}) from the solution of Eq. 6 with the pressure function of Eq 8 and $\tau = 30$ μs. Configuration 2a - concentric annulus.

5.5 Estimated strain for 3013 cans

Figure 17 and Table 9 describe the estimated strain ϵ_{model} for 3013 cans from the solution of Eq. 6 with the defined pressure load of Eq. 8. The estimated strain, $\epsilon_{CJ,\Phi=2}$, using $\Phi = 2$

and P_{CJ}(appropriate for the annular gap), is also plotted for comparison. The values of ϵ_{model} is very close to but slightly larger than the values of $\epsilon_{CJ,\Phi=2}$ for all three mixtures. With increasing P_0, the trend for strains estimated by both methods is identical, and the maximum strain is still in elastic regime for $P_0 < 3.5$ bar.

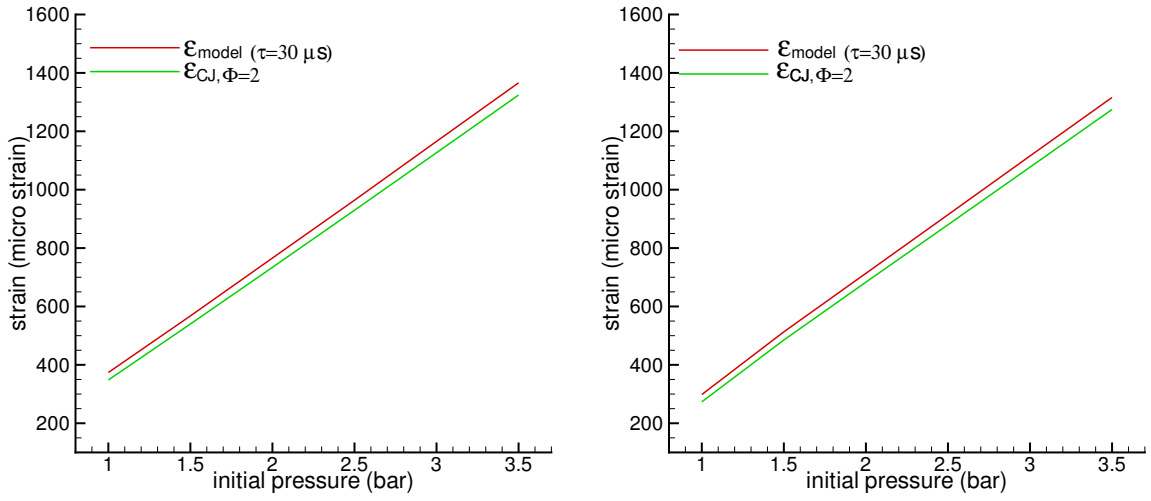

a) mix A

b) mix B

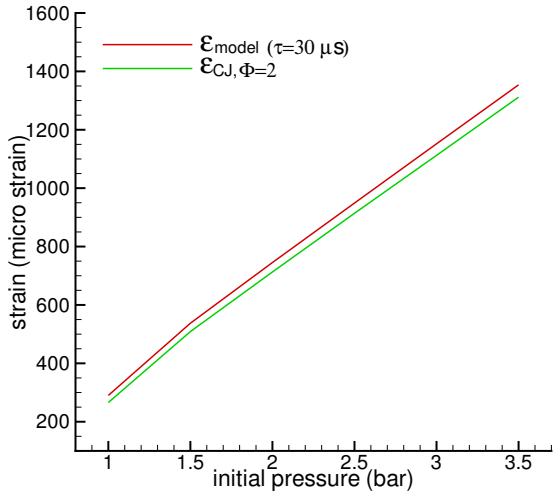

c) mix C

Figure 17: Estimated strain for 3013 outer cans; red lines are given by the solution of Eq. 6 with the pressure load of Eq. 8 and $\tau = 30$ μs; green lines are given by DLF model using P_{CJ} and $\Phi = 2$. Appropriate for explosions in the annular gap region.

Table 9: Estimated maximum strain for 3013 outer cans from the solution of Eq. 6 with the pressure load of Eq. 8 and $\tau = 30$ μs. Appropriate for explosions in the annular gap region.

P_0 (bar)	P_{CV} (MPa)	P_{CJ} (MPa)	ϵ_{max} μstrain
mixture A			
1.0	0.956	1.872	373.8
1.5	1.454	2.848	567.6
2.0	1.958	3.836	765.9
2.5	2.466	4.832	963.9
3.0	2.978	5.834	1165.5
3.5	3.492	6.841	1366.1
mixture B			
1	0.766	1.491	298.3
1.5	1.316	2.569	513.1
2	1.831	3.578	713.5
2.5	2.341	4.579	914.1
3	2.853	5.582	1115.5
3.5	3.366	6.589	1316.0
mixture C			
1	0.742	1.453	290.2
1.5	1.375	2.69	537.3
2.0	1.905	3.729	745.3
2.5	2.426	4.752	949.0
3	2.941	5.762	1151.9
3.5	3.459	6.777	1353.9

6 Summary

Our findings can be summarized as follows:

1. When the tube was empty (no insert), the DDT threshold was observed at $P_0 = 2.6$ bar for mix A, and all the transitions occurred close to the tube end for $2.6 \leq P_0 \leq 3.5$ bar. The maximum strain was also observed close to the tube end. The dynamic load factor Φ_{exp} in DDT region was about 2-2.5 in terms of the measured pressure, the dynamic load factor Φ_{CJ} was between 3-3.5 in terms of P_{CJ}. For mix B and C, no DDT transition was observed for $P_0 \leq 3.5$ bar.

   These transition thresholds are consistent with the preliminary experiments carried out at Caltech (Liang et al., 2006).

2. For the concentric annular gap of 0.08 in, the DDT threshold was P_0 =1.0 bar for mix A, between 1.0 and 1.5 bar for mix B, and between 1.5 and 2.0 bar for mix C. The maximum hoop strain was measured to occur near the tube end. The dynamic load factorΦ_{exp} was close to 1 and Φ_{CJ} was about 2.

   These transistion thresholds are consistent with the planar gap tests carried out at Caltech with these mixtures.

3. The size of the end gap (between the end surface of the solid bar and the interior surface of the ignition flange) has no noticeable influence on DDT threshold or the peak strain.

   This is reasonable since we have already seen from the planar gap experiments that the transition to detonation pressure thresholds for the annular gap height (0.08 in) are equal to (0.08 in end gap) or much lower (0.5 in end gap) than those of the end gap.

4. The eccentricity of the tube insert resulted in different DDT transition behavior at different annular locations. This is consistent with the previous finding that the smaller the gap size is, the smaller the DDT transition distance at the same pressure. However the peak hoop strain was similar for eccentric and concentric cans.

   These results indicate that for the purposes of structural response evaluation, the eccentricity of the gap is not an important factor.

5. The estimated strains using P_{CJ} and $\Phi = 2$ show reasonable agreement with the measured values for all three mixtures in annular configurations. A dynamic load factor of $\Phi = 2$ and ΔP_{CJ} are appropriate for estimating the upper bound for the peak

hoop strains from explosions in the annular gap region between the outer and inner cans.

6. The estimated strains obtained by solving Eq. 6 with the pressure function of Eq. 8 and a pulse width $\tau = 30$ μs also show good agreement with the measured values for the annulus configuration 2a.

   The SDOF model with a simple model of the pressure history that combines an initial impulse with subsequent constant pressure is appropriate for estimating peak hoop strains for explosions in the annulus between the outer and inner 3013 cans.

7. For an empty can, the peak hoop strains are higher than for the annulus configurations. The structural response for the empty can may be bounded by using a dynamic load factor of $\Phi_{CJ} = 5$.

7 Implications for Safety Assessment

In Part II of the test program, we have examined DDT transition and structural response of a model of the 3013 outer can with and without inserts simulating the inner can. We have shown that the DDT transition thresholds within the annular gap of 0.08 in (2.03 mm) are consistent with our studies performed in Part I with the planar gap fixture. We conclude that it is definitely possible for DDT to occur in the annular region at sufficiently high pressures for all three mixtures.

The hoop strain of the thick-tube fixture were measured in the tests. Two methods were examined for using estimates of the pressure loading to predict peak strain. The first method used an assumed dynamic load factor (DLF) and a step-function CJ pressure load and the second method used a mixed impulsive-step load function and a SDOF model.

For the dynamic load factor method, we used the computed CJ pressure and bounding dynamic load factors Φ of either 2 or 5 to estimate the maximum possible hoop strain. The estimated maximum strains with $\Phi_{CJ} = 2$ show a good agreement with the measured peak strains for the annular configuration when the initial pressure is below 3.5 bar. In the worst case, where DDT occurs close to the tube end for the empty tube, the maximum strain is bounded with $\Phi_{CJ} = 5$.

For the impulse method, we solved the single-degree-of-freedom equation of motion of the structure with a model pressure loading consisting of an initial impulse of P_{CJ} with the pulse width of 30 μs and followed by a constant pressure P_{CV}. The estimated maximum strains from this model also show very good agreement with the measured peak strains.

After developing and testing these methods on our test fixture, we estimated the maximum hoop strains for the 3013 cans and an explosion in the annular region between the inner and outer cans. We predict that for all mixtures, the peak hoop strain will be less than 1500 μstrain when the initial pressure is below 3.5 bar. The two methods give essentially identical results and for the purpose of the safety assessment, the dynamic load factor technique is the easiest to apply.

We conclude that although transition to detonation will occur at sufficiently high initial pressure in the annulus between outer and inner cans, the structural response of the outer can will remain elastic and no permanent deformation or other structural failure of the outer can will occur if an the explosion takes place in the annular region.

The hoop strains in proposed tests with instrumented 3013 outer cans are expected to be higher than the present predictions for the annular configuration since the inner can will not be present in the 3013 outer can tests. Based on the present test results, limited (less than 1%) plastic deformation of the "empty" outer can may occur at initial pressures above 2 bar with Mix A. We expect that this will provide an upper bound on the plastic deformation that is possible in the actual 3013 can system since the loading is less severe when an intact inner can is present.

We have not examined several issues are that related to the inner can.

1. Explosion within inner can.

   a) If an explosion takes place within the inner can, outward deformation of the inner can will occur and the inner can may expand sufficiently to impact the outer can. We have not examined the response of the outer can to mechanical impact from the inner can .

   b) The inner can wall is thinner than the outer can so the extent of plastic deformation will be larger. This should be considered in the final safety assessment. A SDOF plastic deformation model with a model loading function based on the present "empty can" (configuration 1) results should be sufficient to address this issue.

2. Deformation of the inner can due to an explosion in the annulus.

   In the case of an explosion in the annulus, the load will act to crush or buckle the inner can. We have not condsidered this process or the implications.

Bibliography

W.M. Beltman and J.E. Shepherd. Linear elastic response of tubes to internal detonation loading. *Journal of Sound and Vibration*, 252(4):617–655, 2002.

J. Biggs. *Introduction to structural dynamics*. McGraw-Hill, Inc., 1964. ISBN 07-005255-7.

T.A. Duffey and D. Mitchell. Containment of explosions in cylindrical shells. *Int. J. Mech. Sci.*, 15:237–249, 1973.

Z. Liang, J. Karnesky, and J.E. Shepherd. Deflagration-to-detonation transition tests in H_2-O_2-N_2-He mixtures. Technical Report FM2006.004, GALCIT, August 2006. Explosion Dynamics Laboratory Report to Los Alamos National Laboratory.

V.I. Manzhalei. Low-velocity detonation limits of gaseous mixtures. *Combustion, Explosion, and Shock Waves*, 35(3):296–302, 1999.

M. Paz and W. Leigh. *Structural Dynamics*. Springer, fifth edition, 2004.

F. Pintgen and J.E. Shepherd. Structural response to deflagration-to-detonation transition events in a tube. Technical Report FM2005-005, Graduate Aeronautical Laboratories California Institute of Technology, August 2005.

F. Pintgen and J.E. Shepherd. Elastic and plastic structural response of thin tubes to deflagration-to-detonation transition events. Technical Report FM2005-008, Graduate Aeronautical Laboratories California Institute of Technology, January 2006.

W.C. Reynolds. The element potential method for chemical equilibrium analysis: implementation in the interactive program STANJAN. Technical report, Mechanical Engineering Department, Stanford University, 1986.

A Specification and characterization of gas mixture

The specifications of each mixture and the results of computations of peak pressures and reaction zone lengths are given in the tables below. In Tables 10- 12, the first column is the total pressure. In Tables 10- 12, the next three columns give the partial pressure of the components in the initial mixture. The next four columns are the constant volume explosion pressure (P_{CV}), CJ pressure (P_{CJ}), reflected CJ pressure (P_{CJref}) and CJ detonation velocity U_{CJ}. The last column Δ_{CJ} is the ZND reaction zone thickness for a CJ detonation. The static strain corresponding to constant volume (ϵ_{CV}), CJ (ϵ_{CJ}) and reflected CJ (ϵ_{CJref}) pressures were computer from the computed pressure.

Table 10: Mixture A: stoichiometric hydrogen-oxygen.

P_0 (kPa)	P_{H_2} (kPa)	P_{O_2} (kPa)	P_{CV} (MPa)	P_{CJ} (MPa)	P_{CJref} (MPa)	U_{CJ} (m/s)	Δ_{CJ} (mm)
100	66.67	33.33	0.956	1.872	4.602	2840.3	0.042
150	100.00	50.00	1.454	2.848	7.006	2862.7	0.030
200	133.33	66.67	1.958	3.836	9.441	2878.6	0.024
250	166.67	83.33	2.466	4.832	11.895	2890.9	0.021
300	200.00	100.00	2.978	5.834	14.364	2900.9	0.019
350	233.33	116.67	3.492	6.841	16.842	2909.4	0.018

Table 11: Mixture B: hydrogen-oxygen-nitrogen.

P_0 (kPa)	P_{N_2} (kPa)	P_{H_2} (kPa)	P_{O_2} (kPa)	P_{CV} (MPa)	P_{CJ} (MPa)	P_{CJref} (MPa)	U_{CJ} (m/s)	Δ_{CJ} (mm)
100	60	26.67	13.33	0.77	1.49	3.60	1904.3	0.304
150	60	60.00	30.00	1.32	2.57	6.28	2199.6	0.075
200	60	93.33	46.67	1.83	3.58	8.77	2351.2	0.046
250	60	126.67	63.33	2.34	4.58	11.24	2450.4	0.036
300	60	160.00	80.00	2.85	5.58	13.71	2521.5	0.031
350	60	193.33	96.67	3.37	6.59	16.19	2575.5	0.027

Table 12: Mixture C: hydrogen-oxygen-nitrogen-helium.

P_0 (kPa)	P_{N_2} (kPa)	P_{He} (kPa)	P_{H_2} (kPa)	P_{O_2} (kPa)	P_{CV} (MPa)	P_{CJ} (MPa)	P_{CJref} (MPa)	U_{CJ} (m/s)	Δ_{CJ} (mm)
100	16	60	16.00	8.00	0.74	1.45	3.46	2860.4	0.277
150	16	60	49.33	24.67	1.38	2.69	6.57	2997.6	0.051
200	16	60	82.67	41.33	1.91	3.73	9.14	2995.7	0.030
250	16	60	116.00	58.00	2.43	4.75	11.67	3000.1	0.022
300	16	60	149.33	74.67	2.94	5.76	14.16	2985.8	0.019
350	16	60	182.67	91.33	3.46	6.78	16.67	2983.2	0.017

Table 13: Computed static strain. The unit for strain is micro strain.

P_0	mix A			mix B			mix C		
(kPa)	ϵ_{CV}	ϵ_{CJ}	ϵ_{CJref}	ϵ_{CV}	ϵ_{CJ}	ϵ_{CJref}	ϵ_{CV}	ϵ_{CJ}	ϵ_{CJref}
100	8.1	16.7	42.4	6.3	13.1	33.0	6.1	12.8	31.6
150	12.8	25.9	65.1	11.5	23.3	58.2	12.0	24.4	61.0
200	17.5	35.2	88.0	16.3	32.8	81.7	17.0	34.2	85.3
250	22.3	44.6	111.2	21.1	42.2	105.0	21.9	43.9	109.1
300	27.1	54.0	134.5	26.0	51.7	128.3	26.8	53.4	132.5
350	32.0	63.5	157.8	30.8	61.2	151.7	31.7	62.9	156.2

B Characterization of thick-walled tube and 3013 cans

The axi-symmetric radial vibrations of long cylindrical tubes (axially unconfined) have a fundamental frequency of

$$f = \frac{1}{2\pi R}\sqrt{\frac{E}{\rho(1-\nu^2)}}, \tag{9}$$

where R is the average radius of the tube, $R = (OD - h)/2$, E is the modulus of elasticity, ρ is the density and ν is Poisson's Ratio. This is the characteristic frequency with which we expect to observe oscillations in the strain signals.

When the transit time through the wall of the tube of thickness h is much less than the period of oscillation of the radial mode of the tube, the radial deflections of the tube can be described as a simple forced harmonic oscillator.

For a travelling load like a detonation, the peak structural deflection can be predicted as a function of wave speed - the lowest critical speed V_{c0}, which corresponds to the group velocity of flexural waves that consist of coupled radial-bending oscillations. There is a closed form for the first critical speed V_{c0} (Beltman and Shepherd, 2002), which is useful for estimation

$$V_{c0} = \sqrt{\frac{Eh}{\rho R}}\left(\frac{1}{3(1-\nu^2)}\right)^{1/4} \tag{10}$$

According to the previous studies of Beltman and Shepherd (2002), the dynamic load factor Φ is close to 1, i.e. close to static loading, when the internal loading travels slower than V_{c0}, and Φ is close to 2 when detonations travels faster than V_{c0}, but when the load speed is close to V_{c0}, Φ has a peak value as high as 3 to 4. In the current tests, $U_{CJ} > 2000$ m/s for all cases. For the thick-walled tube, we expect $\Phi > 2$ since $V_{c0} = 2865$ m/s is very close to U_{CJ}, but for 3013 cans, $V_{c0} = 864$ m/s is much less than U_{CJ}, therefore Φ is expected to have a maximum value on the order of 2. The actual value of Φ can be less than the value quoted, depending on the duration of the Taylor wave following the detonation.

Table 14 lists the parameters and fundamental frequency for the thick-walled tube and the 3013 cans.

Table 14: Fundamental frequency for the aluminium and steel tubes.

Tube	E (GPa)	ν	ρ (kg/m^3)	ID (in)	h (in)	R (in)	f (kHz)	T (μs)	V_{c0} (m/s)
thick-walled tube	207	0.35	$7.8{\cdot}10^3$	4.685	1.61	3.146	10.8	93.0	2865
3013 can	193	0.3	$7.8\cdot10^3$	4.685	0.118	2.402	13.7	72.9	864

C Measured gap size for configuration 2a

Table 15: Measured annular gap size at eight locations with 45° increments for configuration 2a.

Location	Gap size (mm)	Gap size (in)
1	2.464	0.097
2	2.438	0.096
3	1.676	0.066
4	1.626	0.064
5	1.651	0.065
6	2.108	0.083
7	1.981	0.078
8	2.413	0.095

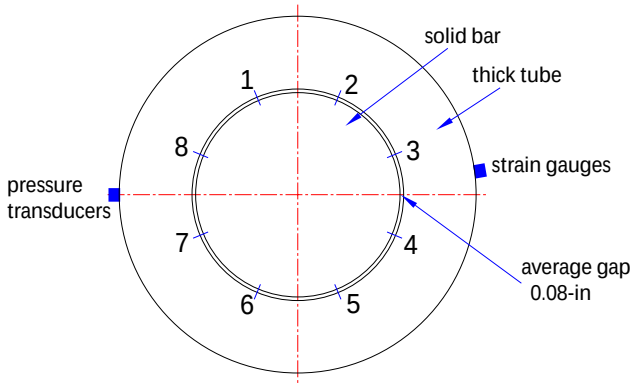

Figure 18: Diagram of the concentric configuration 2a and eight measured gap size locations.

D Measured gap size for configuration 3b

Table 16: Measured annular gap size at eight locations with 45° increments for configuration 3b.

Location	Gap size (mm)	Gap size (in)
1	2.464	0.097
2	1.295	0.051
3	0.508	0.020
4	0.432	0.017
5	1.270	0.050
6	2.337	0.092
7	3.124	0.123
8	3.175	0.125

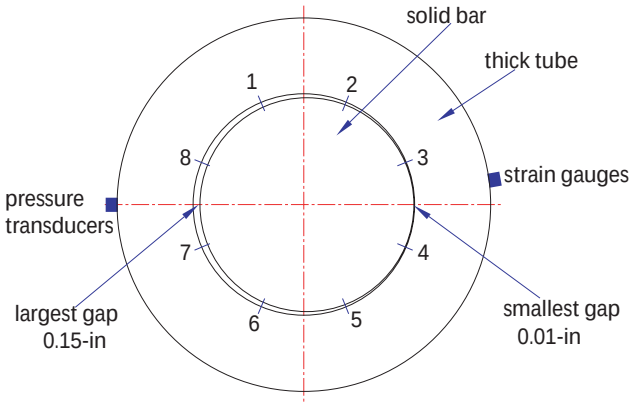

Figure 19: Diagram of the eccentric tube configuration 3b and eight measured gap size locations.

E Configuration 1 (empty)

Table 17: Summary of the peak pressure and strain for configuration 1 (empty tube).

shot	P_0	P_{CV}	P_{CJ}	P_{CJref}	$P_{1,max}$	$P_{2,max}$	$P_{3,max}$	$P_{4,max}$	DDT location
	(bar)	(MPa)							
mixture A									
1	2.0	1.958	3.836	9.441	2.814	2.414	2.384	3.149	–
3	2.5	2.466	4.832	11.895	3.737	3.249	3.371	3.149	–
5	2.6	2.568	5.032	12.387	6.119	12.884	5.241	6.835	P_4
4	2.75	2.721	5.332	13.128	6.465	5.544	6.415	7.036	P_4
2	3.0	2.978	5.834	14.364	8.808	13.463	5.825	9.783	P_4
mixture B									
6	2.5	2.341	4.579	11.239	2.378	2.197	2.224	2.211	–
7	3.0	2.853	5.582	13.712	3.305	2.841	2.933	3.015	–
8	3.5	3.366	6.589	16.194	3.830	3.709	3.836	3.685	–
mixture C									
9	3.0	2.941	5.762	14.160	3.056	2.815	2.787	2.814	–
10	3.5	3.459	6.777	16.666	3.727	3.249	3.371	3.149	–
shot	P_0	ϵ_{CV}	ϵ_{CJ}	ϵ_{CJref}	$S_{1,max}$	$S_{2,max}$	$S_{3,max}$	$S_{4,max}$	S_{max} location
	(bar)	(μstrain)							
mixture A									
1	2.0	17.5	35.2	88.0	25.5	33.7	49.2	60.0	S_4
3	2.5	22.3	44.6	111.2	28.6	37.3	59.6	77.3	S_4
5	2.6	23.3	46.5	115.8	83.0	83.1	101.1	143.6	S_4
4	2.75	24.7	49.3	122.8	95.0	85.8	113.1	168.0	S_4
2	3.0	27.1	54.0	134.5	99.6	91.1	127.7	164.0	S_4
mixture B									
6	2.5	21.1	42.2	105.0	26.2	30.0	47.3	57.3	S_4
7	3.0	26.0	51.7	128.3	27.9	36.9	51.6	64.9	S_4
8	3.5	30.8	61.2	151.7	32.5	37.9	57.0	72.8	S_4
mixture C									
9	3.0	26.8	53.4	132.5	18.7	23.0	17.9	24.3	S_4
10	3.5	31.7	62.9	156.2	31.6	36.9	60.4	73.1	S_4

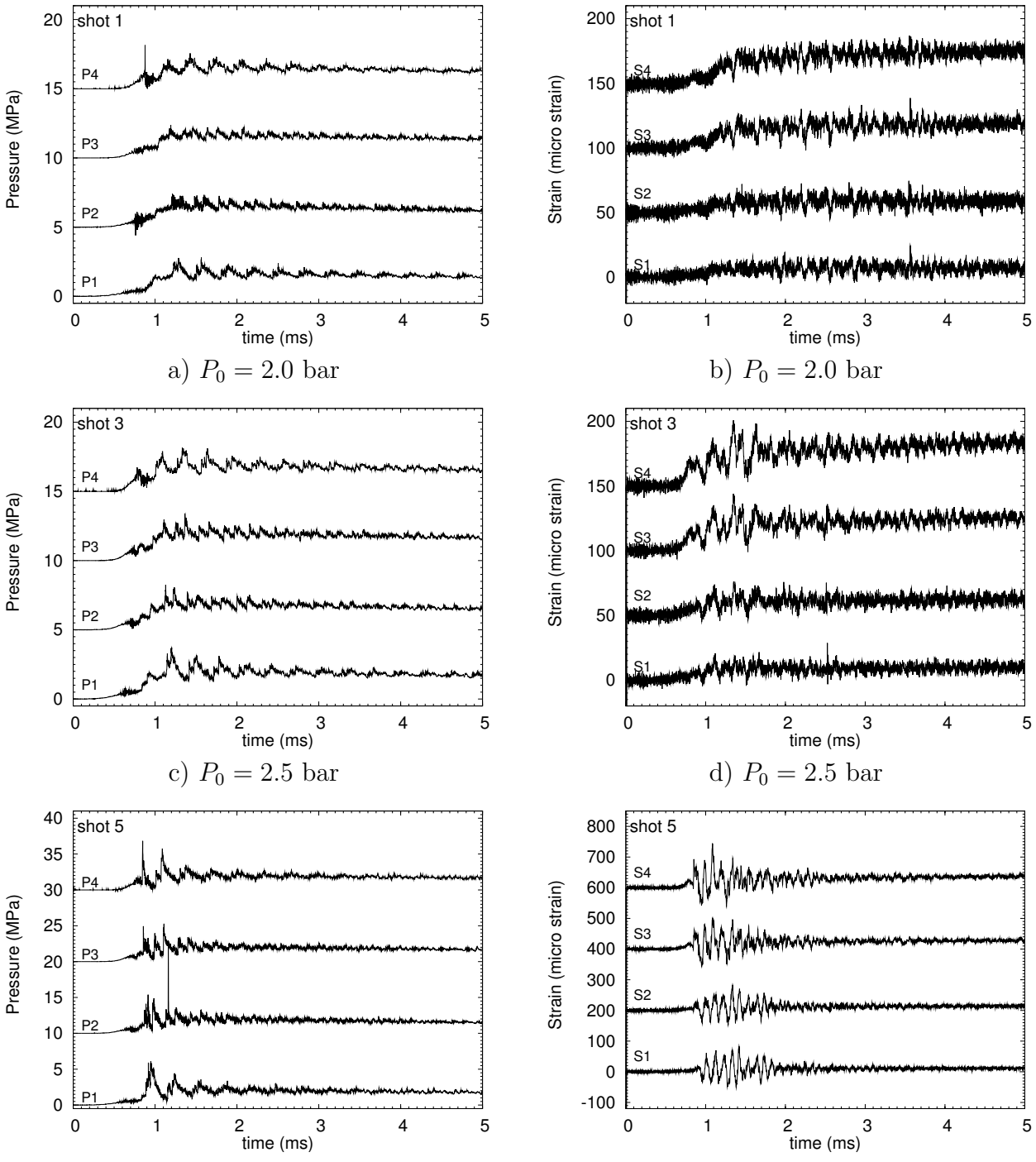

a) $P_0 = 2.0$ bar

b) $P_0 = 2.0$ bar

c) $P_0 = 2.5$ bar

d) $P_0 = 2.5$ bar

e) $P_0 = 2.6$ bar

f) $P_0 = 2.6$ bar

Figure 20: Pressure and strain traces for mixture A with the empty thick-walled tube.

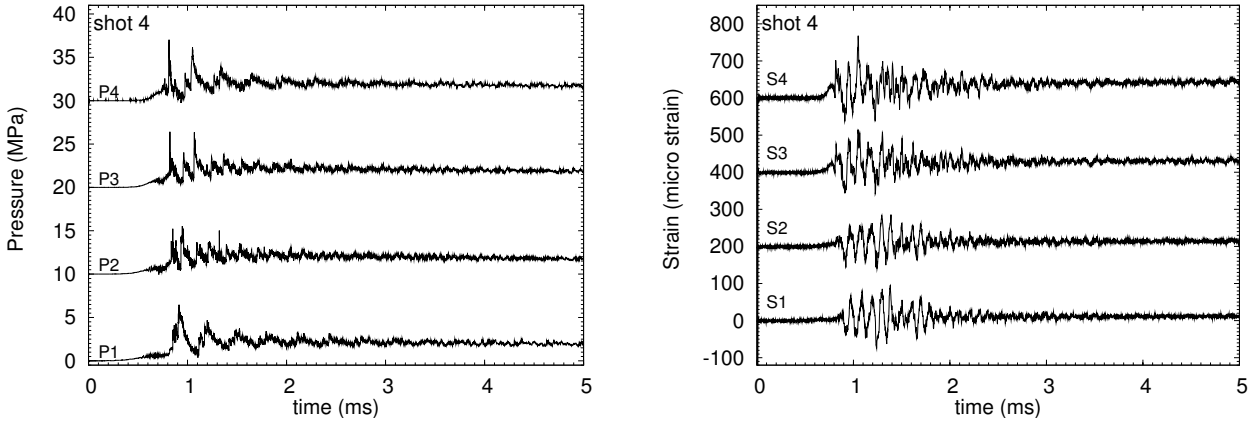

a) $P_0 = 2.75$ bar

b) $P_0 = 2.75$ bar

c) $P_0 = 3.0$ bar

d) $P_0 = 3.0$ bar

Figure 21: Pressure and strain traces for mixture A with the empty thick-walled tube.

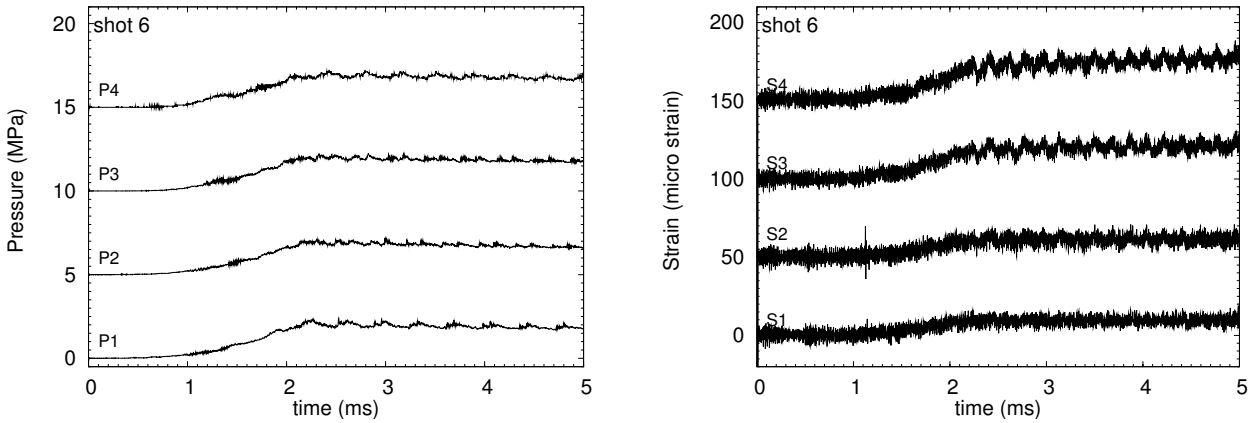

a) $P_0 = 2.5$ bar b) $P_0 = 2.5$ bar

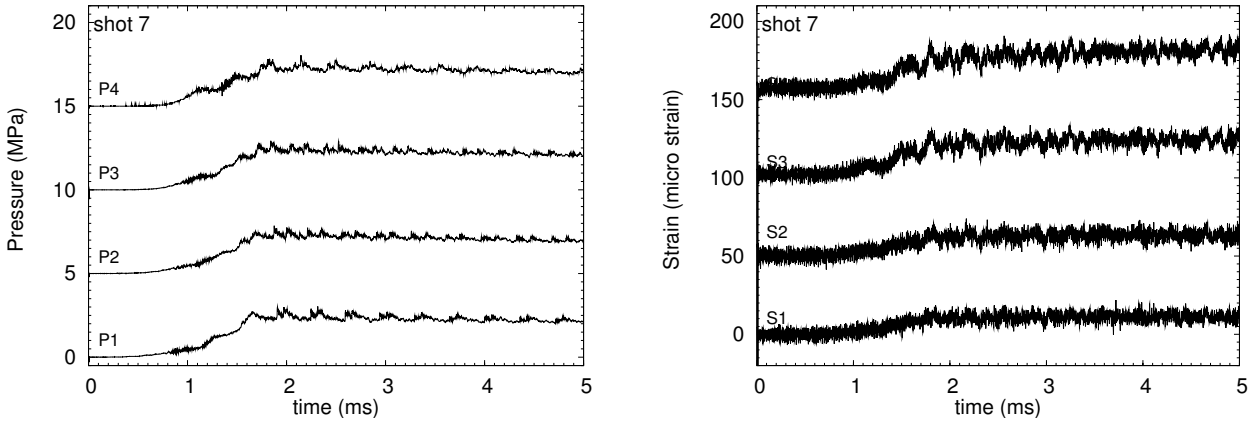

c) $P_0 = 3.0$ bar d) $P_0 = 3.0$ bar

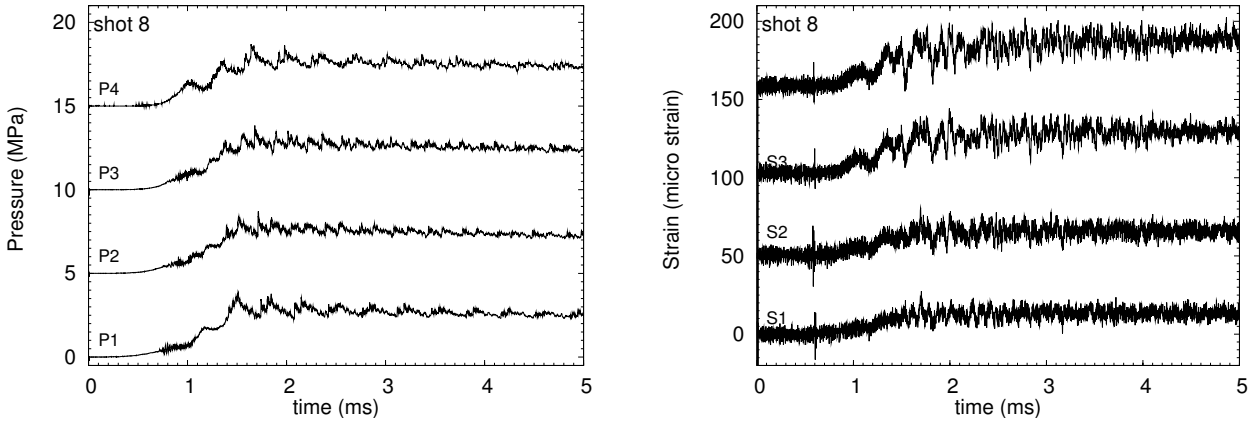

e) $P_0 = 3.5$ bar f) $P_0 = 3.5$ bar

Figure 22: Pressure and strain traces for mixture B with the empty thick-walled tube.

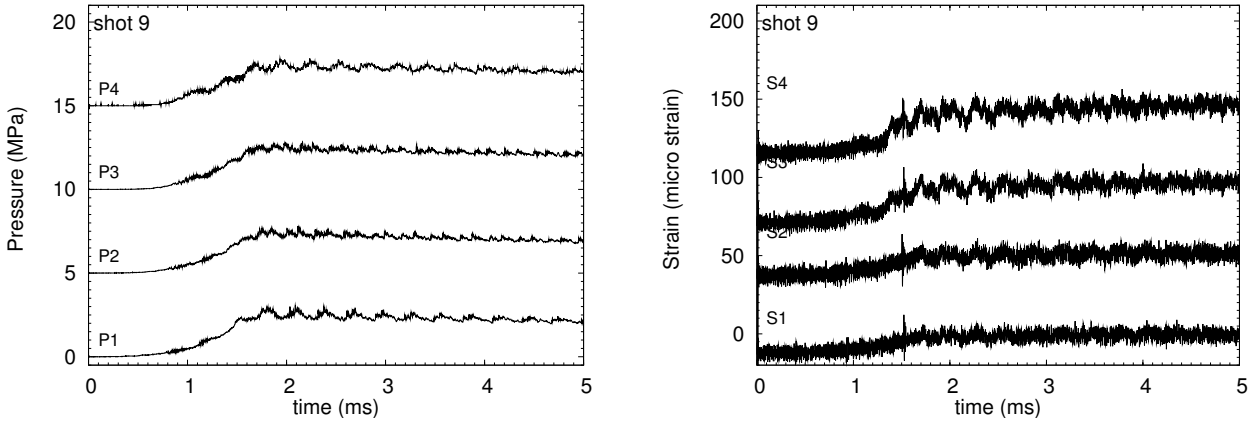

a) $P_0 = 3.0$ bar

b) $P_0 = 3.0$ bar

c) $P_0 = 3.5$ bar

d) $P_0 = 3.5$ bar

Figure 23: Pressure and strain traces for mixture C with the empty thick-walled tube.

F Configuration 2a (concentric, 0.08 in end gap)

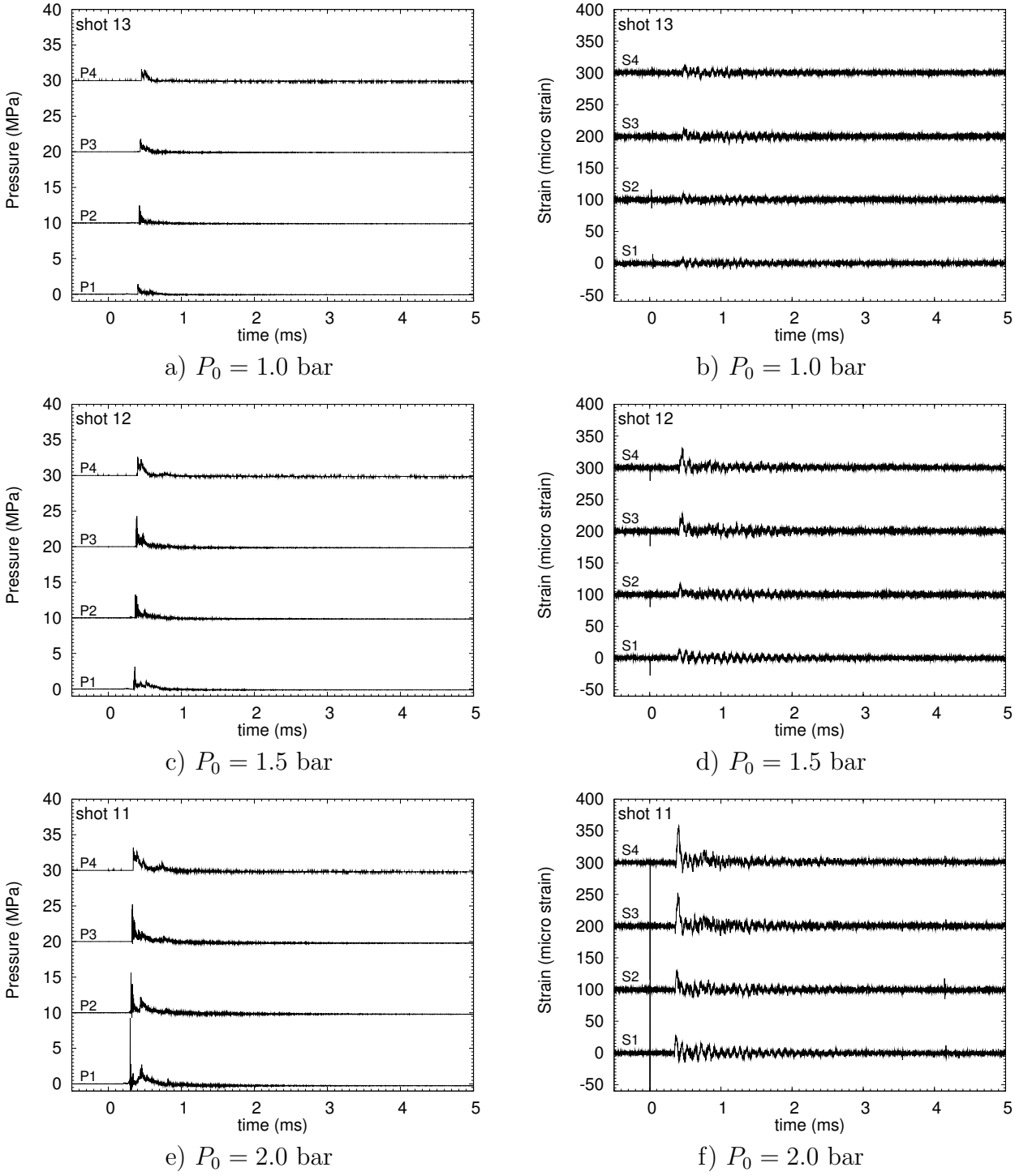

a) $P_0 = 1.0$ bar

b) $P_0 = 1.0$ bar

c) $P_0 = 1.5$ bar

d) $P_0 = 1.5$ bar

e) $P_0 = 2.0$ bar

f) $P_0 = 2.0$ bar

Figure 24: Pressure and strain traces for mixture A with the solid bar in the tube. Annular gap: 0.08 in; end gap: 0.08 in.

Table 18: Summary of the peak pressure and strain for configuration 2a (concentric, annular gap: 0.08 in, end gap 0.08 in).

shot	P_0	P_{CV}	P_{CJ}	P_{CJref}	$P_{1,max}$	$P_{2,max}$	$P_{3,max}$	$P_{4,max}$	DDT location
	(bar)	(MPa)							
mixture A									
13	1.0	0.956	1.872	4.602	1.417	2.460	1.849	1.608	P_1
12	1.5	1.454	2.848	7.006	3.146	3.262	4.275	2.613	P_1
11	2.0	1.958	3.836	9.441	9.244	5.617	5.206	3.216	P_1
14	2.5	2.466	4.832	11.895	8.795	5.380	5.873	4.422	P_1
15	3.0	2.978	5.834	14.364	6.091	7.597	6.909	6.366	P_1
24	3.5	3.492	6.841	16.842	6.126	5.696	5.670	5.160	P_1
mixture B									
17	1.0	0.766	1.491	3.599	0.055	0.053	0.062	0.134	slow flame
16	1.5	1.316	2.569	6.278	1.410	1.993	1.397	3.685	P_4
18	2.5	2.341	4.579	11.239	2.939	5.814	4.316	3.484	P_2
19	3.5	3.366	6.589	16.194	9.057	6.656	5.797	4.825	P_1
mixture C									
23	1.5	1.375	2.690	6.573	0.366	0.342	0.382	0.402	slow flame
20	2.0	1.905	3.729	9.144	2.206	1.947	4.289	7.706	P_4
21	2.5	2.426	4.752	11.669	2.800	8.202	6.005	4.221	P_2
22	3.5	3.459	6.777	16.666	7.820	5.413	4.844	4.355	P_1
shot	P_0	ϵ_{CV}	ϵ_{CJ}	ϵ_{CJref}	$S_{1,max}$	$S_{2,max}$	$S_{3,max}$	$S_{4,max}$	S_{max} location
	(bar)	(μstrain)							
mixture A									
13	1.0	8.1	16.7	42.4	14.7	19.0	14.2	14.0	slow flame
12	1.5	12.8	25.9	65.1	13.5	19.5	28.3	31.2	S_4
11	2.0	17.5	35.2	88.0	26.5	29.9	52.4	58.2	S_4
14	2.5	22.3	44.6	111.2	29.0	35.2	64.3	85.8	S_4
15	3.0	27.1	54.0	134.5	30.9	37.2	59.8	73.6	S_4
24	3.5	32.0	63.5	157.8	35.7	49.2	75.5	94.0	S_4
mixture B									
17	1.0	6.3	13.1	33.0	13.6	18.1	14.6	11.6	slow flame
16	1.5	11.5	23.3	58.2	15.5	19.4	26.2	27.3	S_4
18	2.5	21.1	42.2	105.0	22.7	26.5	44.3	42.8	S_4
19	3.5	30.8	61.2	151.7	35.4	48.7	91.8	135.5	S_4
mixture C									
23	1.5	12.0	24.4	61.0	12.8	19.4	12.4	10.3	slow flame
20	2.0	17.0	34.2	85.3	15.3	21.2	38.7	45.9	S_4
21	2.5	21.9	43.9	109.1	20.0	28.6	63.2	83.6	S_4
22	3.5	31.7	62.9	156.2	51.8	62.6	105.6	135.7	S_4

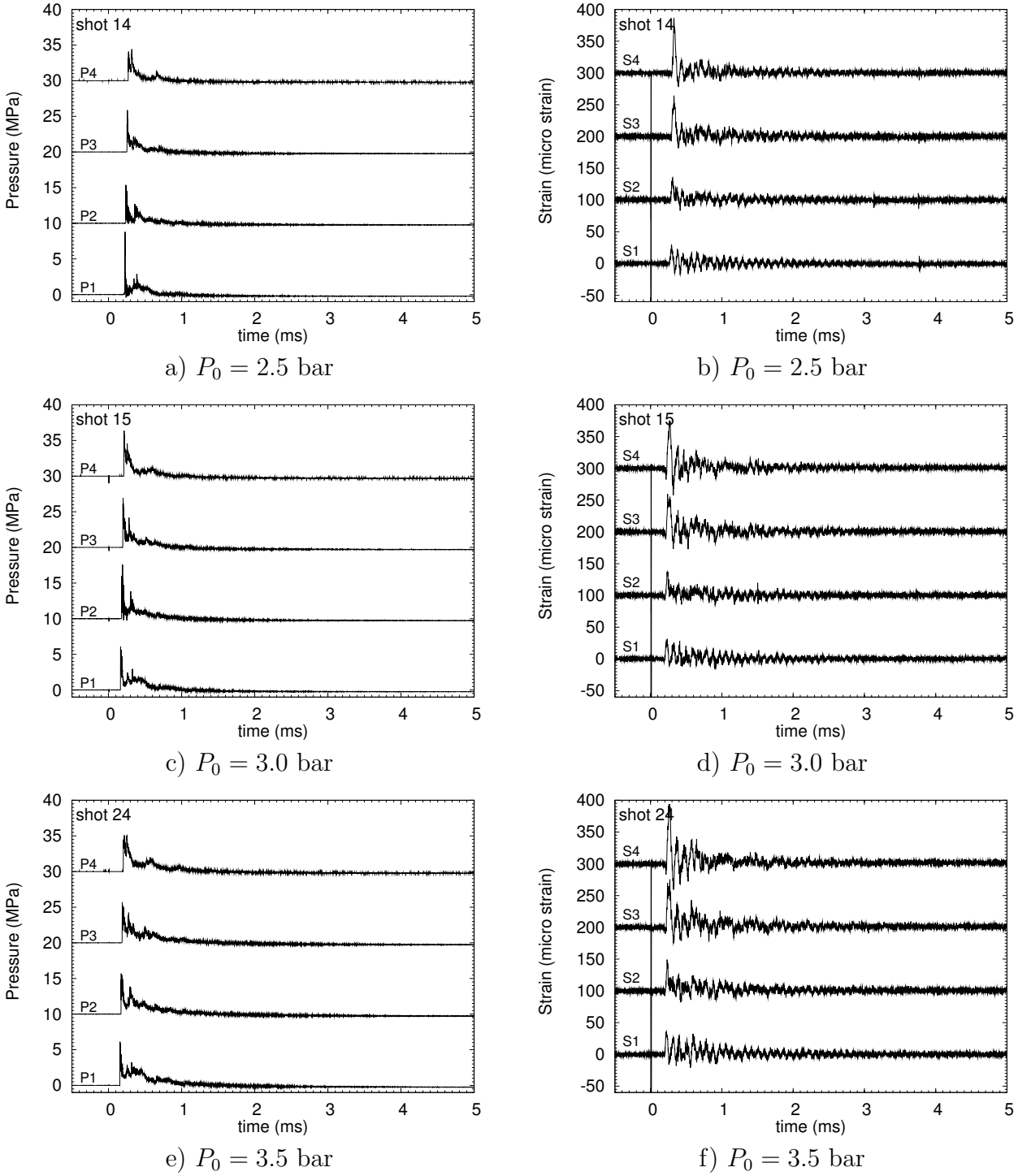

a) $P_0 = 2.5$ bar

b) $P_0 = 2.5$ bar

c) $P_0 = 3.0$ bar

d) $P_0 = 3.0$ bar

e) $P_0 = 3.5$ bar

f) $P_0 = 3.5$ bar

Figure 25: Pressure and strain traces for mixture A with the solid bar in the tube. Annular gap: 0.08 in; end gap: 0.08 in.

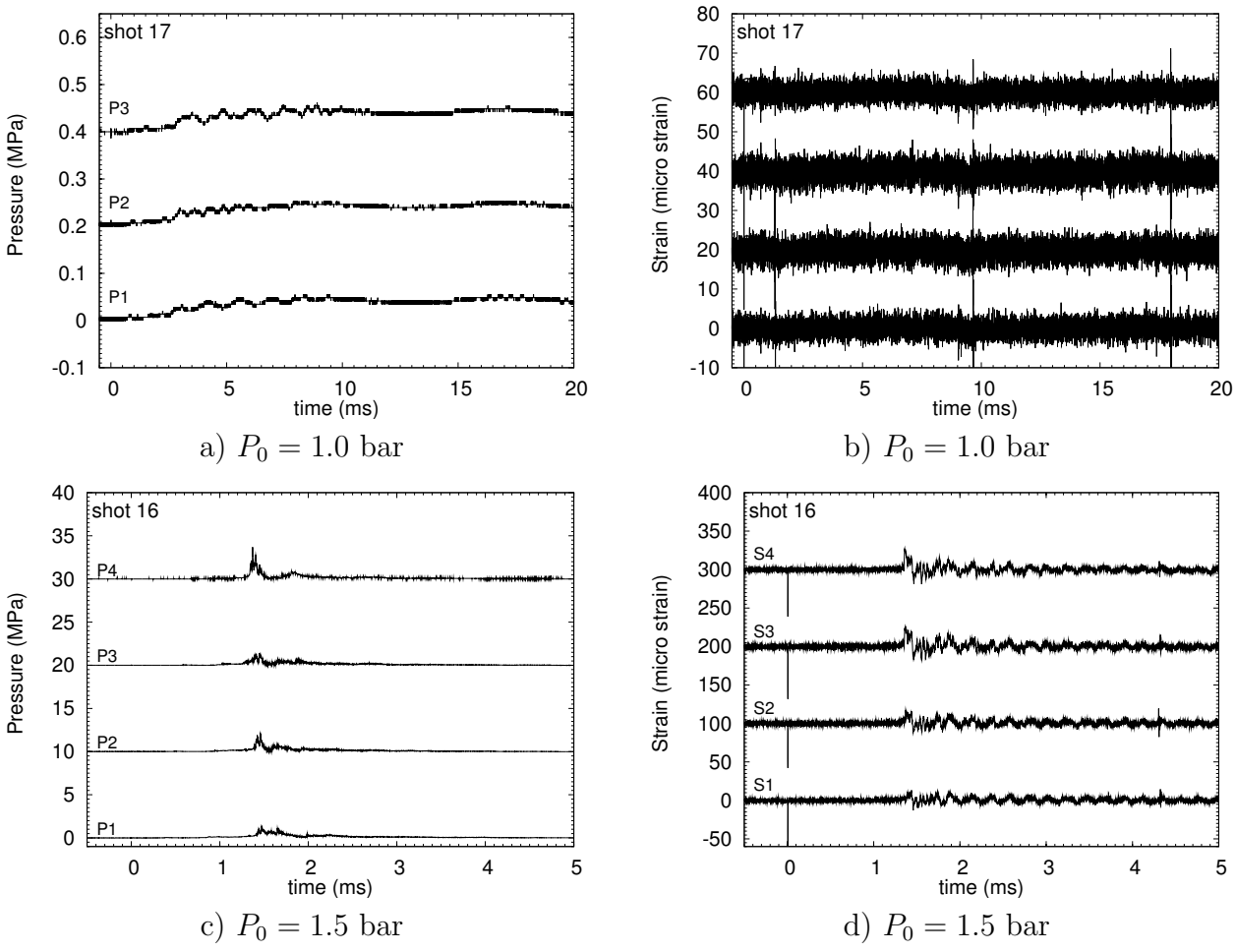

a) $P_0 = 1.0$ bar

b) $P_0 = 1.0$ bar

c) $P_0 = 1.5$ bar

d) $P_0 = 1.5$ bar

Figure 26: Pressure and strain traces for mixture B with the solid bar in the tube. Annular gap: 0.08 in; end gap: 0.08 in.

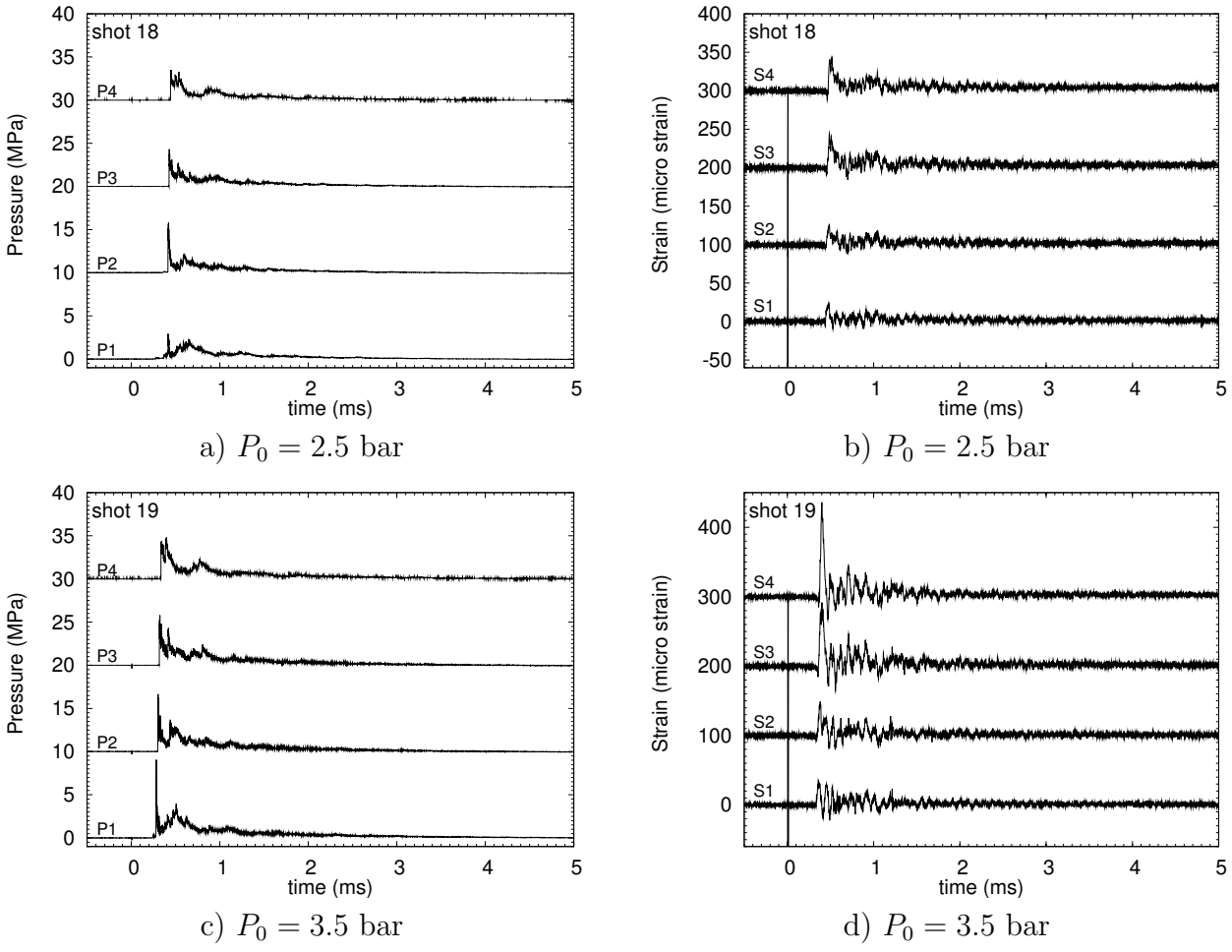

a) $P_0 = 2.5$ bar

b) $P_0 = 2.5$ bar

c) $P_0 = 3.5$ bar

d) $P_0 = 3.5$ bar

Figure 27: Pressure and strain traces for mixture B with the solid bar in the tube. Annular gap: 0.08 in; end gap: 0.08 in.

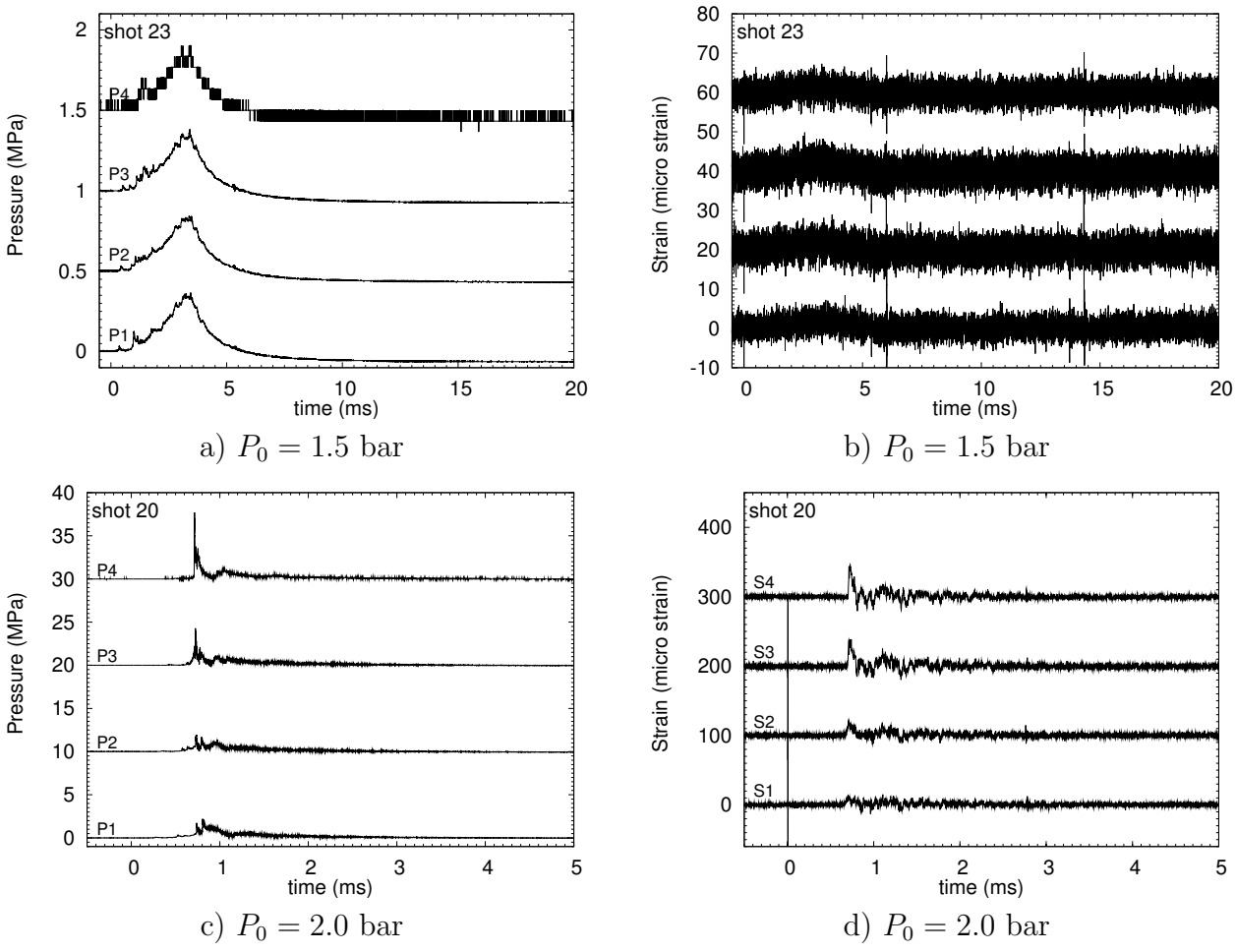

a) $P_0 = 1.5$ bar

b) $P_0 = 1.5$ bar

c) $P_0 = 2.0$ bar

d) $P_0 = 2.0$ bar

Figure 28: Pressure and strain traces for mixture C with the solid bar in the tube. Annular gap: 0.08 in; end gap: 0.08 in.

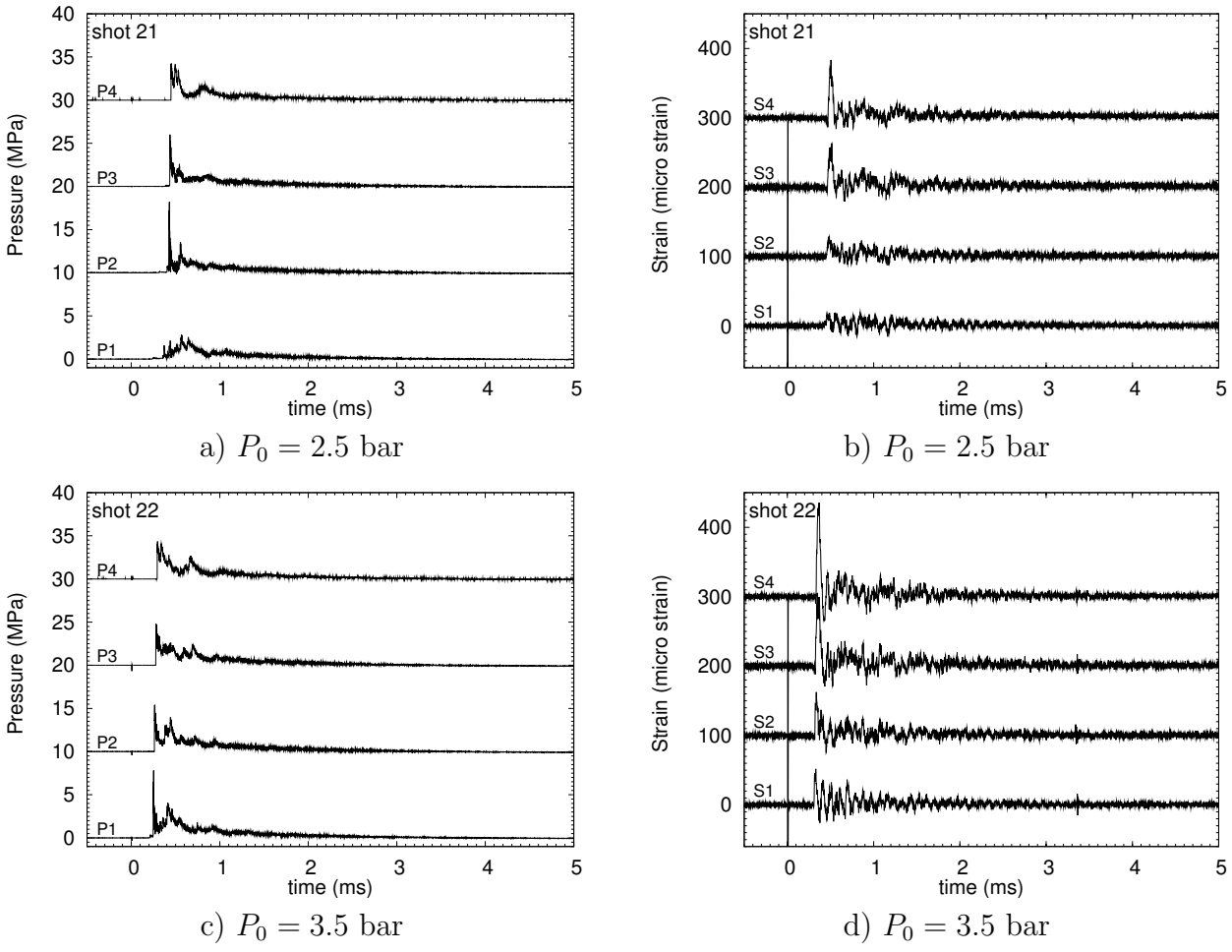

a) $P_0 = 2.5$ bar

b) $P_0 = 2.5$ bar

c) $P_0 = 3.5$ bar

d) $P_0 = 3.5$ bar

Figure 29: Pressure and strain traces for mixture C with the solid bar in the tube. Annular gap: 0.08 in; end gap: 0.08 in.

G Configuration 2b (concentric, 0.5 in end gap)

Table 19: Summary of the peak pressure and strain for configuration 2b (concentric, annular gap: 0.08 in, end gap 0.5 in).

shot	P_0	P_{CV}	P_{CJ}	P_{CJref}	$P_{1,max}$	$P_{2,max}$	$P_{3,max}$	$P_{4,max}$	DDT location
	(bar)	(MPa)							
mixture A									
28	1.0	0.956	1.872	4.602	4.238	4.301	4.414	2.948	P_1
25	1.5	1.454	2.848	7.006	6.278	6.321	4.031	3.350	P_1
26	2.5	2.466	4.832	11.895	8.408	7.879	6.763	4.758	P_1
27	3.5	3.492	6.841	16.842	12.128	9.385	7.660	6.634	P_1
mixture B									
29	1.0	0.766	1.491	3.599	0.207	0.210	0.222	0.268	slow flame
30	3.5	3.366	6.589	16.194	8.470	11.714	10.655	6.902	P_1
mixture C									
31	1.5	1.375	2.690	6.573	2.717	3.025	3.955	4.489	P_1
32	3.5	3.459	6.777	16.666	10.060	13.463	14.193	11.190	P_1
shot	P_0	ϵ_{CV}	ϵ_{CJ}	ϵ_{CJref}	$S_{1,max}$	$S_{2,max}$	$S_{3,max}$	$S_{4,max}$	S_{max} location
	(bar)	(μstrain)							
mixture A									
28	1.0	8.1	16.7	42.4	13.1	18.1	21.9	20.9	S_3
25	1.5	12.8	25.9	65.1	21.7	24.4	41.8	50.0	S_4
26	2.5	22.3	44.6	111.2	37.9	44.2	71.1	83.0	S_4
27	3.5	32.0	63.5	157.8	35.9	47.5	79.9	88.5	S_4
mixture B									
29	1.0	6.3	13.1	33.0	14.9	21.1	14.5	13.3	S_2
30	3.5	3.5	30.8	61.2	46.1	57.1	95.2	109.5	S_4
mixture C									
31	1.5	12.0	24.4	61.0	18.2	19.6	29.8	24.3	S_3
32	3.5	31.7	62.9	156.2	43.6	49.8	84.6	106.6	S_4

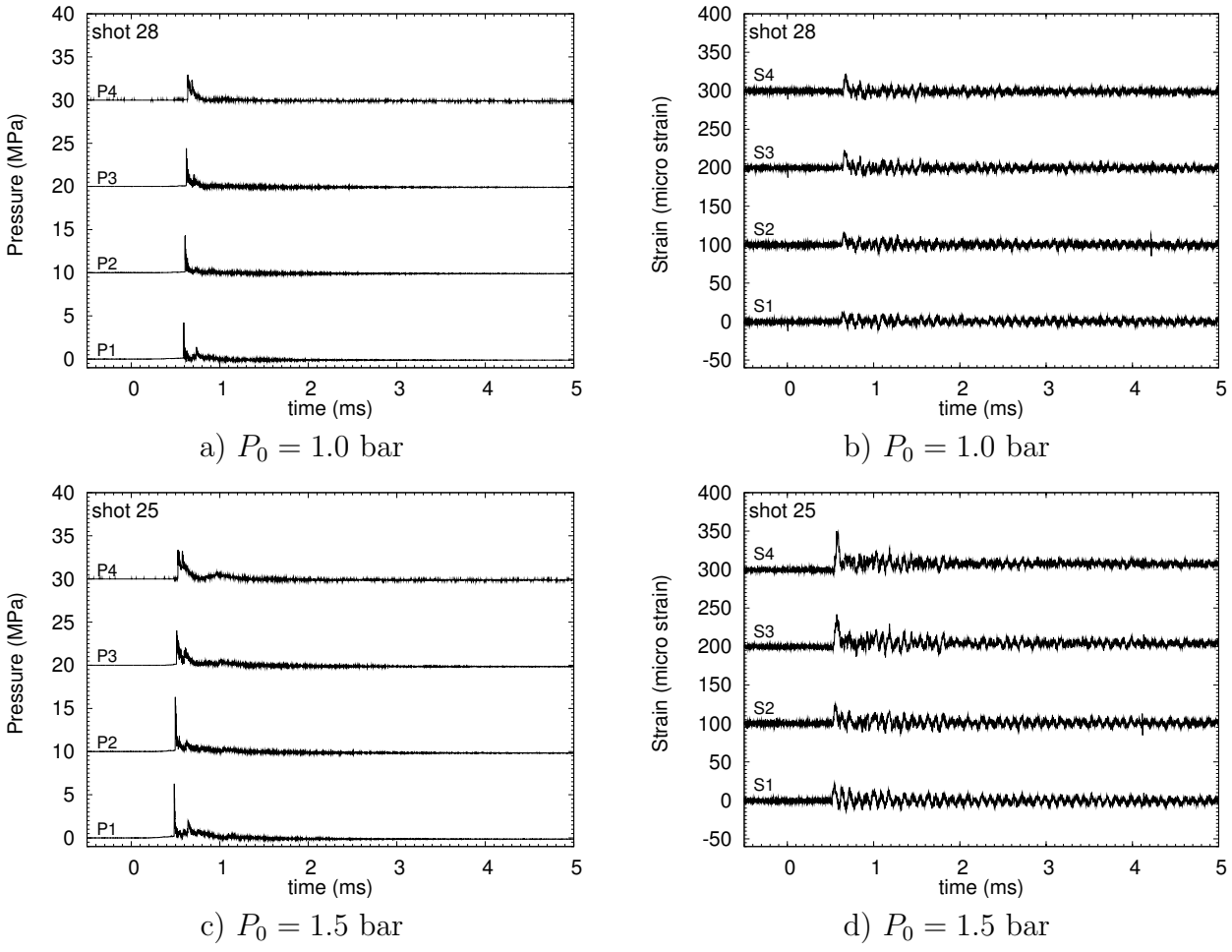

a) $P_0 = 1.0$ bar

b) $P_0 = 1.0$ bar

c) $P_0 = 1.5$ bar

d) $P_0 = 1.5$ bar

Figure 30: Pressure and strain traces for mixture A with the solid bar in the tube. Annular gap: 0.08 in; end gap: 0.5 in.

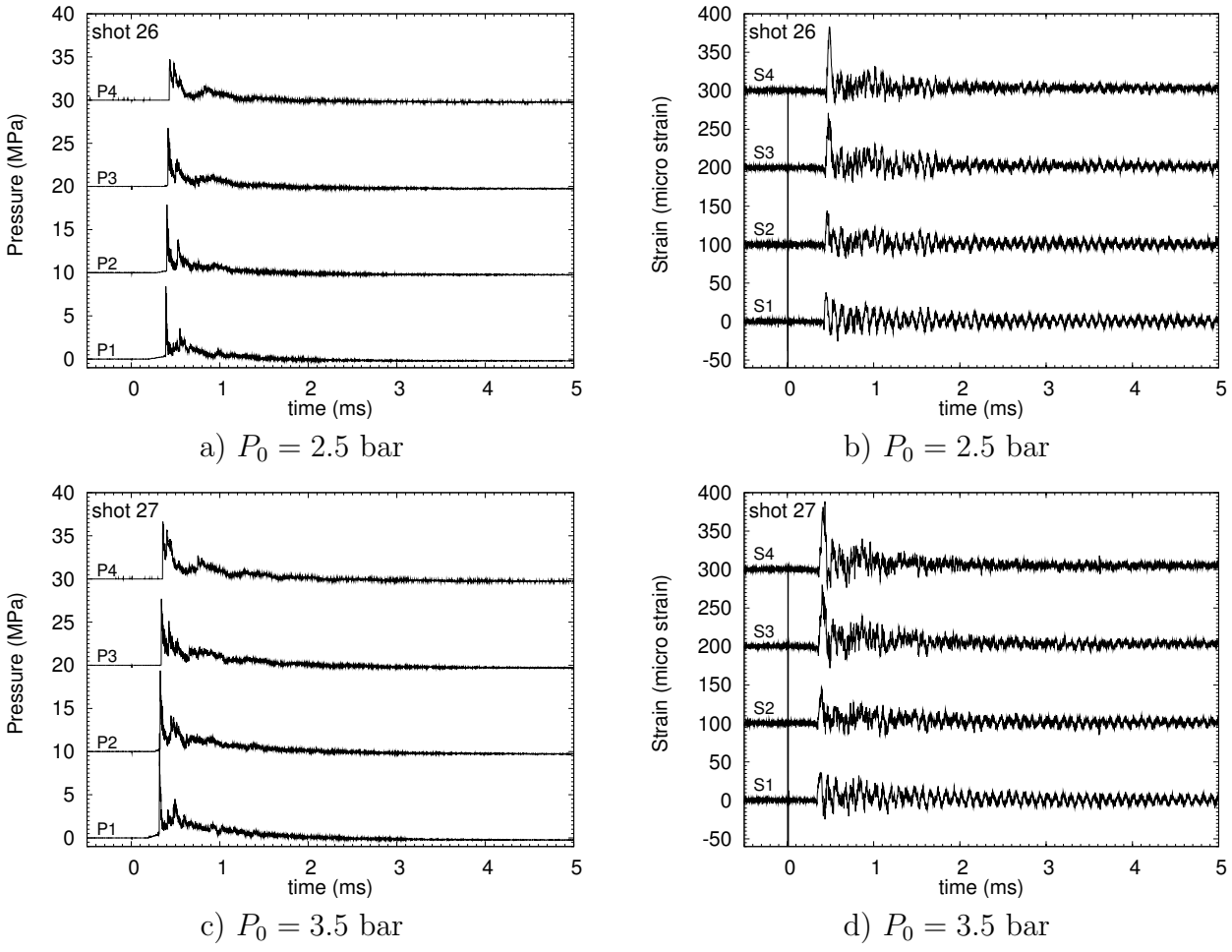

a) $P_0 = 2.5$ bar

b) $P_0 = 2.5$ bar

c) $P_0 = 3.5$ bar

d) $P_0 = 3.5$ bar

Figure 31: Pressure and strain traces for mixture A with the solid bar in the tube. Annular gap: 0.08 in; end gap: 0.5 in.

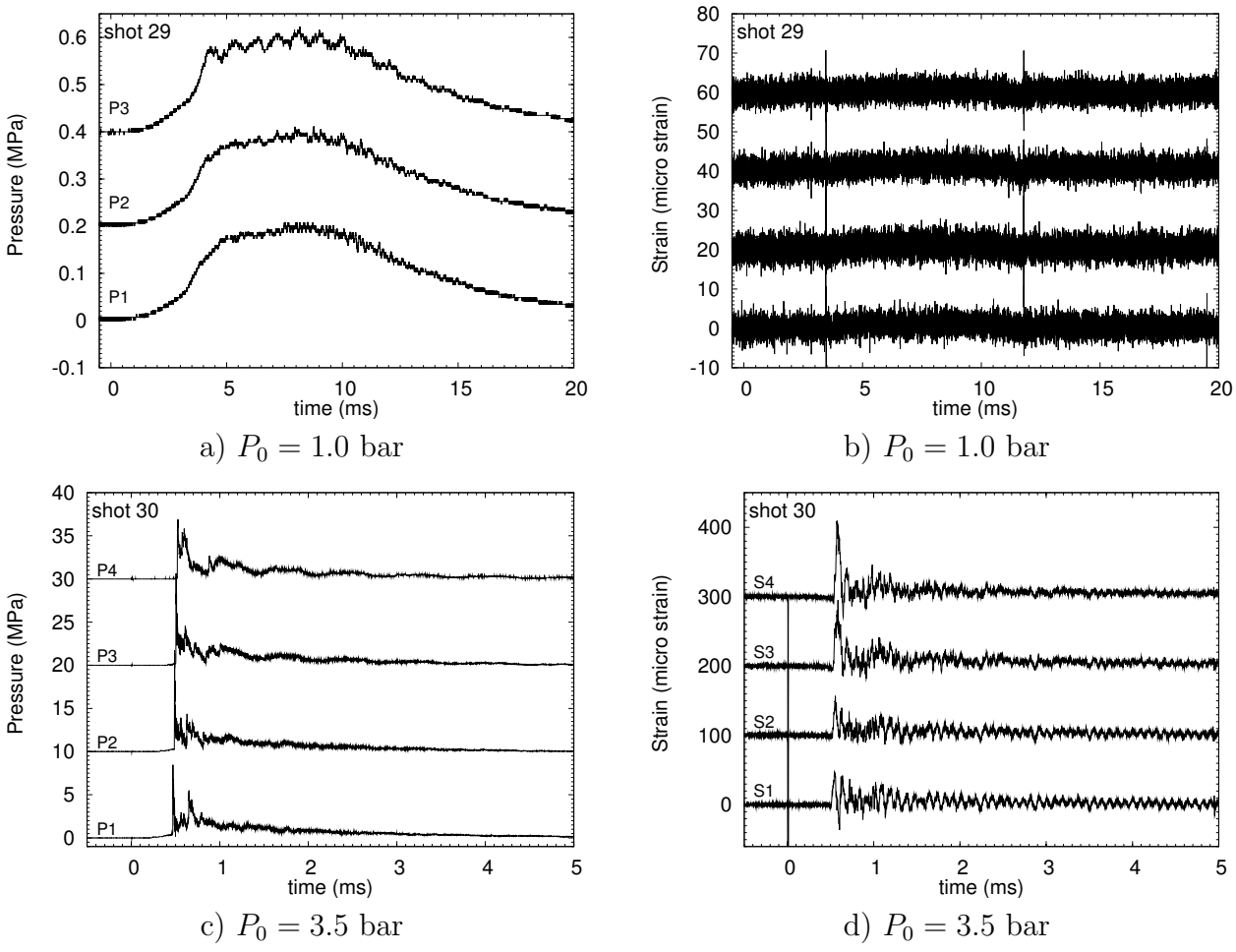

a) $P_0 = 1.0$ bar

b) $P_0 = 1.0$ bar

c) $P_0 = 3.5$ bar

d) $P_0 = 3.5$ bar

Figure 32: Pressure and strain traces for mixture B with the solid bar in the tube. Annular gap: 0.08 in; end gap: 0.5 in.

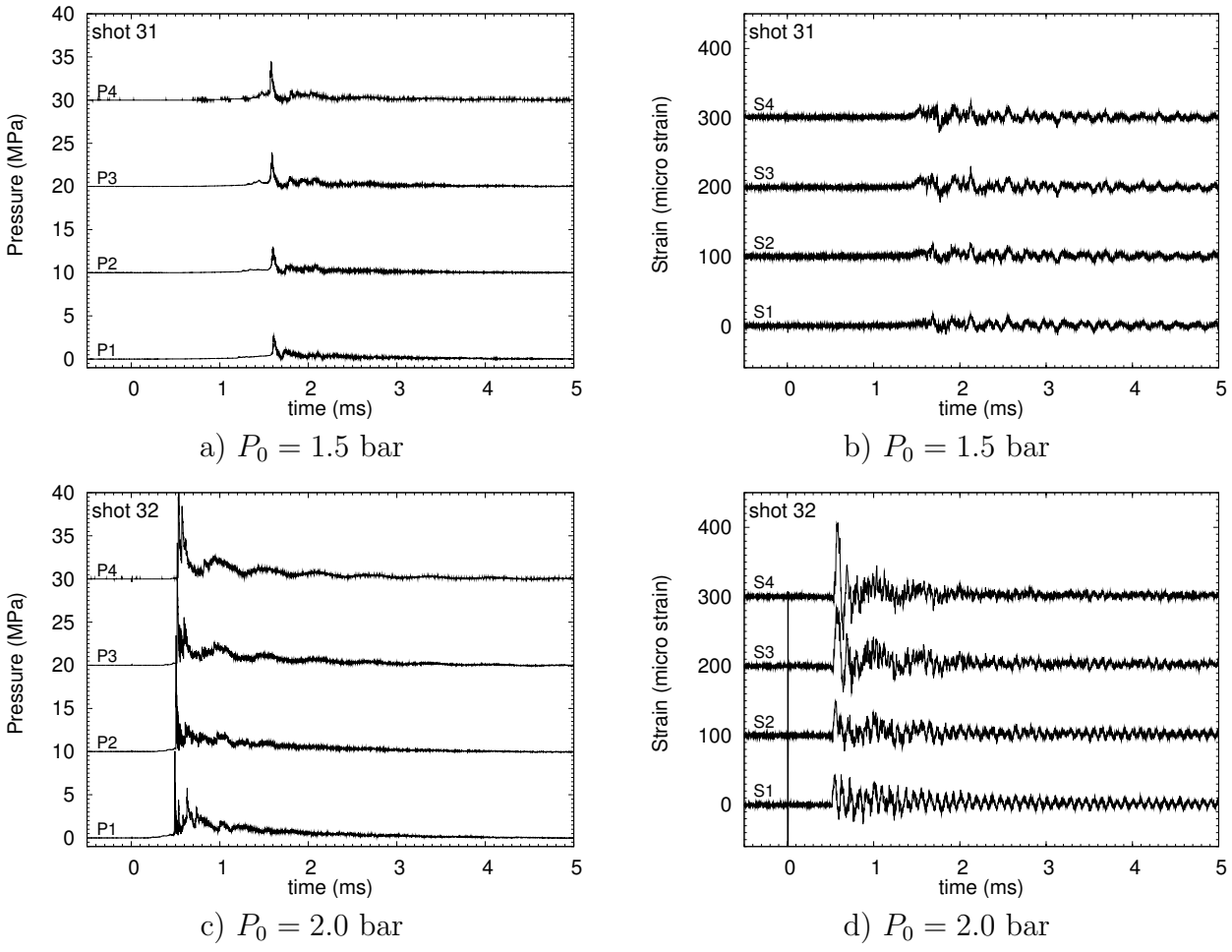

a) $P_0 = 1.5$ bar

b) $P_0 = 1.5$ bar

c) $P_0 = 2.0$ bar

d) $P_0 = 2.0$ bar

Figure 33: Pressure and strain traces for mixture C with the solid bar in the tube. Annular gap: 0.08 in; end gap: 0.5 in.

H Configuration 3a (eccentric)

Table 20: Summary of the peak pressure and strain for configuration 3a (eccentric, 0.01 in on PT side and 0.15 in on SG side.

shot	P_0	P_{CV}	P_{CJ}	P_{CJref}	$P_{1,max}$	$P_{2,max}$	$P_{3,max}$	$P_{4,max}$	DDT location
	(bar)	(MPa)							
mixture A									
33	1.0	0.956	1.872	4.602	4.404	2.986	2.217	2.613	P_1
34	2.5	2.466	4.832	11.895	9.908	6.176	5.227	6.165	P_1
35	3.5	3.492	6.841	16.842	11.886	8.754	7.340	6.432	P_1
shot	P_0	ϵ_{CV}	ϵ_{CJ}	ϵ_{CJref}	$S_{1,max}$	$S_{2,max}$	$S_{3,max}$	$S_{4,max}$	S_{max} location
	(bar)	(μstrain)							
mixture A									
33	1.0	8.1	16.7	42.4	14.0	16.2	26.6	23.7	S_3
34	2.5	22.3	44.6	111.2	30.3	35.3	65.2	84.8	S_4
35	3.5	32.0	63.5	157.8	39.2	47.9	74.1	103.1	S_4

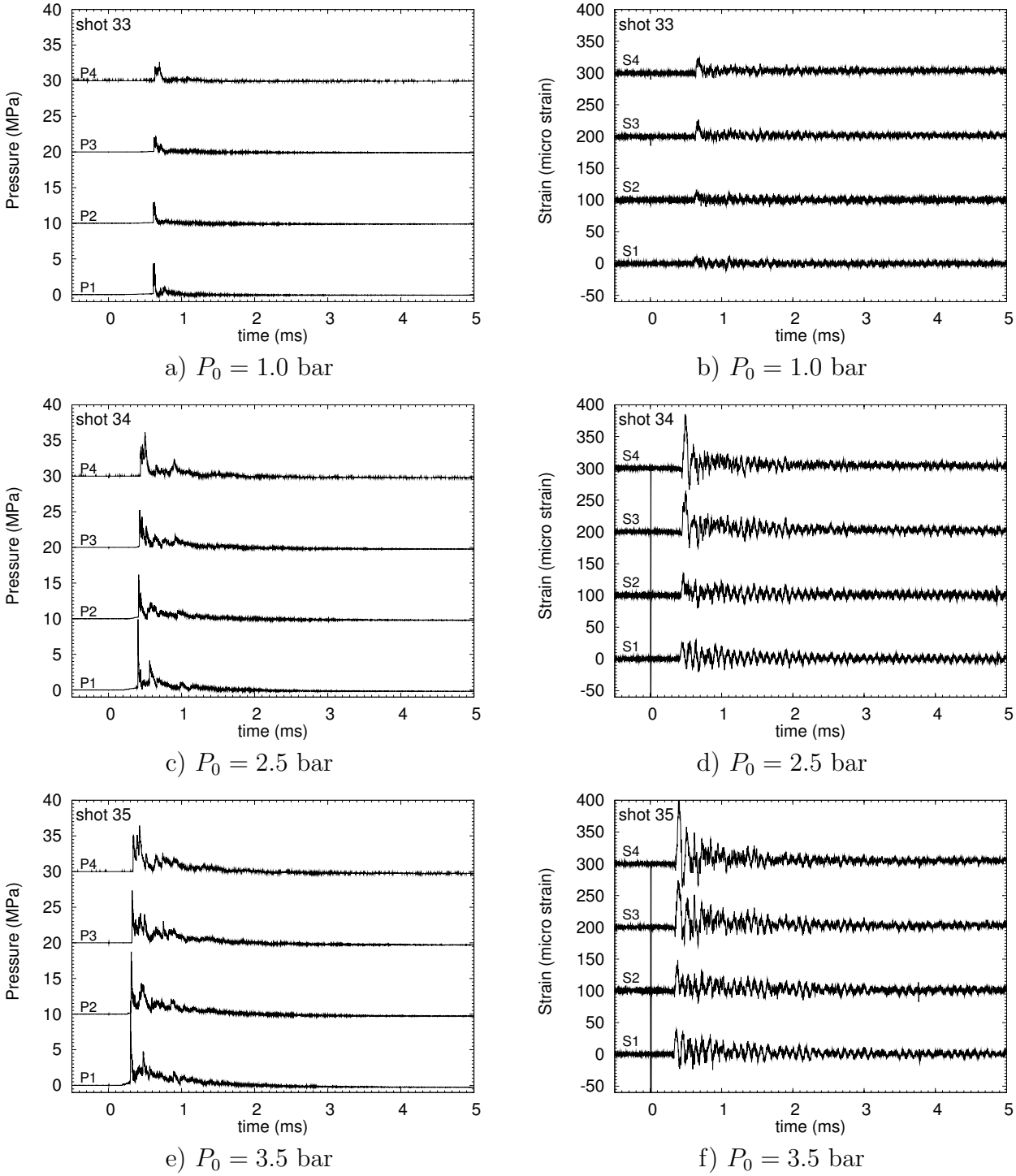

a) $P_0 = 1.0$ bar

b) $P_0 = 1.0$ bar

c) $P_0 = 2.5$ bar

d) $P_0 = 2.5$ bar

e) $P_0 = 3.5$ bar

f) $P_0 = 3.5$ bar

Figure 34: Pressure and strain traces for mixture A with the solid bar in the tube. Eccentric, smallest gap 0.01 in close to the pressure transducer side; end gap: 0.5 in.

I Configuration 3b (eccentric)

Table 21: Summary of the peak pressure and strain for configuration 3b (eccentric, 0.15 in on PT side and 0.01 in on SG side.

shot	P_0	P_{CV}	P_{CJ}	P_{CJref}	$P_{1,max}$	$P_{2,max}$	$P_{3,max}$	$P_{4,max}$	DDT location
	(bar)	(MPa)							
mixture A									
36	1.0	0.956	1.872	4.602	1.314	1.111	5.70	3.015	P_3
37	2.5	2.466	4.832	11.895	5.884	7.531	6.652	5.227	P_1
38	3.5	3.492	6.841	16.842	12.50	8.767	6.603	5.495	P_1
shot	P_0	ϵ_{CV}	ϵ_{CJ}	ϵ_{CJref}	$S_{1,max}$	$S_{2,max}$	$S_{3,max}$	$S_{4,max}$	S_{max} location
	(bar)	(μstrain)							
mixture A									
36	1.0	8.1	16.7	42.4	14.6	16.6	18.3	20.2	S_4
37	2.5	22.3	44.6	111.2	36.1	35.4	63.4	85.7	S_4
38	3.5	32.0	63.5	157.8	45.0	43.1	86.3	101.8	S_4

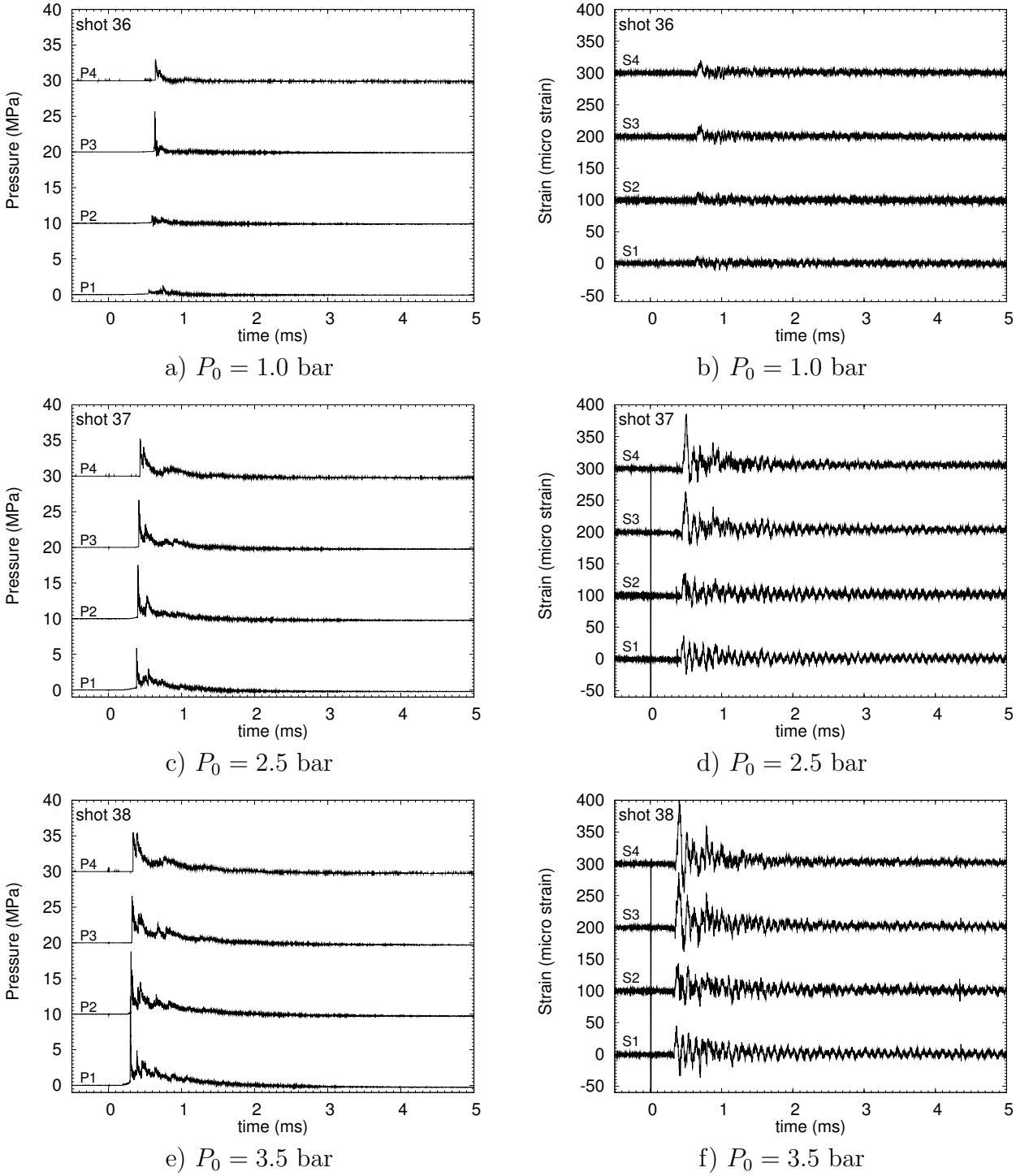

a) $P_0 = 1.0$ bar

b) $P_0 = 1.0$ bar

c) $P_0 = 2.5$ bar

d) $P_0 = 2.5$ bar

e) $P_0 = 3.5$ bar

f) $P_0 = 3.5$ bar

Figure 35: Pressure and strain traces for mixture A with the solid bar in the tube. Eccentric, smallest gap 0.01 in close to the strain gauge side; end gap: 0.5 in.

Explosion Testing of Nested Can Containment System Part III: 3013 Outer Can

Z. Liang and J. E. Shepherd
Graduate Aeronautical Laboratories, California Institute of Technology
Pasadena, CA 91125

Explosion Dynamics Laboratory Report FM2007.001

May 9, 2007

Sponsored by Los Alamos National Laboratory, Subcontract 46222-001-07.

Contents

List of Figures

List of Tables

1 Introduction

This report describes the final series of tests being carried out on this contract to provide data for the safety assessment of the triple-nested containers with the DOE-STD-3013 outer can used in the DOE complex. The tests use deliberate ignition of explosive mixtures to determine structural loading (pressure history) and structural response (stain history) in actual specimens of the 3013 outer can. The threshold for Deflagration-to-Detonation Transition (DDT) was determined and compared with the thick-walled tests. All three mixtures, A, B and C (see report (Liang and Shepherd, 2007a) and (Liang and Shepherd, 2007b)), were tested at room temperature (20–26°C) and pressures of 1.0–3.5 bar.

2 Fixture and Procedure

All the tests were conducted in 3013 outer cans supplied by the Savannah River Site (SRS). The cans are nominally 4.685 in ID, 4.921 in OD and 9.2 in long and constructed of stainless steel to the DOE-STD 3013 specifications. The cans were modified by SRS with small weldment adapters (Fig. 1) to attach pressure transducers and threaded holes in each end for gas fill and ignition feed-thrus, Fig. 2b. Five piezo-electric (PCB) pressure transducers were mounted in the adapters, with gauges P_1-P_4 along the can side and P_5 was located on the end opposite the igniter. The sensitive surface of the transducers was nominally flush with the interior surface of the can.

For shots 01-06 and 1-13, nine strain gauges (S_1-S_9) were mounted on the outer tube surface close to the end of the can opposite the igniter. For the last four shots, 14-17, five more strain gauges (S_{10}-S_{14}) were added closer to the ignition end. As shown in Fig. 2b, the gauges were placed in sets, P_1-S_{12}-S_{14}, P_2-S_{11}-S_{13}, P_3-S_{10}-S_1, P_4-S_9-S_2, S_3-S_5-S_7, S_4-S_6-S_8. Each set was located at the same axial distance from the igniter (the inside surface of the left-hand side of the can as shown in Fig. 2b) and gauges within a set were spaced 90 deg apart. The location of the pressure transducers and strain gauges is listed in Table 1.

The experimental procedure was the same as the tests with the planar and thick-walled fixtures. The spark plug ignition source (Fig. 3a) was used initially and we switched to a glow plug (Fig. 3b) after shot 5 due to the damage to the spark plug in high pressure shots. A voltage of 10 VAC was applied to the glow plug (Bosch 0-250-202-051) and the measured surface temperature of the glow plug reached about 1000°C in 15 s.

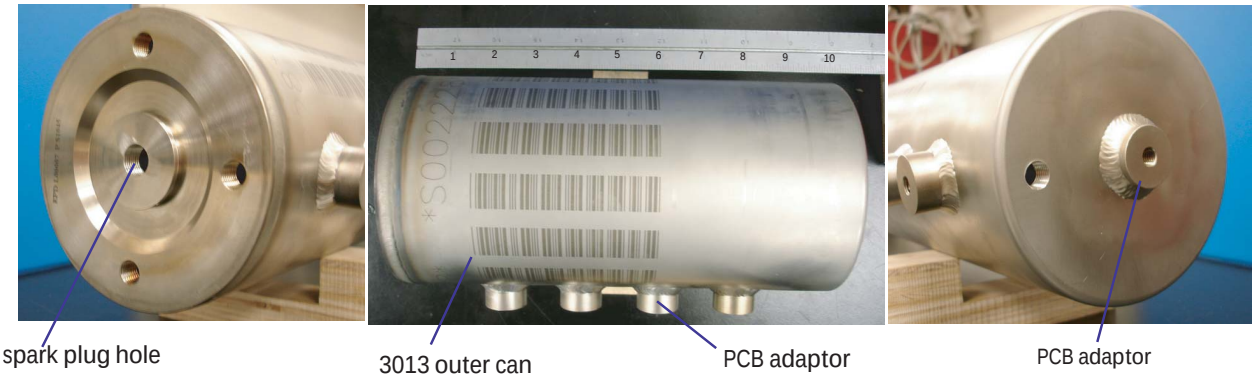

Figure 1: Modified 3013 outer can.

Table 1: Distance (along long axis) from the pressure transducers (P_1-P_4) and strain gauges (S_1-S_{14}) to the igniter location (see Fig. 2b).

pressure transducer	X (m)	X (in)	strain gauge	X (m)	X (in)
P_1	0.047	1.85	S_{12}, S_{14}	0.047	1.85
P_2	0.094	3.70	S_{11}, S_{13}	0.094	3.70
P_3	0.141	5.55	S_1, S_{10}	0.141	5.55
P_4	0.188	7.40	S_2, S_9	0.188	7.40
P_5	0.234	9.20	S_3, S_5, S_7	0.203	8.15
			S_4, S_6, S_8	0.219	8.90

3 Results

A total of 23 shots were performed in this part of the project. A summary of the test conditions is given in Table 2. The pressure and strain traces for each shot are given in Appendix A. The testing history is summarized below.

1. Shots 01-06 were performed first. Nine strain gauges were attached to the can. Strain signals S_7 and S_8 were noisy, possibly because they were damaged by the can supports. The original spark plug failed after shot 06 and was replaced.

   We noticed that after each shot the can would heat up to as much as 40°C due to the heat transfer from the combustion products. We found that in the planar fixture (Liang and Shepherd, 2007a), the DDT transition shifted to higher initial pressure with higher initial temperature. To avoid this effect, two fans were used to cool the can after each shot and the next test was performed only when the gas temperature was below 26°C.

2. Shots 1-4 and 8 were conducted with the same can as shots 01-06 but with a new spark plug and replacement strain gauges for S_7 and S_8. However the new spark plug failed after shot 8.

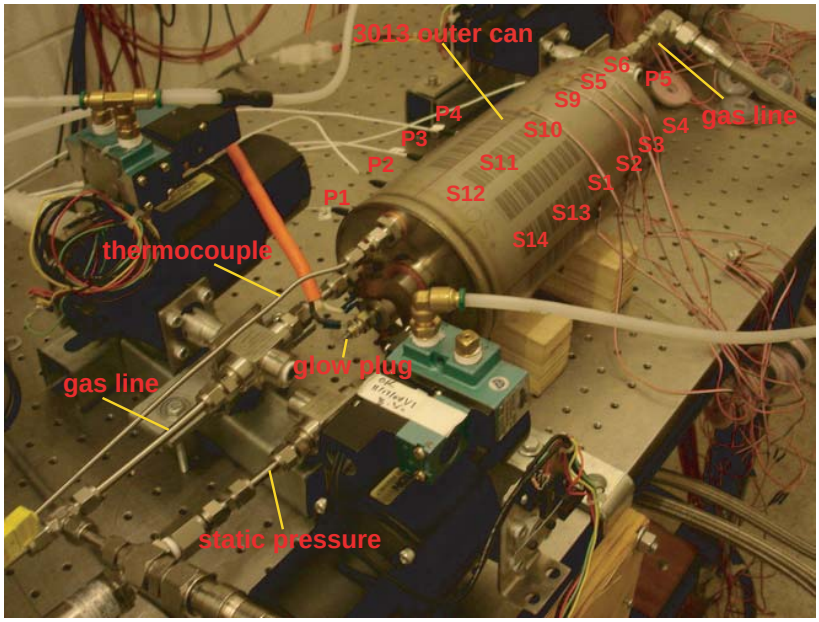

a)

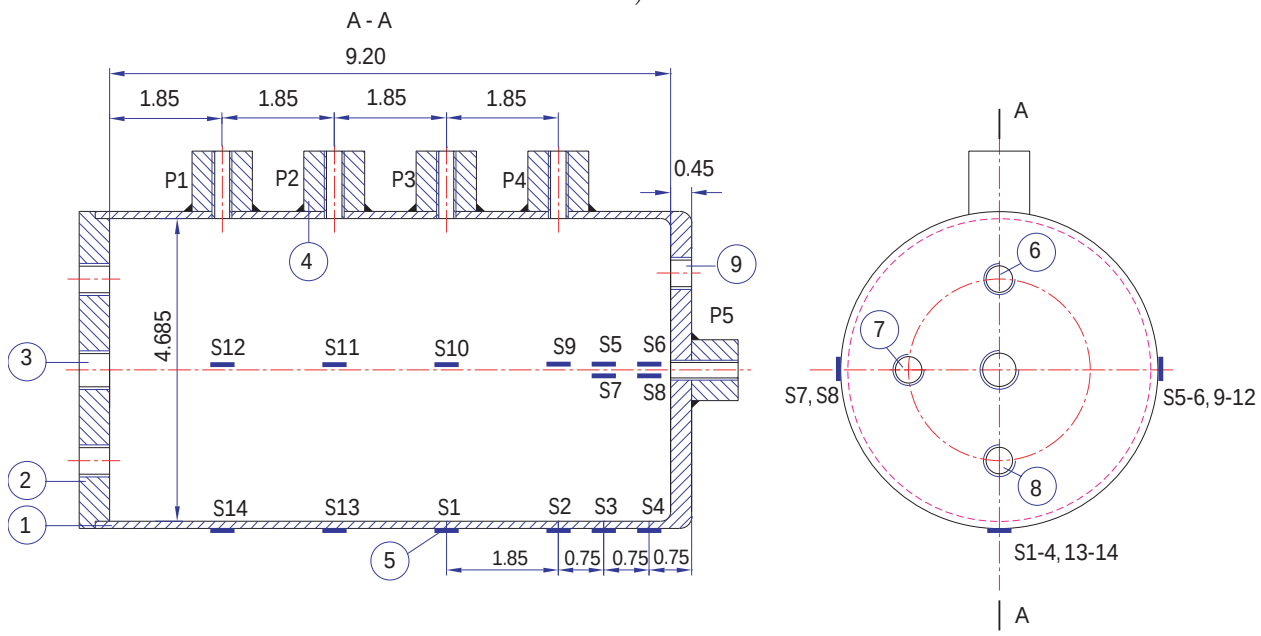

b)

Figure 2: a) 3013 outer can attached to experimental system. b) CAD drawing showing modified 3013 outer can with instrumentation locations. 1-3013 outer can, 2-welded flange, 3-spark/glow plug, 4-pressure transducer adapters, 5-strain gauges, 6-thermocouple, 7-static pressure gauge, 8 and 9-gas fill/circulation lines.

3. A glow plug was then used for ignition in shots 5-17 at the same location as the spark plug. When shot 9 was being performed, the 3013 outer can (S002244) was found to be leaking through the welds.

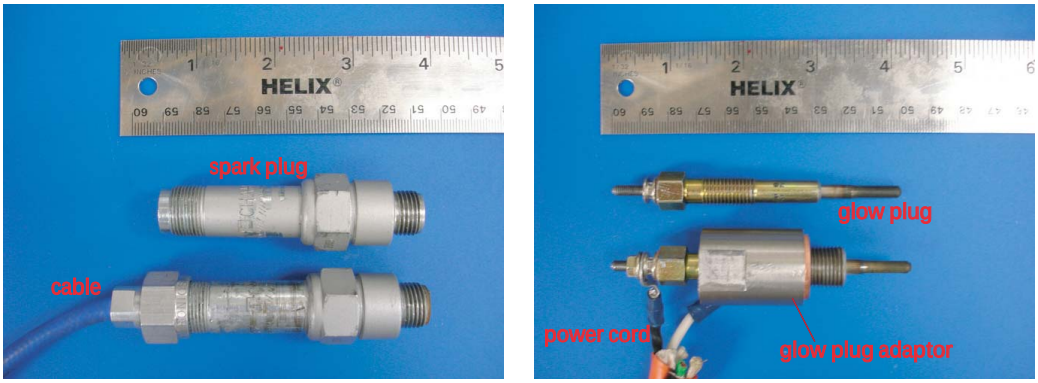

a) b)

Figure 3: a) spark plug and b) glow plug.

4. A new 3013 can (H000463) was used for shots 10-17. For shots 10-13, the strain signal S_3 was noisy. One possible reason is the bonding glue degraded when the can was repeatedly heated by the combustion process. Another possibility is that the strain gauge was damaged due to microcracking by the large amplitude vibrations.

5. For shots 14-17, five new strain gauges S_{10}-S_{14} were added in order to determine the location of the maximum strain on the can and S_3 was replaced. The signal S_{10} was noisy for all the shots and S_{14} became noisy in shot 17.

Figure 4 shows the recorded peak pressures on P_1-P_5, and peak strains on S_1-S_9 for all the shots and mixtures. The values for CJ pressure (P_{CJ}), reflected CJ pressure (P_{CJref}) and constant volume explosion pressure (P_{CV}) for each test were calculated using the chemical equilibrium program of Reynolds (1986) with realistic thermochemical properties. The static strains, ϵ_{CJ}, ϵ_{CJref}, ϵ_{CV}, corresponding to the CJ, reflected CJ and constant volume explosion pressures, were inferred from the approximate stress-strain relation for a uniformly, statically loaded tube

$$\epsilon = \frac{(P - P_a)R}{Eh} \,, \tag{1}$$

where ϵ, E, R, h and P_a are strain, Young's modulus, average radius (mean value of the inner and outer radius), thickness of the can, and atmosphere pressure (P_a=1 bar), respectively. For the 3013 outer can, $E = 193$ GPa, $R = 2.40$ in, and $h = 0.118$ in.

For the empty 3013 outer can configuration, the DDT transition was observed at $P_0 = 2.6$-2.7 bar for mix A. This is essentially the same threshold $P_0 = 2.5$-2.6 bar as observed for the empty thick-walled fixture (Liang and Shepherd, 2007b). The thresholds are not precise due to the limited number of tests and statistical nature of the DDT process. Small variations

Table 2: Summary of test series. The bar codes for cans 1 and 2 are S002244 and H000463 respectively. $P_{0,exp}$ and $T_{0,exp}$ represent the actual initial pressure (bar) and temperature (°C) before the tests.

Can	Shots	Mix	$P_{0,exp}$	$T_{0,exp}$	Igniter	SG	Note
1	01	B	3.0	23.7	spark plug	S_1-S_9	S_7 & S_8 noisy
1	02	B	3.54	28.2	spark plug	S_1-S_9	S_7 & S_8 noisy
1	03	C	3.0	25.3	spark plug	S_1-S_9	S_7 & S_8 noisy
1	04	C	3.47	30.0	spark plug	S_1-S_9	S_7 & S_8 noisy
1	05	A	2.48	26.7	spark plug	S_1-S_9	S_7 & S_8 noisy, P_2 loose cable
1	06	A	2.67	26.2	spark plug	S_1-S_9	S_7 & S_8 noisy, P_2 & P_3 loose cable
1	1	B	2.99	24.2	spark plug	S_1-S_9	
1	2	B	3.50	25.3	spark plug	S_1-S_9	
1	3	C	3.02	25.3	spark plug	S_1-S_9	
1	4	C	3.50	25.4	spark plug	S_1-S_9	
1	5	A	2.52	23.5	glow plug	S_1-S_9	
1	6	A	2.58	25.3	glow plug	S_1-S_9	
1	7	A	2.72	25.7	glow plug	S_1-S_9	P_1 and P_2 loose cables
1	8	A	2.01	22.0	spark plug	S_1-S_9	
1	9	A	2.91	25.6	glow plug	S_1-S_9	no DDT due to system leak
2	10	A	1.0	22.6	glow plug	S_1-S_9	S_3 noisy
2	11	A	3.0	24.5	glow plug	S_1-S_9	S_3 noisy, P_1 loose cable
2	12	A	2.62	24.4	glow plug	S_1-S_9	S_3 noisy
2	13	A	3.52	26.0	glow plug	S_1-S_9	S_3 noisy
2	14	A	1.0	23.9	glow plug	S_1-S_{14}	S_{10} noisy
2	15	A	3.01	24.6	glow plug	S_1-S_{14}	no DDT due to hot can
2	16	A	3.54	23.2	glow plug	S_1-S_{14}	S_{10} noisy
2	17	A	3.04	24.2	glow plug	S_1-S_{14}	S_{10}, S_{14} noisy

may be due to gas fill variations as well as a slight difference in the length of the two fixtures. The inside dimension of the 3013 outer can is approximately 9.35 in, and the thick-walled tube is 9.2 in. For $2.6 < P_0 < 3.5$ bar, DDT transition was always observed close to the can end opposite the igniter, apparently due to shock reflection.

The maximum peak strain was usually observed near the middle of the can on either S_1 or S_2 instead of close to the reflecting end as observed for the thick-tube fixture (Liang and Shepherd, 2007b). This difference can be explained by considering the construction of the fixtures, particularly the stiffness of the ends. The thick tube was closed with a 1-in thick flange bolted to the tube on the end surface; the end of the 3013 can consists of a 0.4 in thick flat section and a 1.25 in long tube section, welded to the tube making up the main

part of the can. The weld is located between the circle S_3-S_5-S_7 and S_4-S_6-S_8.

The strain amplitudes were smaller on gauges S_4, S_6 and S_8, which are 0.3 in away from the end, than on S_2, S_9 (1.8 in away from the end); The strains are shown on figures b in Appendix A). Peak strain increases with increasing initial pressure P_0; the overall trend is linear with sharp increase in the vicinity of the DDT threshold. Below the threshold at $P_0 = 2.6$ bar, the peak strain was on the order of 700 μstrain, which is 1.33 times larger than ϵ_{CJ}. Above the threshold at $P_0 = 2.7$ bar, the peak strain was on the order of 1800 μstrain, which is 1.34 times larger than ϵ_{CJref} and very close to the convention for the onset of plastic behavior (2000 μstrain). For mix B and C, no DDT transition was observed for P_0 up to 3.5 bar with the empty can, which is consistent with the findings with the thick-walled tube, and the peak strains recorded were also comparable to ϵ_{CJ} (see Figure 4d, f).

4 Dynamic Load Factor

The peak value of the strain signals are analyzed in terms of the dynamic load factor (DLF) Φ, which is defined as the ratio of the measured peak strain to the peak strain expected in the case of quasi-static loading.

$$\Phi = \frac{\epsilon_{max}}{\frac{\Delta PR}{Eh}} \tag{2}$$

Table 3 summarizes the DLF computed with Eq. 2 for shots performed with mix A. For Φ_{exp}, $\Delta P = P_{max}$, P_{max} is the maximum value of the measured pressures on transducers 1-4 in Table 4. For Φ_{CJ}, $\Delta P = P_{CJ}$ - P_a. ϵ_{max} is the maximum value of the measured strains on gauges 1-14 in Table 5.

As shown in Table 3, the values of Φ_{exp} ranged between 0.4 and 1.2, values between 1.2 and 2.6 were measured for the empty thick tube configuration. The values obtained indicate loading of the mixed type, intermediate between impulsive and sudden regimes. The values of Φ_{CJ} varied between 1.2 and 3.2, values between 1.7 and 3.5 were measured for the thick tube. The slightly higher values measured for the thick tube configuration may be due to differences in the structural response associated with detonation loads. The critical traveling load speed (Beltman and Shepherd, 2002) for the 3013 cans is approximately 864 m/s, which is much smaller than the ideal detonation velocity ($\approx$ 2900 m/s), but for the thick tube, it is 2865 m/s, which is of the same order as the detonation velocity.

In Fig. 5, the measured strains are compared with estimated strains based on P_{CJ} with dynamic load factors of 1 (static loading), 2 (sudden loading) and 5 (reflected detonation). For the empty can within the DDT range ($P_0 > 2.6$ bar), the maximum measured strains are all larger than $\epsilon_{CJ,\ \Phi=2}$, which is consistent with the results from the thick-walled tube.

Table 3: Dynamic load factors for the empty 3013 outer cans and mixture A.

shot	P_0 (bar)	P_{CJ} (MPa)	P_{max} (MPa)	S_{max} (μstrain)	Φ_{exp}	Φ_{CJ}
10	1	1.872	1.266	244	1.02	1.24
8	2	3.836	3.531	664	1.03	1.64
5	2.5	4.832	5.664	844	0.43	1.66
12	2.6	5.032	4.531	699	1.22	1.32
06	2.7	5.232	7.267	1822	0.69	3.3
7	2.75	5.332	9.825	1583	0.62	2.82
11	3	5.834	9.991	1973	0.60	3.21
17	3	5.834	11.861	1554	0.55	2.53
13	3.5	6.841	9.793	1632	0.75	2.26
16	3.5	6.841	8.129	1607	0.97	2.23

This is because DDT occurred close to the tube end, producing much higher strains than the case where detonation was initiated promptly.

5 Summary

In Part III of the test program, we have examined DDT transition and structural response of the actual 3013 outer can without the inner can. Our findings can be summarized as follows:

1. For mix A, the DDT threshold was observed at P_0=2.6-2.7 bar for the empty 3013 outer can, and all the transitions occurred close to the tube end for $2.7 \leq P_0 \leq 3.5$ bar.

2. For mix B and C, no DDT transition was observed for $P_0 \leq 3.5$ bar. The transition thresholds for all three mixes are consistent with the results of thick-wall tube tests.

3. The hoop strain on the 3013 cans at fourteen locations were measured in the tests. The maximum strain observed was ≈2000 μstrain near the middle of the tube for an initial pressure of 3.0 bar and Mix A.

4. The measured strains are in agreement with estimates using the computed CJ pressure and a dynamic load factor $\Phi \approx 3.5$ (see Liang and Shepherd, 2007b, Table 5). For example, this estimation method predicts a peak strain of about 1970 μ strain at 3.0 bar for Mix A. The peak value of the maximum strain was found at 3 bar, which is just above the threshold pressure range for transition to detonation. This is consistent with other studies carried out at Caltech that show the maximum strains are always

found close to the threshold for transition to detonation. Below the threshold, the peak strains are substantially smaller (less than 1000 μstrain) since the combustion mode is deflagration and much lower over-pressures are produced for deflagrations than for DDT. Above the DDT threshold, transition to detonation occurs with less precompression prior to the DDT event than in the onset regime. As a consequence, the peak pressures and strains are slightly lower (1760 μstrain) at 3.5 bar than at 3 bar.

5. We were not able to test an annular configuration with an inner can inside the 3013 outer can due to limitations in the manufacturing process. However, the estimated maximum strains (see Liang and Shepherd, 2007b, Table 9) based on the measured pressure histories from the thick-wall tube (annular configuration 2a) and a single degree of freedom model (see Liang and Shepherd, 2007b, Section 5.2) are substantially smaller than the measured values for the 3013 outer can. For example, the SDOF method predicts a peak strain of 1165 μstrain for an initial pressure of 3.0 bar and Mix A vs a peak measured value of 1970 μstrain in the 3013 can. Based on these results, we predict that the effect of the annular space created by the inner can will be to reduce the peak strain by 60% from the values measured for DDT in this report. However, as discussed in earlier reports (Liang and Shepherd, 2007a,b), the presence of the annular gap will significantly lower the threshold pressures for DDT compared to the empty can.

6 Implications for Safety Assessment

The tests of the 3013 cans show that up to the maximum initial pressure of 3.5 bar, minimal permanent deformation occurred with peak strains of 0.2% or less even with the most energetic mixture (mix A) of stoichiometric hydrogen-oxygen.

The tests were carried out without an inner can, which is a much more severe condition for testing than the annular configuration that is expected to exist in practice. Testing without the inner can results in delaying the transition threshold to higher pressures compared to the annular configuration and only mix A will undergo DDT at the maximum pressures we were able to test.

In the worst case, where DDT occurs close to the end of the can, the maximum strain can be bounded by using a dynamic load factor of $\Phi_{CJ} = 5$. This is conservative since the peak measured strains have a maximum value of $\Phi_{CJ} = 3.5$. However, considering the peak strains that might be possible due to detonation reflection, a value of $\Phi_{CJ} = 5$ will bound

all cases and provide some margin.

We believe that we have addressed the most serious potential explosion hazard that can occur within the 3013 cans. All of our testing and estimates indicate that there is no possibility of rupture of the outer can and the peak deformations will be limited to a maximum of 0.2%.

As we have stated in the thick-walled tube report, there are several additional issues associated with the inner can that we have not addressed. These include the buckling of the inner can due to an explosion in the annulus and the plastic deformation of the inner can due to an internal explosion. Some simple estimates are given in the Appendices for these processes and show that some limited buckling or plastic deformation of the inner can may be expected. Given the demonstrated capacity of the outer can for containing an internal explosion, the response of the inner can is not expected to play a significant role in determining the overall integrity of the containment system.

Acknowledgments

George Rawls of the Savannah River Site worked with us to design the modifications and supervised the manufacture of the modified 3013 cans.

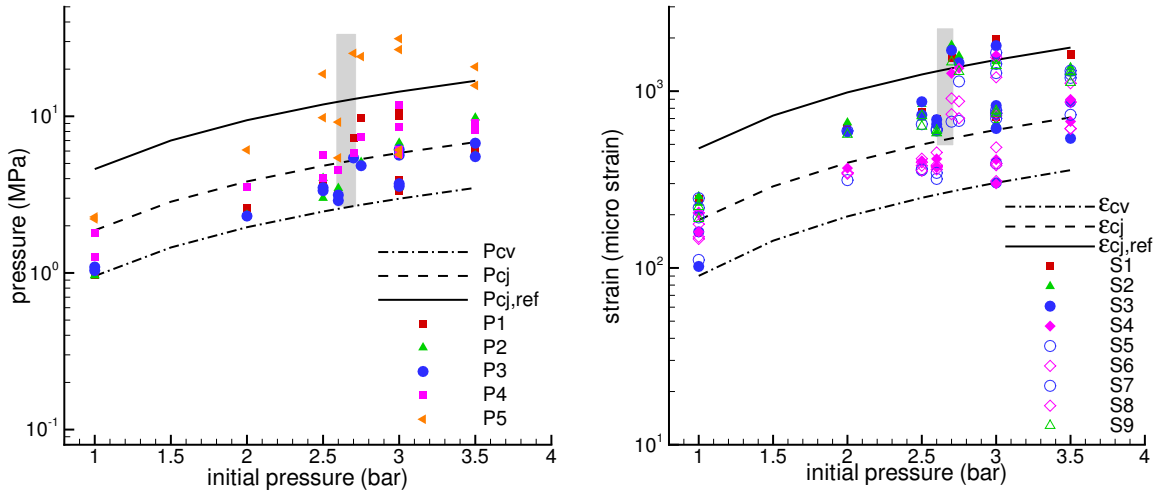

a) peak pressure, mix A

b) peak strain, mix A

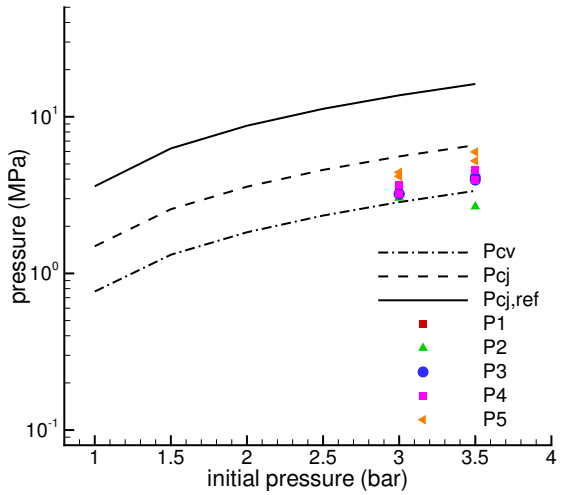

c) peak pressure, mix B

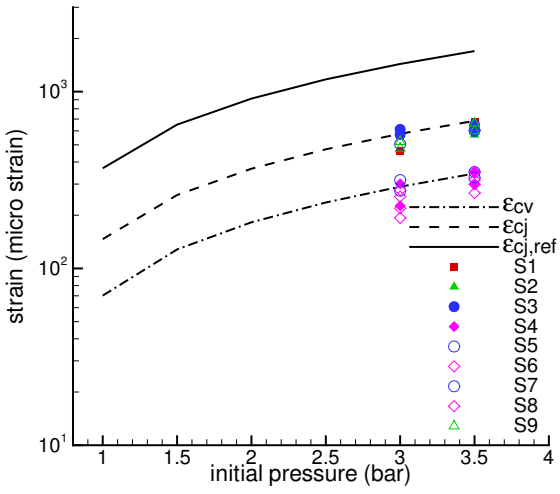

d) peak strain, mix B

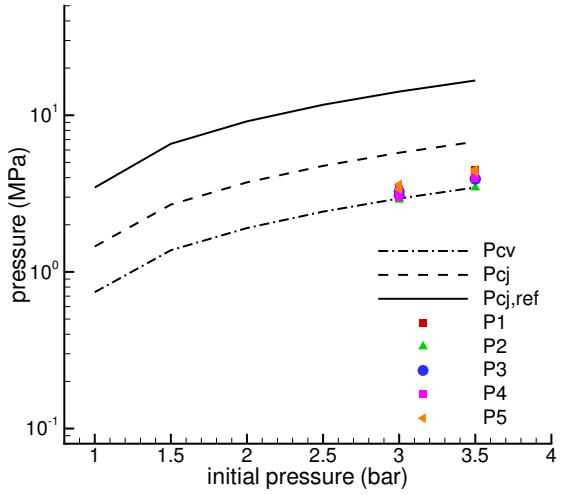

e) peak pressure, mix C

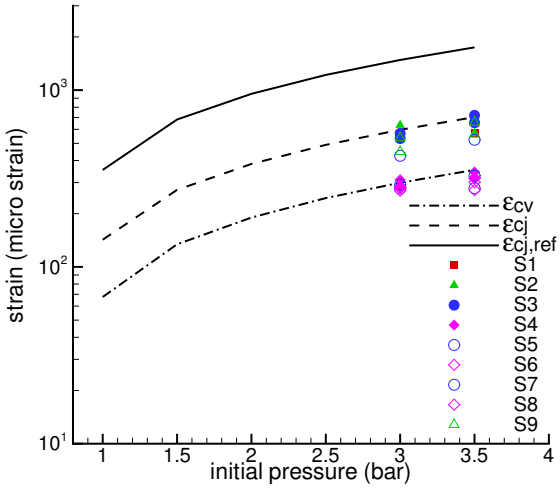

f) peak strain, mix C

Figure 4: Comparison of DDT thresholds and peak pressures for three mixtures and empty can. Gray vertical shaded region indicates the DDT threshold. No DDT observed for mix B and C.

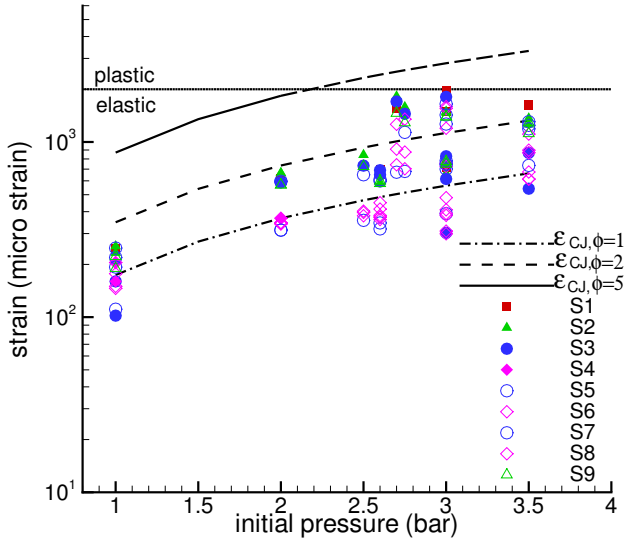

Figure 5: Comparison between the measured strains for S_1-S_9 the estimated strain (ϵ_{CJ}) based on P_{CJ} and $\Phi = 1$, 2 and 5 for empty cans and mix A. The values for S_{10}-S_{14} are not shown in the figure since the peak values are all smaller than for hose shown for S_1-S_9. The peak values of the noisy signals are not included

Bibliography

W.M. Beltman and J.E. Shepherd. Linear elastic response of tubes to internal detonation loading. *Journal of Sound and Vibration*, 252(4):617–655, 2002. 10

Z. Liang and J.E. Shepherd. Explosion testing of nested can containment system part I: Planar fixture. Technical report, Graduate Aeronautical Laboratories California Institute of Technology, January 2007a. 5, 6, 12

Z. Liang and J.E. Shepherd. Explosion testing of nested can containment system part II: Thick-walled tube. Technical report, Graduate Aeronautical Laboratories California Institute of Technology, Febuary 2007b. 5, 8, 9, 11, 12

W.C. Reynolds. The element potential method for chemical equilibrium analysis: implementation in the interactive program STANJAN. Technical report, Mechanical Engineering Department, Stanford University, 1986. 8

W. C. Young and R. G. Budynas. *Roark's Formulas for Stress and Strain.* McGraw-Hill, 1989. 43, 44

A Shot list

Table 4: Summary of the peak pressure .

shot	P_0	P_{CV}	P_{CJ}	P_{CJref}	$P_{1,max}$	$P_{2,max}$	$P_{3,max}$	$P_{4,max}$	$P_{5,max}$	DDT
	(bar)	(MPa)								
mixture A										
10	1.0	1.958	3.836	9.441	1.023	0.967	1.091	1.266	2.278	–
14	1.0	1.958	3.836	9.441	0.975	0.960	1.036	1.800	2.211	–
8	2.0	1.958	3.836	9.441	2.586	2.348	2.308	3.531	6.098	–
05	2.5	2.466	4.832	11.895	3.644	3.005	3.350	4.020	9.800	–
5	2.5	2.466	4.832	11.895	3.402	4.032	3.503	5.664	18.628	–
6	2.6	2.568	5.032	12.387	3.208	3.052	3.142	4.531	9.180	–
12	2.6	2.568	5.032	12.387	2.904	3.479	2.898	4.531	5.428	–
06	2.7	2.670	5.232	12.881	7.267	5.571	5.421	5.830	25.22	P_4
7	2.75	2.271	5.332	13.128	9.825	5.097	4.838	7.396	24.056	P_4
9	3.0	2.978	5.834	14.364	3.353	3.519	3.573	5.730	6.097	–
11	3.0	2.978	5.834	14.364	9.991	6.360	5.650	8.596	31.29	P_4
15	3.0	2.978	5.834	14.364	3.920	3.696	3.712	6.064	5.696	–
17	3.0	2.978	5.834	14.364	11.291	6.761	6.130	11.861	26.669	P_4
13	3.5	3.492	6.841	16.842	6.499	9.793	6.735	9.129	20.705	P_4
16	3.5	3.492	6.841	16.842	6.105	5.637	5.526	8.129	15.747	P_4
mixture B										
01	3.0	2.853	5.582	13.712	3.291	3.039	3.204	3.216	4.172	–
1	3.0	2.853	5.582	13.712	3.506	3.045	3.225	3.665	4.422	–
02	3.5	3.366	6.589	16.194	4.135	2.669	4.115	3.953	5.231	–
2	3.5	3.366	6.589	16.194	4.052	3.907	3.941	4.598	5.964	–
mixture C										
03	3.0	2.941	5.762	14.160	3.277	2.881	3.079	3.015	3.377	–
3	3.0	2.941	5.762	14.160	3.229	2.953	3.267	3.398	3.618	–
04	3.5	3.459	6.777	16.666	4.446	3.453	3.906	3.953	4.503	–
4	3.5	3.459	6.777	16.666	3.893	3.834	3.934	4.331	4.355	–

Table 5: Summary of the peak strains. The noisy strain signals were not processed.

shot	P_0	ϵ_{CV}	ϵ_{CJ}	ϵ_{CJref}	S_1	S_2	S_3	S_4	S_5	S_6	S_7	S_8	S_9	S_{max}
	(bar)	(μstrain)												
mixture A														
10	1.0	196	394	984	244	233	160	205	111	150	193	205	190	S_1
14	1.0	196	394	984	246	254	102	160	219	146	248	177	222	S_2
8	2.0	196	394	984	616	664	589	367	314	341	596	346	569	S_2
05	2.5	249	499	1240	767	706	871	401	362	355	–	415	632	S_3
5	2.5	249	499	1240	725	844	733	403	357	379	650	396	725	S_2
6	2.6	260	520	1295	651	682	690	414	319	373	599	381	599	S_3
12	2.6	260	520	1295	699	578	650	372	345	361	611	450	580	S_1
06	2.7	271	541	1346	1546	1822	1702	1262	672	741	–	910	1460	S_2
7	2.75	276	551	1373	1471	1583	–	1350	679	876	1135	703	1289	S_2
9	3.0	303	604	1503	797	754	–	410	390	381	746	391	774	S_3
11	3.0	303	604	1503	1973	1474	–	1592	700	725	1649	1198	1393	S_1
15	3.0	303	604	1503	711	659	303	299	749	310	781	481	748	S_7
17	3.0	303	604	1503	1492	1490	615	–	1266	757	1426	1554	1391	S_8
13	3.5	357	710	1764	1632	1260	–	674	735	613	1189	1109	1289	S_1
16	3.5	357	710	1764	1607	1365	541	898	1305	615	1245	868	1118	S_1
shot	P_0	ϵ_{CV}	ϵ_{CJ}	ϵ_{CJref}	S_{10}	S_{11}	S_{12}	S_{13}	S_{14}					
	(bar)	(μstrain)												
14	1.0	196	394	984	–	238	203	237	273					S_2
15	3.0	303	604	1503	–	721	689	696	725					S_7
17	3.0	303	604	1503	–	1540	1425	1177	–					S_8
16	3.5	357	710	1764	–	1127	1419	1221	1286					S_1
mixture B														
01	3.0	290	578	1434	565	571	612	226	275	193	–	219	571	S_2
1	3.0	290	578	1434	459	590	573	301	316	277	505	255	478	S_2
02	3.5	344	684	1696	619	570	595	301	327	267	–	352	662	S_1
2	3.5	344	684	1696	672	621	649	352	351	317	603	299	599	S_1
mixture C														
03	3.0	299	597	1481	543	634	569	283	292	270	–	279	537	S_2
3	3.0	299	597	1481	550	526	532	311	278	282	425	283	448	S_1
04	3.5	354	704	1745	648	707	720	321	328	272	–	318	657	S_3
4	3.5	354	704	1745	572	569	654	344	279	317	524	301	562	S_1

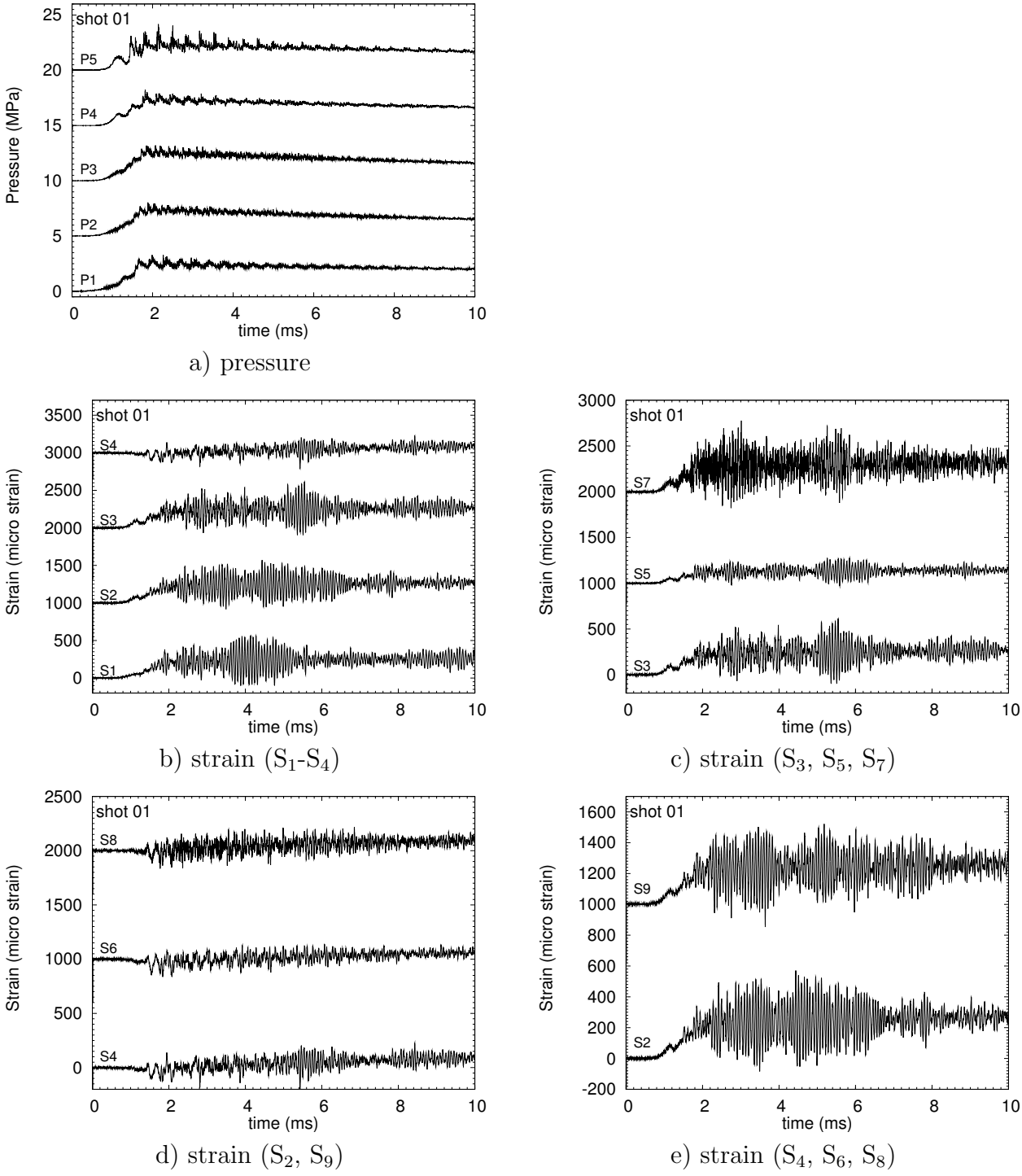

a) pressure

b) strain (S_1-S_4)

c) strain (S_3, S_5, S_7)

d) strain (S_2, S_9)

e) strain (S_4, S_6, S_8)

Figure 6: Pressure and strain traces for mixture B and P_0=3 bar with empty tube, shot 01.

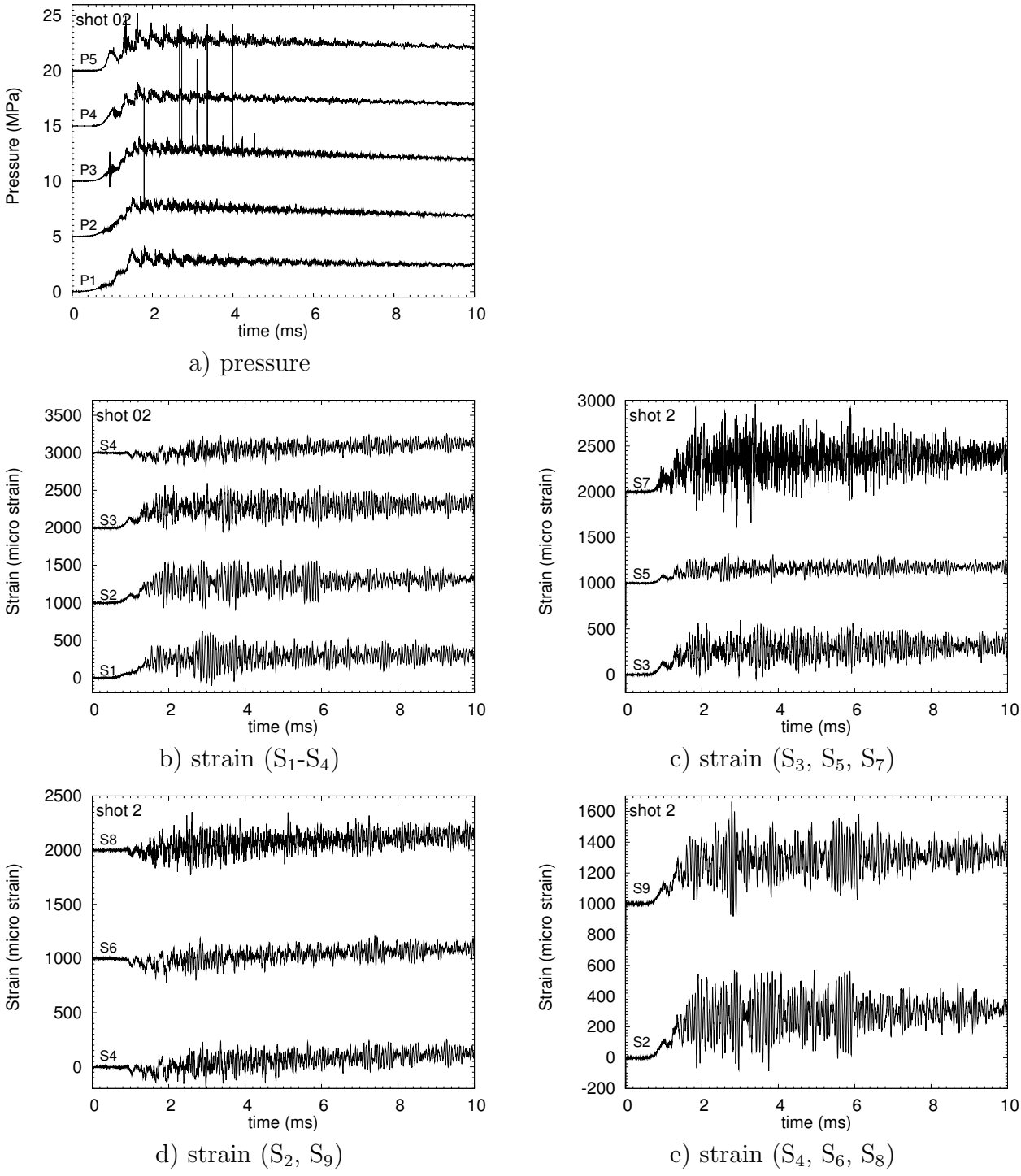

Figure 7: Pressure and strain traces for mixture B and P_0=3.5 bar with empty tube, shot 02.

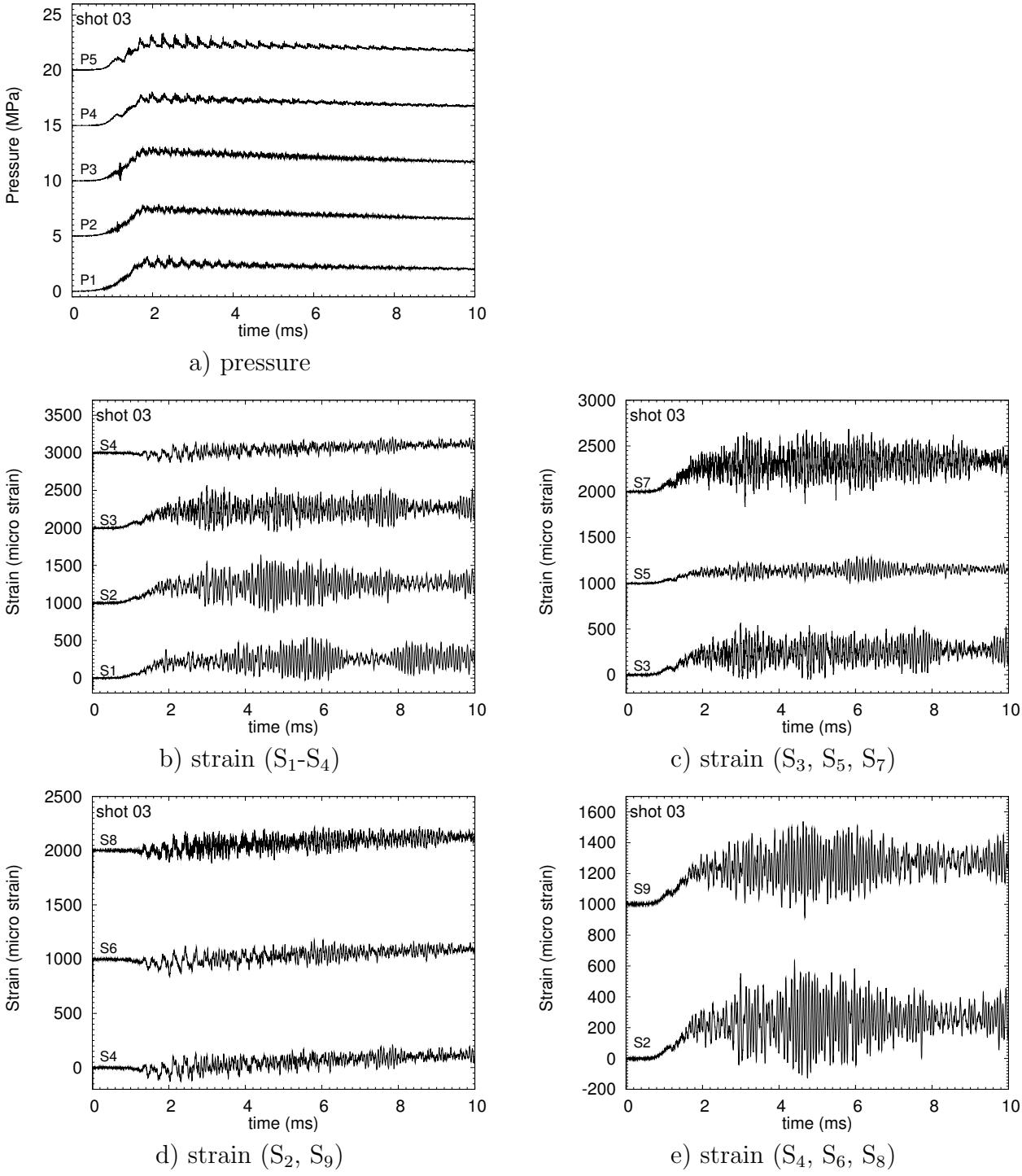

a) pressure

b) strain (S_1-S_4)

c) strain (S_3, S_5, S_7)

d) strain (S_2, S_9)

e) strain (S_4, S_6, S_8)

Figure 8: Pressure and strain traces for mixture C and P_0=3 bar with empty tube, shot 03.

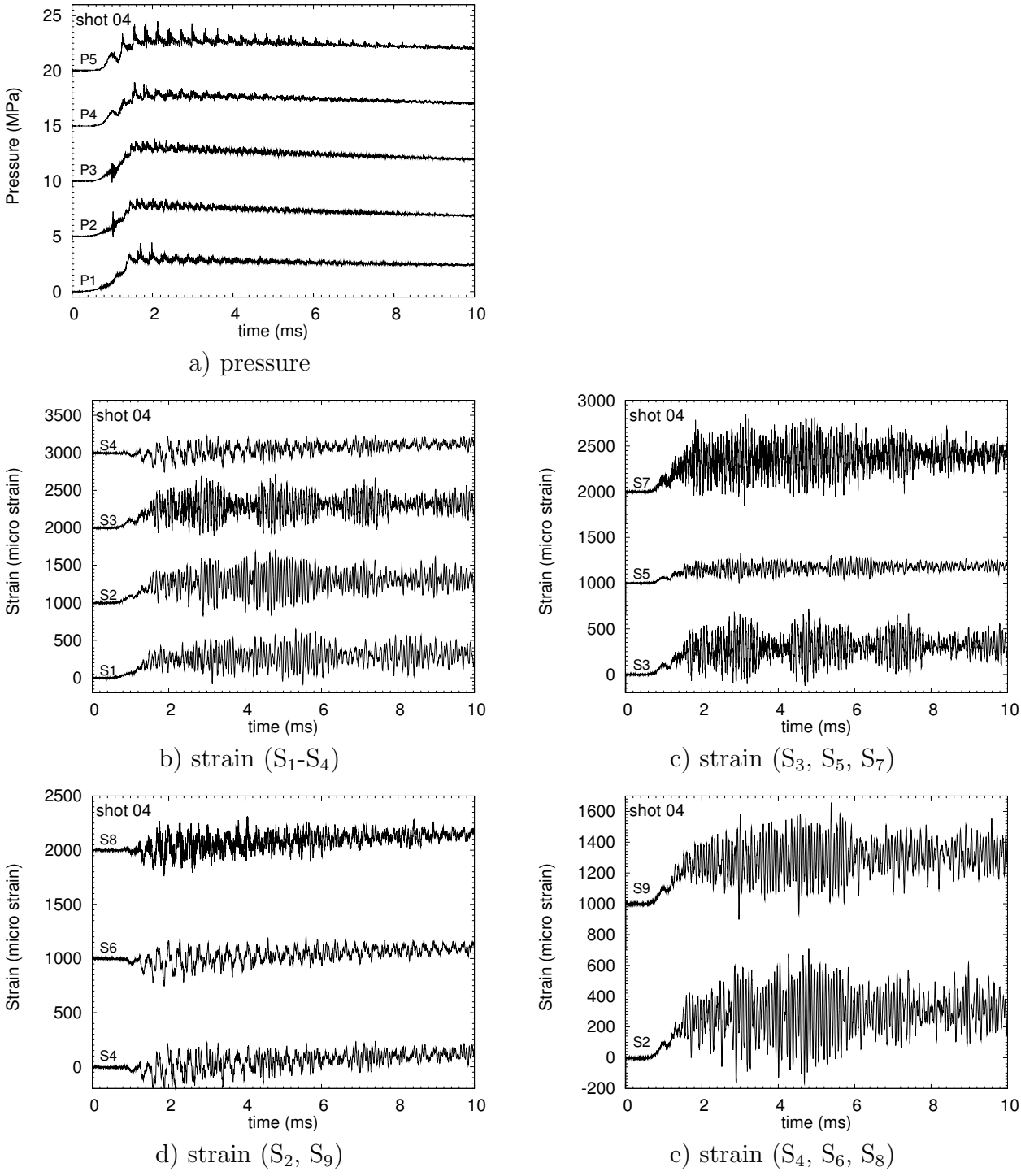

Figure 9: Pressure and strain traces for mixture C and P_0=3.5 bar with empty tube, shot 04.

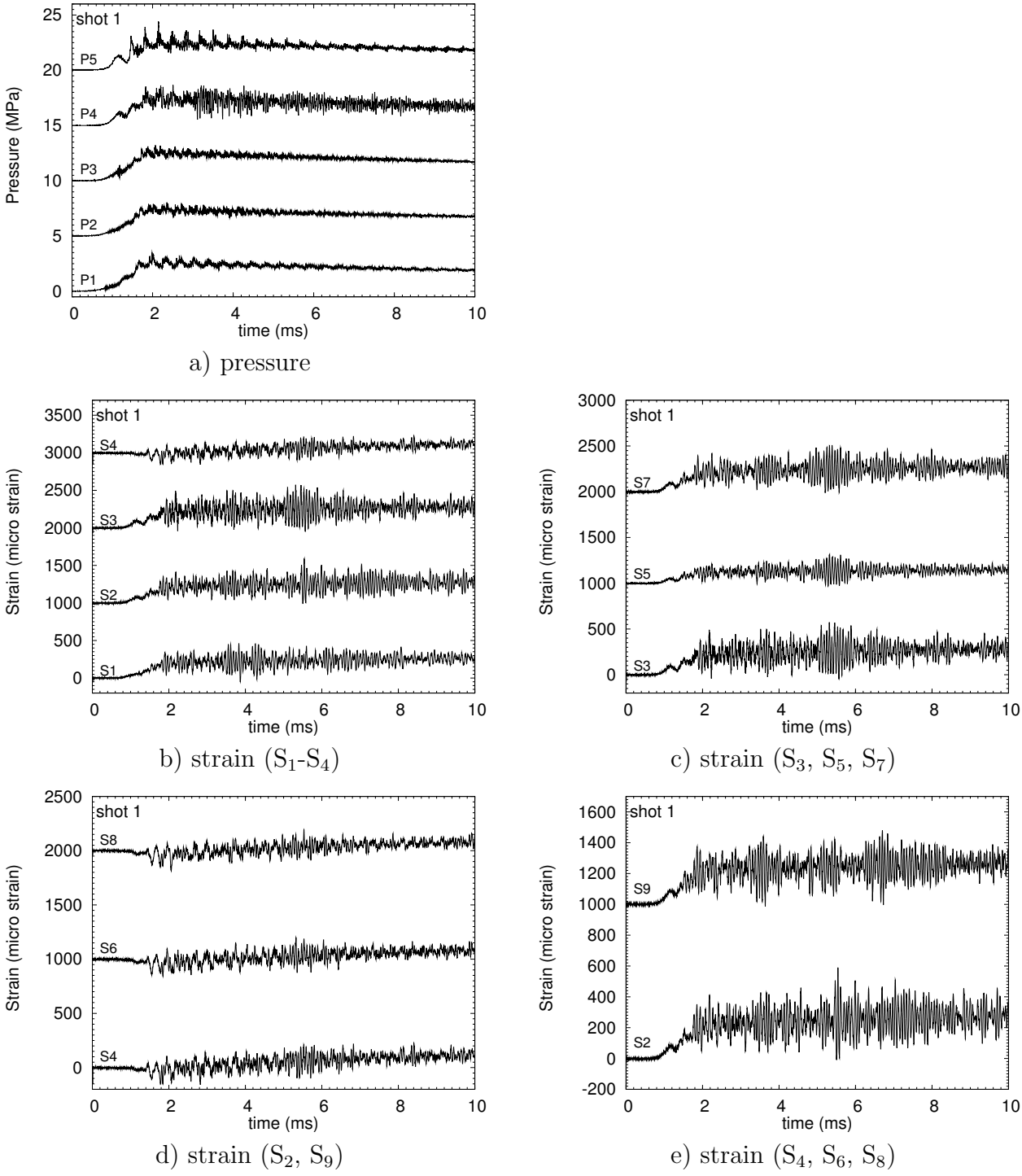

Figure 10: Pressure and strain traces for mixture B and P_0=3 bar with empty tube, shot 1.

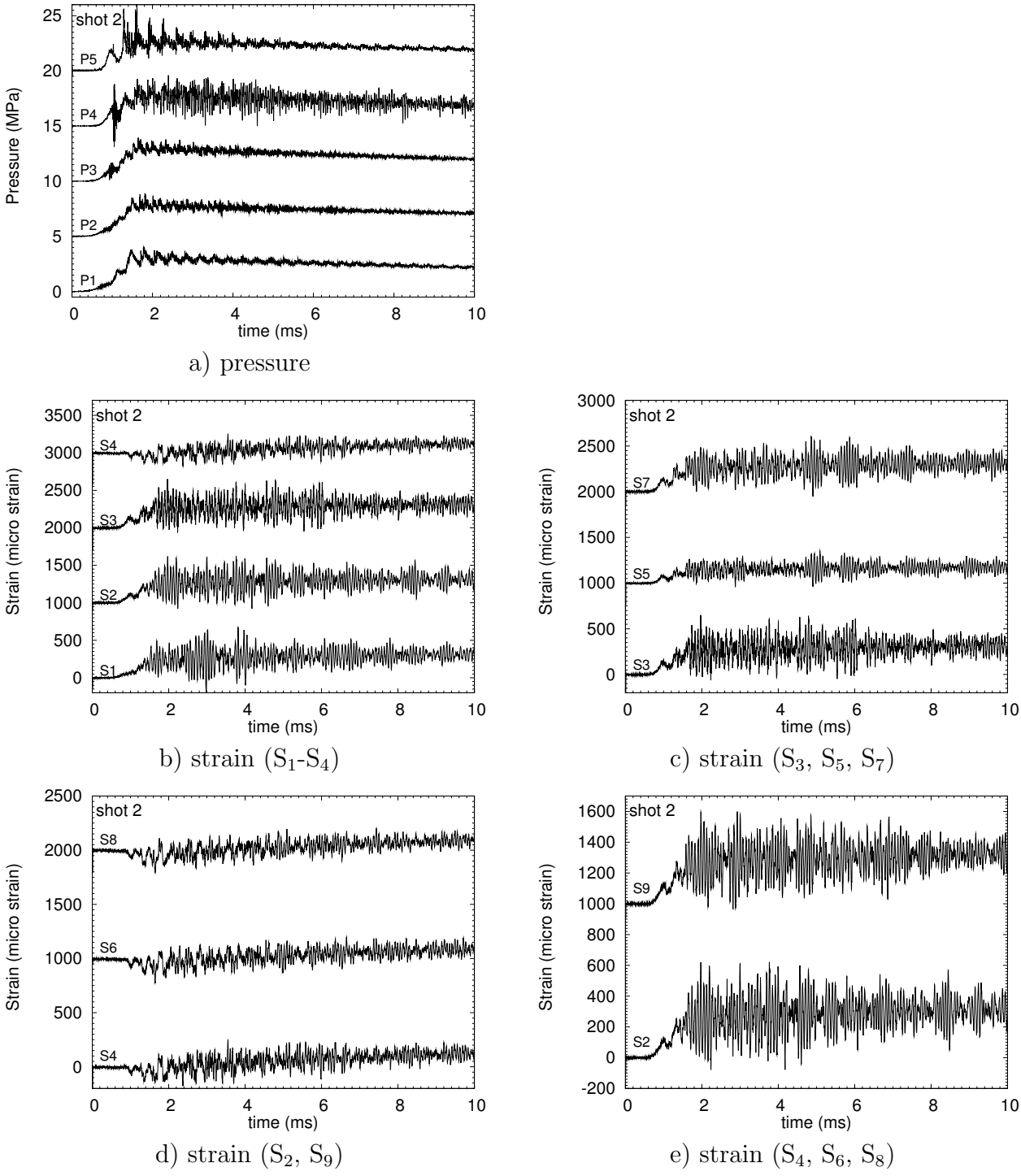

Figure 11: Pressure and strain traces for mixture B and P_0=3.5 bar with empty tube, shot 2.

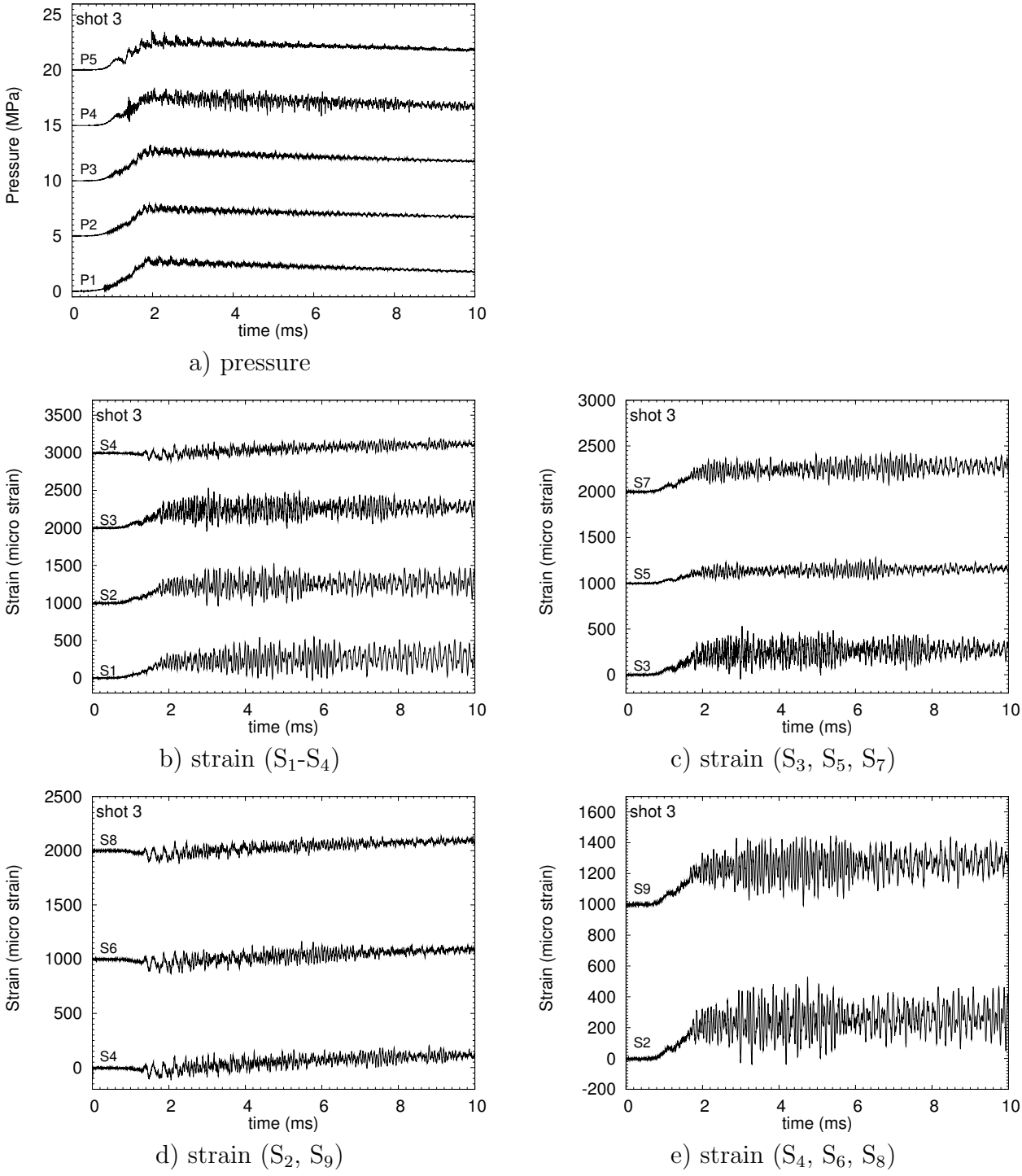

Figure 12: Pressure and strain traces for mixture C and P_0=3 bar with empty tube, shot 3.

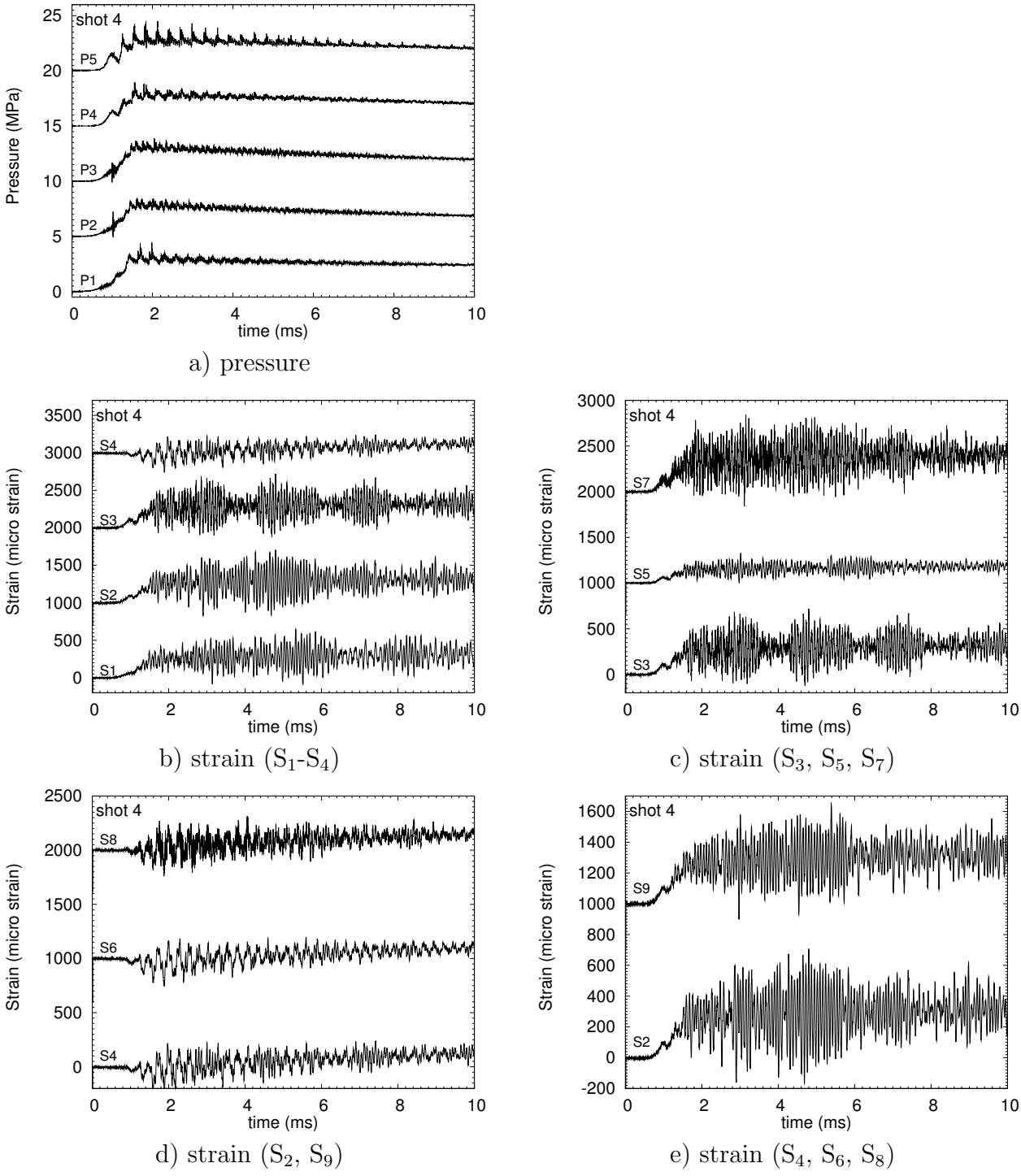

Figure 13: Pressure and strain traces for mixture C and P_0=3.5 bar with empty tube, shot 4.

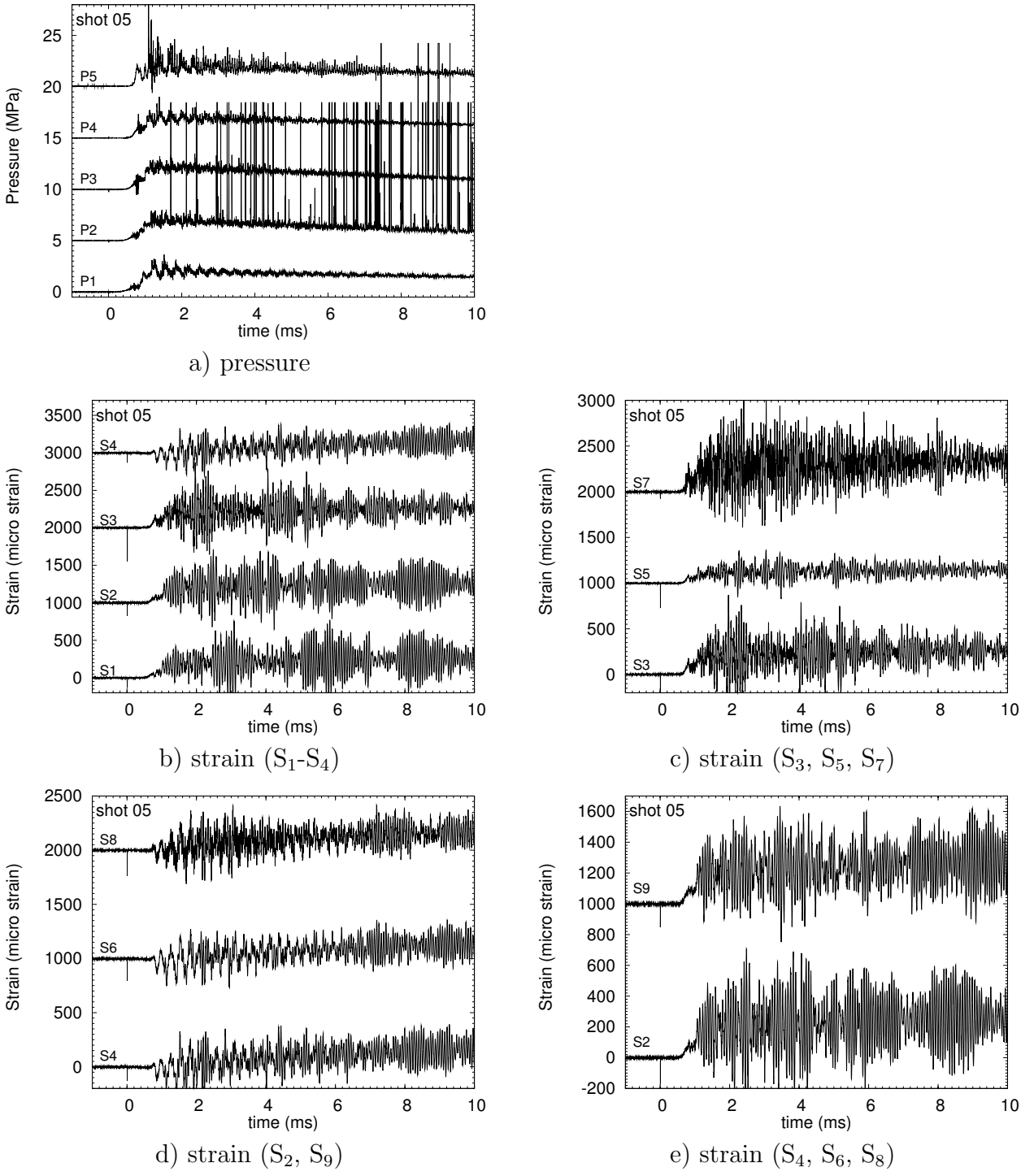

Figure 14: Pressure and strain traces for mixture A and P_0=2.5 bar with empty tube, shot 05.

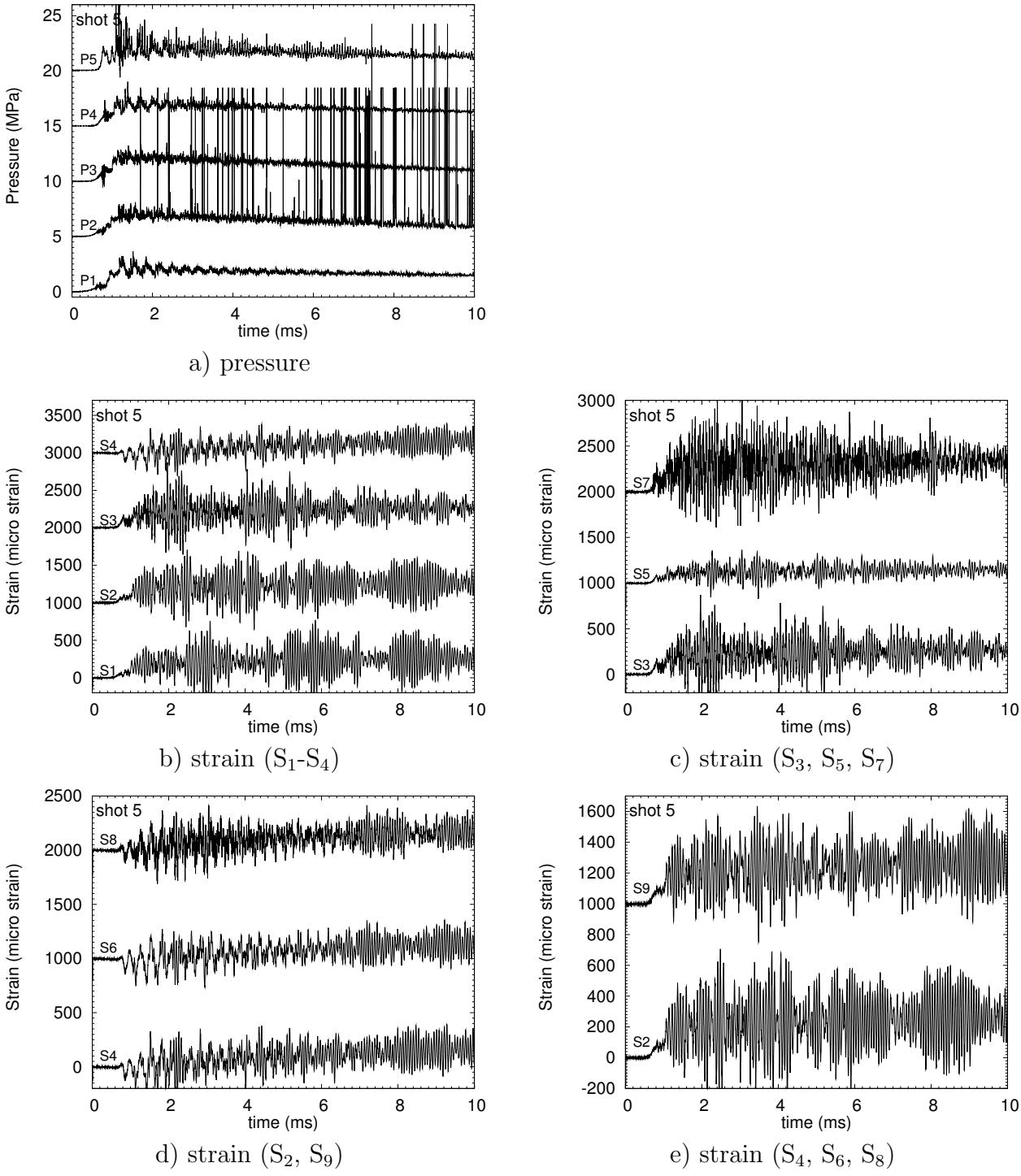

a) pressure

b) strain (S_1-S_4)

c) strain (S_3, S_5, S_7)

d) strain (S_2, S_9)

e) strain (S_4, S_6, S_8)

Figure 15: Pressure and strain traces for mixture A and P_0=2.5 bar with empty tube, shot 5.

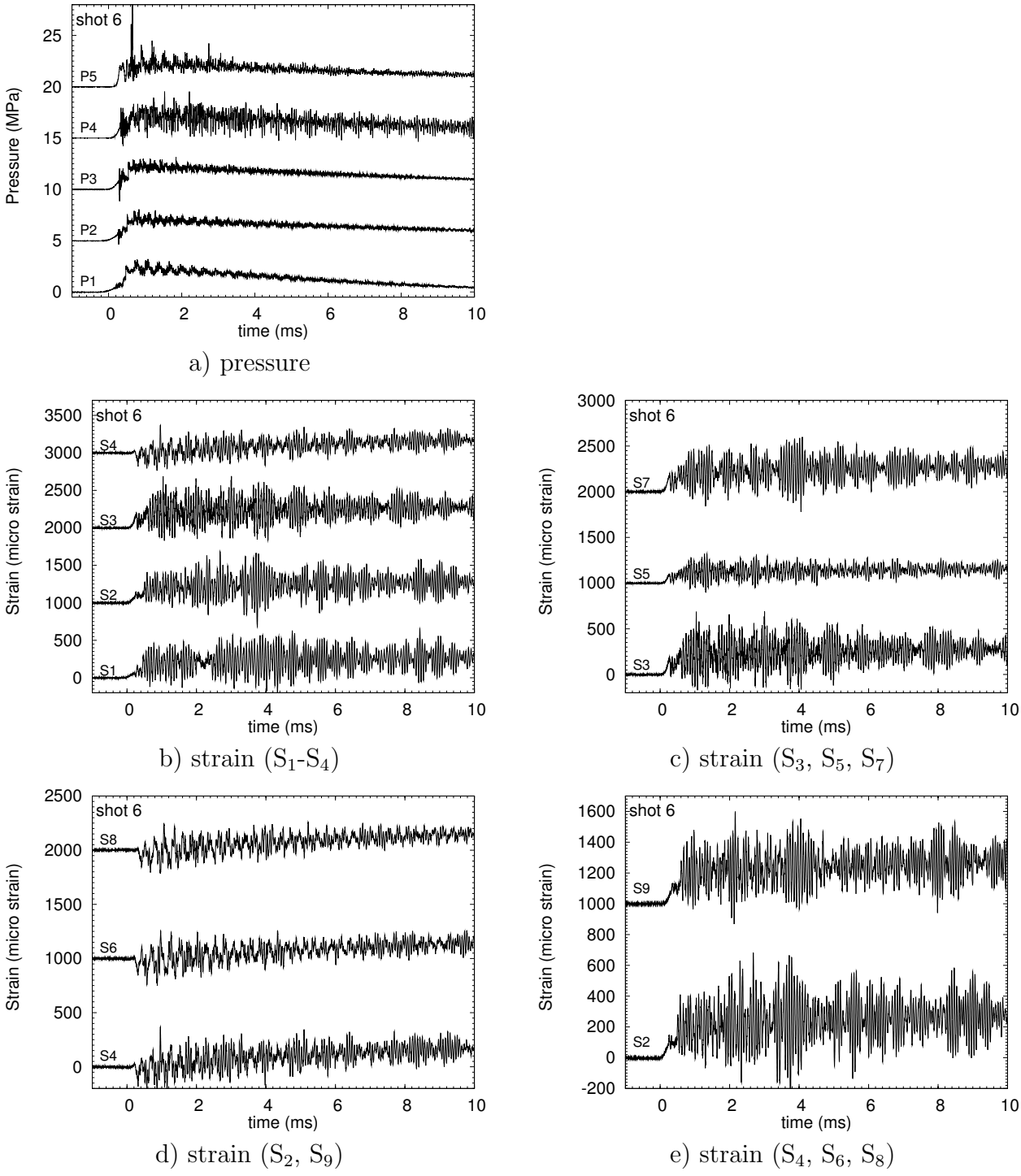

Figure 16: Pressure and strain traces for mixture A and P_0=2.6 bar with empty tube, shot 6.

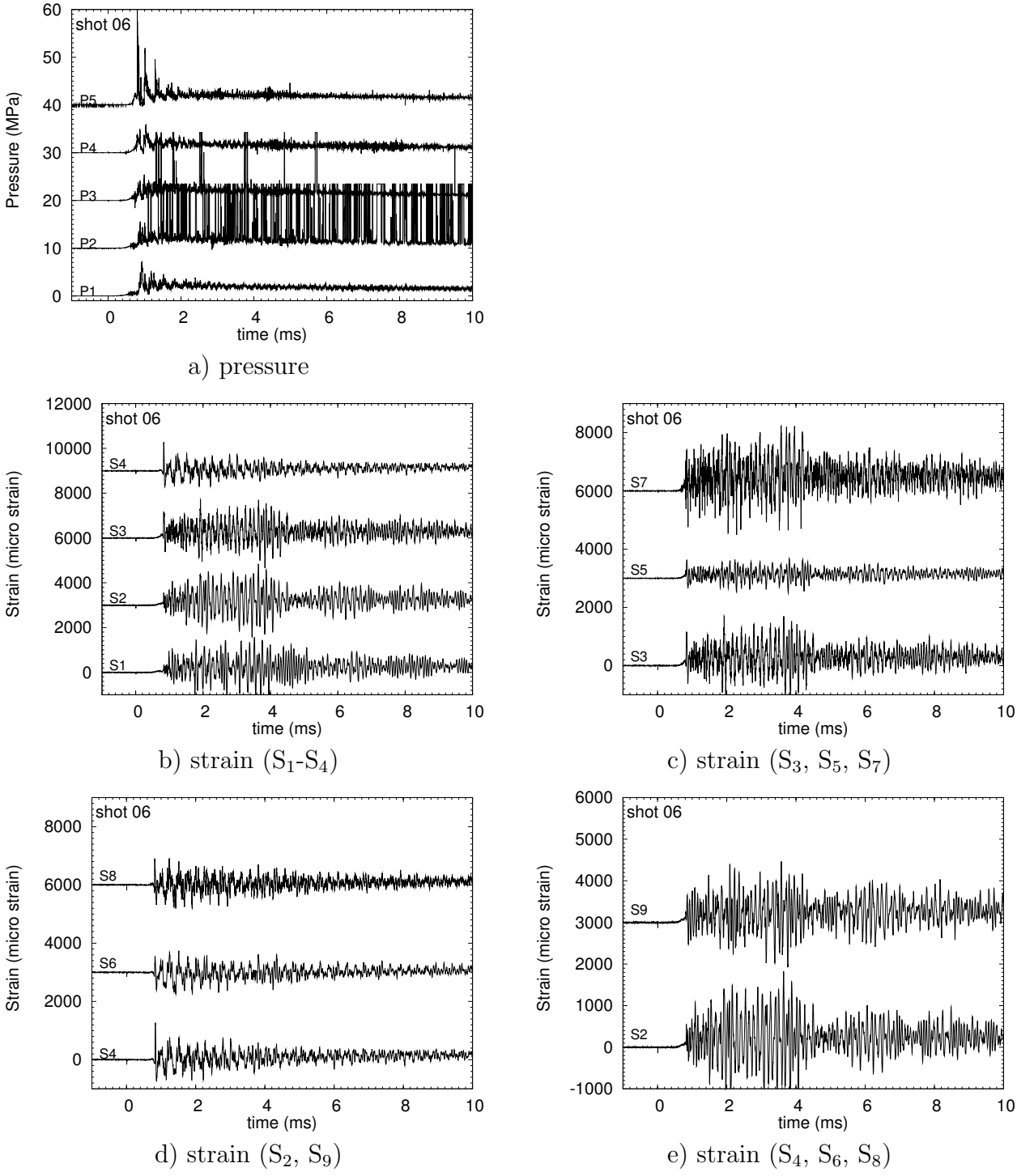

Figure 17: Pressure and strain traces for mixture A and P_0=2.7 bar with empty tube, shot 06.

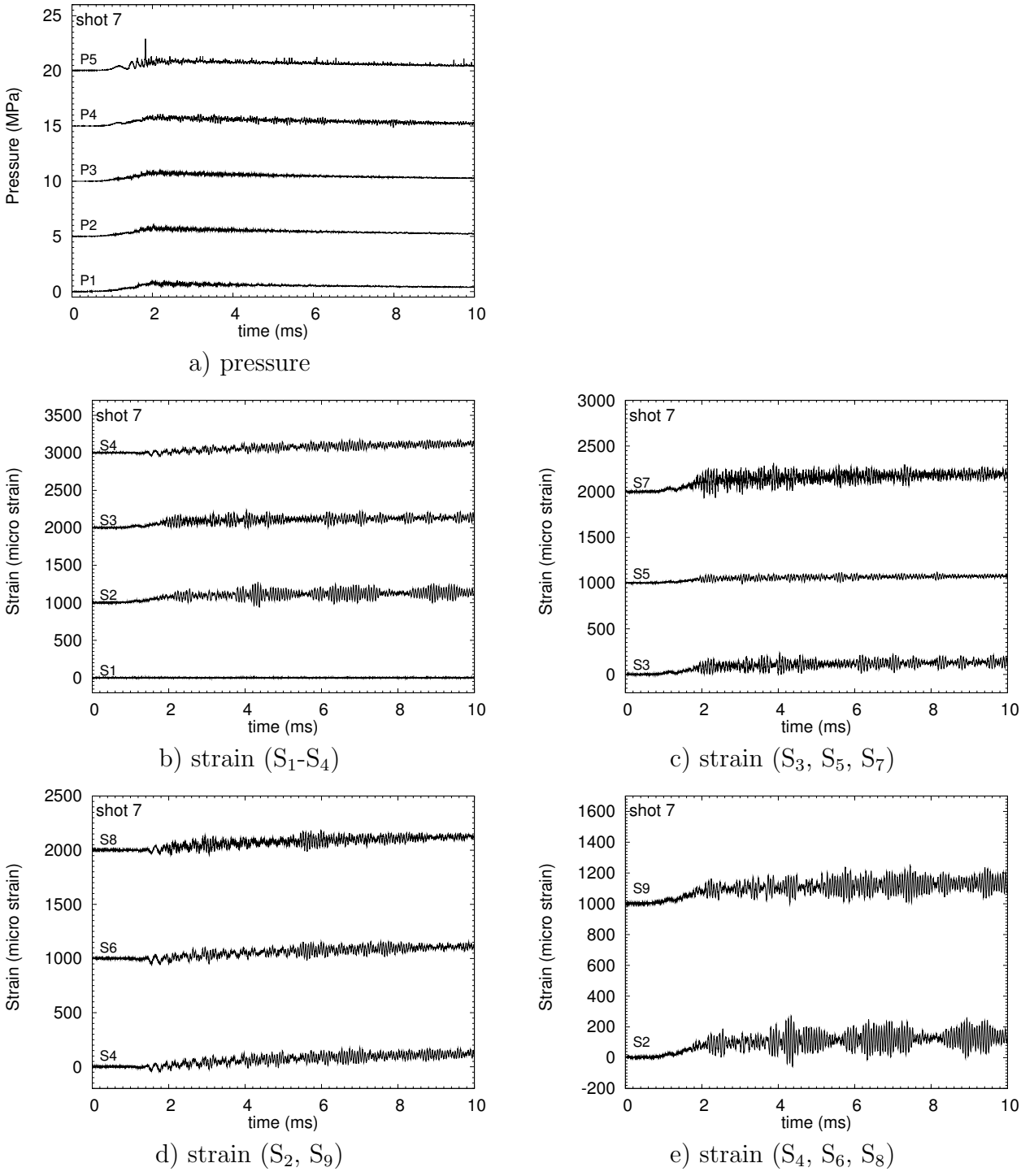

Figure 18: Pressure and strain traces for mixture A and P_0=2.75 bar with empty tube, shot 7.

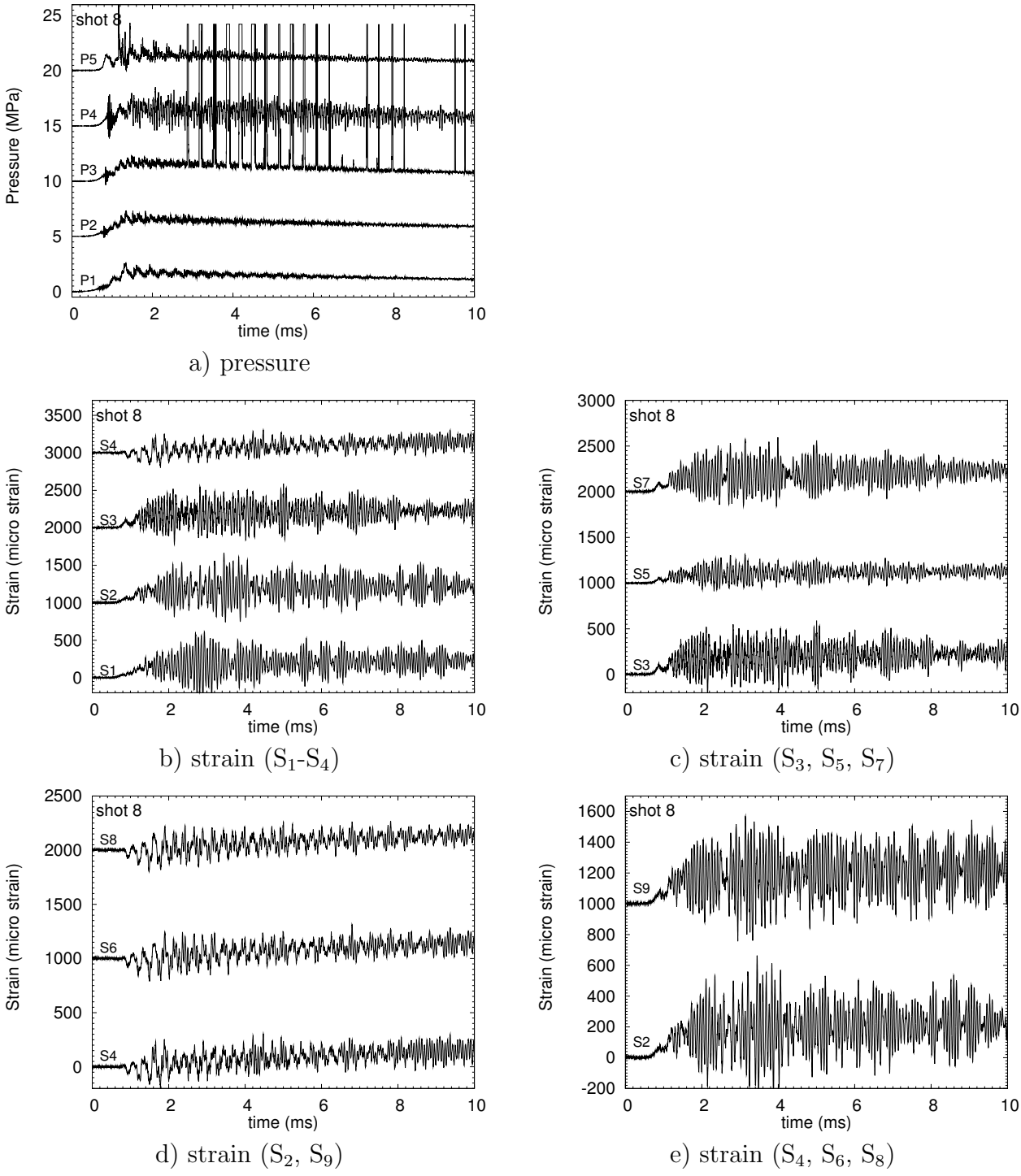

Figure 19: Pressure and strain traces for mixture A and P_0=2.0 bar with empty tube, shot 8.

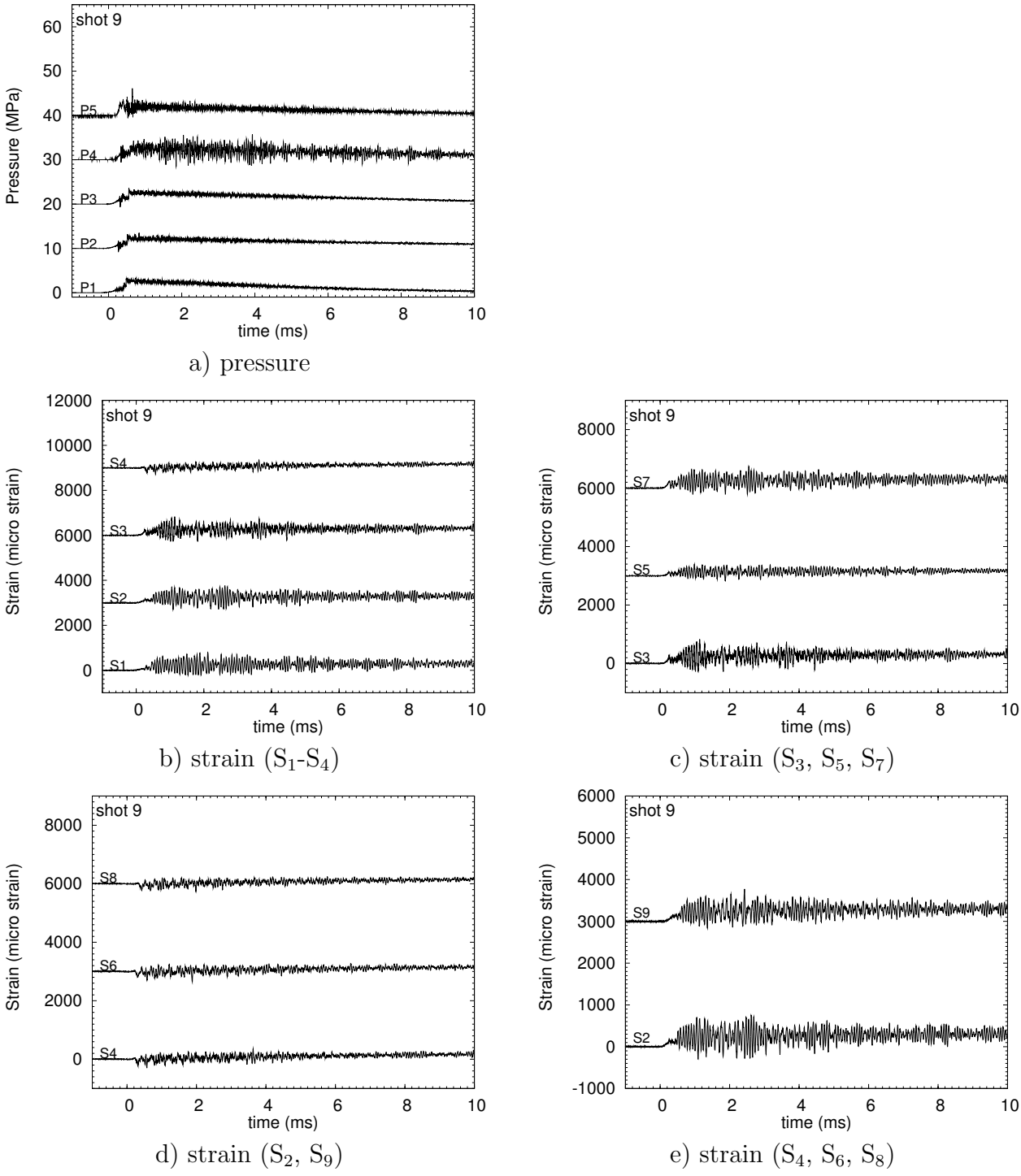

a) pressure

b) strain (S_1-S_4)

c) strain (S_3, S_5, S_7)

d) strain (S_2, S_9)

e) strain (S_4, S_6, S_8)

Figure 20: Pressure and strain traces for mixture A and P_0=3.0 bar with empty tube, shot 9.

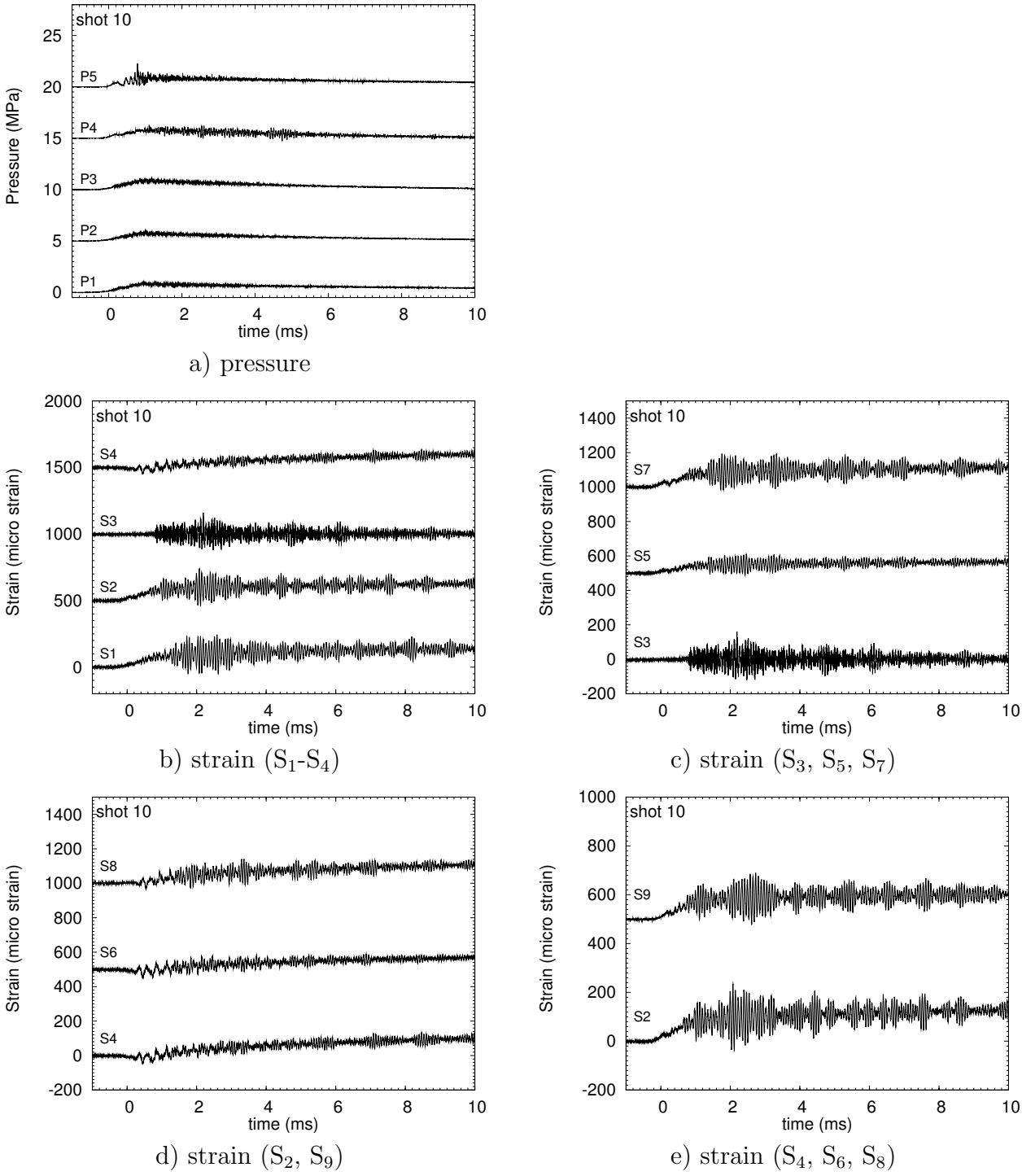

Figure 21: Pressure and strain traces for mixture A and P_0=1.0 bar with empty tube, shot 10.

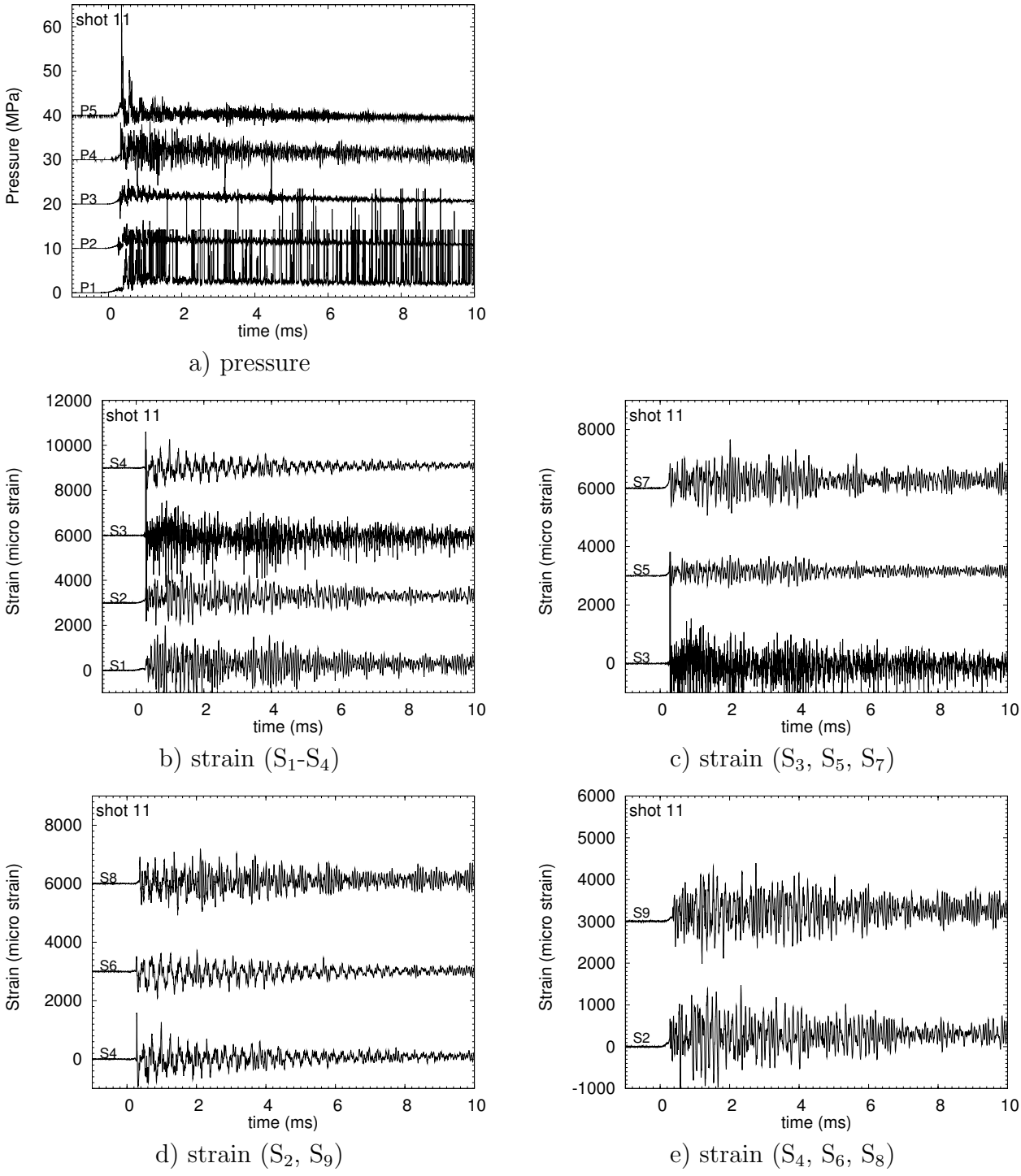

a) pressure

b) strain (S_1-S_4)

c) strain (S_3, S_5, S_7)

d) strain (S_2, S_9)

e) strain (S_4, S_6, S_8)

Figure 22: Pressure and strain traces for mixture A and P_0=3.0 bar with empty tube, shot 11.

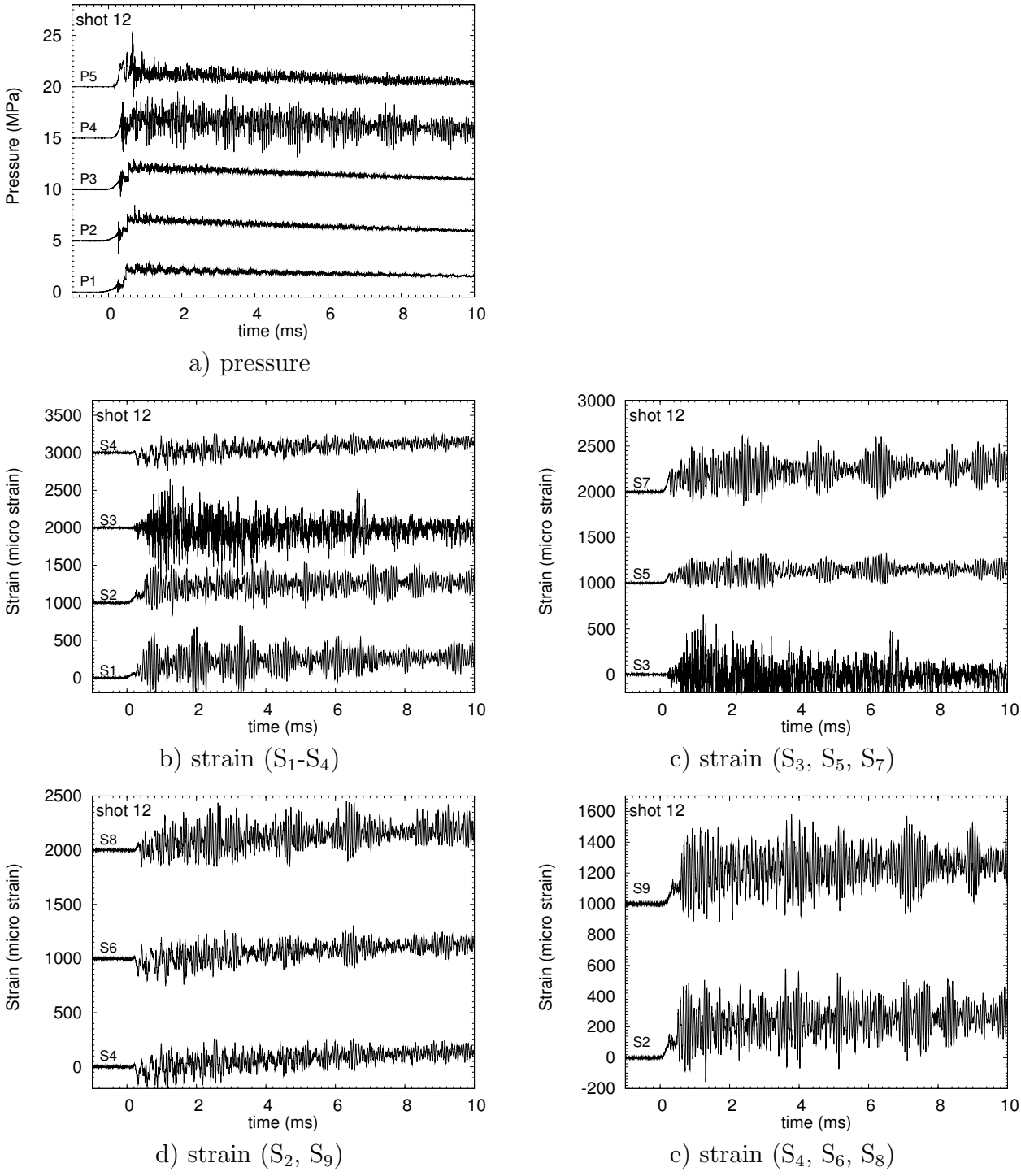

Figure 23: Pressure and strain traces for mixture A and P_0=2.6 bar with empty tube, shot 12.

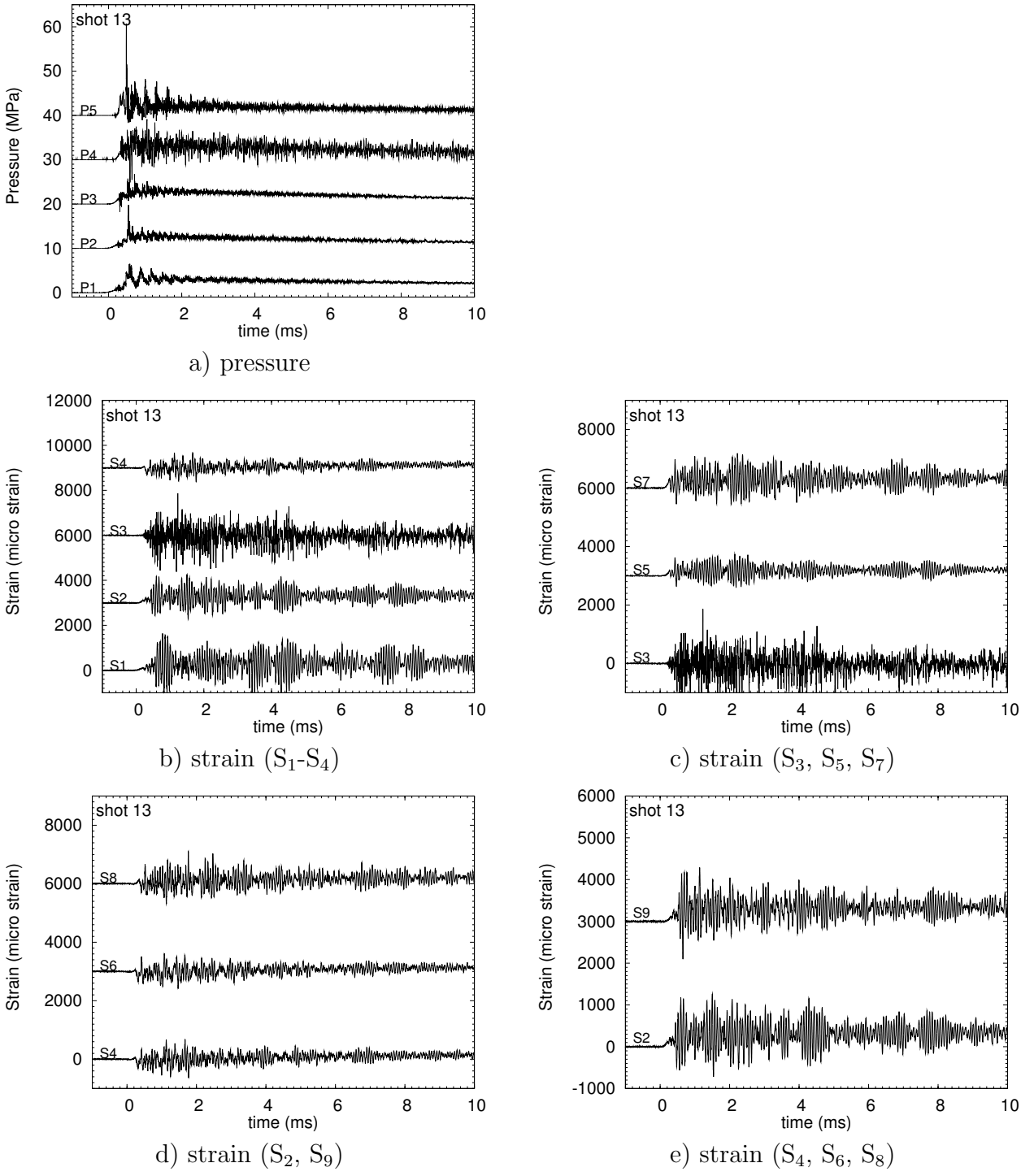

Figure 24: Pressure and strain traces for mixture A and P_0=3.5 bar with empty tube, shot 13.

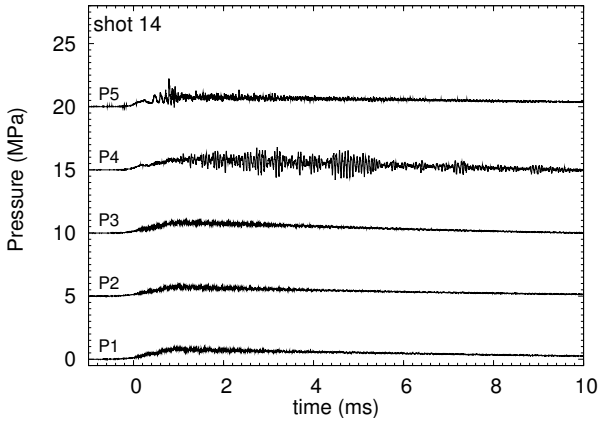

a) pressure

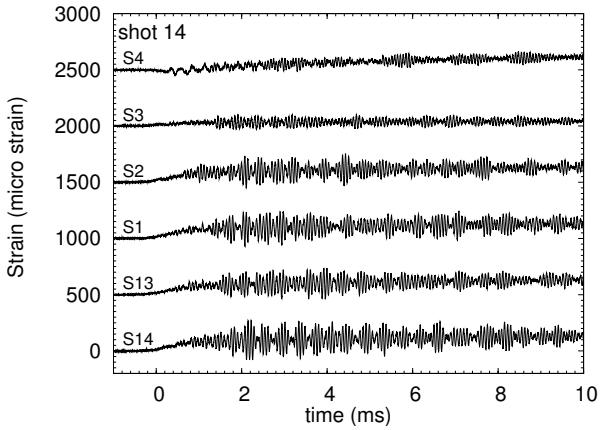

b) strain (S_{13}, S_{14}, S_1-S_4)

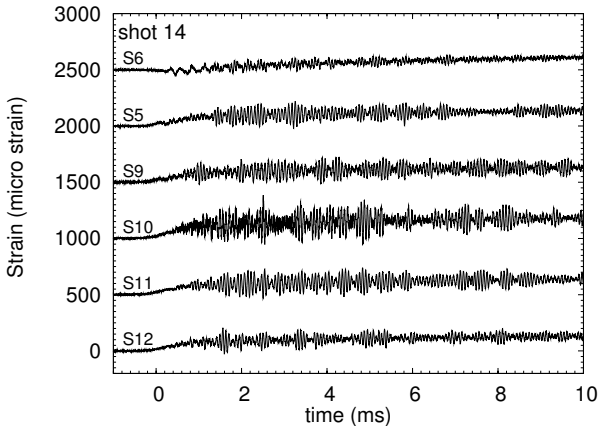

c) strain (S_9-S_{12}, S_5, S_7)

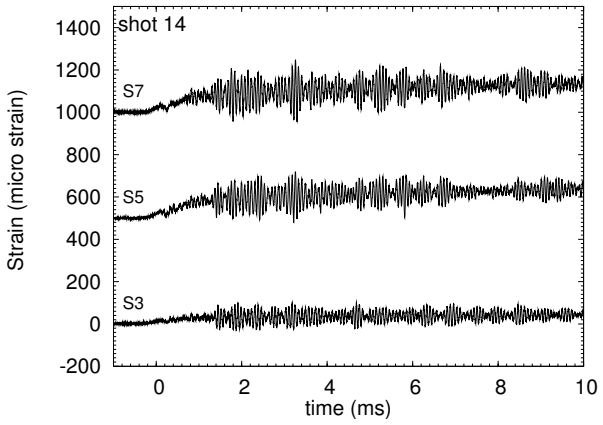

d) strain (S_3, S_5, S_7)

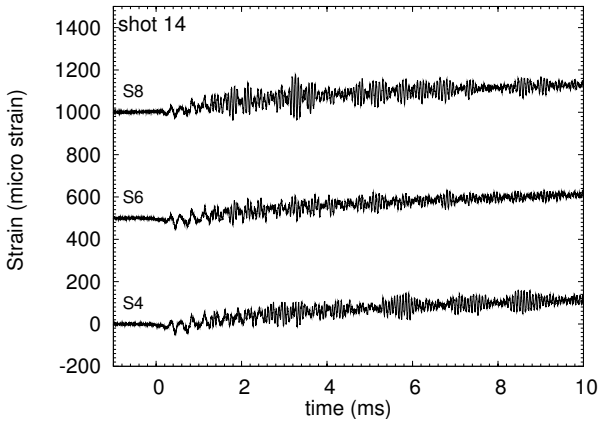

e) strain (S_4, S_6, S_8)

Figure 25: Pressure and strain traces for mixture A and P_0=1.0 bar with empty tube, shot 14.

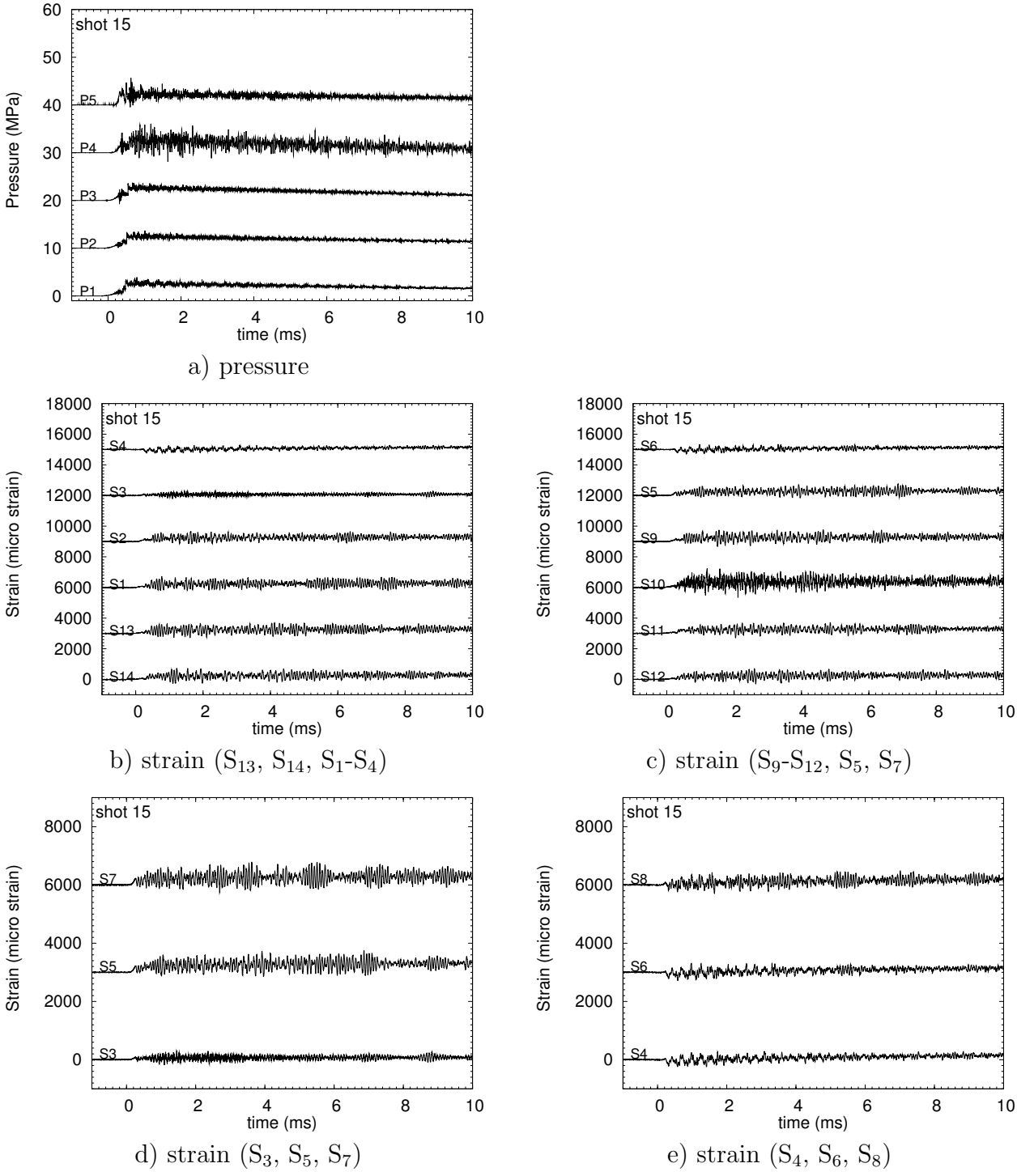

Figure 26: Pressure and strain traces for mixture A and P_0=3.0 bar with empty tube, shot 15.

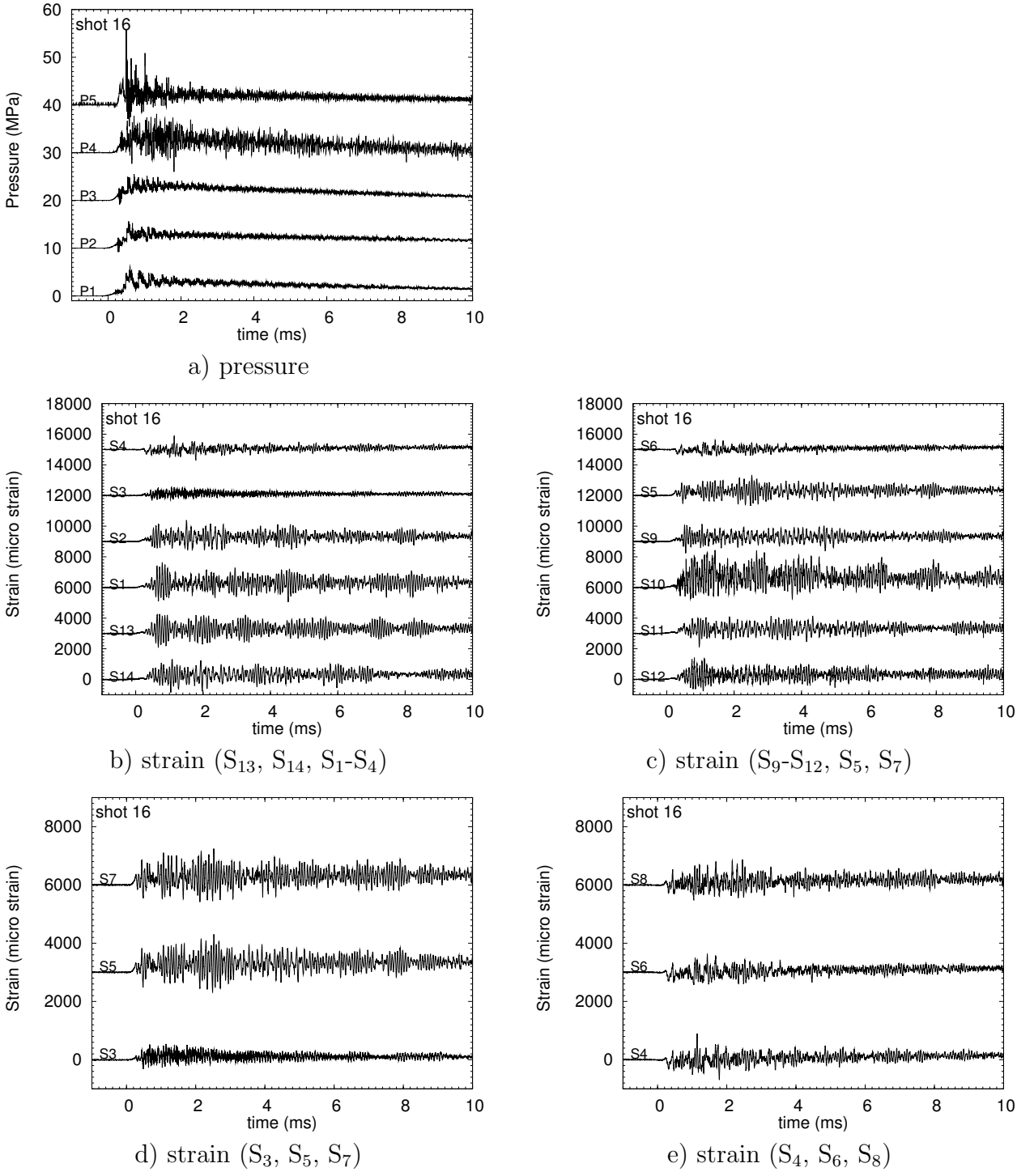

Figure 27: Pressure and strain traces for mixture A and P_0=3.5 bar with empty tube, shot 16.

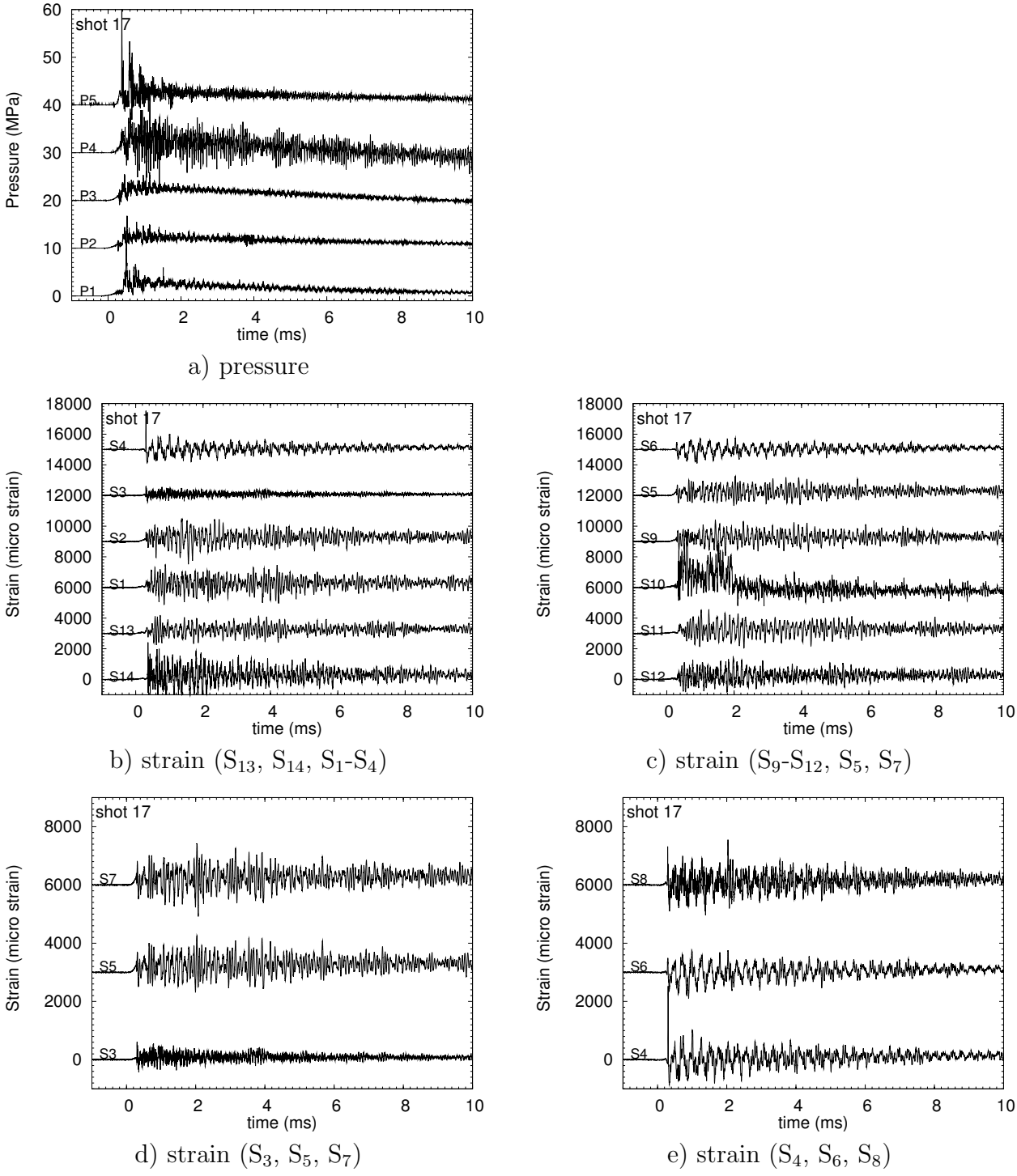

Figure 28: Pressure and strain traces for mixture A and P_0=3.0 bar with empty tube, shot 17.

B Estimates for the deformation of the inner cans

If an explosion takes place within the inner can or convenience can, deformation may occur in those cans. The resulting deformation could be higher than for the outer can since the wall thickness of the convenience can (0.039 in) or inner can (0.059 in) is much smaller than that of the outer can (0.123 in). In addition, the inner diameter of the inner cans (4.5 in) is smaller than the outer cans (4.685 in), so we would also expect DDT transition would occur at an initial pressure smaller than 2.6 bar.

Using the simplified approach that we have applied to analyzing the test results on the outer can, we have made predictions of the deformation of the inner can due to an internal explosion. Figure 29 and Table 6 show the estimated strains for inner cans and mixture A using P_{CJ} and $\Phi = 1$, 2 and 5. For $\Phi = 2$, the estimates approach the elastic limit (0.2% strain) when $P_0 > 2.75$ bar, but for $\Phi = 5$, the estimated strains are all above the limit when $P_0 > 1.2$ bar. When DDT occurs within an empty can, the dynamic load factor based on P_{CJ} may reach 3.5 according to both thick tube and 3013 outer can results. Therefore we expect plastic deformation of the inner can for an explosion of Mix A at an initial pressure higher than 2.75 bar and possibly at lower pressures, depending on the actual DDT threshold for the inner can. At the highest initial pressure with Mix A, sufficient plastic deformation might occur that the inner can expands to contact the outer can. We have not considered this possibility in detail.

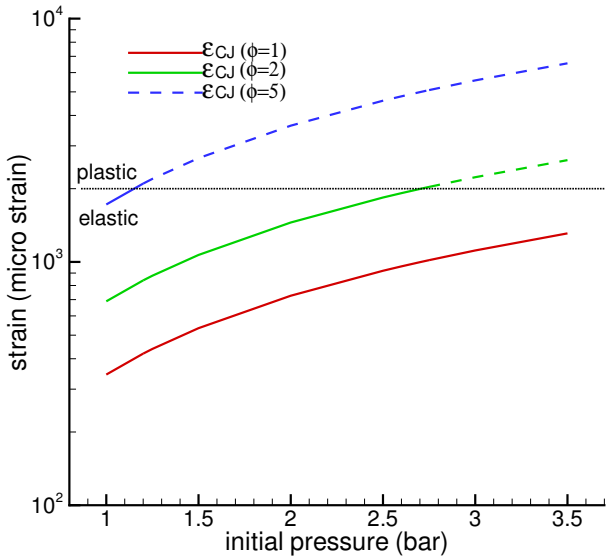

Figure 29: Estimated strain for the inner cans based on P_{CJ} in terms of dynamic load factors of 1, 2 and 5, and mix A. For the inner cans, ID = 4.50 in, OD = 4.62 in, $h = 0.06$ in, $R = 2.28$ in, and $E = 196$ GPa.

Table 6: Estimated strain for the inner cans with mix A using $\Phi = 1$, 2 and 5, and computed CJ pressure P_{CJ}. For inner cans, ID = 4.50 in, OD = 4.62 in, $h = 0.06$ in, $R = 2.28$ in, and $E = 196$ GPa.

P_0	P_{CJ}	$\epsilon_{CJ,\ \Phi=1}$	$\epsilon_{CJ,\ \Phi=2}$	$\epsilon_{CJ,\ \Phi=5}$
(bar)	(MPa)	μstrain		
1	1.872	344.4	688.9	1722.2
1.5	2.848	534.2	1068.3	2670.8*
2	3.836	726.2	1452.4	3631.0*
2.5	4.832	919.8	1839.6	4599.1*
3	5.834	1114.6	2229.2*	5572.9*
3.5	6.841	1310.3	2620.6*	6551.6*
*Not reliable, indicates plastic deformation.				

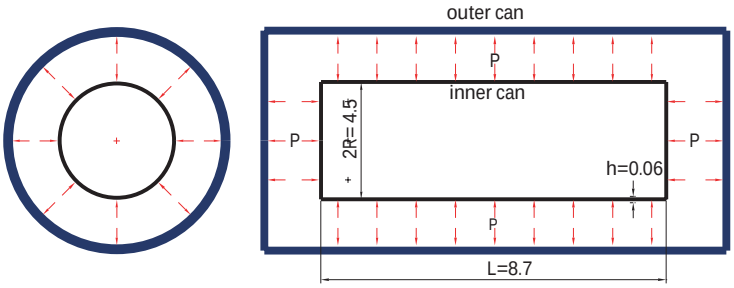

Figure 30: Schematic of 3013 inner and outer cans.

If an explosion takes place in the annulus between the outer and inner cans, the pressure will not only act to expand the outer can but also crush the inner can (see Fig. 30). All of our previous work has focused on the expansion of the outer can due to an internal explosion. The crushing of the inner can is more difficult to estimate than the deformation of the outer can since the inner can will fail by buckling; a process that is well-known to be very difficult to accurately estimate since it is quite sensitive to small variations in tube wall thickness and deviations from assumed cylindrical symmetry. We can make a rough estimate of the potential for buckling by assuming that the explosion in the annulus can be treated as applying a uniform quasi-static pressure load on the entire outer surface of the inner can. The critical external pressure at which elastic buckling occurs (see Young and Budynas, 1989, page 736, formula 20) can be estimated as

$$P_{critical} = \frac{E\frac{h}{R}}{1+\frac{1}{2}(\frac{\pi R}{nL})^2}\left(\frac{1}{n^2\left(1+\left(\frac{nL}{\pi R}\right)^2\right)^2}+\frac{n^2h^2}{12R^2(1-\nu^2)}\left(1+\left(\frac{\pi R}{nL}\right)^2\right)^2\right) \tag{3}$$

where $E = 196$ GPa, $h = 0.06$ in, $R = 2.28$ in, $L = 8.7$ in, $\nu = 0.3$, and $n =$ number of lobes

formed by the tube in buckling. Table 7 shows that $P_{critical}$ approaches a minimum value of 5.25 MPa when $n = 3$. The recommended (Young and Budynas, 1989) minimum critical pressure is 0.8 $P_{critical}$=4.2 MPa. This estimate is for a static load so it is problematic to apply this directly to a potential explosion situation. However, using a load factor of $\Phi_{CJ} = 2$, we expect that buckling will occur if the initial pressure exceeds 2 bar and transition to detonation takes place.

Table 7: Critical external buckling pressure for inner cans.

n	$P_{critical}$ (MPa)
2	23.32
3	5.25
4	5.34
5	7.58
6	10.65
7	14.35
8	18.64

We conclude that explosions within the inner can may result in plastic deformation of the inner can and possibly, contact with the outer can. Explosions outside the inner can may causing buckling or crushing of the inner can, absorbing some of the energy from the explosion.